Integrated Approach Towards the Application of Horizontal Wells to Improve Waterflooding Performance

FINAL REPORT

Submitted by

Mohan Kelkar

Department of Petroleum Engineering

Chris Liner

Dennis Kerr

Department of Geosciences

The University of Tulsa

Tulsa, Oklahoma 74104

Reporting Period: January 1, 1993 – August 31, 1999

Work Performed Under Contract No. DE-FC22-93BC14951

Prepared for

U.S. Department of Energy

Assistant Secretary for Fossil Energy

Contracting Officer's Representative

Mr. Daniel Ferguson

U.S. Department of Energy

National Petroleum Technology Office/DOE

Post Office Box 3628

Tulsa, Oklahoma 74101

TABLE OF CONTENTS

LIST OF ILLUSTRATIONS

LIST OF TABLES

DISCLAIMER

ACKNOWLEDGMENT

The research effort described in this report was supported by the U.S. Department of Energy under Contract DE-FC22-93BC14951. Additional support is provided by Amoco Production Company and Uplands Resources, Inc. The computer facilities were provided by the University of Tulsa.

We would like to thank Dan Richmond from Uplands Resources, Inc. for his valuable contribution and insight to our work. We also would like to acknowledge the guidance provided by Rich Chambers, Henry Tan, John Eager and Chandra Rai from Amoco Production Co. Lastly, our special thanks go to Rhonda Lindsey and Dan Ferguson from the Department of Energy for their enthusiasm and valuable suggestions.

September, 1999

Mohan Kelkar

ABSTRACT

This final report describes the progress during the six years of the project on "Integrated Approach Towards the Application of Horizontal Wells to Improve Waterflooding Performance." This project was funded under the Department of Energy's Class I program which is targeted towards improving the reservoir performance of mature oil fields located in fluvial-dominated deltaic deposits. The project involved an integrated approach to characterize the reservoir followed by drilling of horizontal injection wells to improve production performance.

The project is divided into two budget periods. In the first budget period, many modern technologies were used to develop a detailed reservoir management plan; whereas, in the second budget period, conventional data was used to develop a reservoir management plan. The idea was to determine the cost effectiveness of various technologies in improving the performance of mature oil fields.

In the first budget period, we applied several new technologies. These included integrated approach, use of cross borehole tomography, detailed geological analysis using micro-resistivity logs, facies biased mapping of sands using a concept of discrete genetic intervals (DGI), geostatistics and flow simulation. Out of these technologies, integrated approach, geological description using DGI's, geostatistics and flow simulation proved to be very effective. The other two technologies – cross borehole tomography and micro-resistivity logs – were not effective because of either the cost and/or uncertainties in application of these technologies.

The field implementation at the end of the first budget period resulted in significant increase in oil production. More important, our predictions matched very well with the observed performance.

In the second budget period, we concentrated on using conventional data to develop a detailed reservoir description. We used the existing well core and log data as well as production data to develop reservoir description. We continued to use technologies which were proven to be effective in the first budget period – namely, use of DGI's to describe geology, geostatistics and flow simulation.

Based on the evaluation of conventional data, we proposed drilling a deviated well using surface steered drilling assembly. Unfortunately, due to problem during drilling, the well had to be abandoned. We, therefore, never had the opportunity to test our reservoir management plan in the second budget period. Based on the experience during the first budget period, we are confident that we would have been able to improve the performance had the well been successful.

To compliment our technical effort, we also conducted vigorous technology transfer activities. These included publications and presentations at various technical meetings and journals, conducting technology transfer workshops for small operators and independents, and publishing two newsletters for interested audience. These activities resulted in reaching a wide cross section of audience, and making the operators aware about technologies that can help them in the future.

EXECUTIVE SUMMARY

This final report discusses the various approaches used in attempting to improve the performance of mature oil field. The results of the implementation and the lessons learned from the implementation are also included in the report. The field selected for the implementation is Glenn Pool oil field, which has been producing for more than 90 years. Overall, the technologies that proved to be effective include integrated approach to describe reservoirs, geological description using Discrete Genetic Intervals (DGI's), ranking of reservoir using productivity index mapping, geostatistics and flow simulation. The technologies which proved to be only marginally effective or ineffective include: use of micro-resistivity logs for detailed geological description, cross borehole tomography and drilling of deviated hole using surface steered drilling assembly.

The first budget period of the project focused on the Self-unit, a 160-acre tract of Glenn Pool field operated by Uplands Resources, Inc. The data available from the unit were wireline logs and core reports, and historical production records. Using log and core data, the reservoir was first divided into seven DGI's, each composed of contiguous facies deposited during a limited, discrete increment of time. Based on the preliminary geological evaluation, a test well (Self-82) was drilled and cored. Additional log data including micro-resistivity log (Formation Microscanner Imaging) data were collected from the same well. Using this well as a source well, three cross borehole tomography surveys were conducted between Self-82 and the surrounding three wells. With the help of a modified geological description as well as geophysical and engineering data, a detailed reservoir description was constructed. After validating the description by comparing the simulated flow performance with the historical data, several operating scenarios were simulated to optimize the flow performance under modified conditions. A combination of recompletion and stimulation of most wells followed by increasing the water injection rate in the field was observed to be the most optimal change to improve the flow performance of the Self-unit.

The proposed reservoir management plan was implemented, and the unit performance was monitored for over three years. At the base level, the Self-unit was producing between 15 to 17 bbls/day. The initial increase in the incremental oil production was predicted to be in the range of 18 to 21 bbls/day.

The actual increase was 21 bbls/day. After 3 years, the incremental increase was predicted to be about 10 to 12 bbls/day. Currently, the field is producing 10 incremental bbls of oil per day over its base rate. In short, we were able to correctly predict the performance of the reservoir. Although in terms of actual production, this increase is not much, note that it still represents about 150% increase in the production rate. Further, the field is more than 90 years old, and has been subjected to many technologies in the past. If we can cost effectively increase production from such a mature field, we would be able to do better in other, relatively younger, fields. The economic evaluation indicated finding cost of oil is in the range of $4.50 to $6.00 per barrel. This cost can be reduced substantially if we only use the cost-effective technologies and eliminate the use of other technologies.

The effectiveness of technologies applied during the first budget period was critically examined. The use of integrated approach in developing reservoir description was found to be very useful. By combining various disciplines, we were better able to identify the uncertainties in reservoir description as well as were better able to understand the importance of most relevant scales in describing the reservoirs. The use of DGI's was helpful in identifying the intervals where the remaining oil is most likely located. Geostatistics helped us in developing tools that were capable of integrating various types of data, and quantifying uncertainties in the description. Flow simulation allowed us to evaluate various scenarios in determining an appropriate reservoir management plan. On the other hand, use of micro-resistivity logs did not add significantly more information compared to the actual core. For shallow, marginal reservoirs like Glenn Pool, the use of micro-resistivity logs was not very effective. The cross borehole imaging was expensive, and resulted in images that were dependent on the algorithm used to process the data. The cross borehole technology is relatively new, and technical uncertainties in the evaluation simply do not allow us to use the technology on a routine basis in a cost-effective manner.

For the second budget period of the project, we expanded the scope to other parts of the Glenn Pool field. Unlike the first budget period, we did not collect any new data during this period. Instead, we concentrated on using the existing data to develop a detailed reservoir description. We evaluated the entire area operated by Uplands Resources for the second budget period. In addition, we also evaluated an adjacent unit, which used to be operated by Chevron. The Chevron miceller-polymer unit

was successfully flooded in early 80's using miceller-polymer flood. We wanted to understand the reasons for the success.

Since it was difficult to study all parts of the reservoir in great details, we graded the reservoir based on a method of potential index mapping. This mapping involves evaluating various areas in the reservoir based on the permeability, thickness, porosity, saturation as well as prior access to that area by already existing wells. In addition to potential index mapping, we also examined the primary and secondary recovery production from various units. Based on the grading of various parts of the reservoir, we decided to concentrate on tracts 7 and 9.

We began our evaluation by studying the Chevron unit. Our evaluation indicated that the success of the Chevron unit could be partly attributed to re-completion of the upper intervals in the Glenn sand. Unlike other operators, Chevron concentrated on the upper and middle Glenn sand, and implemented the miceller-polymer flood in those sands. The increase in oil production as well as reduction in water cut was substantial. We re-simulated the Chevron unit assuming that it is water flooded with same completion as Chevron had used. The response indicated that Chevron would have achieved a substantial increase in the oil production with reduction with water cut just by using water flood. Although not as impressive as the miceller-polymer flood, the simulation indicated to us that we could use a similar approach in other parts of the field. We studied both tracts 7 and 9, and investigated various scenarios for improving the performance of those units.

Based on our evaluation, we decided to drill a deviated well in tract 9, which would be completed in the upper and middle part of the Glenn sand. To achieve the drilling in a cost-effective manner, we employed a relatively new technology of surface steered drilling which is much cheaper than conventional deviated hole drilling. Unfortunately, drilling of deviated hole proved to be much more challenging than anticipated. We lost the drilling assembly twice. During the second time, we could not fish it, and the hole had to be abandoned. As a result, our reservoir management plan during the second budget period could not be validated. Because of budget constraints, another attempt at drilling the deviated hole could not be made. Hopefully, private owners will take an initiative, and with favorable oil price, drill deviated wells in the same field to validate the concept.

To compliment our technical effort, we vigorously pursued various technology transfer activities. These activities resulted in 26 publications and 10 presentations. In addition, four technology transfer workshops were conducted for the benefit of small operators and independents. These workshop locations included Tulsa, Houston, Denver and Ft. Worth. We also published two newsletters and sent them to over 300 interested parties.

To summarize, although the project ended with a failure of deviated well, we accomplished a great deal. We demonstrated that even a ninety-year old field could be rejuvenated using cost effective technologies. We evaluated various technologies and determined their cost-effectiveness. We were able to transfer many aspects of the technology to small operators and independents.

INTRODUCTION

The overall report is divided into four sections. In the first section, we provide the background of the field that was the subject of investigation. The project was divided into two budget periods. In the second section, we describe the activities during the first budget period. The first budget period involved using modern technology to describe the reservoir in part of the field followed by implementing an appropriate reservoir management plan to improve the performance. In the third section, we describe the activities during the second budget period. The second budget period involved using conventional technology to develop a reservoir description followed by implementing an appropriate reservoir management plan to improve the performance. Comparing the two periods, we were successful in improving the performance of the field during the first budget period. In contrast, due to problems in drilling the horizontal well, we were unable to validate our approach during the second budget period. In the last section of the report, we summarize some of the technology transfer activities carried out as part of the project.

BACKGROUND

The DOE Class I Program is targeted towards improvement of production performance of existing mature oil fields located in fluvial-dominated deltaic sandstone reservoirs. This project was selected under the near-term program which required that existing new technologies be applied in these fields to prevent any premature abandonment of these mature fields. The Glenn Pool field selected for this project fits the desired characteristics under this program.

The Glenn Pool field is located in portions of Tulsa and Creek Counties of Oklahoma. The field was discovered in 1905, and it is estimated as having produced 330 MM barrels of oil from the Middle Pennsylvanian (Desmoinesian) age Bartlesville sandstone. Glenn Pool field, like other fields developed in the Bartlesville sandstone, is located on the northeastern Oklahoma platform, a paleotopographic and structural depression of mid-Mississippian-Pennsylvanian age lying between the Ozark uplift to the east, the Nemaha ridge on the west and the Arkoma basin to the south (see **Figure 1**). The figure also shows the area of study for this project. The Self-unit indicated in the figure was the subject of first budget period investigation, whereas the gray area surrounding the Self-unit was the subject of the second budget period.

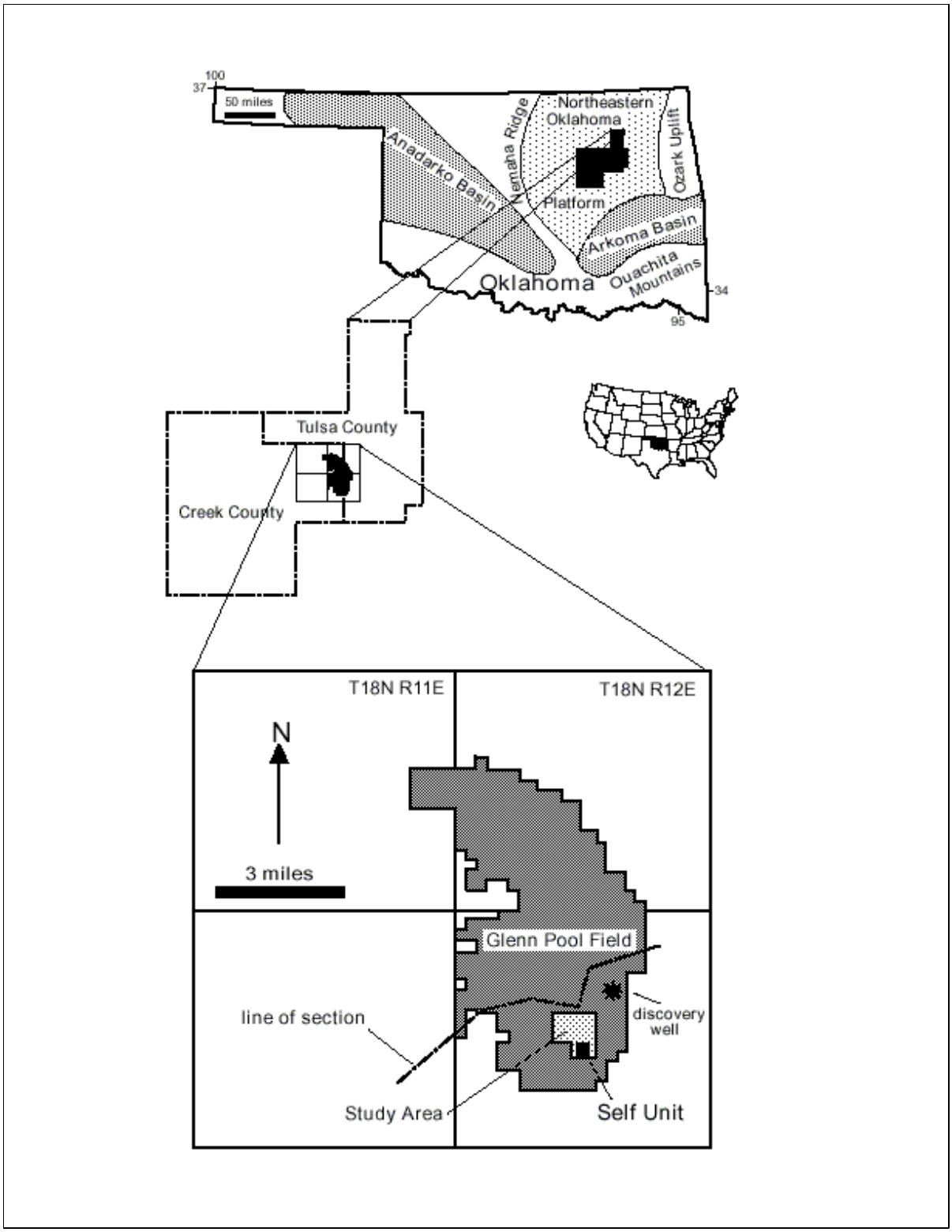

Figure 1 – Location of Glenn Pool field

The field encompasses 27,440-acres. Initial production from the wells ranged from 75-500 BOPD to 4,000 BOPD. After discovery in 1905, the field reached peak production in 1907. The first well in the field was drilled in fall of 1905. The well was located on the Ida Glenn farm near the center of the SE/4 of section 10, T17N, R12E, in Tulsa County (see Figure 1). The well was 1,458-ft deep and produced at a flowing rate of 75 BOPD. The producing interval was called "Glenn sandstone" and in the subsequent years became the target pay zone. The average producing span was estimated to be close to 240-ft and was the most productive compared to the other nearby fields.

Initial wells were drilled by cable tools. Surface casing of 8-5/8 inch size was set at 275-ft and open hole drilling was carried out to the top of Bartlesville reservoir. The hole size was reduced to 6 inches through the pay zone interval. The producing interval was shot with 250-300 quarts of nitroglycerine, casing set to the top of the sandstone, and the shot hole cleaned out. By 1906, well drilling averaged at the rate of 3 wells per day. In this process, orderly spacing of the wells was neglected. Subsequently, the completion was on a ten-acre pattern. Earthen lakes were used for storage on many leases, and oil was shipped to the Texas Gulf Coast by railroad. In 1908, 100 companies were operating in the field. By 1912, several BCF of natural gas is estimated to have been flared, vented or used as fuel for lighting field operations. The field limits had been defined by 1920. A pipeline through Coffeyville, Kansas connected the field to the Chicago and Great Lakes markets. By 1926, 22 refineries served the area.

With depletion of production, gas injection was introduced in 1940, and gas collected at producing wells was recycled to injection wells. Water flooding operations began in 1944. Cumulative oil production records prior to field-wide water flooding are incomplete. By 1943, it was estimated that the production throughout the field was between 222 and 236 MMBO. Over 100 MMBO had been produced up to 1990 by secondary gas repressuring, water flooding, and tertiary recovery methods bringing total production to 330 MMBO. The field is being depleted at present. Several large production units are under water flood, and a few units have undergone testing and implementation of micellar-polymer enhanced recovery methods. Results have shown the possibility for significant additional volumes of recoverable oil.

The Glenn sand has been conventionally divided into 3 units: upper, middle and lower Glenn.[1] Each is separated by apparent permeability barriers consisting of interbedded siltstones and shales. In the central portion of the Glenn Pool field the Glenn sand is present at a depth of approximately 1,500 feet, and the thickness varies from 100 to 185-feet. The upper and middle Glenn are the producing intervals in the central portion of the field and the lower Glenn is below the oil-water contact.

Oil from the Glenn sand has a gravity of 35.8° to 41.3°. It contains 3.12 to 11.46% paraffin and a sulfur content of 0.3%. Initial reservoir pressure has been estimated in the range of 600 to 700 psi. Current water flooding injection pressure ranges from 100 to 1,100 psi.[1]

From regional studies, the Bartlesville sandstone is regarded as having been deposited by a fluvial-dominated delta system.[2] In the Glenn Pool field area, the Glenn sand is predominantly the deposits of delta plain depositional environments. The lower Glenn sandstones are subangular to subrounded, moderately sorted, silty fine- to medium-grained sandstone, with abundant sand-size rock fragments, and thin beds of shale and siltstone.[1] The lower non-porous break consists of interbedded, laminated silty sandstone and shale with localized thin beds of shale, sideritic clay pebbles and with intervals of carbonate-cemented sandstone.[1] The middle Glenn is subangular to subrounded and well-sorted fine- to very-fine-grained sandstone.[1] It is primarily massively bedded, with portions containing medium-scale crossbedding.[1] The middle Glenn forms the major part of the reservoir.

The upper non-porous break consists of thin silty shale or interbedded laminated, silty sandstone and silty shale.[1] It is an effective permeability barrier but limited lateral extent may result in localized contacts between the upper and middle Glenn. The upper Glenn is in part massively bedded and in part medium-scale crossbedded. It is angular to subangular, moderately sorted very fine- to medium-grained sandstones,[1] and contains abundant carbonaceous fragments and a few sand-sized rock fragments. The upper portion of the upper Glenn contains poorly sorted very fine- to medium-grained sandstones with silty interlaminations, sparse carbonate or silica cement, and visible porosity.

Tectonism associated with the Ouachita collisional event caused the platform to tilt southward into the subsiding Arkoma foreland basin of southeastern Oklahoma.[2-4] Regional uplift during the Jurassic and

Cretaceous resulted in a gentle, westward dipping monocline with locally developed low-relief closures.[1, 5] Glenn Pool field structure contour data at the top of the Bartlesville (Glenn) sandstone show a broad feature, open to the northwest, with about 200-ft (61 m) of relief.[1] The productive limits of Glenn Pool field only generally coincide with this feature. Within the field, structural relief is variable (50-75-ft, 15-23 m) as a result of Bartlesville (Glenn) sandstone thickness variations and stratigraphic termination along the eastern margin of the field.

Stratigraphically, the Bartlesville sandstone and its outcrop equivalent, the Bluejacket sandstone, are members of the Boggy formation, which is included within the Krebs group of the Desmoinesian series (**Figure 2**). The Bartlesville is underlain by the Savanna formation (Krebs group) and is overlain by the Inola limestone and, locally, by the Red Fork member (zone). Black shales within the Inola limestone, a member of the Boggy, and Brown limestone, a member of the Savanna, are used as marker beds for detailed stratigraphic correlation (**Figure 3**). Within Glenn Pool field, the Bartlesville (Glenn) has been traditionally divided into upper, middle, and lower Glenn sand intervals, all of which pinchout at the eastern edge of the field.[1] Entrapment within the field is a result of this updip termination of reservoir-quality sandstones (Figure 2).

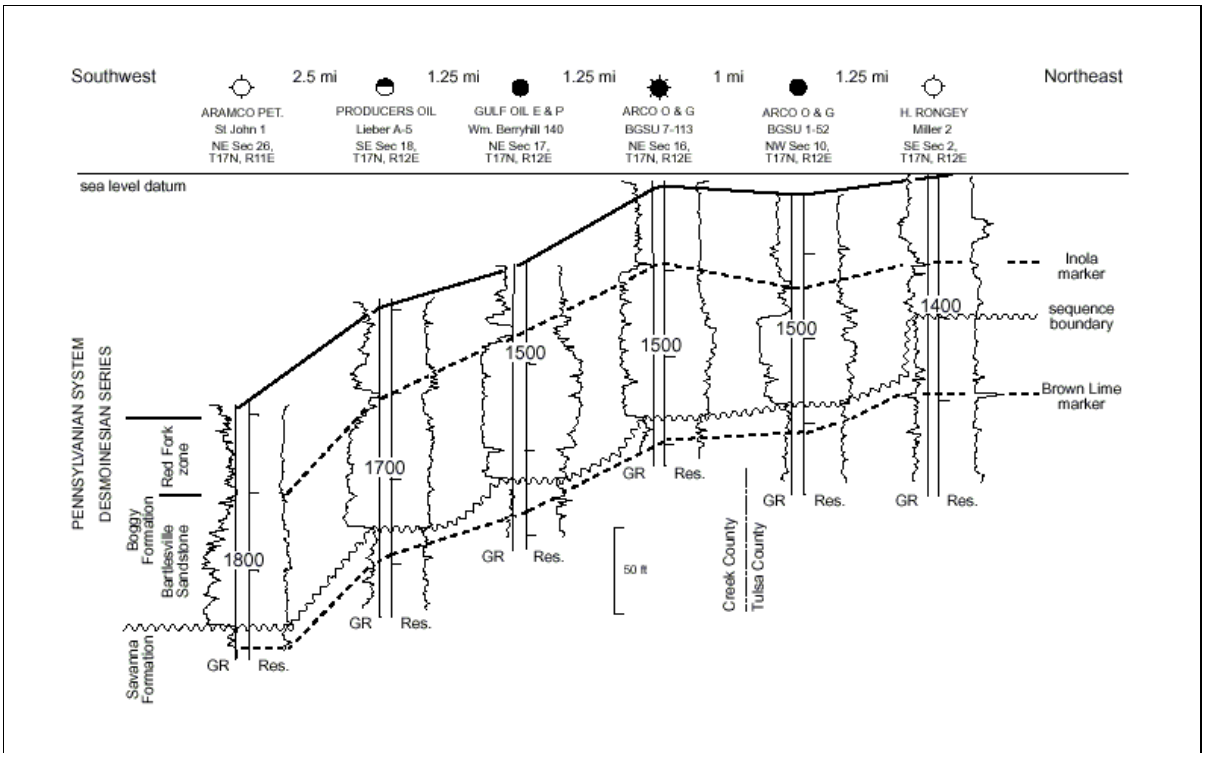

Figure 2 – Stratigraphic location of Bartlesville sandstone

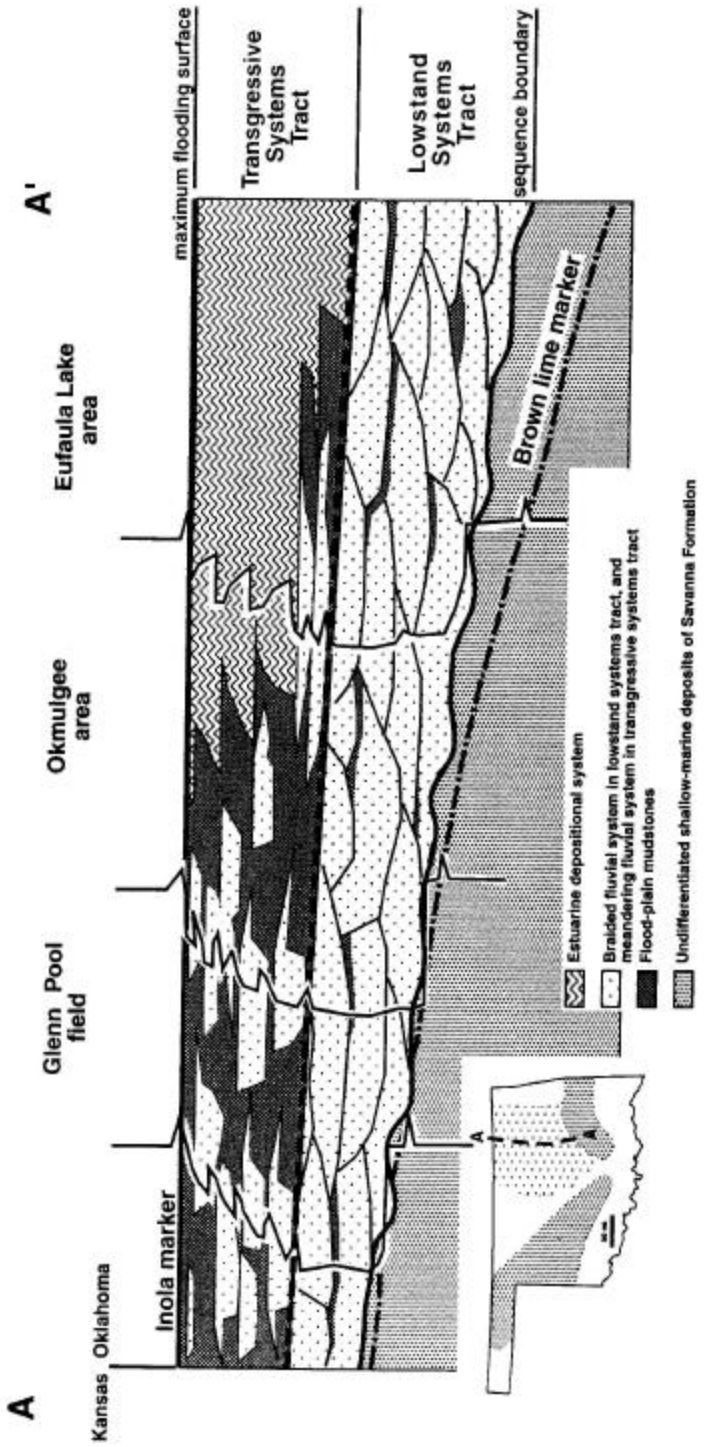

Figure 3 – Marker beds for Glenn Pool field

The conventional interpretation of the Bluejacket (outcrop) and Bartlesville (subsurface) sandstone was established in studies conducted by Visher[2] and his students at The University of Tulsa during the 1960s and 70s. This interpretation proposes that the Bartlesville was deposited within a fluvial-dominated deltaic system that prograded southward into the subsiding Arkoma Basin (see Figure 1), essentially during a single regressive event. An alluvial valley system extending from the Kansas-Oklahoma state line is inferred to show southward transition to a fluvial-dominated deltaic system across northeastern Oklahoma. Within this scheme, Glenn Pool field lies well within the deltaic portion of the overall system, close to the depositional boundary between upper and lower delta plain facies.

During this investigation, the conventional geological model of Bartlesville sandstone has been substantially revised in light of new information. The details of this revision are discussed in the following sections.

BUDGET PERIOD I

Introduction

In the first budget period, our effort concentrated on Self-unit located in the southeast portion of the Glenn Pool field (see Figure 1). During this period, we applied several new technologies to improve the reservoir description. These technologies include integrated reservoir description, geological description using DGI's (discrete genetic intervals), modern logs, cross borehole tomography, geostatistics and reservoir flow simulation. The description and success of each of these technologies is discussed in this section.

Self-Unit

The Self-unit, area of investigation of project during budget period one is a 160-acre tract located in southeast portion of Glenn Pool oil field in section 21-17N-12E (**Figure 4**). Currently Uplands Resources, Inc. operates the unit. The first well on the lease was put on production November 6, 1906. In all, 5 wells were put on production in 1906. Out of the three Glenn sand intervals, the upper and middle are present while lower Glenn is absent in the Self-unit. ARCO's report by Heath[6] on the Glenn sand unit gives a brief history about the performance of the Self-unit.

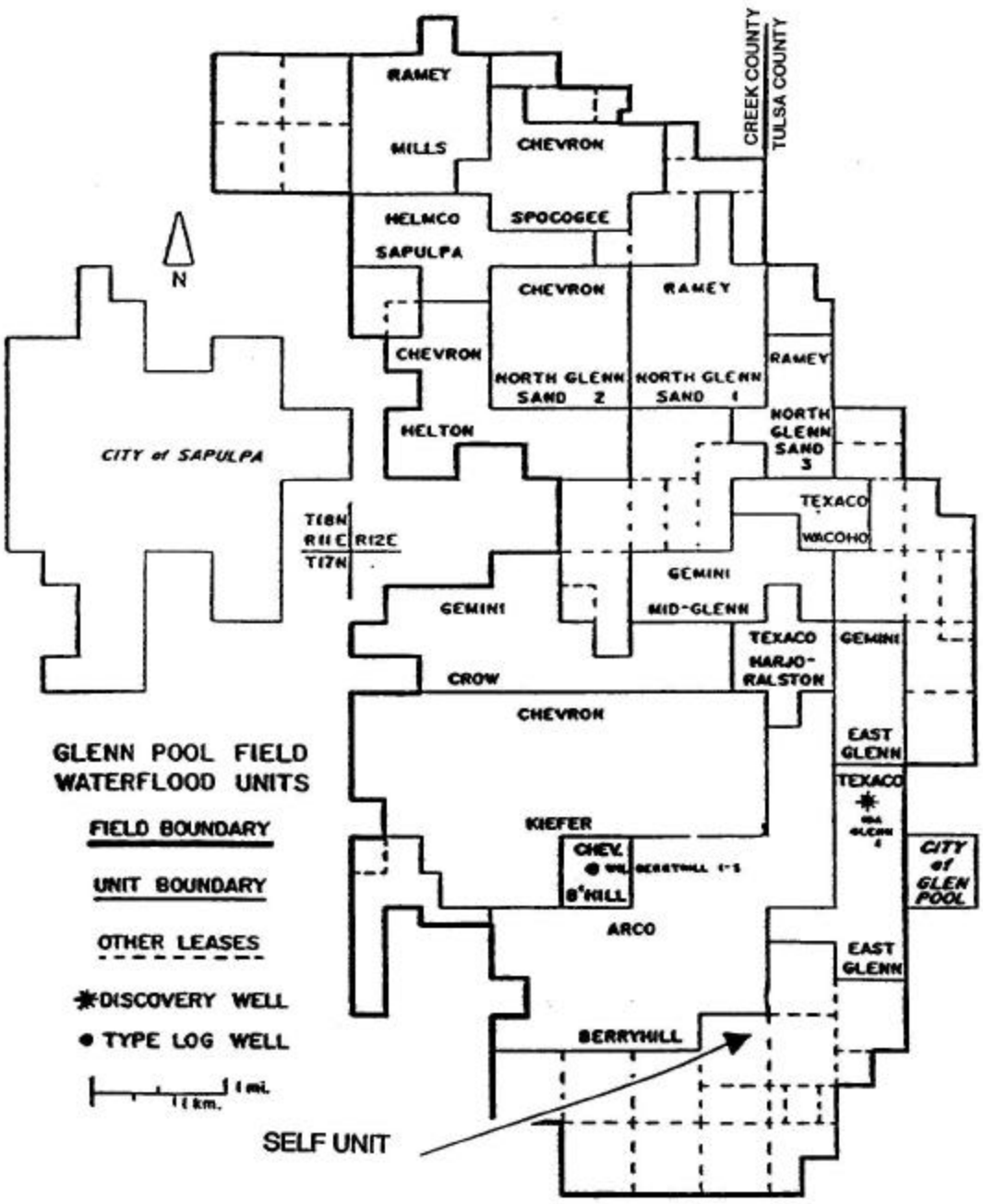

Figure 4 – Self-unit location[1]

The original oil in place (OOIP) for the unit has been estimated to be 13.009 MMBO. Primary production during 1906-1945 resulted in the production of 1.809 MMBO representing 13.91% of

OOIP. In 1945, gas repressuring began in the unit. This resulted in a recovery of 0.231 MMBO representing 1.8% of OOIP. During 1954-1966 the unit was put on a pilot water flood resulting in production of 0.169 MMBO (1.3% of OOIP). The recoveries were higher in the areas surrounding the pilot and the gas injectors. In 1966, water flooding was extended to the majority of the field. In the initial period of water flooding, the production increased across the entire Self-unit. The total production during 1966-1978 was 0.235 MMBO, representing 1.8% of OOIP. The unit was re-drilled in 1978 on a ten-acre 5-spot pattern. During 1978-1983, 0.146 MMBO production representing 1.12% of OOIP was obtained. From 1984-1992, production was 0.157 MMBO representing 1.2% of OOIP. Total production obtained to date from the unit is around 20% of the OOIP.

The Self-unit experienced good primary recovery, but response to the subsequent secondary recovery efforts has not been encouraging. Study of the available well logs and core reports indicate that lithologic heterogeneities and permeability vary throughout the lease. Well logs taken in the 1980's indicate higher water saturations in middle Glenn portions rather than in the upper Glenn. Upper Glenn portions could not be swept by water flooding, perhaps, because of lower permeabilities in these portions and inadequate perforation coverage.

Despite subsequent water flooding, water injection could not be contained on the lease and water possibly migrated to other parts of the field. Large permeability variations in upper and middle Glenn also contributed to this inefficient use of water injection. Injection pressures and rates vary throughout the lease; pressures range from 50 to 700 psi, and the rates range from 40 to 2,000 barrels of water per day. At the start of budget period one, oil production from the unit was less than 18 bbls/d with water cut of 99%.

In total, 81 wells have been drilled on the Self-lease. The study required the availability of all well records. Though starting production and abandonment data for most of the wells are available, information with regards to the production history for individual wells could not be traced. The lease-wide production records are not available before the year 1935. Well chronology has been established by analyzing two well maps, well map as of 12-August-1955, well map as of 15-May-1981 and the

other sparsely available well records. Information pertaining to the number of producing wells each year is available from production documents but information regarding the location or respective number had to be estimated based on the documents mentioned above. The chronological development of the Self-unit on a well by well basis till the start of the project is included in **Table 1**. The well map depicting all the wells drilled in the Self-unit is shown in **Figure 5**. Initial development occurred along the periphery of the unit; subsequently, development occurred in the interior.

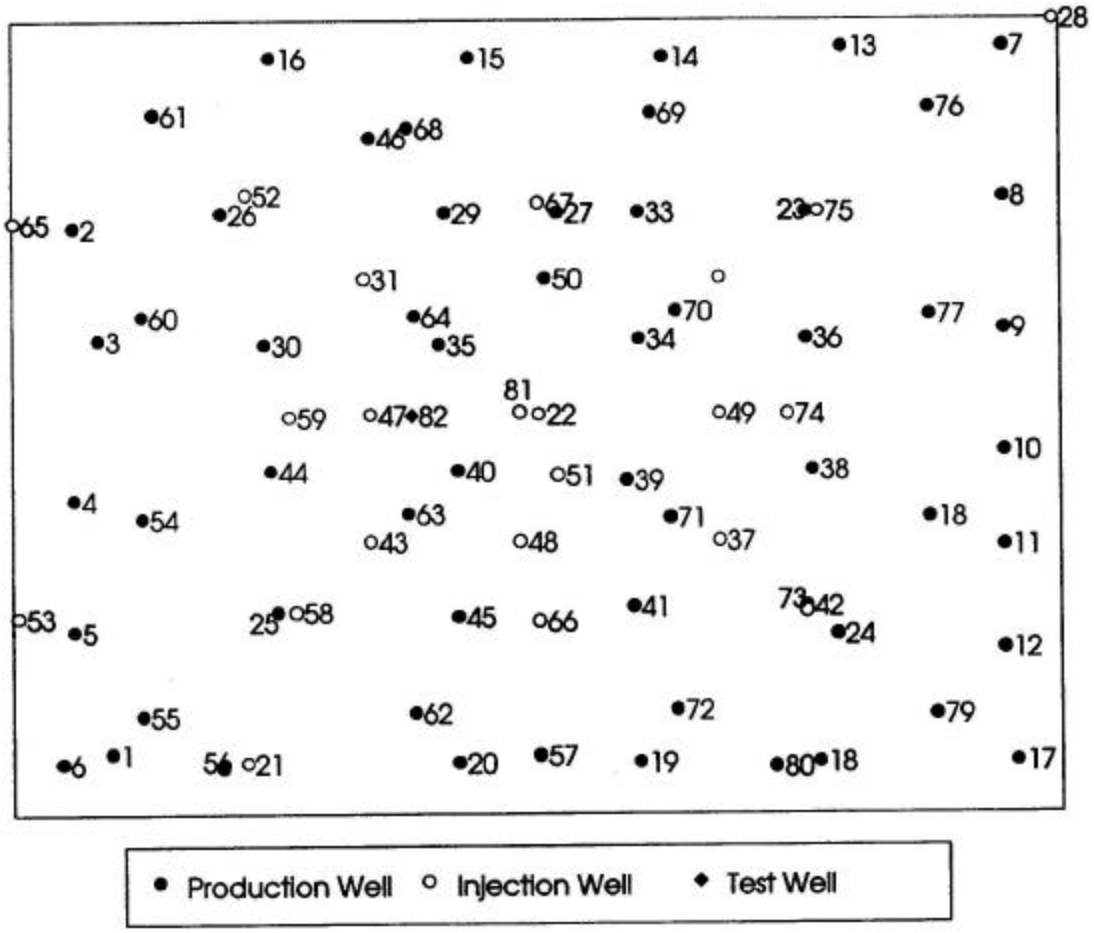

Figure 5 – Well locations

Table 1 – Historical Information on Self-unit							
Year	Number of Producers	Gas Injectors	Water Injector	Water Disposal	Wells Drilled	Wells Plugged	Well Number
1906	5	-	-	-	5(1, 2, 3, 4, 7)	-	1, 2 ,3, 4, 7
1907	27	-	-	-	22(5, 6, 8-27)	-	1-27
1911	26	0	0	0	0	1(4)	1-3,5-27
1923	24	-	-	-	-	2(3, 5)	1,2,6-27
1927	20	-	-	-	-	4(11, 12, 17, 18)	1, 2, 6-10, 13-16, 19-27
1930	18	-	-	-	-	2(19, 24)	1, 2, 6-10, 13-16, 20-23, 25-27
1936	18	-	-	-	-	-	1, 2, 6-10, 13-16, 20-23, 25-27
1946	16	4(21, 28, 31, 32)	-	-	5(28-32)	1(27)	1, 2, 6-10, 13-16, 20, 22, 23, 25, 26 Inactive 29, 30
1947	19	5(21, 28, 31, 32, 37)	-	-	7(33-39)	-	1, 2, 6-10, 13-16, 20, 22, 23, 25-26, 29, 30, 33 Inactive 34-36, 38-39
1948	25	6(21, 28, 31, 32, 37, 43)	-	-	6(40-45)	-	1, 2, 6-10, 13-16, 20, 22, 23, 25-26, 29, 30, 33, 34, 35, 36, 38, 39, 40 Inactive 41, 42, 44, 45
1950	27	8(21, 28, 31, 32, 37, 43, 47)	-	-	2(46, 47)	-	1, 2, 6-10, 13-16, 22, 23, 25, 26, 29, 30, 33-36, 38-42, 44 Inactive 20, 45-46

Year	Number of Producers	Gas Injectors	Water Injector	Water Disposal	Wells Drilled	Wells Plugged	Well Number
1954	27	8(21, 28, 31, 32, 37, 43, 47)	3(22, 48, 49)	1(20)	2,(48,49)	-	1, 2, 6-10, 13-16, 23, 25, 26, 29, 30, 33-36, 38-42, 44-45 Inactive 46
1957	28	-	11(21, 22, 28, 31, 32, 37, 43, 47, 48, 49, 50)	1(20)	1(50)	-	1, 2, 6-10, 13-16, 23, 25, 26, 29, 30, 33-36, 38-42, 44-45, 46
1965	28	-	12(21, 22, 28, 31, 32, 37, 43, 47, 48, 49, 50, 51)	1(20)	1(51)	-	1, 2, 6-10, 13-16, 23, 25, 26, 29, 30, 33-36, 38-42, 44-45, 46
1967	28	-	12(21, 22, 28, 31, 32, 37, 43, 47, 48, 49, 50, 51)	1(20)	1(52)	-	1, 2, 6-10, 13-15, 23, 25, 26, 29, 30, 33-36, 38-42, 44-45, 46, 52 Inactive 16
1970	28	-	12(21, 22, 28, 31, 32, 37, 43, 47, 48, 49, 50, 51)	1(20)	-	1(16)	1, 2, 6-10, 13-15, 23, 25, 26, 29, 30, 33-36, 38-42, 44-45, 46, 52
1971	27(1st ½) 23(2nd ½)	-	12(21, 22, 28, 31, 32, 37, 43, 47, 48, 49, 50, 51)	1(20)	-	5(7, 9, 13, 14, 15)	1, 2, 6, 8, 10, 23, 25, 26, 29, 30, 33-36, 38-42, 44-46, 52

Year	Number of Producers	Gas Injectors	Water Injector	Water Disposal	Wells Drilled	Wells Plugged	Well Number
1972	20	0	12(21, 22, 28, 31, 32, 37, 43, 47, 48, 49, 50, 51)	1(20)	-	3(29, 33, 34)	1, 2, 6, 8, 10, 23, 25, 26, 30, 35, 36, 38-42, 44-46, 52
1973	20(1st ½) 17(2nd ½)	-	12(21, 22, 28, 31, 32, 37, 43, 47, 48, 49, 50, 51)	1(20)	-	3(10, 35, 36)	1, 2, 6, 8, 23, 25, 26, 30, 38-42, 44-46, 52
1978	16	-	11(21, 22, 28, 31, 37, 43, 47, 48, 49, 50, 51)	1(20)	-	2(2, 32)	1, 6, 8, 23, 25, 26, 30, 38-42, 44-46, 52
1979	6(1st ½) 9(2nd ½)	-	10(21, 22, 28, 31, 37, 43, 478, 49, 50, 51)	1(20)	3(53-55)	8(8, 23-26, 44-47)	1, 6, 30, 38, 42, 52, 53-55 Inactive 39-41
1980 (Jun)	6	-	2(48, 50)	-	-	17(1, 20, 21, 22, 28, 31, 37-43, 49, 51)	6, 30, 52, 53, 54, 55
1981 (Dec)	21	-	11(48, 52, 53, 58, 59, 65, 66, 67, 73-75)	-	24(56-80)	1(6)	30, 50, 54-57, 6-64, 68-72, 76-80
1982	20	-	11(48, 52, 53, 58, 59, 65, 66, 67, 73-75)	-	-	1(30)	50, 54-57, 60-64, 68-72, 76-80
1984	20	-	11(52, 53, 58, 59, 65, 66, 67, 73-75, 81)	-	1(81)	1(48)	50, 54-57, 60-64, 68-72, 76-80
1992							Same status
1993							Same status

As already mentioned, the unit was put to production in 1906, though no exact date could be found. Heath's report[6] lists the cumulative production through 1946 as 1.809 MMBO. Yearly production information from 1935-1906 has been extrapolated based upon the number of wells operating in the respective years and the production information for the years 1935-1946. From 1936-1972, the yearly estimation has been carried out on the basis of production information available for one month, three months, or in some cases six months. 1972 onwards production data availability are complete and detailed. Annual water injection and production rates are available for Self-unit and the adjoining Burrows lease combined. Data for individual leases has been obtained based upon their respective oil production fraction. The overall production history based on the above information is summarized in **Figure 6**. As evident from this figure, every time new technology was implemented in Self-unit the field responded with substantial increase in production. This is evident in 1946, 1965 and 1978. This also gives an indication that if new technology is properly used and a good reservoir management plan is implemented, the Self-unit can respond with an increase in oil production.

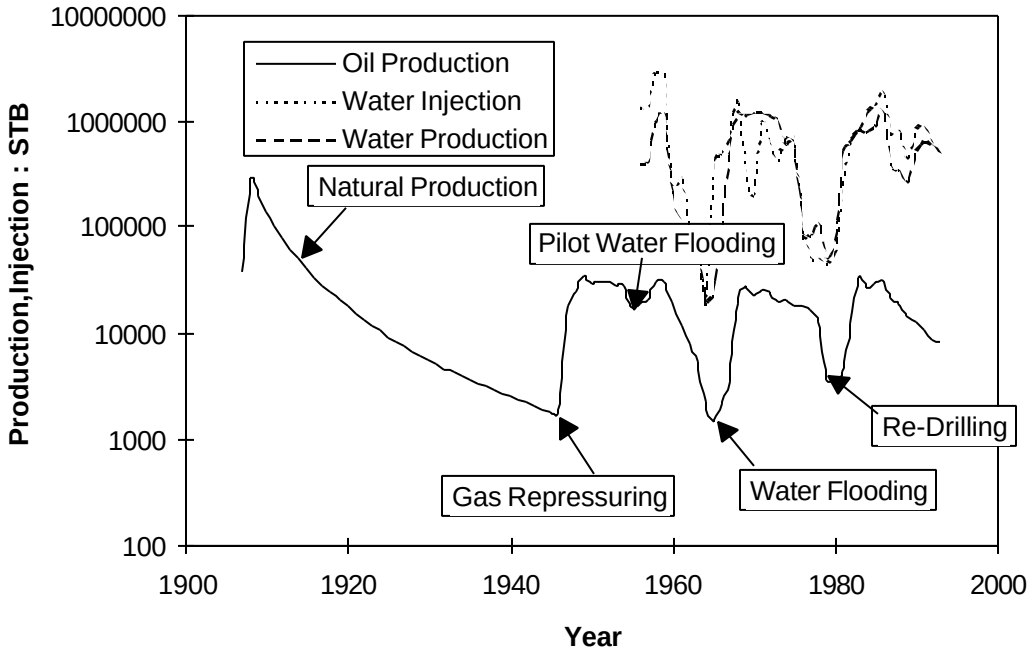

Figure 6 – Production history of Self-unit

For information related to the petrophysical properties, 3 well logs for wells drilled after 1978 are available. Permeability data availability for the Self-unit is not that abundant. Though eight core reports are available from the wells operating during 1940's and 1950's, the logs for those wells could not be traced and as a result no relation between the core and well log of the same well could be established. Furthermore, the existing wells have only been logged and there is no core report relevant to these wells.

Well schedule, water injection and production data have been summarized based on 1002-A forms, production reports, PI forms and other miscellaneous documents available from Uplands Resources, Inc. and the Oklahoma Well Log Library.

Although significant production data were available, the project team believed that an additional well was needed to be drilled for the following reasons.

- We did not have a single core from the Self-unit. The only core available to us was from northern part of the Glenn Pool field. We did not believe that it would be representative of Self-unit.
- We intended to run micro-imaging log to obtain detailed geological architecture. To run the micro-imaging log, we needed an open hole. With the existing wells, no open hole was available.
- We wanted to use cross borehole tomography to generate cross section information between two wells. To properly obtain the image of the reservoir, the well needs to be drilled deeper than the formation. All the existing wells were drilled to the total depth of Glenn sand. To properly obtain the cross borehole imaging information, we needed to have at least one well 400-ft deeper than the bottom of the Glenn sand.

In view of the above considerations, a vertical well was drilled in the Self-unit at the end of 1993. The location of the well, Self-82 is shown in Figure 5. The location was decided based on preliminary geological mapping, as well as distance considerations from the surrounding wells. The well was drilled 400-ft deeper than the Glenn sand. It was cored, a suite of modern logs, including micro-imaging log, was run successfully. The well was completed in January 1994.

In the following sections we will describe various technologies used in improving the reservoir description.

Geological Facies Architecture

Conventional geological analysis has divided the Glenn sand into upper, middle and lower sands. Recent well log, core, and outcrop analyses, however, have resulted in significant revisions to the conventional model.[7-9] These studies strongly suggest the Bartlesville sandstone in Glenn Pool field and much of northeastern Oklahoma consist of incised valley-fill deposits. Advanced reservoir characterization efforts in the southern portion of the field, including the Self-unit, propose a new facies architectural scheme based on a three-level spatial hierarchy of elements.[9] These elements, in increasing volumetric order, include: 1) facies/subfacies; 2) discrete genetic intervals (parasequences); and 3) systems tracts and stratigraphic sequence (Figure 3).

Much valuable data for re-interpretation of the Bartlesville sandstone came from a project cooperative well, the Self-82. A full suite of logs, including a microresistivity borehole image log, as well as a core (87-ft, 26 m) through nearly the entire Bartlesville interval, supplied considerable information for detailed characterization of reservoir sandstones and remaining reserves (**Figure 7**).

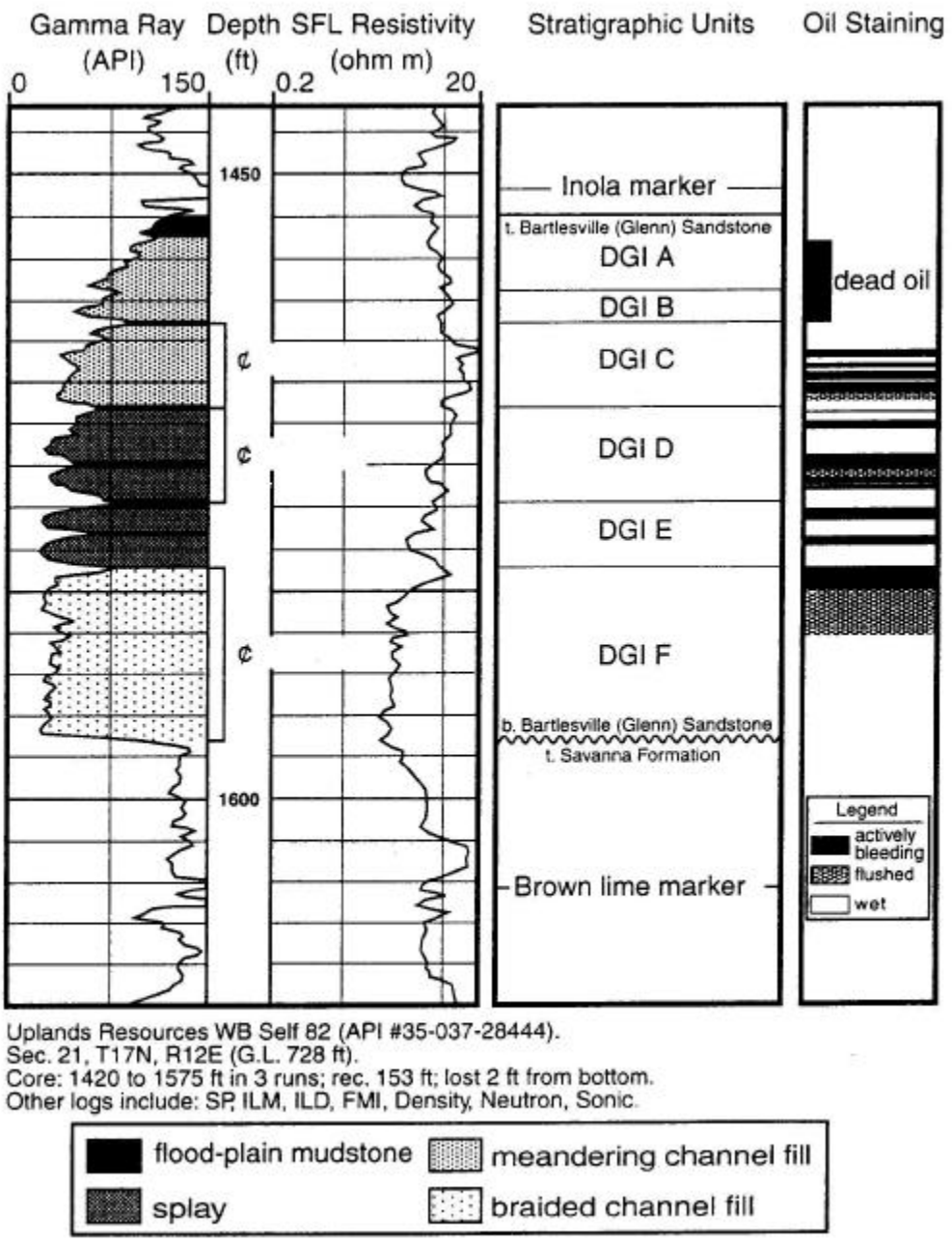

Figure 7 - Self-82 log with stratigraphic units and core oil-staining observations[10]

Facies and Subfacies Elements

The use of the term facies and subfacies is consistent with the traditional concept of sedimentary facies. Each facies and subfacies is characterized by its texture, sedimentary structures and wireline log profile.

Although they are given interpretative names, each is based on its distinctive descriptive characteristics. As architectural elements, facies, and to a more limited degree subfacies, are the volumetrically smallest elements in the hierarchy resolvable by conventional subsurface technologies.

Braided Channel-Fill Facies

Braided channel-fill facies compose the lower 40 to 80 ft (12-24 m) of the Bartlesville sandstone in Glenn Pool field. These deposits consist of structureless to less commonly parallel-bedded, moderately to well-sorted, upper medium- to lower coarse-grained sandstones (**Figure 8**). The basal contact is erosional with the underlying Savanna formation (sequence boundary, Figures 3 and 7). In outcrop, thick, structureless sandstones grade laterally to cross-stratified and/or parallel-bedded sandstone with parting lineations.[9]

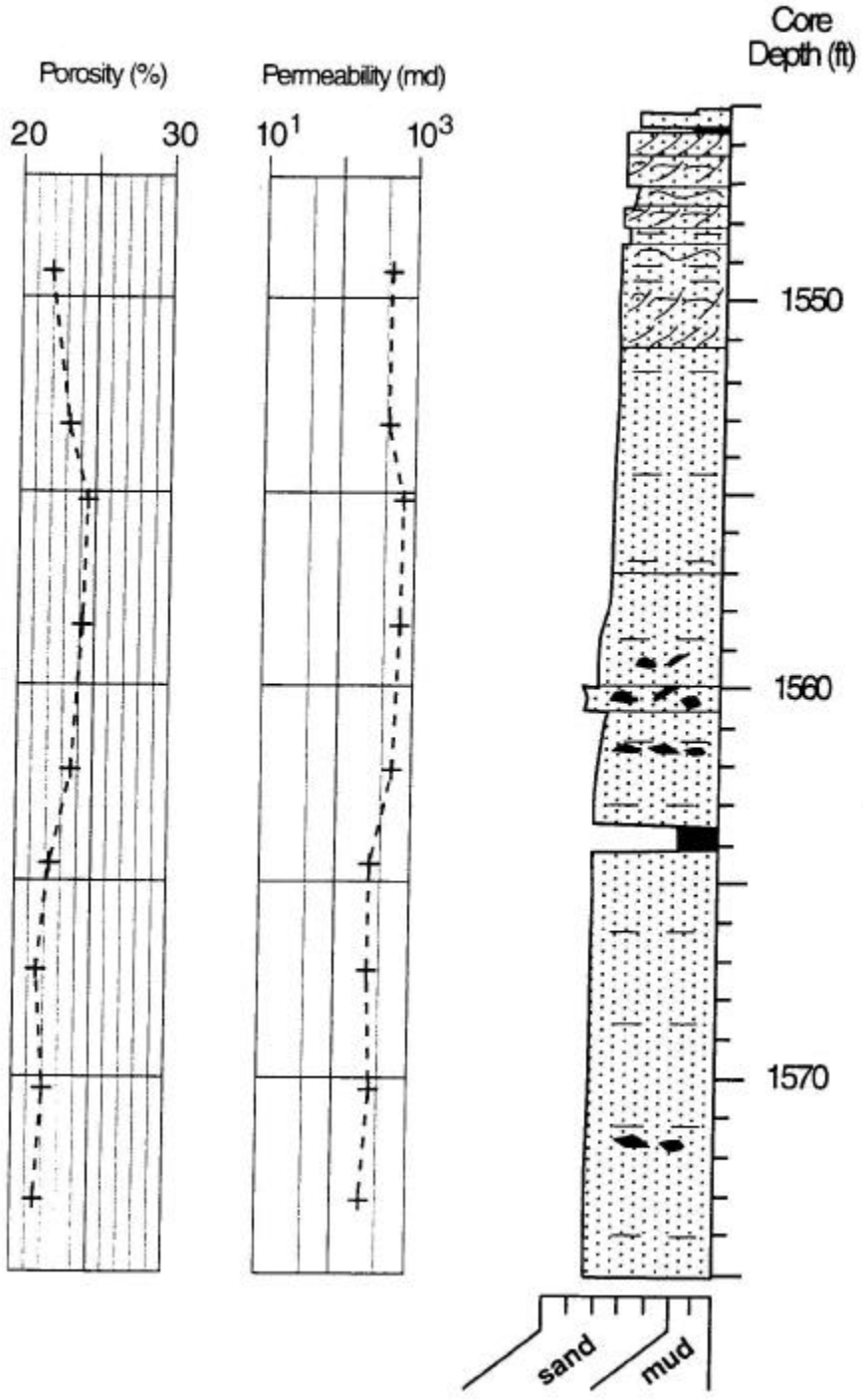

Figure 8 – Self-82 core description of DGI F braided channel-fill facies[10]

Subsurface correlations suggest that braided fluvial sandstones cover much of the southern part of Glenn Pool field. Mapping reveals localized areas where net sand thickness is 40 to 60-ft (12-18 m) over an area of 120 ac (48 ha), elongated in an east-northeast to west-southwest direction. In outcrop, the lateral limits of sand-body complexes are rarely seen, but numerous internal erosional surfaces define individual sand-bodies with width to maximum-net-sand-thickness ratio averaging about 30% and ranging between about 15-50%.[9]

Deposits of this facies exhibit blocky gamma ray well log profiles and excellent reservoir characteristics, as determined by core analysis (Figure 7). Porosities and permeabilities are commonly in the range of 20-25% and 100-1000 md.

Meandering Channel-Fill Facies and Subfacies

Meandering channel-fill deposits dominate the upper 100 to 150-ft (30-45 m) of the Bartlesville sandstone in Glenn Pool field. This facies is further subdivided into lower, middle, and upper channel-fill subfacies that together display a fining upward progression in grain size and an upward increase in proportion of interstratified mudstone. This texture profile and upward increase in mudstone content is also reflected in serrated bell-shaped well log (gamma ray and resistivity) profiles (**Figure 9**).

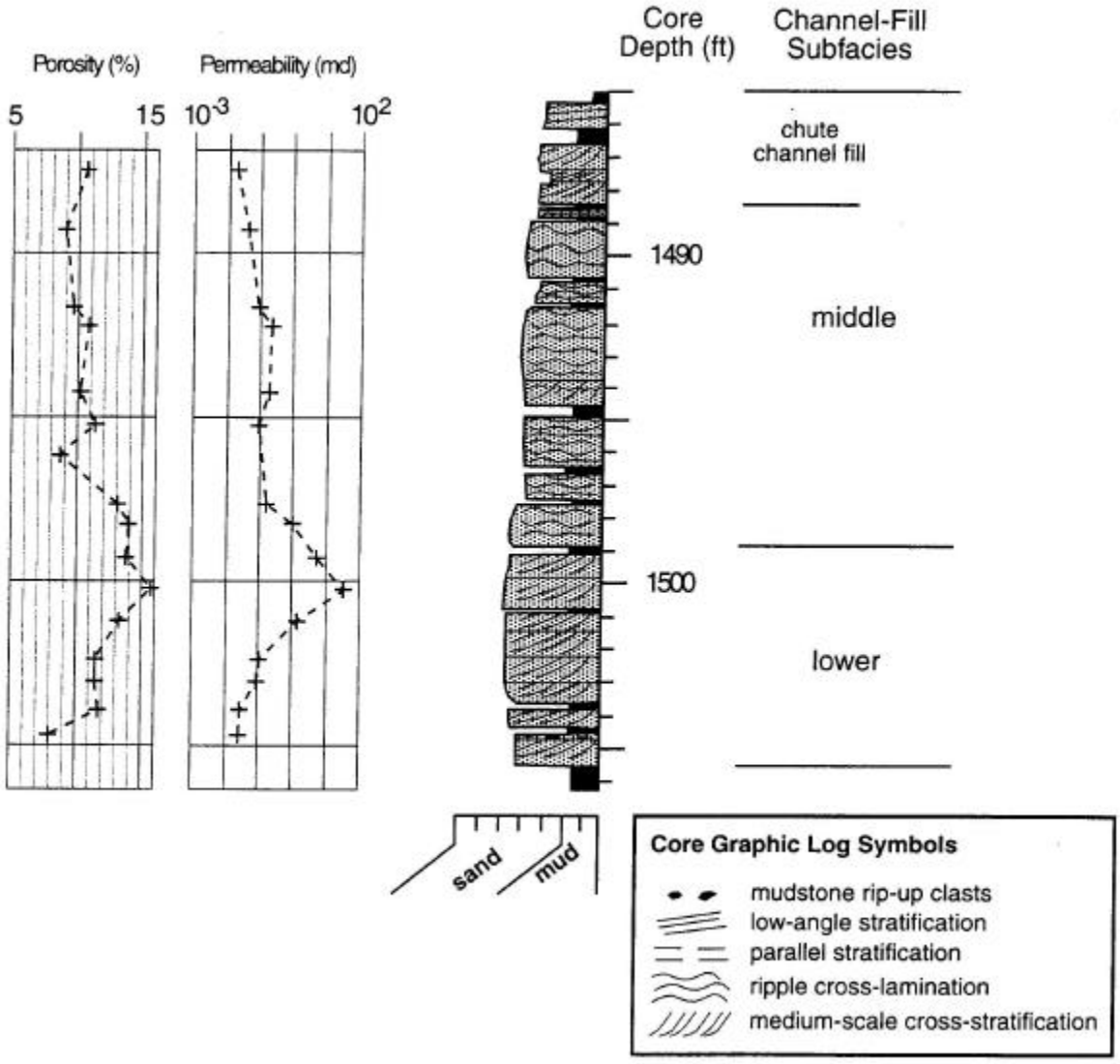

Figure 9 – Self-82 core description of DGI C meandering channel-fill facies[10]

Lower Channel-Fill Subfacies

Consists of moderately to well-sorted, medium-grained sandstone with medium-scale cross stratification. Intraclast lag deposits are common at the base, with similar clasts and mudstone drapes typically occurring along cross strata.

Middle Channel-Fill Subfacies

Deposits include moderately sorted, lower medium-grained sandstones; poorly sorted, silty fine-grained sandstones; and mudstone to silty mudstone with carbonaceous debris. Other physical structures include horizontal stratification and ripple lamination. Medium grained sandstones tend to be cleaner and better sorted. Low-angle bedding planes identified as lateral accretion surfaces show drapes of medium- to very thin-bedded mudstone and silty mudstone containing carbonaceous debris (Figure 9). Inversion in the overall fining-upward texture profile and medium-scale trough cross stratification are regarded as chute channel-fill deposits within the middle channel-fill subfacies. Chute channel-fills are not common in Glenn Pool field, but are common in outcrop exposures northeast of Glenn Pool.[7]

Upper Channel-Fill Subfacies

This subfacies consists of non-reservoir mudstone and silty claystone.

Interpretation of the above described facies and subfacies as meandering channel-fill deposits is consistent with published literature.[11-12] The basal erosional contact is regarded as the record of the channel thalweg (thread of deepest flow) eroding laterally as the channel evolves. The lower channel-fill subfacies are the deposits of crescentic dunes deposited near the thalweg but in shallower, lower current-strength parts of the channel. The middle channel-fill subfacies is the record of lateral accretion bar deposition. The presence of sand-mud couplets and abundance of mudstone interbeds strongly suggests influence by tidal fluctuations.[13] The upper channel-fill subfacies represents the abandonment phase of channel filling; it is expected to be thickest at the last location of the thalweg.

Log correlation and facies mapping in southern Glenn Pool field define north-south oriented meandering channel-fill sand bodies, in contrast to the more east-west orientation of braided channel-fill facies.[9] Meandering channel-fill sand-body geometry is characterized by a width to maximum net sand thickness ratio ranging from 30-80%. Channel-fill widths vary from a typical 1,500-ft (500 m) at lower stratigraphic levels to 200-ft (67 m) at upper stratigraphic levels. Within each channel-fill deposit localized net-sand isopach thicks are interpreted as complex lateral accretion bar deposits.

Analysis of a microresistivity borehole image log run in the Self-82 well demonstrated the utility of using these data for refining the facies architecture at a particular location (**Figure 10**). The meandering channel-fill facies is interpreted as the deposit of a complex lateral accretion bar with the major sand thickness located to the north-northeast of the Self-82. The acute azimuthal angle between the dip of lower channel-fill subfacies cross strata (azimuth average = 153^{o}) and the dip of middle channel-fill subfacies lateral accretion surfaces (azimuth average = 183^{o}) indicates the Self-82 is located on the downstream side of a lateral accretion bar.[14] In addition, the upward rotation observed in lateral accretion surface dip directions suggests that this bar developed by amplitude increase (i.e. increasing thalweg sinuosity) and included secondary nodes.[15]

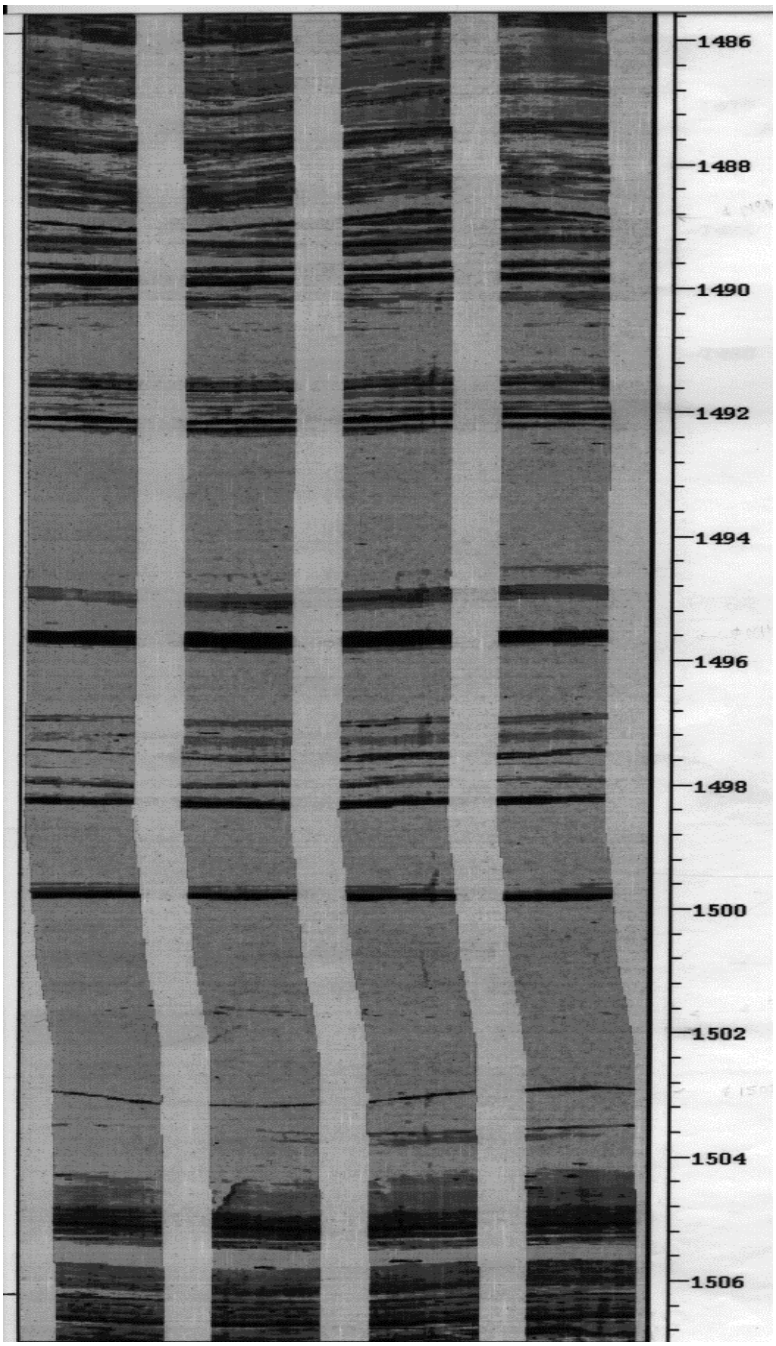

Figure 10 - Microresistivity borehole image for meandering channel-fill facies of DGI C[10]

Splay Facies

Splay facies has a characteristic coarsening-upward textural profile that results from interbedded silty mudstone and fine-grained sandstone grading upward to medium-grained sandstone (**Figure 11**).

Low-angle parallel bedding and ripple cross-lamination are the most common sedimentary structures, with medium-scale cross stratification and contorted bedding less frequently observed. Thin mudstone beds (up to several inches, centimeters) are interstratified throughout and become more numerous in the uppermost portions of the Bartlesville sandstone.

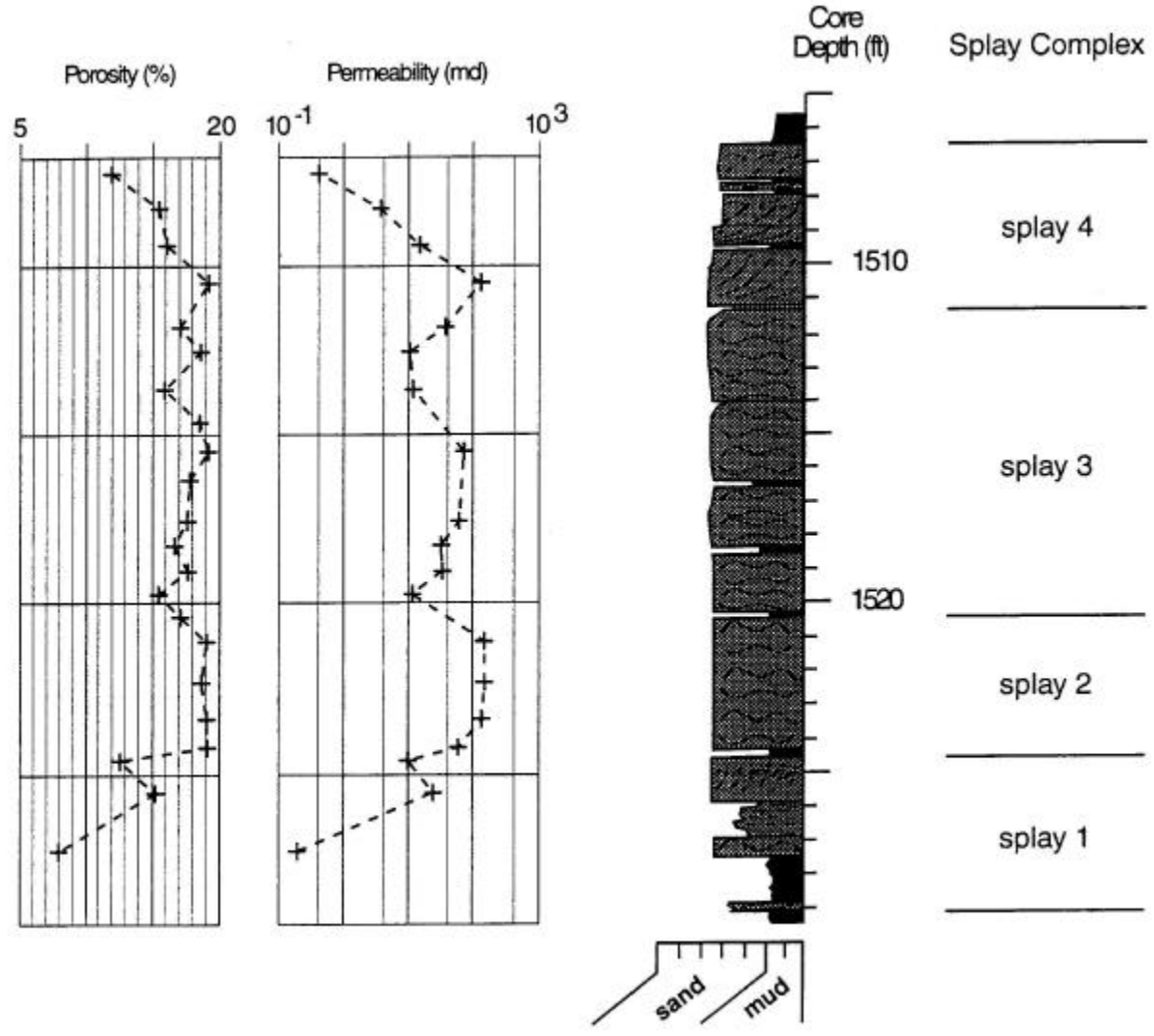

Figure 11 – Self-82 core description of DGI D splay facies[10]

Solitary occurrences of splay facies typically generate a funnel-shaped log profile (Figures 7 and 11). However, where splay complexes formed from two or more crevasse breaks, vertical stacking of

sandstone and mudstone beds, as well as grain size profiles, are more complicated and exhibit undiagnostic log responses (Figure 7).

Floodplain Mudstone Facies

Floodplain mudstone facies consist of strata ranging from siltstones with ripple cross lamination to dark gray mudstones and carbonaceous shale. High gamma ray and low resistivity well log values are characteristic. However, the log response may not reach the "mudline" where these mudstones form thin beds between thick sandstones.

To the south and northwest of Glenn Pool field, the floodplain facies contain coal deposits that are mined locally.[16-17]

Discrete Genetic Interval (Parasequence) Elements

A discrete genetic interval (DGI) is defined as a collection of genetically related contiguous facies deposited during a discrete increment of time. Kerr and Jirik[18] developed the concept of a DGI for the purposes of subsurface mapping of Tertiary fluvial deposits in the south Texas onshore gulf coast region. Thus, a DGI is an operational unit for subsurface mapping. A single DGI is correlated as having a common elevation from the top of gross channel-fill thickness to a stratigraphic datum (marker bed). After correlation through a cross section network has been completed, the facies and their thickness are plotted at each well site for each DGI. If the facies genetic relationships are logical, then the task is complete. If, however, the facies genetic relationships do not make sense, then the correlation must be reconsidered and another iteration is required. Once satisfied with the DGI correlation, facies-biased isopach mapping is performed.

A DGI can also be thought of as a lithostratigraphic unit whose boundaries have chronostratigraphic significance and whose definition in the case of the Bartlesville sandstone is equivalent to that of a parasequence[9] in sequence stratigraphic parlance.[19] Identification of DGI's for the Self-unit portion of Glenn Pool field are indicated in Figure 7. As shown, each DGI is commonly associated with a single facies type in individual wells but will exhibit lateral distribution of coexisting facies in cross sections

(**Figure 12**). The DGI is considered the major subsurface unit for mapping purposes. Within the productive, sand-rich portion of the Bartlesville sandstone, individual DGI's are separated by laterally extensive (except for localized erosional windows) floodplain mudstone horizons. Facies occurrences within a DGI share a common depth relative to the Inola limestone marker (Figures 7 and 12). In correlating Bartlesville DGI's in southern Glenn Pool field, a 5-ft (1.5-m) tolerance is required due to local variations in early compaction and syndepositional slumping off the valley margin.

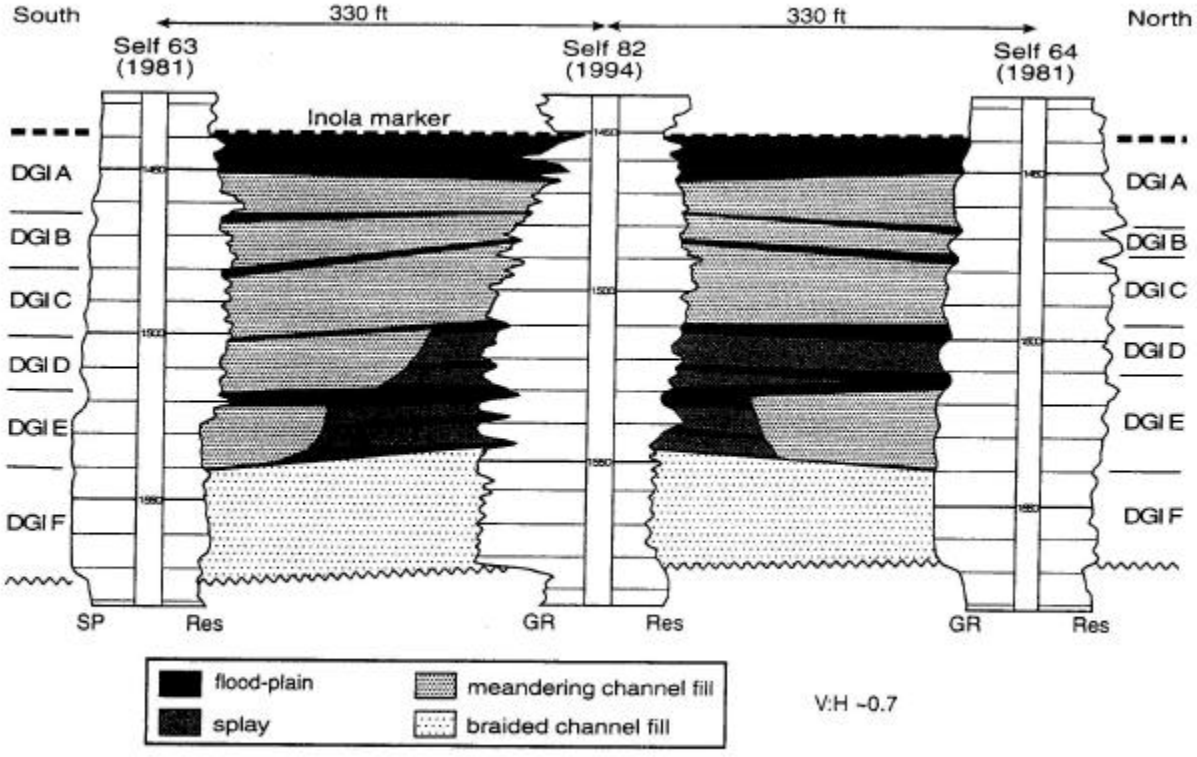

Figure 12 – Cross-section through Self-82 well showing of discrete genetic intervals and facies[10]

In the southern part of Glenn Pool field, a total of 7 DGI's are recognized, labeled A through G in descending order; however, DGI G is not present in the Self-unit (Figure 12).[9] DGI's G and F consist of braided channel-fill facies and limited occurrences of floodplain mudstone facies. DGI's A-E are made up of meandering fluvial facies (channel-fill and splay facies) (Figure 12), with an overall upward increase in the proportion of non-reservoir floodplain mudstone facies. Within the limits of the Self-unit,

DGI G is absent due to onlap pinchout to the south. South of Glenn Pool field, DGI A through E show transition to estuarine bayhead delta facies deposits.[9]

Systems Tracts and Sequence Stratigraphic Elements

The largest stratal volumes considered in study of the Bluejacket (Bartlesville) sandstone are equivalent to systems tracts and stratigraphic sequences. A stratigraphic sequence is a succession of genetically related strata bounded by unconformities and their correlative conformities.[20] A systems tract is a contemporaneous three-dimensional assemblage of facies whose designation is based on position within a stratigraphic sequence and a distinctive parasequence stacking pattern.[19-20] The original conceptualization of sequence stratigraphy has the incised valley being filled during the later stages of relative sea level lowstand.[21-22] However, if the erosional accommodation provided by incision of the former shelf is not filled during relative sea level lowstand, then the incised valley may be filled during subsequent rise in relative sea level.[23]

Based on analysis of facies distribution and DGI (parasequence) stacking patterns, the Bluejacket (outcrop) and Bartlesville (subsurface) sandstone comprises two systems tracts (see Figure 3). In Glenn Pool field, the low-stand systems tract is represented by DGI G and F, which include braided channel-fill facies sandstones in an aggradational stacking pattern. An overlying transgressive systems tract is interpreted for DGI A through E, with meandering fluvial facies dominant in the area of Glenn Pool field. The Inola marker is considered to represent a compressed section associated with the maximum flooding surface (Figure 3).

The basal contact of the Bartlesville sandstone with the underlying Savanna formation is an unconformity identified as a type-1 sequence boundary. This conclusion is based on outcrop observations and detailed subsurface correlations and conforms to the overall interpretation of the Bartlesville as representing the lower portion of a type-1 stratigraphic sequence.[9] The sub-Bartlesville unconformity shows truncation of parasequences in the Savanna formation and, as noted, is onlapped by Bartlesville parasequences (DGI's).[9]

Petrophysical Properties and Architectural Elements

The above analysis of facies architectural elements is considered of direct importance to defining, mapping, and explaining the distribution of reservoir quality and remaining oil reserves in the Bartlesville sandstone. Core analysis performed on samples from the Self-82 well demonstrated that porosity and permeability are strongly DGI-related, with both parameters showing progressive increase from DGI B downward to DGI F (**Figure 13**). Highest reservoir quality and the greatest degree of homogeneity are indicated for DGI F, with *Kv/Kh* ratios as high as 0.8-0.9 (**Figure 14**). Moderate to good reservoir quality exists in meandering channel-fill and splay facies sandstones, which display considerably greater permeability anisotropy (*Kv/Kh* of 0.3-0.5) than do braided channel-fill deposits. Figure 14 suggests that both lateral and vertical fluid flow are significantly more complex in meandering channel-fill and splay sandstones, and that large portions of these potential reserves remain unflushed by waterflooding to date.

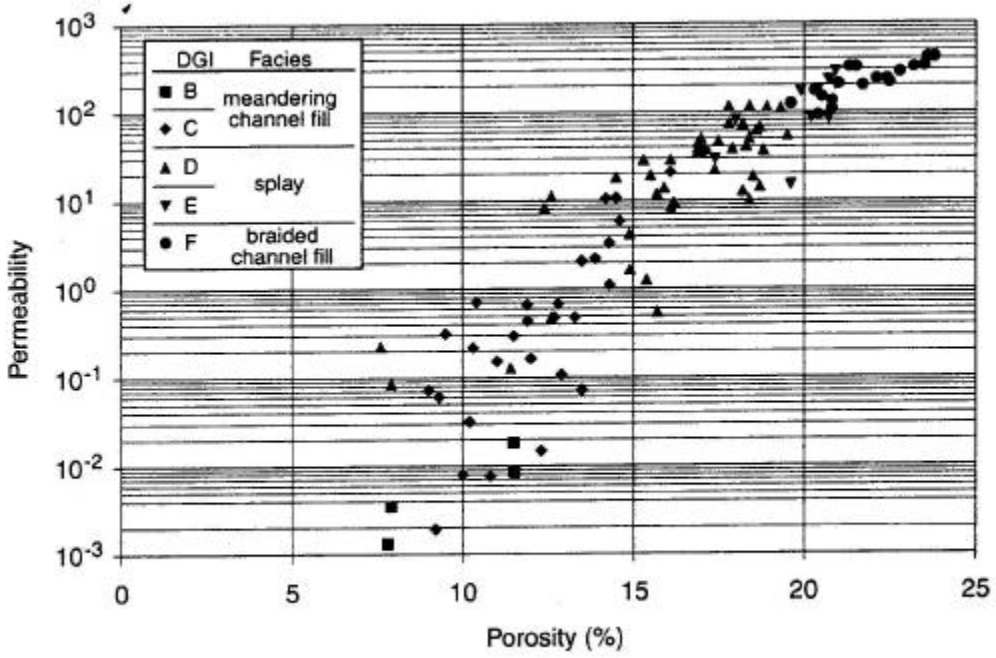

Figure 13 – Permeability vs. porosity from core plug measurements in Self-82[10]

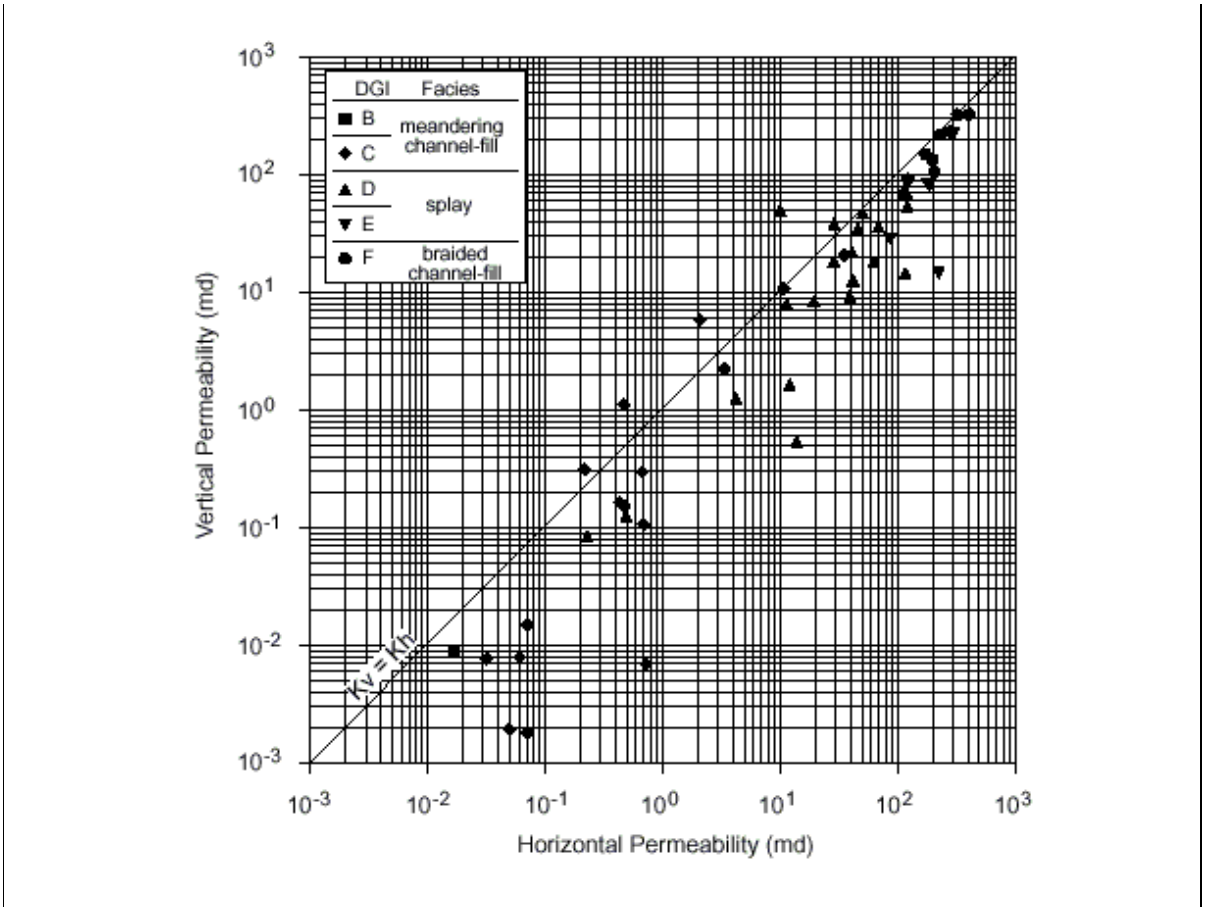

Figure 14 - Vertical permeability vs. horizontal permeability from core plug measurements in Self-82[10]

This conclusion is strongly supported by observations of oil staining in the Self-82 core (see Figure 7). Such observations showed that DGI C, the lower channel-fill subfacies, was water bearing (i.e., appeared to be flushed), whereas actively bleeding oil was seen in middle channel-fill sandstones between mudstone drapes on lateral accretion surfaces. For DGI D, in which individual splay sandstone layers are separated by mudstones, oil was observed bleeding from all except one of the sandstones, assumed to be flushed (see Figure 7).

The combined quantitative and qualitative data on the Self-unit indicate that the largest amount of remaining oil reserves, after nine decades of development, are concentrated in middle channel-fill subfacies and splay facies of DGI A through E (transgressive systems tract).

Structure Southeast Side of Glenn Pool Field

Preparation for drilling the Self-82 well included picking the expected depths to the top of the Inola limestone and Glenn sandstone for establishing a coring point. Offset wells were about 600-ft apart from the Self-82 staked location. The coring point was picked at 1420-ft drill depth; the point was estimated independently by two geologists whose estimations were very similar. After coring and logging of the Self-82, it was realized that the estimated and actual depths were 30-ft off. This discrepancy was most puzzling given the close distance to offset wells. Consideration to the possibility of additional structural relief within the broad Glenn Pool field closure was discussed, but not given a high priority within the project work schedule.

A study area was selected along the southeastern margin of Glenn Pool field (sections 27, 28, 33 and 34 of T17N R12E) for the investigation of this question of localized structural relief. The working hypothesis was that such structures are large-scale slumps located along the incised valley margin. The study area is located closer to the margin than the Self-unit. Logs from 21 wells were available for this effort. Well spacing ranges from 2,600-ft to less than 300-ft apart. Structure cross sections were compiled through the well array.

The stratigraphic interval of interest spanned the Pink limestone to the Brown limestone. Top of the Pink is about 260-ft above the Glenn sandstone. Top of the Brown is about 120-ft below the top of the Glenn sandstone. The interval thickness between the top Brown and base of Glenn is highly irregular as a result of erosional relief along the base of the Glenn. Structure maps were produced for top Pink, top Inola, and top Brown.

The top Inola structure map provides evidence of localized structures similar to what would be expected for slumping. The relief within the study area measured from well log tops is 50-ft over about 1 mile. Locally, however, the relief is as high as 30-ft vertically in 400-ft laterally; relief comparable to that developed around the Self-82 well. From careful correlation, it is clear that stratigraphic section if faulted out of wells where the structural relief is high. The faults appear to be listric normal in geometry, with associated antithetic faults and rollover anticlines. The normal faults trend northeast southwest

(parallel to the local orientation of the incised valley margin) with open curvature to the northwest and down to the northwest separation. Laterally discontinuous antithetic faults mirror the normal faults. Structural separation is 30-ft across the listric faults with localized antithectic faults; is 15-ft across listric faults without antithetic faults; and is 10-ft across antithetic faults. Separation up through the Pink limestone is only locally developed.

The implication for reservoir compartments depends on the stratigraphic level within the Glenn sandstone. Faulting of the braided fluvial section probably has little effect in that fault gouge of this sand-rich interval is not likely to be a barrier to fluid flow. On the other hand, faulting of the meandering fluvial section could produce reservoir compartments in that fault gouge of this mud-rich interval that will likely produce reservoir barriers/baffles. Thus, DGI A through E reservoir compartments could be developed locally in these listric faulted areas.

Geophysical Analysis

As part of applying new technology, we evaluated the effectiveness of cross borehole tomography in improving the reservoir description. In this section we detail our efforts and provide some results.

Introduction

Seismic crosswell tomography is a method of determining seismic velocity (wave speed) between boreholes. The tomographic image has a resolution of 10 to 25-ft and can supply otherwise unavailable information on geological and reservoir characterization parameters.

Seismic tomography is similar in principle to medical tomographic methods, but several factors conspire to make seismic tomography more difficult than the medical case. This is illustrated in the comparison below.[24]

Medical X-Ray Tomography

- Imaged object can be completely surrounded by sources and receivers (full aperture).
- Image rays travel at constant velocity (speed of light) and are straight.

- Uniform ray coverage.
- Resolution dictated by x-ray wavelength on the order of Angstroms.

Seismic Tomography

- Imaged object cannot be completely surrounded by sources and receivers (limited aperture).
- Image rays travel at variable velocity (sound speed in rocks) and are bent.
- Irregular ray coverage due to ray bending and limited recording aperture.
- Resolution dictated by seismic wavelength on the order of 25-ft.

These differences mean that medical tomography technology has not been of direct use in the seismic case. Rather, it has been necessary to develop methods of acquisition, processing and interpretation that directly account for the nature of seismic tomography measurements. This new technology has, until recently, only been available in research labs of major oil companies. We feel that seismic tomography an important tool for reservoir analysis. The information to be gained from seismic tomography includes details of geological variations within the reservoir and estimates of parameters of interest to petroleum engineering.

In this project we acquired seismic tomography across a five-spot well pattern in order to visualize and understand important parameters controlling reservoir quality. The acquisition and initial processing of this data was performed by Amoco Production Company under the direction of Larry Lines and Henry Tan of the Tulsa Research Center. The survey planning and interpretation was integrated with petroleum engineering and geological data.

Four separate tomography data sets were acquired inside the Self-unit of the Glenn Pool field. The geometry included a centrally located source well, S, and four receiver wells, R. Each tomography survey results in an image plane between the source well and the receiver well active for that survey. By shooting in four substantially perpendicular directions, we planned to maximize the probability of observing geologic trends in the data (e.g., channels, depositional fabric, etc.).

The source well is referred to as Self-82. This was drilled as part of this research project. The advantages of using a new well for the source, as opposed to an existing well, are:

1) Hole will be clean, uncased and untreated.
2) Hole will be logged, including sonic.
3) TD approximately 500-ft below reservoir level.
4) Hole will be cored through the reservoir.
5) Hole will have micro-imaging log through the reservoir.

Items 1 through 3 are of direct importance to the tomography, while 4 and 5 are critical to integrating tomography results with reservoir parameters. In addition to the logs mentioned here, a deviation survey was performed in the source and receiver wells.

The tomography acquisition was done with equipment and personnel provided by Amoco Production Company, under the direction of Dr. Larry Lines and Dr. Henry Tan. This team had extensive experience in the acquisition of tomography data[25-29] including several surveys in Oklahoma.[30-31]

The four tomography surveys were not be acquired in one continuous effort. Aside from questions of field crew efficiency in a lengthy shooting program (see below), there was a need to review data from the first survey for data quality and processed image fidelity. This review pointed out the need for modifications to the acquisition parameters.

The field equipment needed for tomography acquisition is two wireline trucks, a down-hole source and a string of down-hole receivers.

There were many tomography sources in use or being developed[32-33] at the time of this project. This study used a Piezoelectric transducer source.[28, 34] Physically, the source is a steel-encased ceramic piezobender with 4 3/4 inch outside diameter (OD), and requires a fluid-filled borehole of inside diameter (ID) not less than 5 inches. It can generate a useful signal up to 2000 Hertz (cycles per second) and actual tests in Oklahoma rocks similar to those at Glenn Pool have shown 1500 Hz signal received across distances of 400 to 500-ft.

The basic receiver for this study is a string of hydrophones connected through wireline cable to a truck-mounted recording system. The use of hydrophones requires the receiver hole, like the source well, to be fluid filled. An important efficiency factor is the number of receivers that can be operated down-hole at one time, termed a receiver group. Current technology (as of the project date) limited this number to about 6 receivers per group. The receivers, wireline cable and recording instruments deliver a time sampling rate of 50 microseconds, with 8000 samples per trace and 24 bits/sample. This general kind of source/receiver tomography acquisition set-up has seen extensive field use.[26, 28, 35]

Data Processing

Once the data is collected it must be processed to create an image of the subsurface between the source well and receiver well. This involves picking first arrival times for each source and receiver then inverting a large, sparse system of algebraic equations. The result is a velocity tomogram which estimates the seismic velocity on a regular grid in the vertical plane between the source and receiver wells. The method is capable of determining interwell velocity variations of 5%, or better.

The plan was to process the data in two fundamentally different ways. First, the data would be processed by Amoco using the system they had developed over the course of several years.[36-37] We considered this to be state-of-the-art processing technology. Second, we planed to process the data at The University of Tulsa using public domain software. We used a seismic tomography processing program written by the U. S. Bureau of Mines called BOMTOM (Bureau Of Mines TOMography).

Since BOMTOM is free and could be run on a standard PC, it is typical of the processing capability that any small operator could possess. By processing the data in two ways we could compare the processing capability available to small operators (e.g., BOMTOM) with the state-of-the-art solution (Amoco processing). This gave some indication whether tools available to the small operator are adequate for reservoir characterization studies using seismic tomography.

Interpretation and Integration

Once the seismic tomography data has been acquired and processed it must be interpreted. It is at this stage, more than any other, that the integration of geophysics, geology and petroleum engineering is required. The raw product of tomography processing is a velocity tomogram showing variations in seismic wave speeds between the source and receiver boreholes. This must be correlated with all available information, including well logs, cores, geological parameters (lithology, porosity, stratigraphy, etc.) and petroleum engineering parameters (oil saturation, fluid contacts, etc.). Our project generated one image between the source well and each of four receiver wells. We planed to interpret this data and gain information on several characteristics of the reservoir. First, structure and lithostratigraphy,[28, 38-40] second, reservoir inhomogeneities,[38] third, acoustic continuity[30, 41] which is a tool for determining whether beds that appear to be the same unit in two wells are physically continuous; and fourth, correlation of stratigraphic units between tomography surveys to determine their orientation in three-dimensional space.

Any interpretation goal depends on data quality, but these require only average data quality. In addition, if the data quality were excellent it might also be possible to infer porosity[31] and/or oil saturation.[38, 42]

Crosswell Seismic Test

The primary goal before acquisition was to test operational procedures and data acquisition parameters in advance of the full crosswell test scheduled in late 1993 or early 1994.

The test was conducted on 24-25 August between wells 62 and 72 of the Self-unit. The well locations are shown in **Figure 15**. The acquisition team consisted of equipment and personnel from Amoco Production Company's Tulsa Research Center (H. Tan, L. Colethorp and J. Beck). Also represented were The University of Tulsa (C. Liner, M. Kelkar, D. Kerr, and graduate students), Uplands Resources, Inc. (D. Richmond, J. Helm), and the Department of Energy (R. Lindsey).

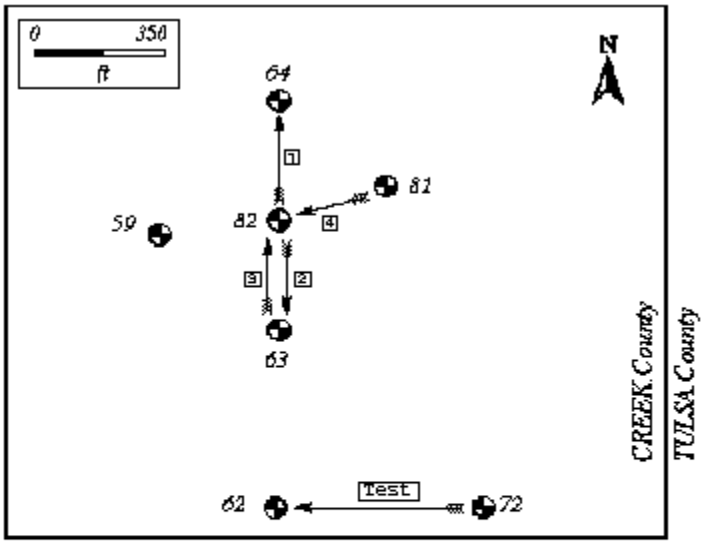

Well Pair	Distance (ft)
72-62	660
82-64	341
82-63	324
81-82	361
82-59	347

Data	Survey	Date
	Test	24 August 93
14736	1	27 January 94
17759	2	28 January 94
16696	3	29 January 94
travel times	4	30 January 94

Figure 15 – Map and shooting schedule for crosswell seismic data acquisition

These particular wells were chosen because they were widely spaced (about 660-ft) and intermittently shut down. Well 62 served as the receiver well and 72 as the source well. The seismic source, **Figure 16**, is an annular piezoelectric transducer, which produces a swept signal. For day 1 shooting the signal sweep contained frequencies from 200-2000 Hz. Other acquisition parameters are listed in **Table 2**. The recorded data traces were cross-correlated with the pilot sweep to create impulse-like correlated data traces. The correlation process allows more energy to be input over a time window (0.25 seconds) than could be injected by an impulsive source. An impulsive source of similar strength would be damaging to downhole equipment and the borehole. The test operation involved two wireline trucks, one each for source and receiver well, and a control truck. Each shot generated 6 channels of time-dependent data: one channel for each of the 3 receivers, one channel for the pilot signal, and two dead channels.

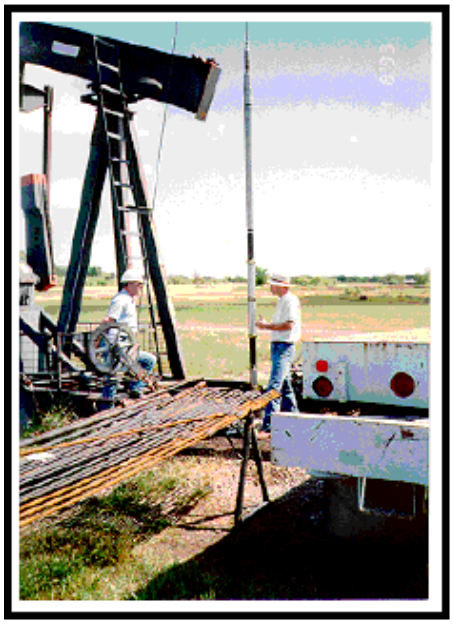

- Piezoelectric Transducer
- Sweep Signal
- 200-2000 Hz
- 0.25 s Sweep Time
- 4 ft Source Interval

Figure 16 – Photo of source and some characteristics

Table 2 – Properties of tomography software used in this project

Group	Rays	Anisotropy	Access
Utulsa	Curved	Yes	In development
Amoco	Curved	Yes	Proprietary
MUN	Curved	Approximate	Consortium
BOMTOM	Straight	No	Public

The receiver apparatus, **Figure 17**, consisted of three hydrophones on wireline spaced 8-ft apart. The hydrophones return electrical signals in response to the passage of acoustic, or sound, waves. The receivers are suspended freely in the borehole while the source is continuously moved in the receiver well. Both source and receiver wells must be fluid-filled for the crosswell system to operate.

- Hydrophones
- Fluid-filled Borehole
- Array of 15
- 8 ft Spacing

Figure 17 – Photo of receiver and some characteristics

Four common receiver fans were shot on day 1, as shown in **Figure 18**. Also shown are the fan numbering system, extent of fans, lithology in source and receiver wells, well separation, and starting/ending depth associated with each fan. Some formation depths are also indicated. The lithology and formation depth information was supplied by the geological team based on well-log interpretation. The deepest sand unit in each well is the Glenn sand, which is the productive interval in the field. From the acquisition geometry we did not expect to determine velocity in the Glenn sand itself during this limited test. The fans were acquired in the order 1, 2, 3, 4.

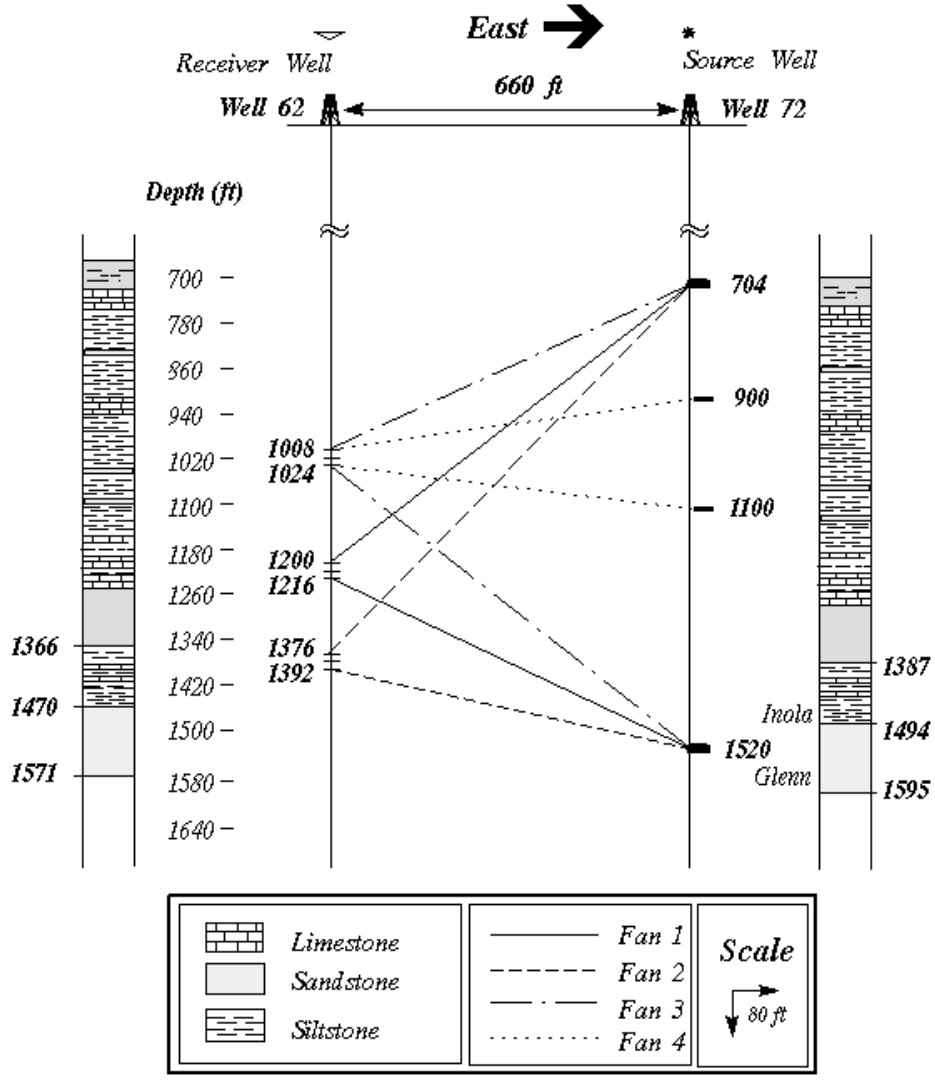

Figure 18 – Details of shooting geometry for the test survey

Fans 1-3 had source spacing of 16-ft, which allowed rapid traverse of the entire section of interest. This source spacing is very large, even for a typical tomographic survey. It was used for testing purposes only, and the total interval covered by sources in Fans 1-3 was approximately 700 to 1,500-ft. High-resolution reflection surveys require smaller source intervals. To test the feasibility of reflection work at Glenn Pool, Fan 4 was shot with source spacing of 4-ft. This was accomplished by moving the source up one-half of the fixed receiver interval of 8-ft.

Vertical stacking is a method of improving data quality and suppressing random noise. The idea is to make repeat measurements without moving source or receiver and summing the repeat results to create a final trace. The signal-to-noise improvement achieved by this process in SQRT[N] where N is the number of vertical stacks. Only random noise is suppressed by this technique. Source generated noise (such as tube wave energy) is not suppressed.

All fans from day 1 used an 8-fold vertical stack. As the source is continuously moved uphole, the source is activated 8 times in a 2-ft zone centered on the stacked source location. The resulting traces are summed to form the stack trace at this level. The vertical stacking process is valid if the stacking interval is much less than a seismic wavelength. We estimate the P-wave wavelength in the data to be approximately 12 to 13-ft, and the S-wave wavelength approximately 6-ft. Therefore, the 2-ft vertical stacking interval is valid.

Data acquired on day 1 showed good data quality and signal transmission. First arrivals (which are the basis of tomographic processing) were well defined, and significant events beyond first arrival energy are also present. These are some combination of direct shear waves, reflected P & S waves, and tube waves. The 16-ft source spacing on Fans 1-3 give the direct arrivals large time delays as source/receiver separation increases. Four 4-ft source spacing on Fan 4 resulted in observation of reflection energy beyond the first arrival. These reflections are important as a source of high-resolution information about the rock configuration.

Detailed examination of Fan 1 showed first arrivals with good continuity and amplitudes significantly above background noise levels. When first break amplitudes fall below background level first breaks cannot be picked for use in tomography. This gives a constraint on the maximum operating range of the crosswell acquisition system. This operating range varies with geographic location and reservoir depth.

Direct arrivals weaken with angular source/receiver separation. Calculations based on data from Fans 1-3 indicate the maximum transmission distance for direct arrivals at the Glenn Pool site is about 735-ft. In the full crosswell test we expected well separation of 450-ft, so the 735-ft maximum range corresponds to a maximum source/receiver angle of 52š. This is well in excess of the design criteria of

45š. Therefore, we expected good direct arrival energy at maximum acquisition angles in the full crosswell test.

A major attraction of crosswell seismic data, relative to surface data, is its higher frequency content. Spectrum analysis of the test data indicated significant frequency content from 300-1300 Hz. No surface seismic data exists at Glenn Pool, but typical surface seismic frequencies are 20-80 Hz. Thus, crosswell seismic data gives a 10 to 20-fold increase in resolution relative to surface seismic data.

The second day of the crosswell test followed up ideas and concerns identified on day 1. Four additional fans were acquired. Fans 5 and 6 have source level spacing of 16-ft. These were designed to test maximum signal range by shooting with large vertical source/receiver separation. The longest source/receiver separation occurs in Fan 6, where the signal clearly faded into background noise levels. At this range no useful source-generated energy is present. This test fan reinforced the maximum range calculations derived from day 1 data.

All of the day 2 data was shot with a source bandwidth of 400-2000 Hz. This change from 200-2000 Hz on day 1 was in response to low frequency tube wave noise (about 200 Hz) interpreted on the day 1 data. The 400 Hz low-cut had a nominal effect on the data quality.

Fans 7 and 8 are reflection-quality common receiver fans with 4-ft source spacing. These are near in depth to the reservoir level and may contain reflections from the reservoir itself. These two fans were shot with the first source in each fan vertically offset by 2-ft. That is, the source levels in Fan 7 are at depth levels 1488, 1484, Š, 1276, while Fan 8 has source levels 1490, 1486, Š, 1278. This acquisition geometry allows the data traces to be interleaved to an effective spacing of 2-ft. Strong tube wave energy was seen to interfere with reflection events. Some advantage was gained by the 2-ft spacing, but no further interpretation was attempted.

Also on day 2, a vertical stack test was performed as part of Fan 5. The source interval 800-928 (fixed receiver location) was shot once with 8-fold vertical stack and again with 32-fold vertical stack. The 32-fold data (lower plot) stands out slightly better from background noise level. The 32-fold data

shows some improvement in signal strength in the 1500-2000 Hz range. Overall the effect is a minor improvement in data quality.

Crosswell tomography involves picking first arrival times on crosswell seismic data and inverting for a velocity distribution between the wells. The quality and reliability of the tomogram depends on highly redundant data. If a great number of travel times are available then the velocity field is well-constrained. With fewer travel times the solution is highly non-unique. The crosswell data acquired on days 1 and 2 was insufficient for full tomographic reconstruction. However, using all day 1 data we were able to estimate velocities, which should be viewed with caution due to insufficient data for full inversion. The average velocity in well-illuminated zones was about 12,000-ft/sec. This is in very good agreement with sonic log velocities from the Self-82, which was drilled in December 1994. The average sonic velocity at a depth of 1,000-ft in the Self-82 is 11,800-ft/sec.

The location of Self-82 was decided in a series of team meetings during third and fourth quarters of 1993. From a geophysical point of view, this location was acceptable because the four surrounding wells were close (about 330-ft) and formed perpendicular seismic image planes. This configuration seemed optimum for delineating reservoir features of interests.

After the Self-82 well was drilled, well preparation began on the 59, 63, 81 and 64 wells. These wells served as receiver wells in the full crosswell survey. It was discovered at this time that the receiver wells were either plugged back or sand-filled to near the top of the Glenn sand.

An important parameter in tomographic acquisition is aperture. This is a measure of how well the acquisition geometry "surrounds" the object of interest. If the object is surrounded then the aperture is good and a well-constrained image can be produced. If the aperture is incomplete, the object is not surrounded and an incomplete image results. The nature of crosswell acquisition is such that it is never possible to acquire full aperture data, but it is important to get the best aperture possible. By having the receiver wells only open through the uppermost Glenn sand, the survey aperture was seriously compromised. It was decided to re-enter these wells for cleaning and/or reaming to the base of the

Glenn. As cleaning these wells was an unanticipated cost, the geophysical team was requested to prioritize the receiver wells in order of importance.

A meeting with geological team members was held on 17 January 1994, and priorities were established. These priorities are given here, together with related comments.

1. 82 → 81
   - Edge of DGI "B" sand (subtle)
   - Thickening of DGI "C" (15 feet)
   - Thinning of DGI "A" (10 feet)
   - Best image plane perpendicular to channel

2. 82 → 63
   - Point-bar to point-bar cross section
   - Erosional edge of DGI "B"
   - Thinning of DGI "A" (10 feet)

3. 82 → 64
   - Thickening of DGI "C" (10-15 feet)
   - Edge of DGI "B"
   - Thinning of DGI "A" (10 feet)

4. 82 → 59
   - Small well casing (4.5" OD; 3.875" ID)
   - Unlikely it can be cleaned well enough to admit seismic receivers
   - Suggest no cleaning of well 59, but run receivers from PBTD.

Tomograms and Interpretation

By late 1994 there were tomography results available from The University of Tulsa (G. Bozkurt), Amoco (A. Vassiliou), Memorial University of Newfoundland (L. Lines), and BOMTOM (G. Bozkurt). Table 2 lists the tomography software characteristics used in this study.

It was quickly apparent that the data presented a difficult geophysical problem because of strong P-wave anisotropy present in shaly rocks above the Glenn sand. This was first recognized by A. Vassiliou of Amoco, and independently discovered by L. Lines of Memorial University. The following discussion is based on ideas originated by A. Vassiliou.

P-wave anisotropy means that the velocity of P-waves depend on direction of propagation. It is customary to refer to speed of horizontally traveling P-waves as *Vh* (horizontal velocity) and vertically traveling ones as *Vv*. If $Vh > Vv$ then the rocks are said to be weakly anisotropic, while $Vh >> Vv$ indicates strong anisotropy. In the Glenn sand itself, we observe negligible anisotropy. However, the presence of strong anisotropy above the Glenn must be accounted for if accurate tomography results are to be obtained. Furthermore, the level of anisotropy observed at Glenn Pool is such that surface reflection data (such as 3-D seismic) may require special processing. For independent operators in the area, this fact could be very important.

Velocity anisotropy is usually indirectly indicated. This can be through core plug measurements at frequencies 100 times (or more) greater than surface seismic frequencies, or tomographic results that are highly processed products or even non-hyperbolic normal move out curves on surface seismic data. At Glenn Pool we have rare direct evidence of strong P-wave anisotropy.

The first piece of evidence is the sonic log on the interval 1200 - 1600. Sonic logs measure velocity by refracting a high-frequency P-wave pulse vertically along wall of the borehole. Thus, sonic measurements indicate *Vv*. For example at the 1,250-ft level in Self-82 the sonic reading is 90 microsecs/ft, corresponding to a *Vv* of 11,110-ft/sec.

From the crosswell data, we can extract traces that have source and receiver at the same level (depth). The pertinent wells at Glenn Pool were surface surveyed to determine relative wellhead location, and a deviation survey was run on each to track subsurface (x, y, z) coordinates of each well bore. From this information, it is possible to construct a constant-level gather for each survey. Since the source and receiver for each trace are at the same depth, the direction of energy travel is horizontal and therefore indicates *Vh*. The crosswell horizontal distance and travel time can be combined to provide a *Vh*

Pseudo-Sonic reading in microsecs/ft. For example, at the 1,250-ft level in the 82->64 survey, the first arrival energy indicates a *Vh Ps*-Sonic value of about 71.5 microsecs/ft, corresponding to a *Vv* of 13,990-ft/sec. This value is consistent in all three crosswell surveys.

To summarize, the sonic log in Self-82 gives *Vv*=11,110-ft/s at 1,250-ft while the crosswell data shows that *Vh*=13,990-ft/s at the same depth. This represents direct evidence for a *Vh* about 26% greater than *Vv* in the rocks at this level. Generally, P-wave anisotropy greater than 10% is considered strong, which makes the level of anisotropy seen at Glenn Pool quite remarkable.

As it relates to the tomography results, the first clear evidence of anisotropy was a characteristic X feature seen in the BOMTOM result. This processing was done at The University of Tulsa using picks from A. Vissiliou of Amoco. This X feature is typical of constant velocity tomography results in an area where anisotropy is present. As seen in **Figure 19**, this feature is present in the constant velocity tomogram (BOMTOM), but not the MUN tomogram, which honors anisotropy and curved rays.

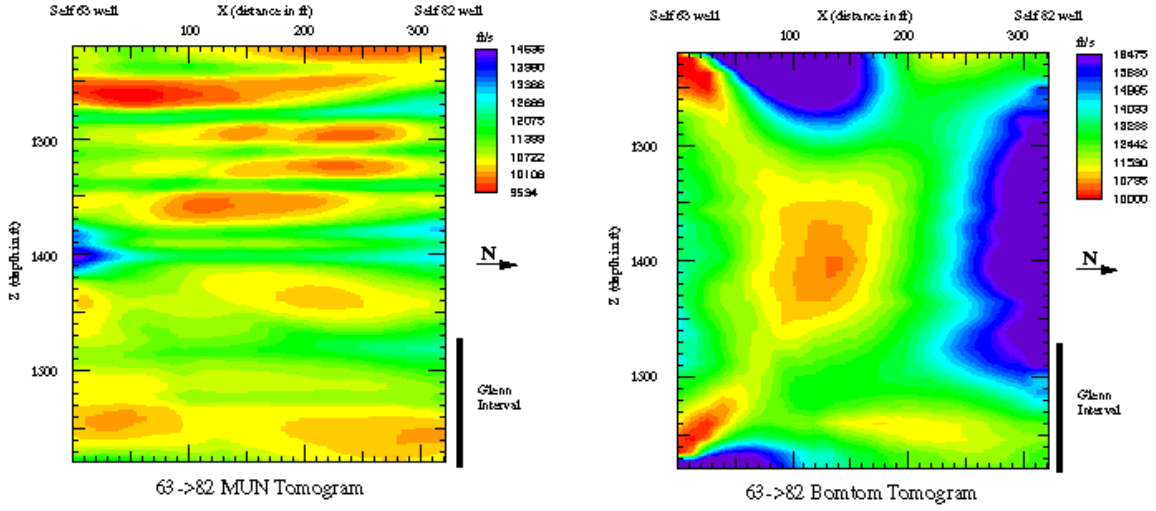

Figure 19 – Comparison of 63-82 tomograms processed by Memorial Univerity and software from the U.S. Bureau of Mines

The Memorial University tomograms were discussed at length at a meeting in Tulsa between Dr. Lines and TU team members on June 29, 1994. This tomogram was significantly different from the Amoco result, particularly the level of detail in lateral variations of velocity. The original of this tomogram was

forwarded to TU for final display and interpretation. **Figure 20** is a side-by-side comparison of the MUN and Amoco results. Finally, The University of Tulsa result is compared with MUN in **Figure 21**.

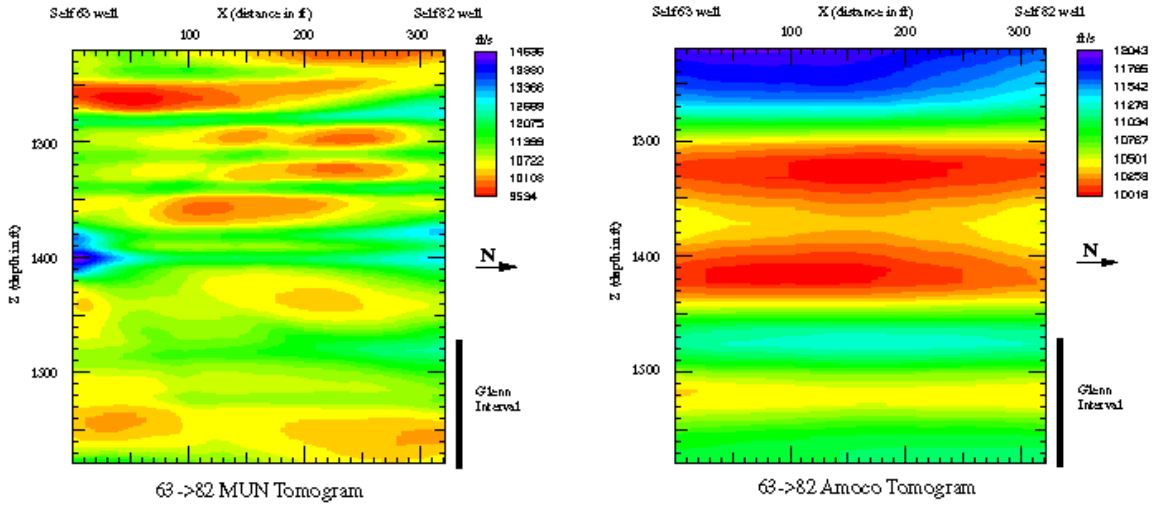

Figure 20 – Comparison of MUN and Amoco tomograms

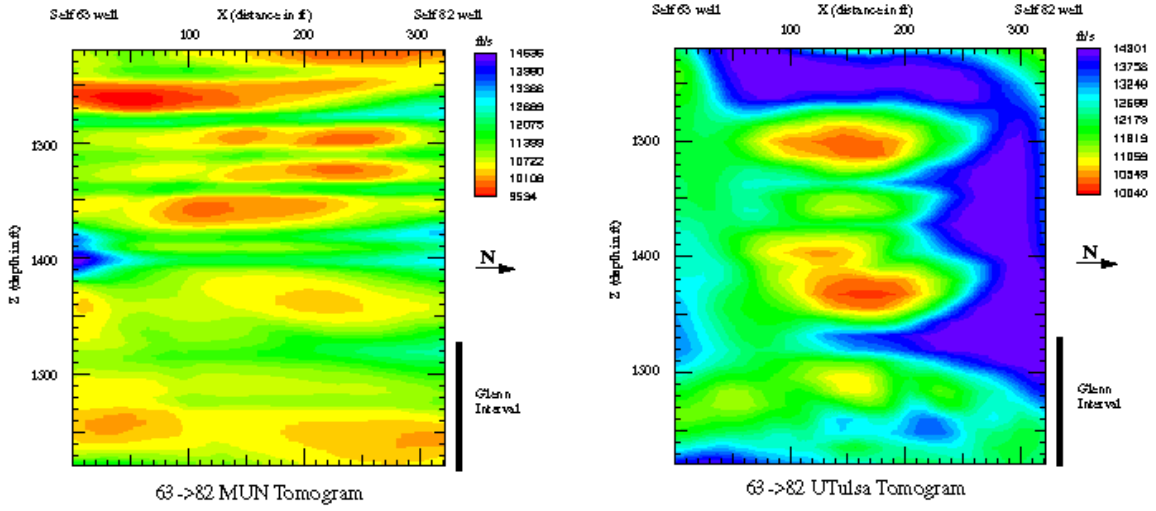

Figure 21 – Comparison of MUN and The University of Tulsa tomograms

Based on discussions with the geological and engineering teams, it was decided that the MUN result best represented the subsurface as tested by well control. Detailed interpretation of the MUN tomogram was undertaken. **Figure 22** shows the full tomogram and a zoom of the Glenn interval showing an interpreted sand body. Properties of the imaged sand body are listed, including width,

height, etc. This is a level of detail that is unavailable from surface seismic measurements, and illustrates the added value of crosswell studies.

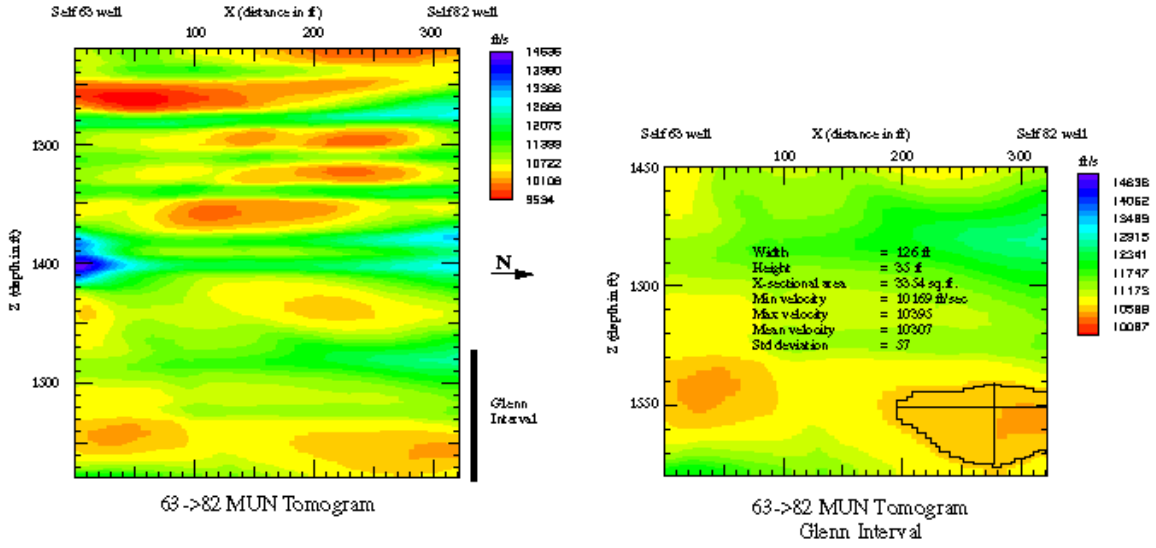

Figure 22 – MUN tomogram and zoom of Glenn interval with interpreted sand body

Using well log data, the geological team had developed a sequence stratigraphic interpretation of the rocks encountered in the 63 and 82 wells. In **Figure 23**, these interpretations are brought into the tomogram. Finally, the interpreted tomogram is shown along side a line drawing of the sequence stratigraphic interpretation in **Figure 24**.

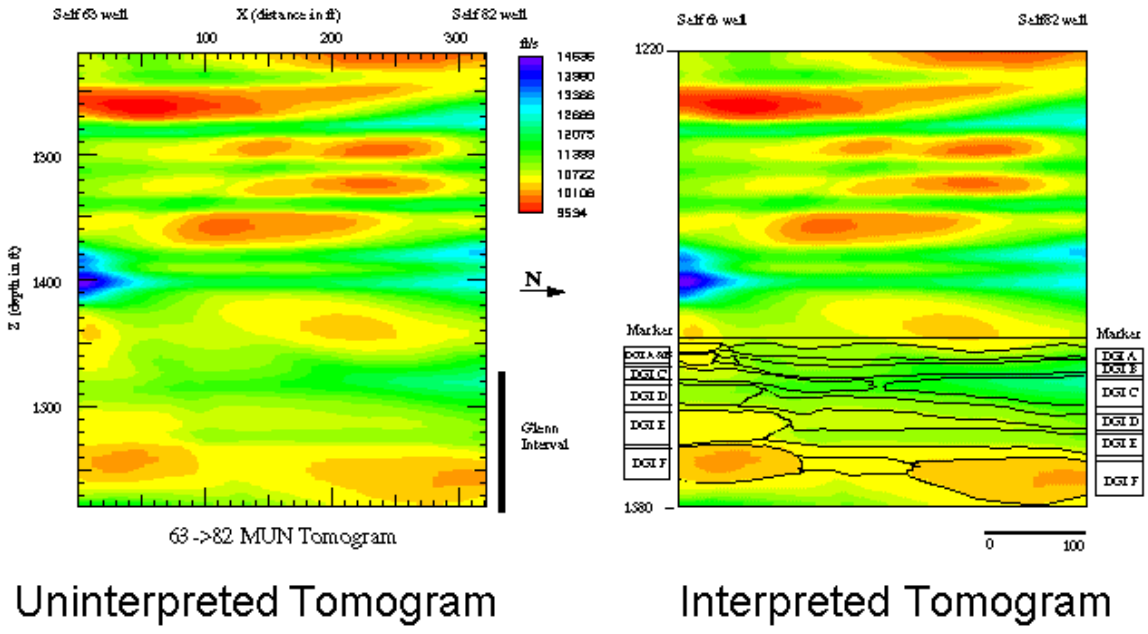

Figure 23 – Detailed stratigraphic interpretation

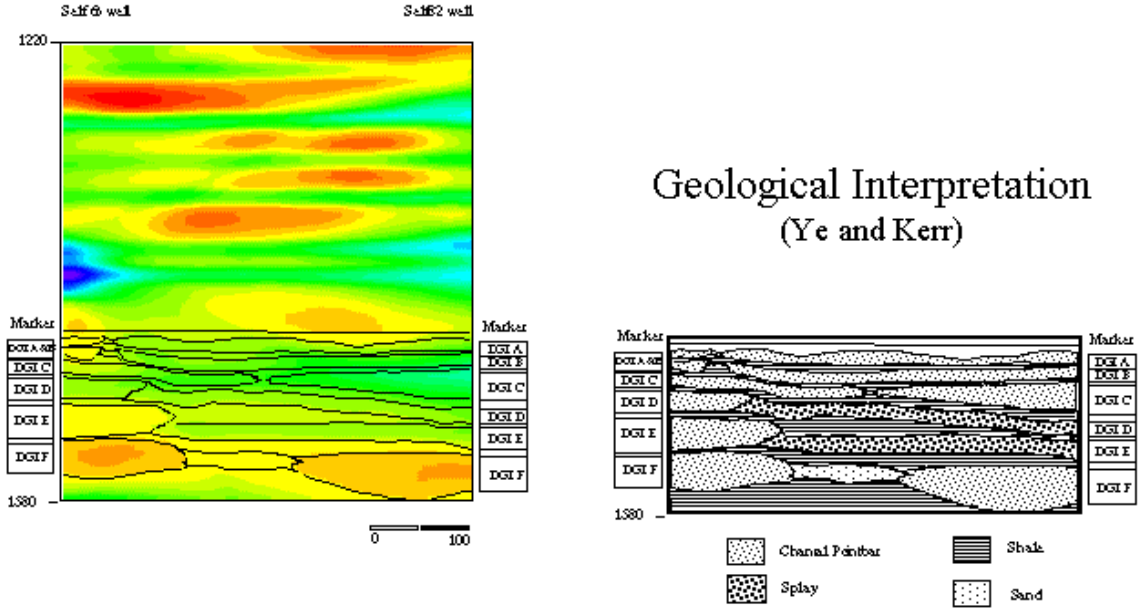

Figure 24 – The tomogram interpretation (left) compared to the geological model (right)

Anisotropic Ray Tracing

As noted above, the Glenn Pool site is characterized by strong seismic anisotropy. This means that seismic wave speed in a vertical plane depend on the direction of travel, which leads to complications with processing crosswell seismic data. If it is not properly taken into account, the resulting tomograms exhibit artifacts, which have no geological meaning. Software has been developed at The University of Tulsa to deal with this problem. The software is an extension of earlier work by Epili and McMechan[43] and is the subject of G. Bozkurt's Ph.D. dissertation.[44]

3-D Seismic

In addition to cross borehole tomography survey, a 3-dimensional surface seismic survey was acquired on the western edge of the Glenn Pool field. This did not include the Self-unit. This survey was organized by C. Liner of The University of Tulsa on the basis of in-kind contributions by Uplands Resources, The University of Tulsa, Mercury International Technology, and Nemeha Resources. Unrelated to the DOE research project involving Uplands Resources and The University of Tulsa, this seismic survey was acquired, processed, and interpreted through in-kind contributions and without use of DOE funds. The market value of the survey is approximately $50,000. The total area of the survey is approximately 2 square miles.

The objective was to acquire (Nemeha), process (MIT), and interpret (TU) a 3-D seismic survey over an area of known Wilcox (Devonian) production.

Specific interpretation objectives included:

- Analysis of the Glenn sand interval for evidence of channels and/or reservoir quality indicators.
- Structural interpretation of the Wilcox formation.
- Structural interpretation of the Arbuckle formation.

With the growing trend toward 3-D seismic use in all phases of exploration and production, we feel this project served as an example and a stimulus to 3-D work in the shallow oil province of northeastern Oklahoma. The data may be released in whole or in part at the discretion of each partner individually.

This is an important project that benefited all parties involved, and enhanced the existing DOE Glenn Pool project.

Geostatistical Modeling

Once the geological and geophysical data are gathered, the next step was to integrate this information. We generated petrophysical properties description such that the description is consistent with underlying geology. The geophysical cross sections generated by cross borehole tomography were used to improve the spatial modeling of different attributes. In this section we describe the approach used to integrate geological and petrophysical properties information. For additional details, please refer to Bahar.[45] The technique is based on the combination of simultaneous sequential Gaussian simulations and conditional distribution technique.

Multiple-Attributes Simulation

The approach used for this work in performing the co-simulation procedure is the combination of simultaneous sequential Gaussian simulation (sGs)[46] and conditional distribution technique. Additionally, the truncated Gaussian technique and indicator kriging are also employed since it involves the simulation of indicator variable in the Gaussian domain. **Figure 25** presents the schematic diagram of the co-simulation technique used in this study.

The key techniques in this procedure are the implementation of the simultaneous sGs and the use of conditional distribution to back transform the secondary and tertiary variables, i.e., porosity and permeability. The back transform of the first variable, i.e., facies, is performed using the truncated Gaussian method.[47] Using this technique, there will be no cross covariances/cross variograms required and no large co-kriging system to solve. This improves the practical application of the technique.

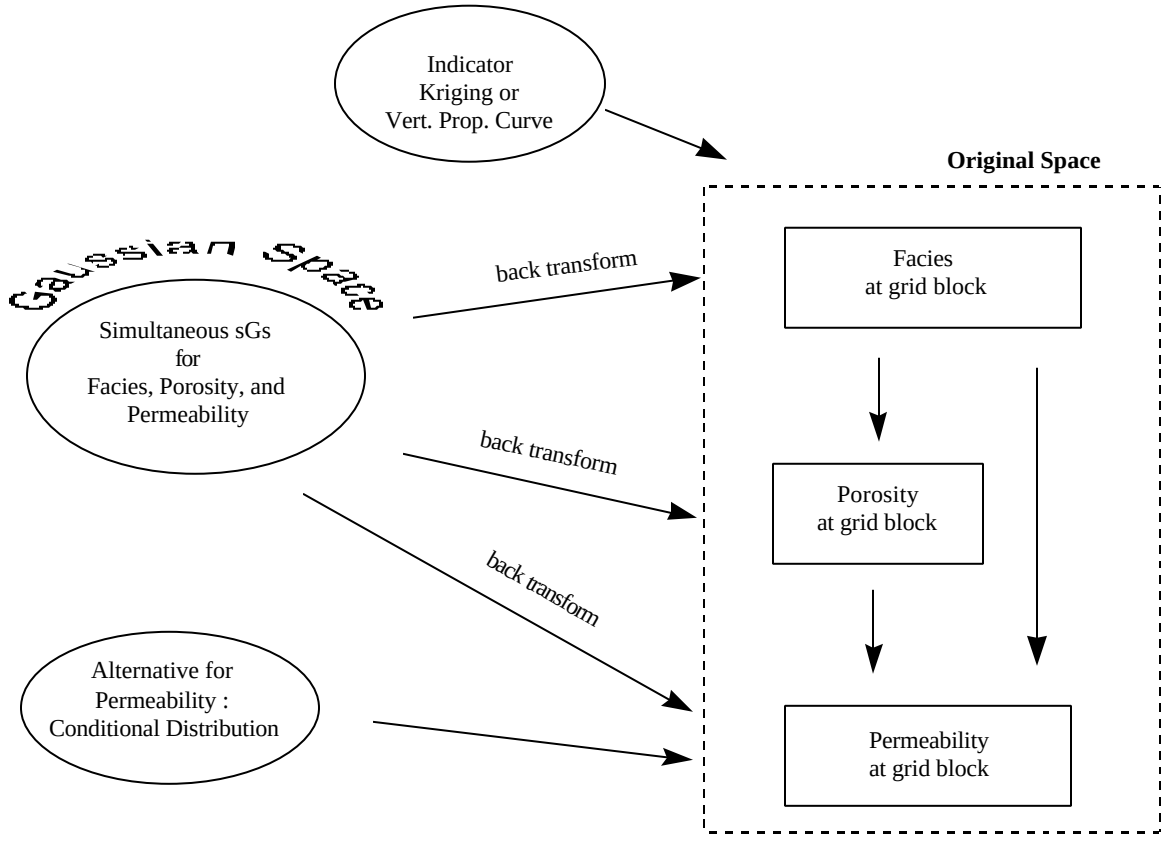

Figure 25 - Schematic diagram of the co-simulation technique

Theoretically, the technique is not limited to only three variables. We can extend it to as many variables as we wish, but the implementation of this technique in this study is limited to these three variables only since these are the most important variables, based on the log and core data, that directly relate the geological information and petrophysical properties.

The first most important aspect about the co-simulation technique developed here is the simultaneous use of sGs procedure for facies, porosity, and permeability. It provides two advantages. First, the ability to incorporate the spatial relationship of each variable. Second, by selecting the same simulation procedure for all three variables, a single search neighborhood can be applied where the same data points are used in the kriging process of each variable. This technique makes the program computationally efficient. As in any sGs procedure, the sample points could either be the original data or the previously simulated nodes and each simulation node is visited only once using the selected random path.

The application of single search neighborhood during the simulation may not always be possible if some data for one or two variables are missing at one particular location. For example, consider the case where at one location facies have been identified but porosity and permeability are not available. For facies, this location is considered as the sampled point but for the other two variables this location needs to be treated as the unsampled location. So, when sampled points are searched during the sought neighborhood process, this point can not be fully used to perform the kriging process of all three variables. It is only good for kriging of facies. Additional search is required for porosity and permeability until the requirement of the minimum number of nodes to complete the kriging is satisfied.

In the most common situation, however, there will be porosity data for each location where facies are identified and limited number of permeability data are available. In this case, it is better to perform the single search neighborhood for facies and porosity simulations only and do separate search for permeability simulation.

In the case where the locations for permeability data are unknown, then only conditional distribution technique can be applied for permeability simulation, i.e., without the sGs. This is the case where the "alternative" procedure of Figure 25 is applicable.

Since the technique uses independent sGs for each variable, the spatial analysis required are the Gaussian variograms for facies, porosity, and permeability. No cross variogram is necessary. Additionally, for the purpose of indicator kriging where its result is used in the truncated Gaussian procedure[47] to back transform the Gaussian facies value, a set of indicator variograms is required. One variogram is needed for each facies.

The second most important aspect of this co-simulation procedure is the use of conditional distribution technique to perform the back transformation from the Gaussian space into the original space. The idea of using conditional distribution is similar to the use of vertical proportion curves in the truncated Gaussian technique. The vertical proportion curves represent the probability or the percentage of geological facies at a particular depth. By using this proportion curve, it restricts the appearance of certain facies and allows other facies at certain depth with some probability. In this case, the use of

conditional distribution technique will restrict the distribution of the simulated value which is consistent with the local relationships between the new and prior simulated variables.

In the standard sGs, the back transform procedure is conducted using the distribution of all data. In this technique, the back transform of porosity, as the secondary variable, is constrained to the porosity distribution for certain facies only. **Figure 26** shows the schematic diagram of the conditional distribution procedure for porosity simulation. From this figure, we can see that, first, distribution functions or correlations between porosity and each facies are built (Figure 26a). Then, the cumulative distribution function (cdf) of porosity data in the original space (Figure 26b) is calculated. The cdf in Gaussian space can be calculated for later use as shown in Figure 26c.

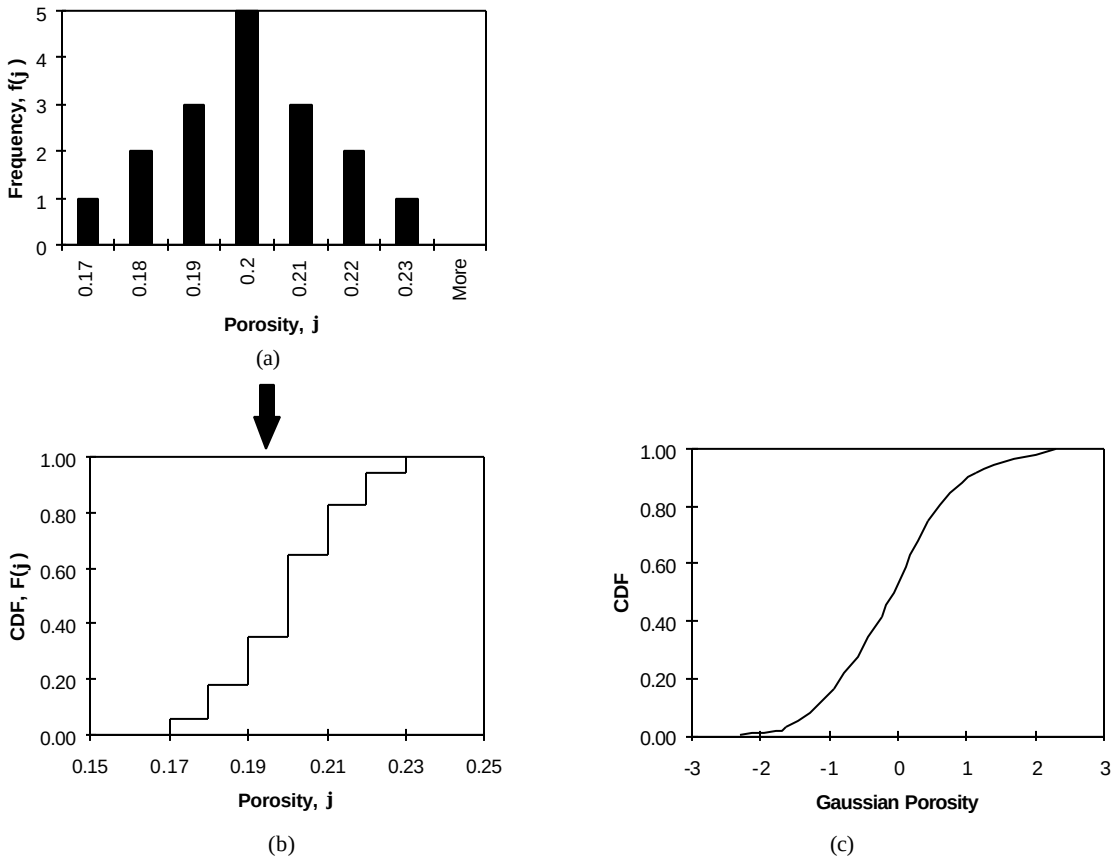

Figure 26 - Conditional distribution procedure for porosity: (a) the frequency plot of porosity data for certain facies type, (b) cumulative distribution function (cdf) of the corresponding porosity correlation, and (c) cdf in Gaussian space

Once a facies is assigned for a certain location, then the cdf for this facies is used to back transform porosity as shown in **Figure 27**. In the example shown in this figure, the facies for a certain location is identified as Facies A. Using the cdf of porosity for Facies A only, the Gaussian porosity obtained from the sGs procedure is back transformed to get the final porosity value. The dotted line on the cdf curve is calculated using linear interpolation of the data in the cdf curve. This line is used in assigning the final porosity. The dotted line with the arrowhead shows the direction of the process during back transform procedure.

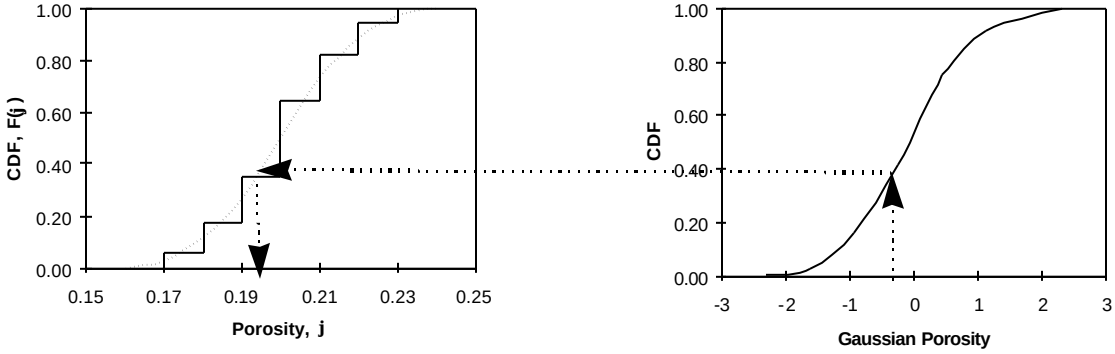

Facies Correlation for Facies A

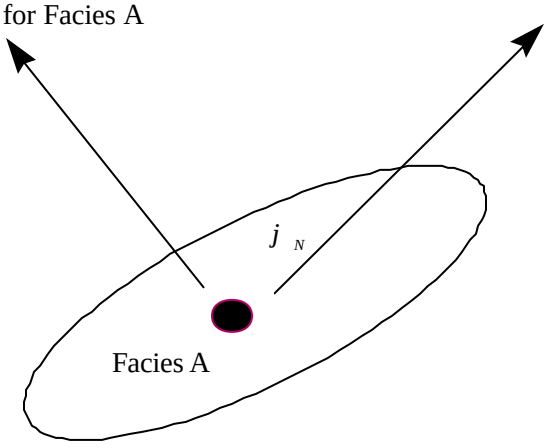

Simulated Facies and Gaussian Porosity

Figure 27 - Example of the use of conditional distribution technique in porosity simulation

The use of this technique can be extended to next variable, the tertiary variable, i.e., permeability. Since permeability is a function of porosity, and porosity is a function of facies then permeability needs to be constrained to both of these variables. **Figure 28** shows the schematic diagram of the back

transformation using conditional distribution technique for permeability. Figure 28a shows the porosity-permeability correlation for one of the facies. As we can see from this figure, several porosity classes are defined in this correlation. This is to minimize the variation of the permeability values. In general, the number of the class can be set as the square root of the number of data points. However, in the implementation of this program the number of class is always set as 4 which corresponds to the quartiles of data. The histogram of permeability for one of the porosity class is shown in Figure 28b. Using this histogram, we can build the cdf of this histogram as shown in Figure 28c. The cdf for Gaussian space can be calculated for later use as shown in Figure 28d.

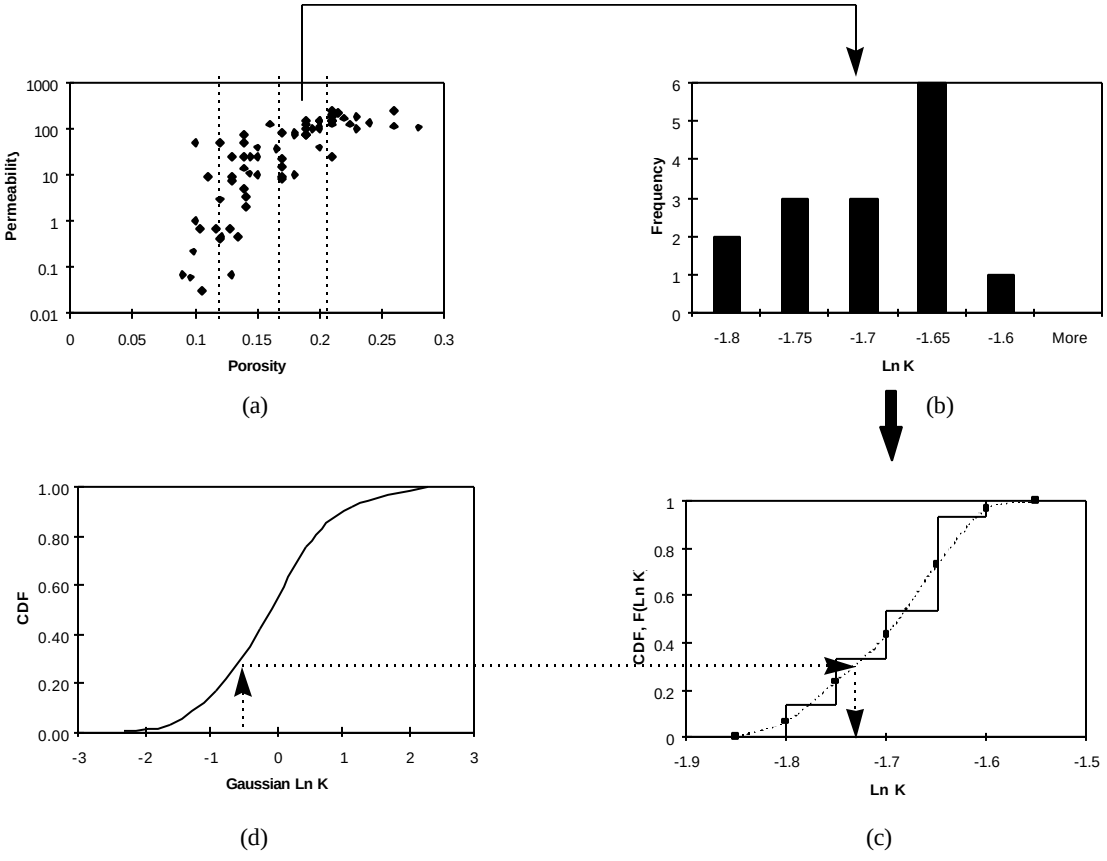

Figure 28 - Conditional distribution technique for permeability

In the simulation procedure, once facies and porosity are assigned for a certain location, then we can assign permeability using the appropriate cdf, i.e., the cdf from the corresponding porosity class, and the Gaussian permeability value from the sGs procedure.

For the case where the sGs is not performed for permeability simulation due to the missing location information, a random number between 0 and 1 can be used instead of the Gaussian transformed value to simulate a permeability value from conditional cdf.

The co-simulation technique described in the previous section uses the data that originate mainly from well logs and well cores. Using these data and other information, the geologist will produce geological interpretation of the reservoir that includes the description of facies at well location. Facies distribution at, for example, 1-ft interval in each well could be generated based on this interpretation. This distribution becomes the hard data for the co-simulation technique. It is considered as hard data since it is based on measured values.

The goal of the geological simulation is to closely replicate the geologist's interpretation. To achieve this goal, it may be important that some other information, other than the hard data, to be incorporated in the geological simulation procedure. This information is commonly known as the soft data.

One type of information that can be considered as the soft data is the geologist's interpretation of facies distribution for the whole reservoir, e.g., the isopach map of the facies. This interpretation is considered soft information since it is not based on measured values. Hard data in the indicator simulation technique are represented by an indicator value that has the value of 1 if present and 0 if absent, e.g. $I(\vec{x}) = [0 \quad 1 \quad 0 \quad 0]$, means facies 2 is present and others are absent at location $\vec{x}$. To incorporate the soft information, certain probability values can be assigned for each facies at one location. This information can be incorporated in the simulation procedure by modifying the definition of indicator function. For example, if there is 50% chance of facies 1 and 50% chance for facies 2 to exist at a certain location, then for a system with 4 facies, the indicator function becomes $I(\vec{x}) = [0.5 \quad 0.5 \quad 0 \quad 0]$. A question mark can be assigned if the probability of one facies is not known with certainty. That is, if the probability of facies 1 is 25% but there is no certainty about the other three facies, then we can assign a question mark for other facies, i.e., $I(\vec{x}) = [0.25 \quad ? \quad ? \quad ?]$.

The value specified in the soft data can be assigned as the result of indicator kriging for that location. In the case where the question mark is provided for several facies then indicator kriging for those facies

needs to be performed. The cumulative value of the kriging results must be rescaled to 1 minus sum probability of the known facies. So, the cumulative value of all facies becomes exactly 1.0. For example, if the soft data for a location $\vec{x}$ are $I(\vec{x}) = [0.25 \quad ? \quad ? \quad ?]$, the kriging for facies 2, 3, and 4 must result with the probabilities that satisfy the following condition,

$$\sum_i p_i = (1 - 0.25) = 0.75, \qquad \text{where } 0 \le p_i \le 0.75, \text{ and } i = 2,3,4 \tag{1}$$

The method was used to generate reservoir description in the Glenn Pool field. The geological unit used by the geologist in describing the Glenn sandstone in the Glenn Pool field is the discrete genetic interval (DGI). Ye[10] has defined 6 DGI's in the vicinity of Self-unit, namely DGI A through F, and 7 DGI's in the vicinity of track 7 unit, namely DGI A through G. Each DGI may consist of several facies such as channel fill, crevasse splay, and flood plain mudstone. Due to the unavailability of porosity log for track 7 unit, at half of the wells, porosity data are simulated using the remaining well data. Permeability data are available from few of the cored wells in track 7.

The first result shown here is the 2-D simulation of DGI A of track 7 unit. In the vicinity of this unit, three facies exist for the DGI A, namely channel-fill, crevasse splay, and shale/mudstone. For simulation purposes, these three facies are named facies 1, 2, and 3, respectively. The dimension of the track 7 unit is 2,640 $\times$ 2,640 sq. ft. The simulation is conducted using 80 $\times$ 80 grid blocks in x and y directions or a total of 6,400 grid blocks.

The detailed spatial modeling analysis is not included here. Only the results of the simulation are presented. **Figure 29** presents the geologist's interpretation of facies distribution for DGI A in the vicinity of track 7. The simulation results for 4 different realizations are shown in **Figure 30**. Total number of realizations simulated is 100. Comparing these figures, we can see that the simulation matches the geologist's interpretation very well.

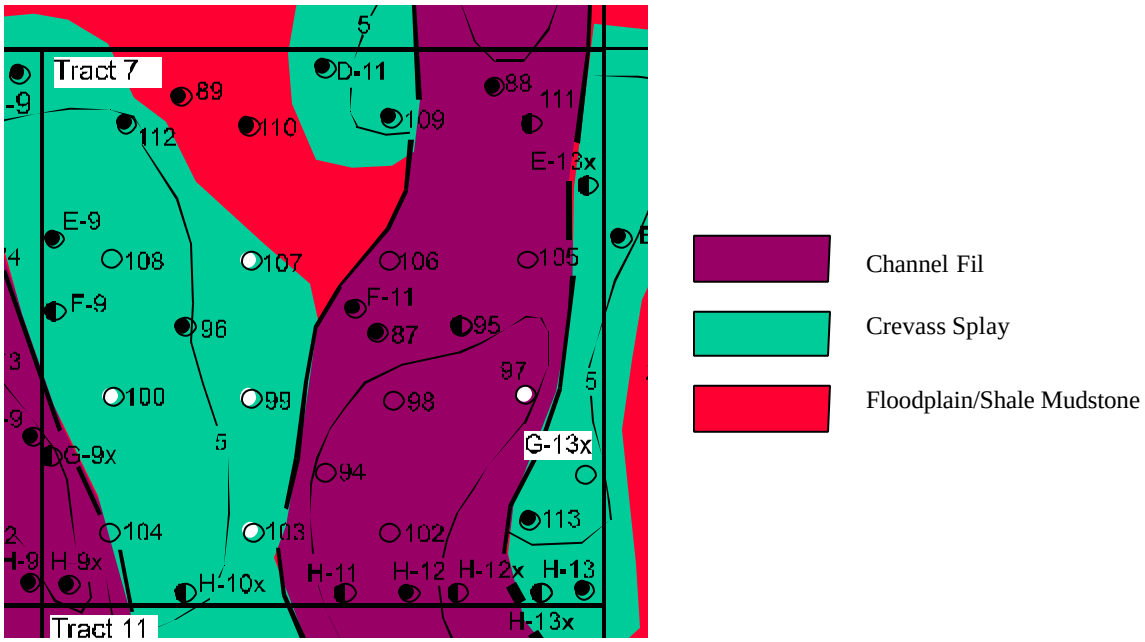

Figure 29 - Geologist's interpretation of facies distribution in the vicinity of track-7 (after Ye)[10]

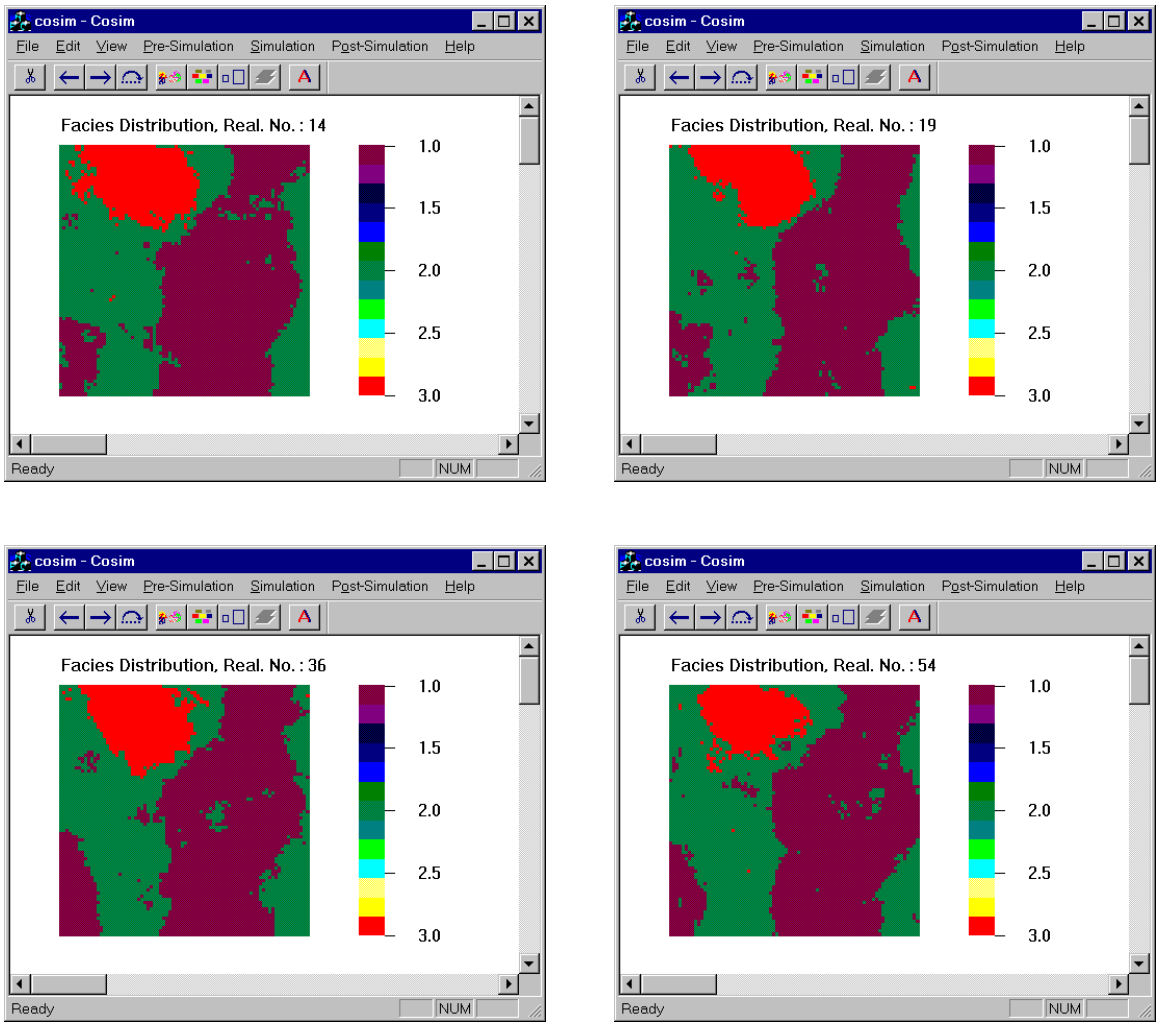

Figure 30 - Multiple realization of facies distribution of DGI A - track 7 unit

The global pdf comparison between the simulation and the conditioning data for all realizations is shown in **Figure 31**. From this figure we can see that, with respect to the conditioning data, the simulation under-estimates the proportion of facies 2 and over-estimates the proportion of facies 3. But, as we refer to Figure 29, we can observe that we only have two samples of facies 3. Therefore, the discrepancy between the two results prevail.

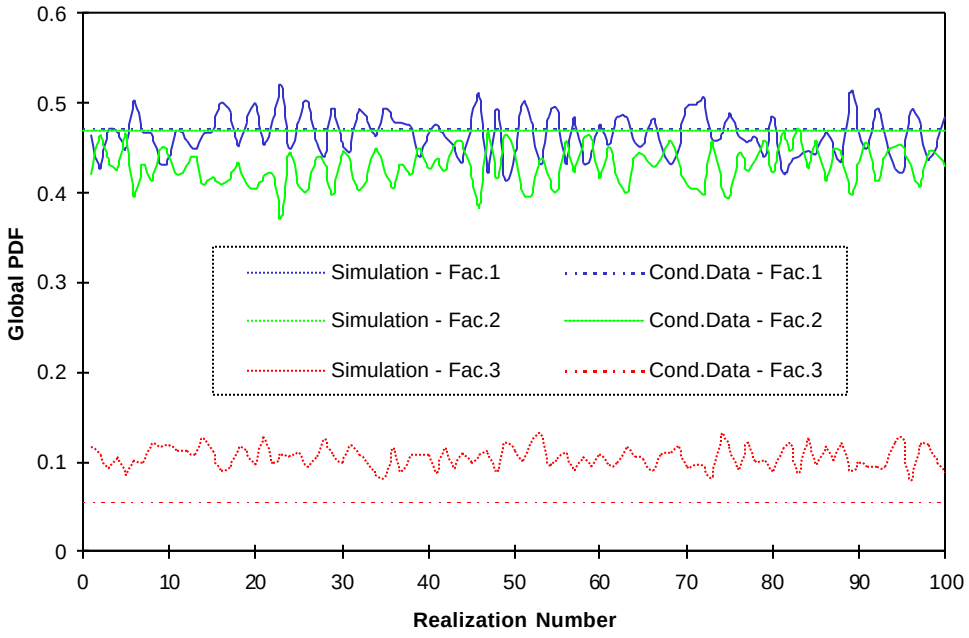

Figure 31 - Global PDF comparison between simulation and data for all realizations

The corresponding petrophysical properties distribution for one of the realizations is shown in **Figure 32**. From this figure we can clearly see that both porosity and permeability distributions follow facies description very well. This result confirms that the petrophysical properties are controlled by underlying geological description. The local variation of the permeability distribution is due to the use of random sampling method since collected permeability data are from wells other than the ones used as conditioning data. The other aspect that is important in this work is the efficiency of the program in replacing the traditional technique, i.e., the two stage approach.[48-49] This aspect will be discussed in the next paragraph.

The amount of time required to complete one simulation run can be considered very small. With the Pentium 200-Pro machine, it takes about 7 seconds. The variation in simulation time using different grid block configuration and different number of realizations is shown in **Figure 33**. As expected, the amount of time varies significantly depending on the number of grid blocks as well as the number of realizations.

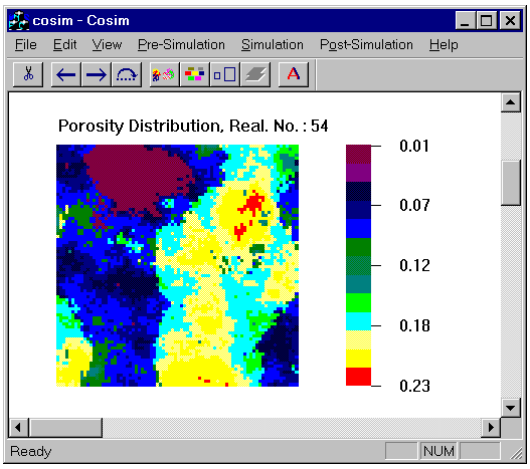

(a)

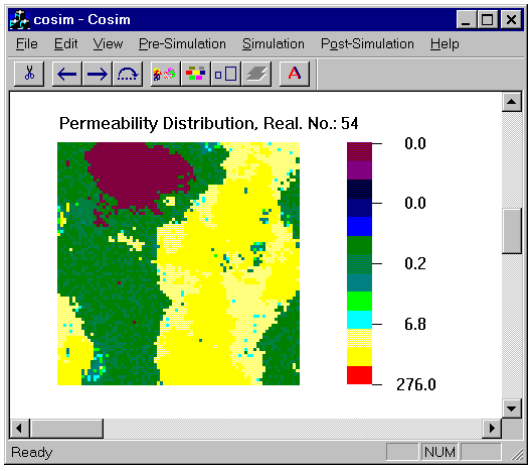

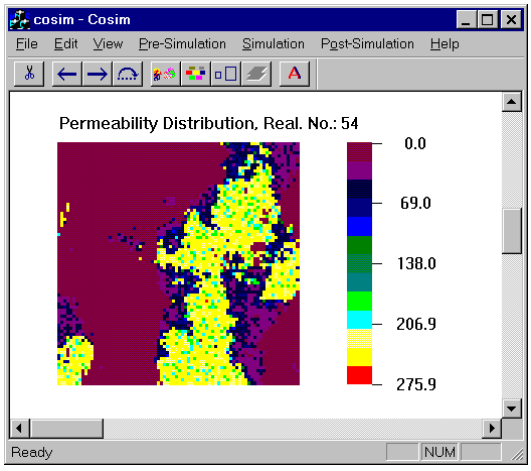

(b) (c)

Figure 32 - Porosity and permeability distribution of DGI A for track 7 unit from one of the realization. Permeability is sampled using random sampling. (a) Porosity distribution. (b) Permeability distribution shown in log scale. (c) Permeability distribution shown in decimal scale.

The efficiency of the program can be much more appreciated if we directly compare the actual time required to complete one case study starting from raw data until the distributions of facies, porosity, and permeability are obtained. This include data preparation and variogram analysis. Using the traditional approach it is estimated that an order of magnitude time will be required compared to the approach proposed here.[45] We have to include the data preparation time in this comparison since the traditional

approach requires a lot of human intervention to complete the work while the co-simulation technique has eliminated a big part of it.

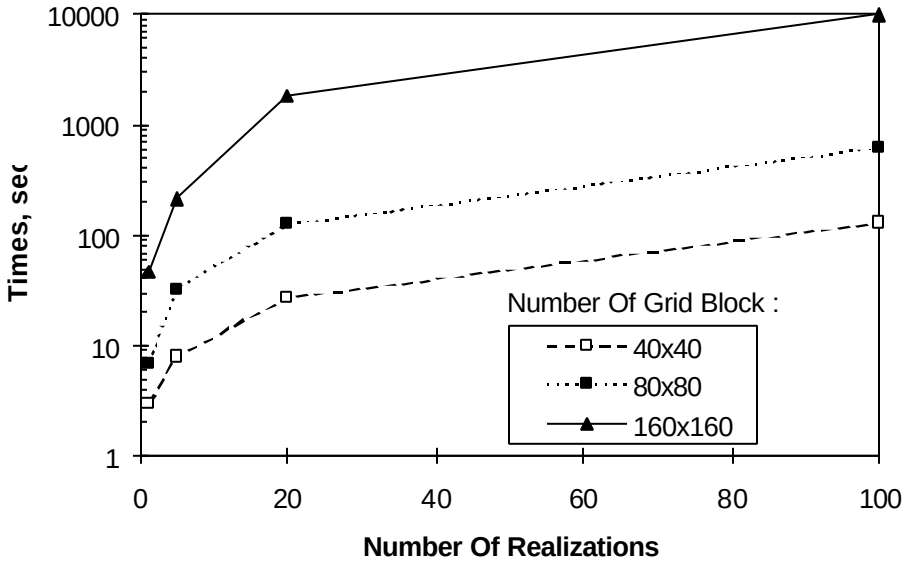

Figure 33 - Computation time comparison for different grid block configurations and different number of realizations

The second result shown in this section is taken from the Self-unit data where the 3-D simulation of DGI, not facies, is conducted. The purpose of this simulation is to show that the simulation is capable of simulating the sequence stratigraphic characteristic of the DGI. The number of grid blocks used in this example is 256,000 ($40 \times 40 \times 160$) grid blocks where the size of each block is $66 \times 66 \times 1$ ft^3. The 3-D view of DGI distribution is shown in **Figure 34**. The corresponding petrophysical distribution is shown in **Figure 35** and **Figure 36**.

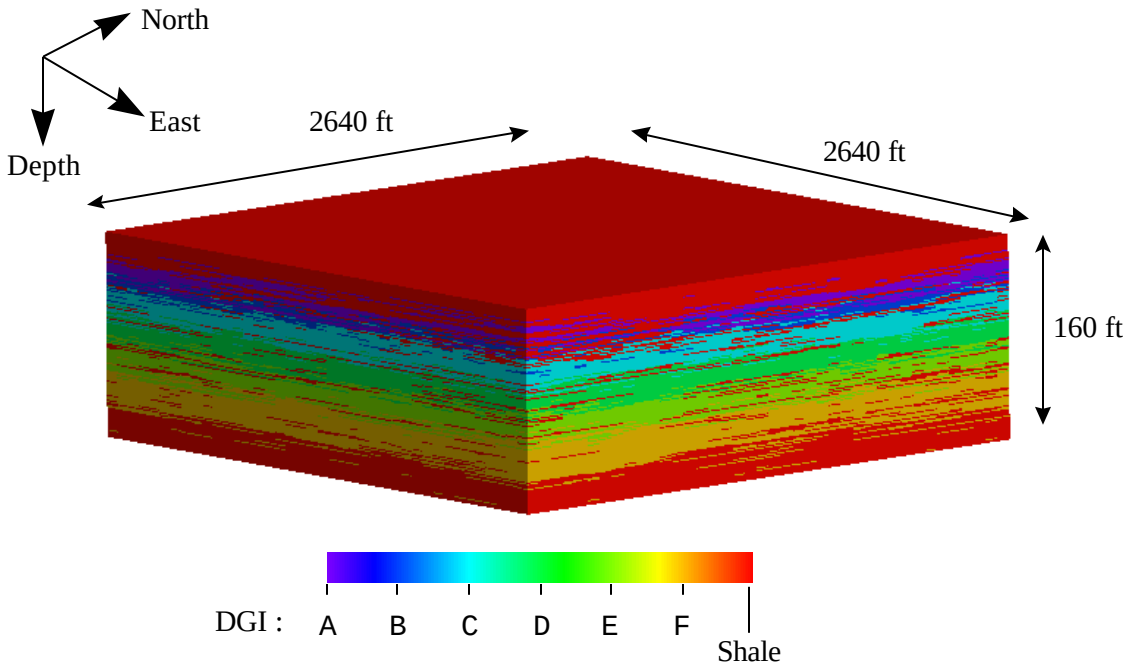

Figure 34 – 3-D view of DGI distribution of the Self-unit data.

From these figures we can see clearly how the DGI's vary from top to bottom with shale on the top and the bottom borders. This distribution is followed very well by the petrophysical properties distribution as shown in Figure 35 and Figure 36. The increase in porosity and permeability from top to bottom are matched very well with the field observation, i.e., from well log and core data.

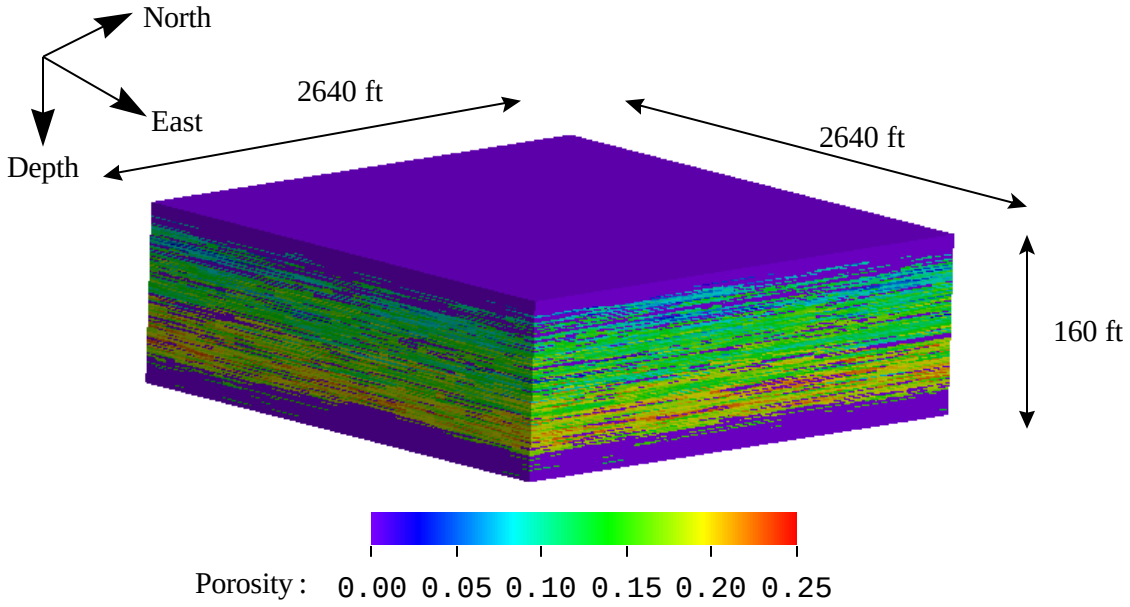

Figure 35 – 3-D view of porosity distribution of the Self-unit data.

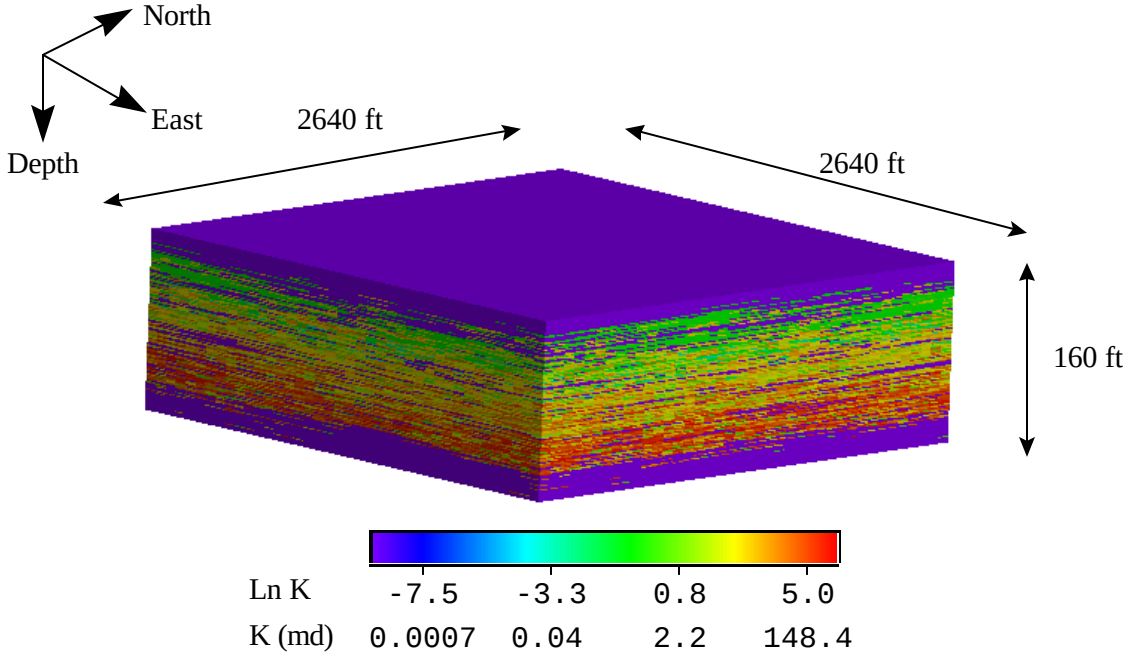

Figure 36 – 3-D view of permeability distribution of the Self-unit data.

The approach used in incorporating tomographic data is very similar to the above discussion. The only difference was the construction of variogram model, which is required for spatial analysis. Instead of

using data from vertical wells only, we also used the data from various cross sections generated by tomography. As a result of incorporating tomographic data, the variogram model improved substantially. However, as discussed in the next section, the overall flow simulation results did not improve substantially.

Flow Simulation

In conducting flow simulation to simulate the reservoir performance, we used three alternative models. These are:

- Deterministic model: It represents traditional approach where cross correlations at interval locations were established based on geological correlations. The petrophysical properties were estimated using traditional interpolation techniques given the well data.
- Stochastic model: This model represents a geostatistical approach where an integrated description was used to generate a detailed reservoir description. Some of the results are shown in the previous section.
- Stochastic model with tomogram: This model represents incorporation of cross borehole seismic data in stochastic model.

Following the reservoir description task, the flow simulation was conducted to match the past performance and also to predict the future production using three different scenarios. Based on the flow simulation results, the economic analysis was conducted as to the most feasible scenario that is applicable to the Self-unit.

Deterministic Model

Geological Simulation

The common problem encountered in generating the reservoir description is how to fill in the information at the unsampled locations, i.e. at the interwell regions. The conventional way of solving this problem is to assume that a certain relationship (correlation between wells and/or based on similarity) exists in these

regions, and that there is a unique set of model output data for a given set of inputs. This is known as a deterministic approach. A model that is commonly used in the conventional approach is known as the layer-cake model.

The geologists involved in this project, Kerr and Ye, have established a stratigraphic framework of the Self-unit that divided the unit into 6 Discrete Genetic Intervals (DGI's). Using each DGI as a layer, a model with 6 sandstone-layers can be developed. From their interpretation, it is observed that for some intervals an impermeable layer exists between two consecutive DGI's. To accommodate this fact, the model is modified to contain this layer in between two DGI's.

For the purpose of flow simulation, each layer is divided into several grid blocks. To cover the 160-acres of the Self-unit, 400 grid blocks (20×20 in X and Y directions respectively) are assigned to each layer. Using this configuration, the dimension of each grid block in X and Y directions becomes 132-ft whereas its thickness is determined using bilinear interpolation based on the well data. **Figure 37** shows the interpolation result for north-south cross section. This figure clearly indicates how each layer is stacked against one another.

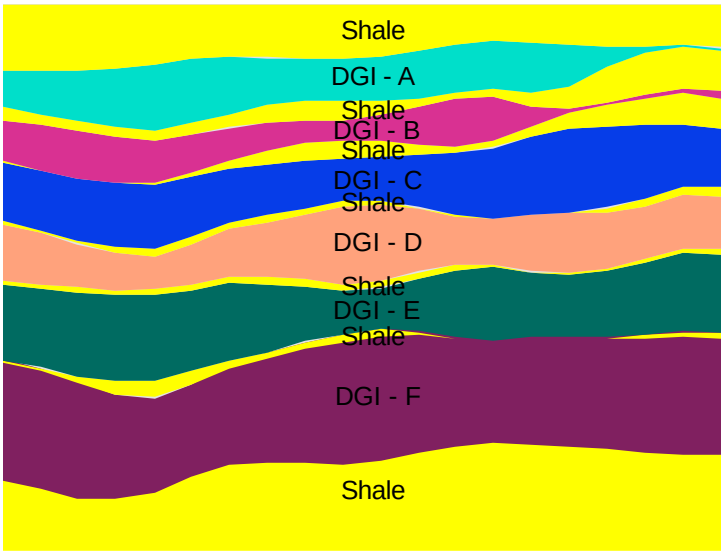

(a)

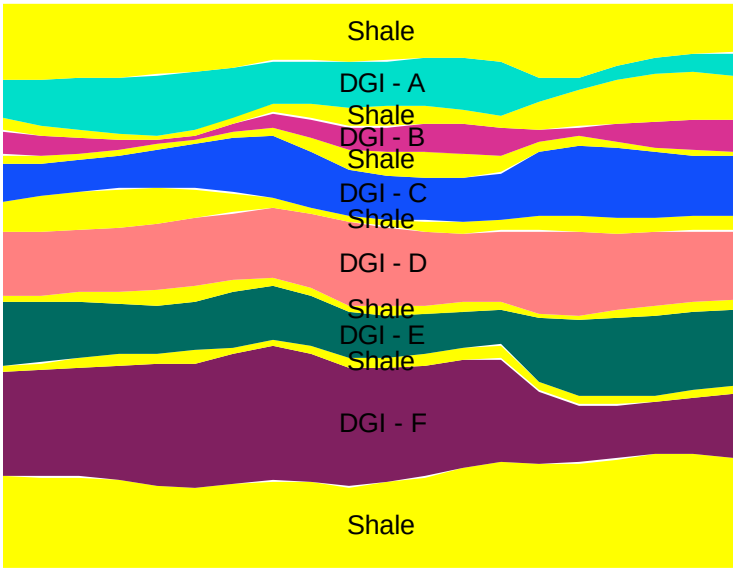

(b)

Figure 37 – Deterministic north-south and east-west sand cross section

Figure 38 shows the thickness comparison of each layer between well data and the model at wells No. 43 and No. 37 respectively. The data from these wells were not used as input in the interpolation process. Thus, these comparisons should validate the interpolation used in generating the model. As these figures indicate, the model conforms to the geological architecture as is commonly observed in the conventional method.

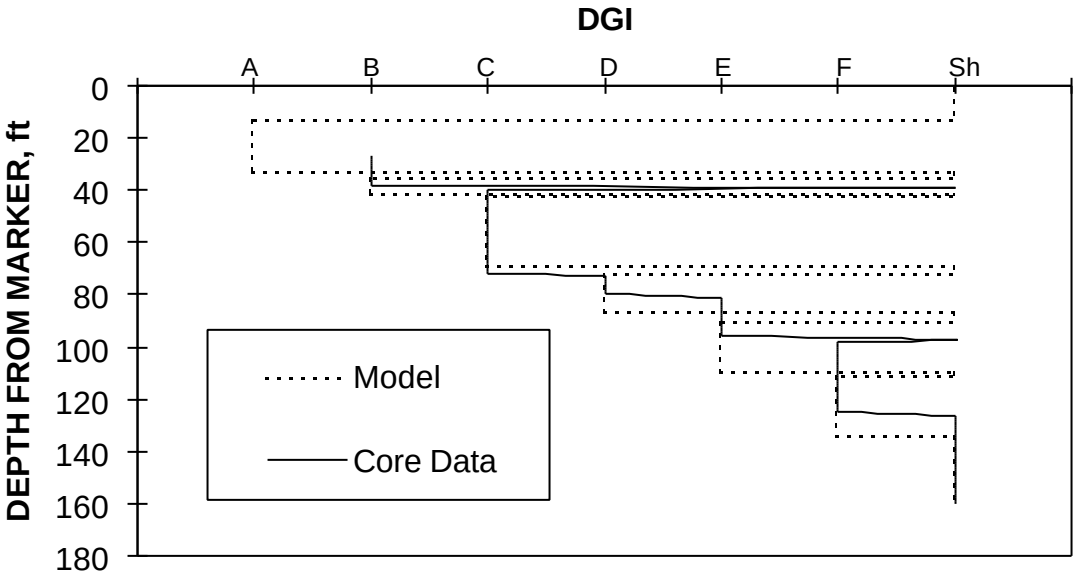

(a) Well 43

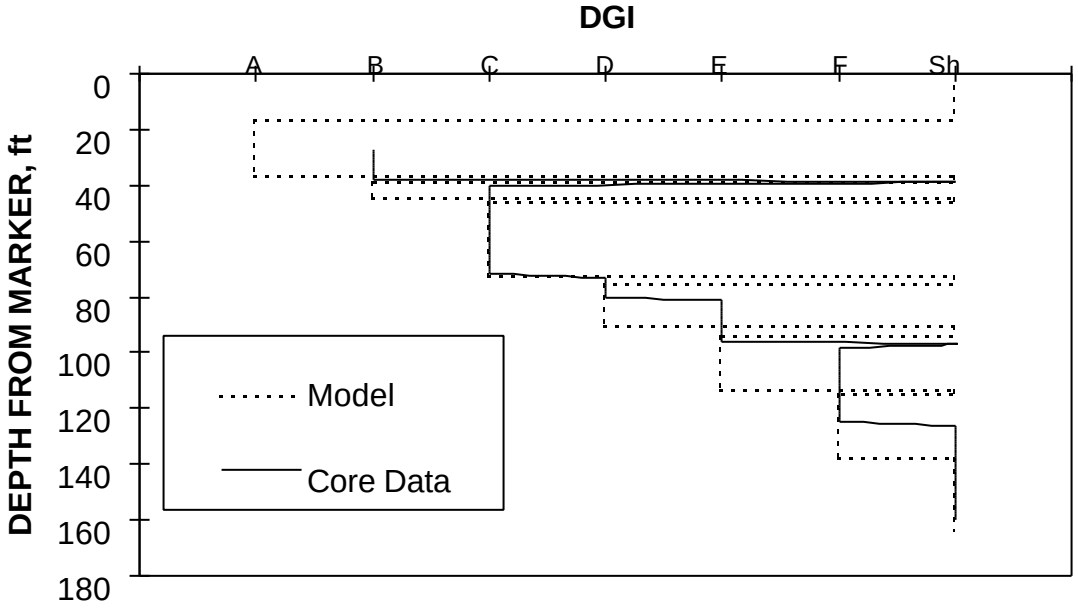

(b) Well 37

Figure 38 - Deterministic - sand thickness well 43 and 37

Porosity Description

In assigning the porosity value to each grid block, the well data is first superimposed on the geology data, i.e.; the porosity of each DGI/layer is separated from the others. An average value is calculated for each layer at each well. Then, the porosity of a grid block at an unsampled location is calculated using bilinear interpolation of the well data that has been averaged previously. The porosity of the impermeable (shale) grid blocks is set as zero. All of the porosity data used in this study were gathered from the log of currently existing wells. No corrections or correlations to core data are made since none of these wells were cored.

Figure 39 shows the porosity distribution of the east-west cross section. It can be observed that the porosity distribution is almost uniform in each layer. Thus, it is clear that this model can not capture the heterogeneity of the reservoir. **Figure 40** presents the porosity at Self-82 to show the comparison of the estimated value with the field data at a specific well. It can be observed that the porosity value from the model seems to be inconsistent. It underestimates at the top part of the reservoir (DGI's A, B, and C), but overestimates at the bottom part of the reservoir (DGI's E and F).

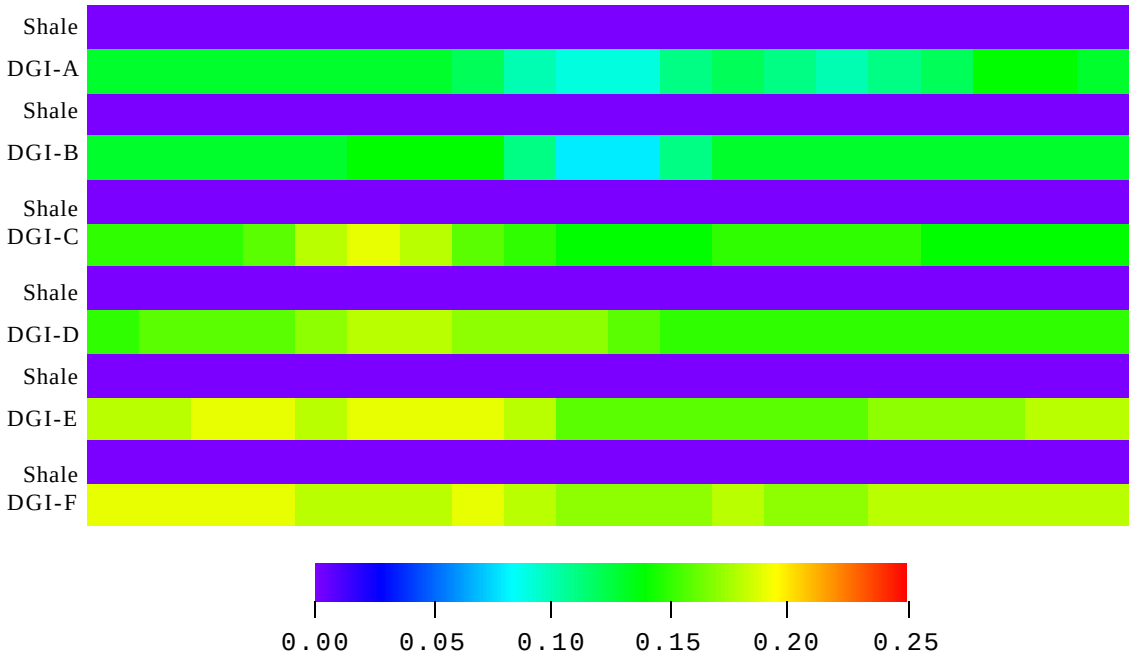

Figure 39 – East west porosity cross section – deterministic model

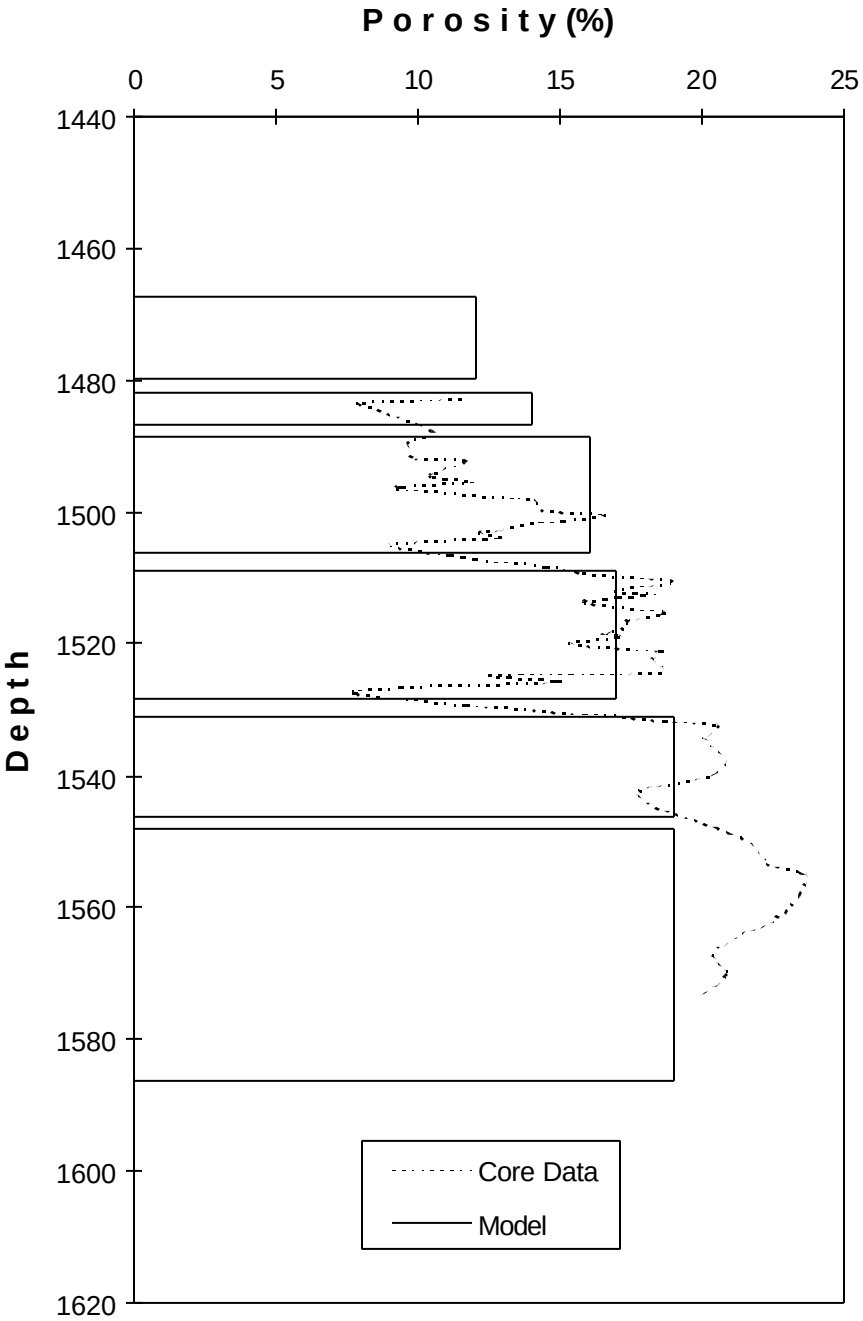

Figure 40 - Porosity comparison at Self-82

Permeability Description

The permeability value for each grid block for this model is estimated using a linear relationship assumption between porosity and the logarithm of the permeability. The only source of data for permeability available for this study is from the core measurements of several old wells, i.e. Well No.'s 28, 31, 32, 37, 43, and 47. Unfortunately, the core data from these wells are not available for the whole intervals. Mostly, they are only from the bottom intervals since those were the most productive intervals. This situation creates difficulty in generating the correlation. In fact, there is no data available for DGI-B and only a few points for DGI-A.

Figure 41 shows the permeability distribution of the north-south cross section. As in the porosity distribution, it can be observed that the areal heterogeneity cannot be captured by this model. Observing the average value for each layer, it is found that the permeability of DGI A (k-average = 15.6 md) and DGI B (k-average = 15.5 md) is higher than the permeability of DGI C (k-average = 8.5 md). This is inconsistent with the field data. The reason for this is the poor quality of the data that were used in generating the porosity-permeability relationship for these DGI's. The core study of Self-82 indicates that the porosity for DGI's A and B is about 12 - 15% with the permeability in the range of 0.1 to 1 md, while the average value from the old core which was used as input data was 17% for porosity and 60 md for permeability. Overestimated distributions resulted for DGI's A and B. **Figure 42** presents the permeability distribution at Self-82. In general, the model predicts a very narrow range of permeability. It overestimates at the top intervals but underestimates at the bottom intervals. Again, the heterogeneity of the reservoir is not captured very well.

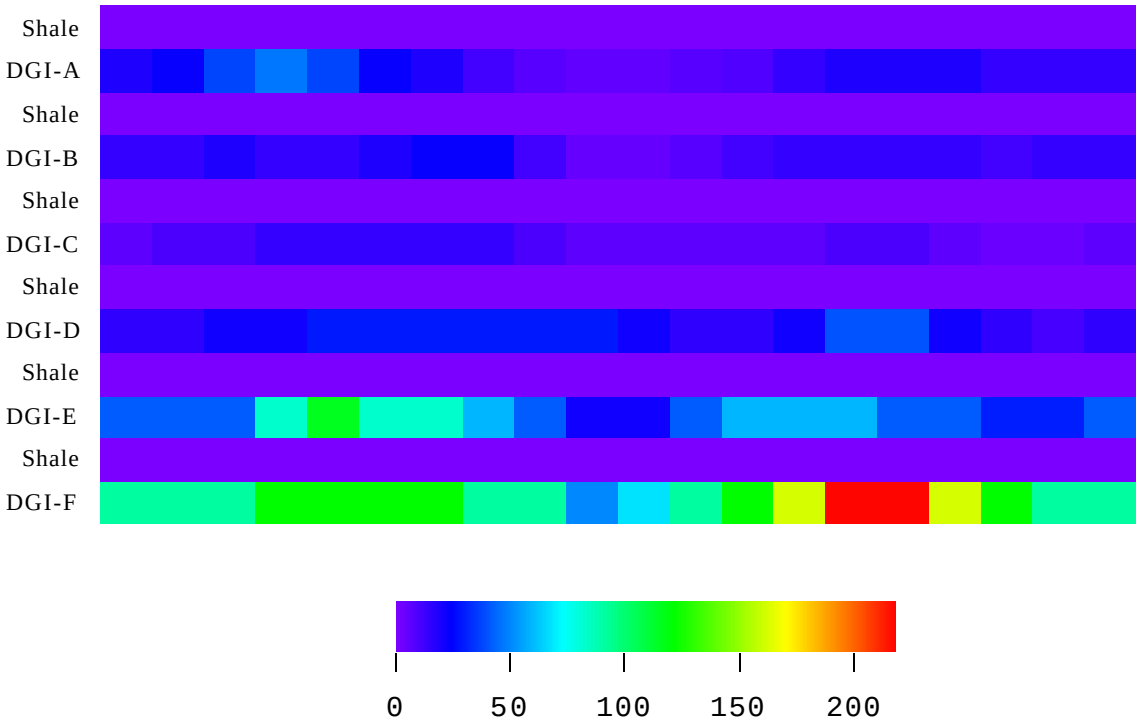

Figure 41 – North-south permeability cross section – deterministic model

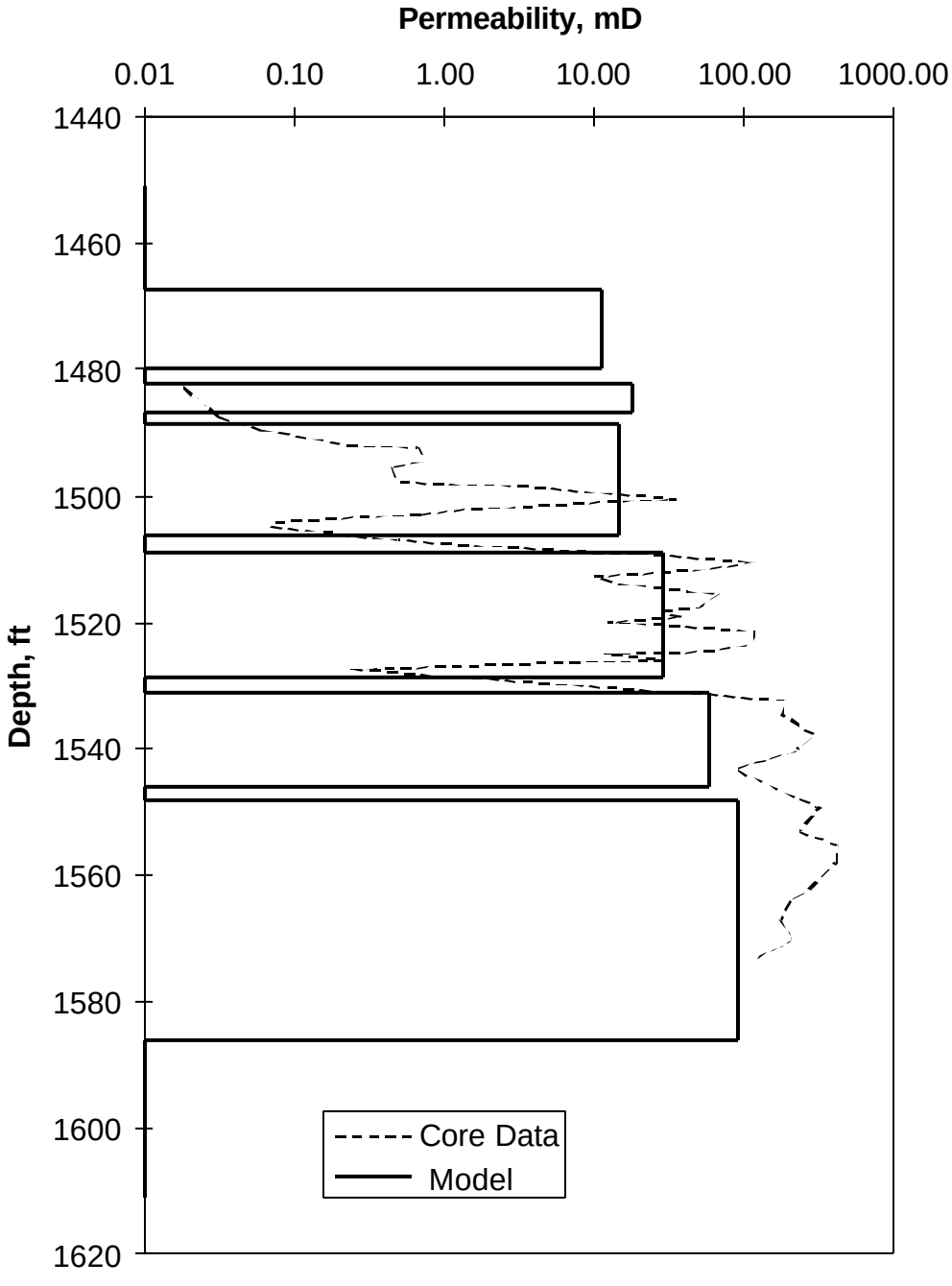

Figure 42 – Permeability comparison at Self-82 – deterministic model

Figure 43 presents the comparison of the permeability thickness product (kh) between the well test interpretation and the model. In this figure, any point that lies on the 45^{o} line is a perfect match. Since

most of the results lie above this line, it indicates that the model overestimates the kh value when compared to the well test results. The procedure that was applied in calculating the kh for the model is as follows.

1. A radius of investigation is defined as half the distance between adjoining wells.
2. The permeability inside this radius was averaged geometrically. The geometric average was calculated only for layers, which are perforated.
3. The kh of the model then was calculated as the summation of kh for each of the layers.

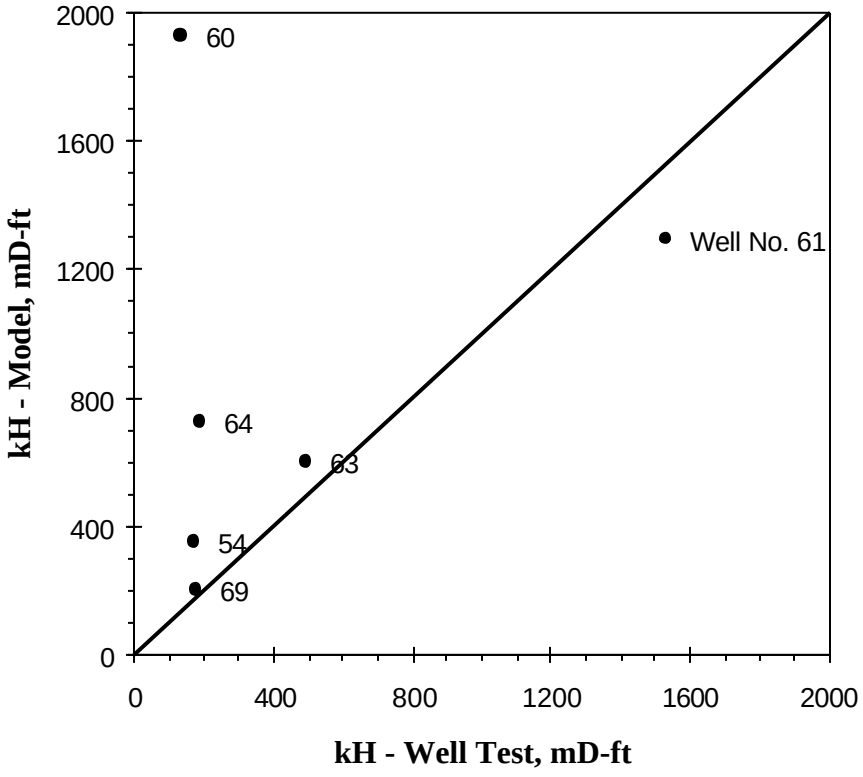

Figure 43 – Permeability thickness product (kh) comparison – deterministic model

The permeability of the model used for comparison with the well test, such as in Figure 43, is the absolute permeability whereas in practice the permeability calculated from the well test is the effective permeability. Considering that most of the field has been flushed with water, especially at the bottom

part of the reservoir, and has been produced with 99% water cut, it is reasonable to assume that the flow in the reservoir is approximately single-phase. Thus, the use of absolute permeability for this comparison is justifiable.

Flow Simulation

In order to have confidence in predicting the future performance of the reservoir, a reasonable match in the flow simulation of the past performance has to be achieved. The next task after generating the reservoir description is to conduct a flow simulation. All of the flow simulations presented in this report were conducted using ECLIPSE-100 Black Oil Simulator.

The flow simulation was performed to match the past production from November 6, 1906 until January 1, 1994. In this model, the same number of grid blocks used in the reservoir description is used in the flow simulation, i.e., $20 \times 20 \times 12 = 4800$ grid blocks. Therefore, no upscaling process required for this model.

In running the flow simulation, at least one parameter should be available as a control parameter. This parameter could be oil production rate, water production rate, or bottom hole pressure, etc. Using one control parameter, the other parameters can be used as the match parameters, to which the flow simulation result is compared. The problem that was encountered in running the simulation is the limited information on any of these parameters. Accurate information about the original oil-water contact was not known. Thus, it was quite difficult to determine the initial conditions of the reservoir. The production data were not available for the early times until 1946. The only data that was available was the first 24 hours production, or the initial potential, of a few early wells. It was decided to make trial and error runs in searching for the bottom hole pressure that could produce the initial potentials at those wells. **Figure 44** presents the initial potential comparison between the simulation and field data using uniform bottom hole pressure (BHP) at all wells of 400 psi. Except for Wells No. 1 and 16, the match is considered reasonable. In order to have a better match for these two wells, a lower BHP value should be used, but lowering the BHP would affect the other well matches. Thus, it is decided to use the BHP of 400 psi for the early production time. Using this value as the control parameter, the

simulation is continued until the reservoir pressure is depleted to this pressure. When this happens a lower value of bottom hole pressure is used as the control parameter and the simulation resumes. This process is repeated until the year 1946.

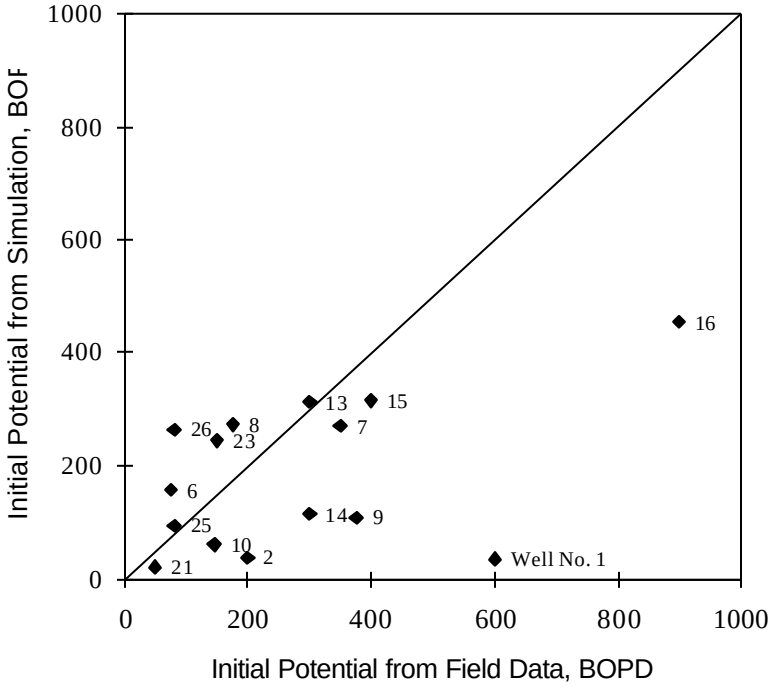

Figure 44 – Initial potential comparison – deterministic model

The production profile derived from this method is presented in **Figure 45**. In this figure, the results from 4 case studies were presented. These case studies were conducted due to the uncertainty of the relative permeability data and the initial water saturation. The definition of each case study is presented in **Table 3**. From Figure 45, it can be seen that at the beginning, the production is optimistic, but close to 1946 the production is low compared to the field data. The flow simulation in the period after 1946 was run using water production rate as a first control parameter with a restriction of a maximum value of oil production rate. These water and oil production rates are the yearly field wide data available for the Self-unit. It can be observed that the simulated results match the field data.

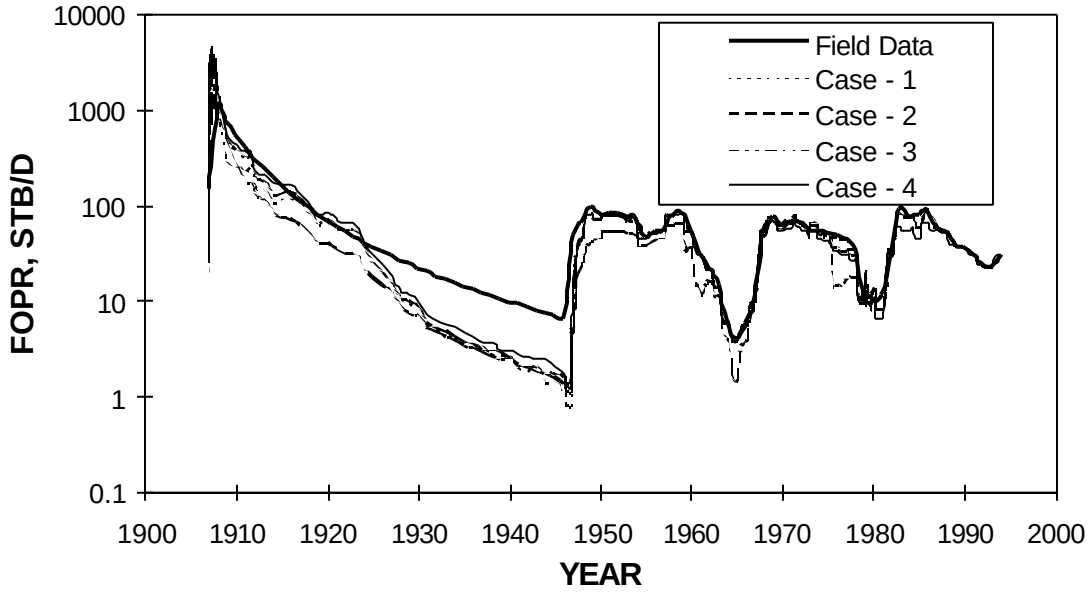

Figure 45 – Field oil production rate (FOPR) – deterministic model

Table 3 - Case definition used in flow simulation	
Legend	Description
Case 1	Uniform *Kr* (Glenn Pool Data), Uniform *Swi* = *Swr*
Case 2	Uniform *Kr* (Modified - Glenn Pool Data), Variable *Swi*
Case 3	Variable *Kr* (3 zones - Glenn Pool Data), *Swi* = *Swr* (3 zones)
Case 4	*Kr* as measured by BDM-Oklahoma (2 zones), *Swi* = *Swr* (2 zones)

Figure 46 presents the Original Oil In Place (OOIP) calculated using this model. As a comparison, the calculated OOIP as reported by Heath[6] is also presented. The difference that is observed among the case studies is due to the difference in the initial water saturation that was assumed in each case.

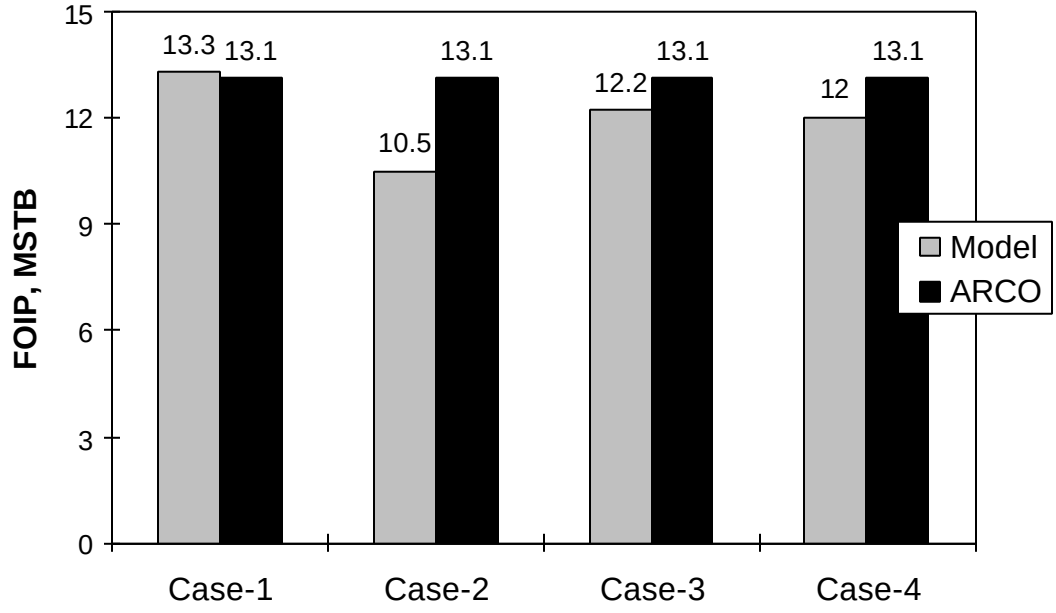

Figure 46 – Original oil in place estimation – deterministic model

Figure 47 presents the water cut predicted from the simulation. The field presently produces with a water cut of 99%. It can be seen that the simulated water cut does not match the field data very well. This is probably due to the limited information about the oil-water contact as well as the relative permeability as suggested by case 2 that gives higher water cut compared to the other cases. In this case the bottom interval (DGI F) was assumed to be saturated with water at the initial conditions and a higher water relative permeability (k_{rw}) was used. Overall information about oil-water contact indicates that water may present in part of the F zone. However, due to limited information, no aquifer model has been used.

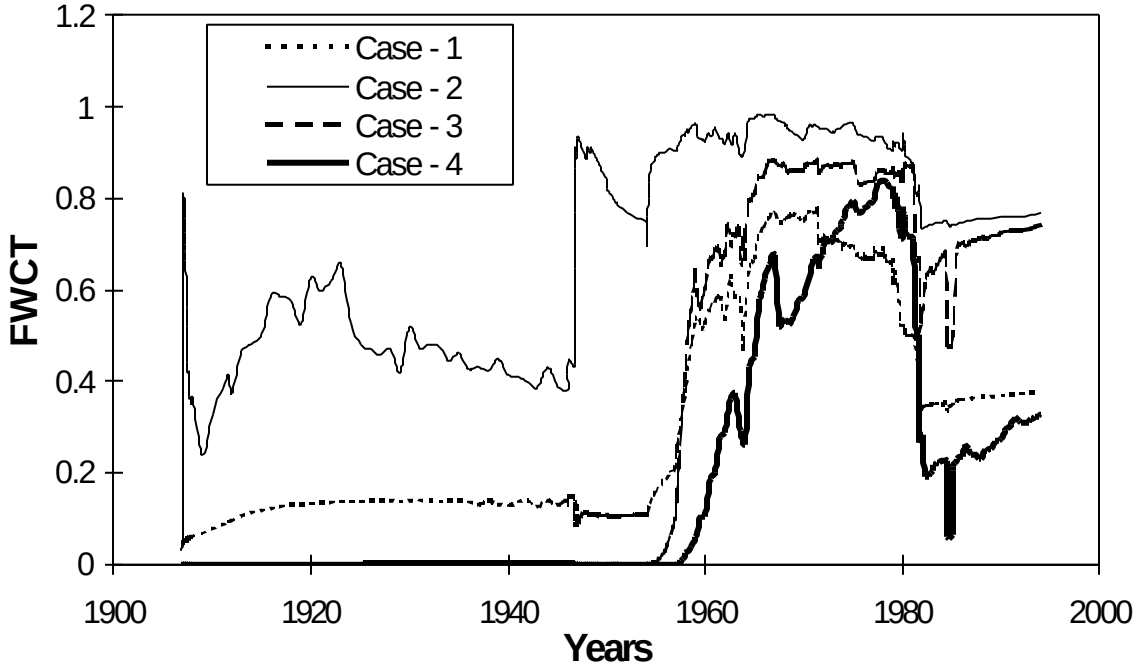

Figure 47 – Simulated field water cut – deterministic model

In order to see the potential for future use, the oil saturation map had to be analyzed. **Figure 48** shows the oil saturation comparison between the simulation and log-derived values at Self-82 for each case. The comparison is reasonable. In general, the simulation shows an optimistic result. All cases predicted high oil saturation at almost all units except unit F. In this unit, cases 2 and 3 predict a relatively lower oil saturation value as observed from the log data. The assumption that the formation is flushed by water at this interval can be justified. Thus, based on this model all the units, except unit F, can be considered good candidates with future potential.

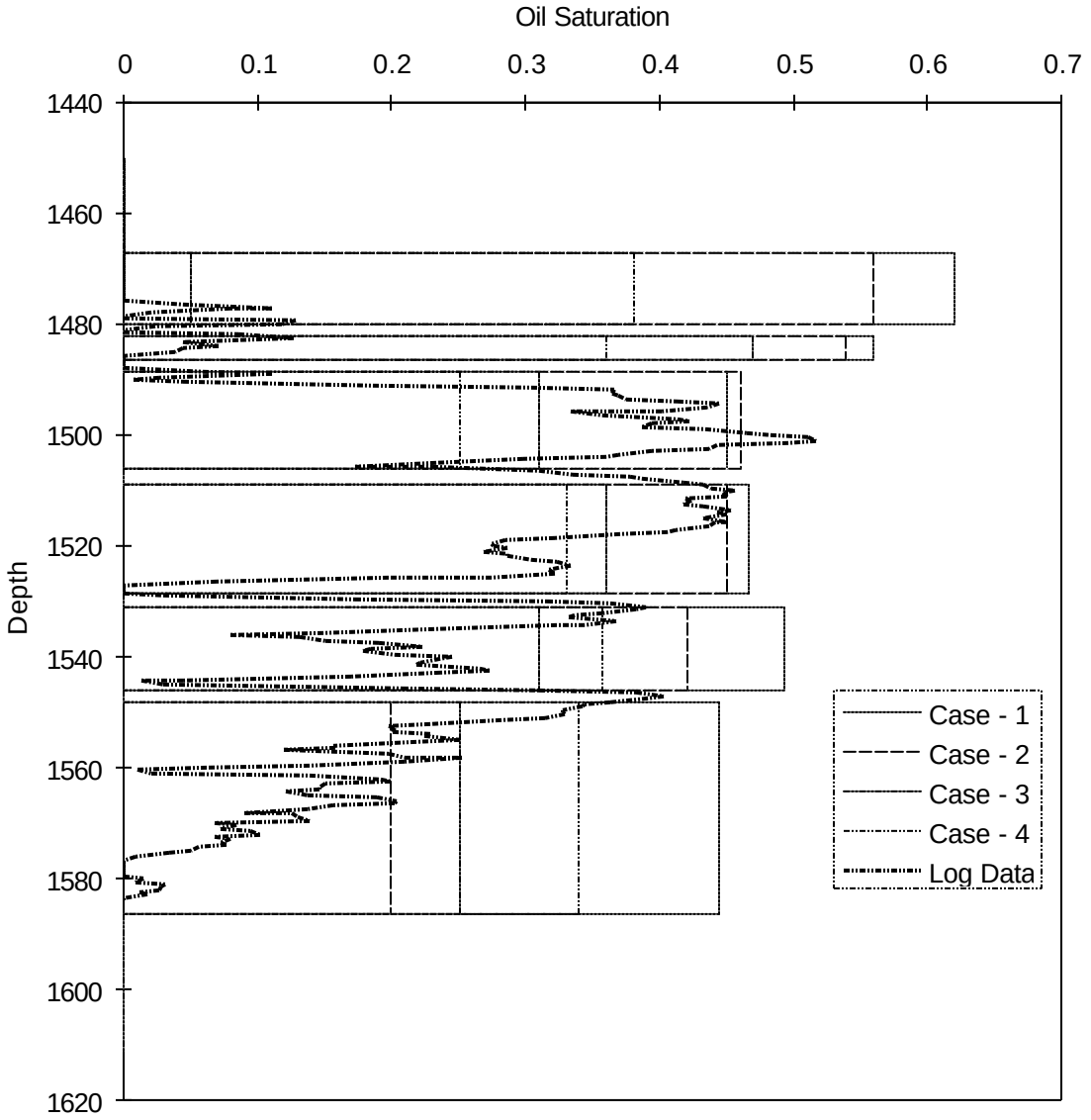

Figure 48 – Oil saturation comparison at Self-82 – deterministic model

Summary

To summarize the findings from this model, a deterministic model was developed for the Self-unit using available log and core data as well as the geological interpretation. The overall results based on the deterministic model are optimistic when compared to the field data. The kh values from the well tests are lower than predicted by the model. In general, variability of the properties observed in the field data

is not preserved when using a deterministic model. In the next two sections, the comparison of this model with the stochastic approach is be presented.

Stochastic Model without Tomography Information

Geological Simulation

The geological facies simulation was carried out using a geostatistical approach. The details and some of the results are already presented in the previous section and will not be repeated here. To summarize, the DGI's were simulated as categorical variables. The description was observed to be consistent with geological mapping developed by geologists. The total number of grid blocks simulated was equal to 256,000.

Porosity Description

Once the geological facies were simulated, the porosity values were simulated consistent with underlying geology. The details are provided in the previous section and will not be repeated here. **Figures 49a** and **b** show the comparison between simulated DGI's and observed DGI's at two wells which were not used in simulation. As can be seen from these two figures, the comparison is reasonable. The porosity from Self-82 was not used as conditioning data. **Figure 50** compares the simulation results with the observed data. Compared to deterministic model, the stochastic model captures the reservoir heterogeneity much better. It also tracks the variation in porosity better than the deterministic model.

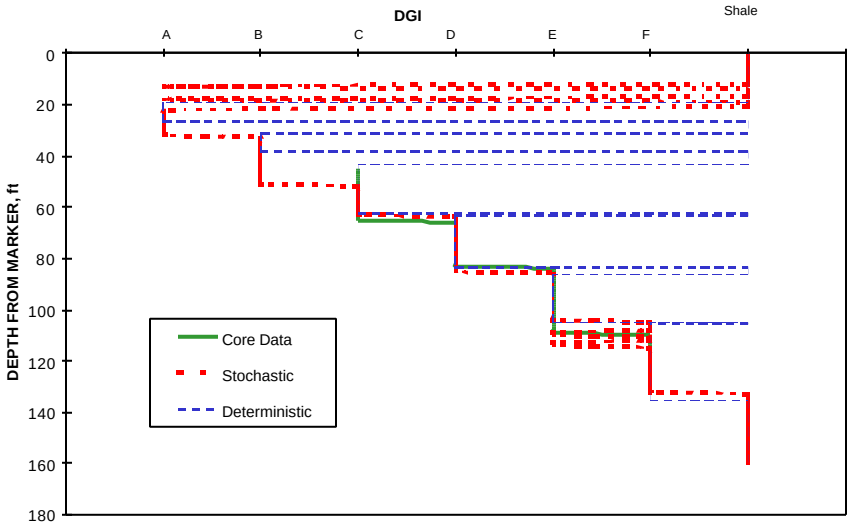

Figure 49a - DGI comparison at well no. 43 - DGI model

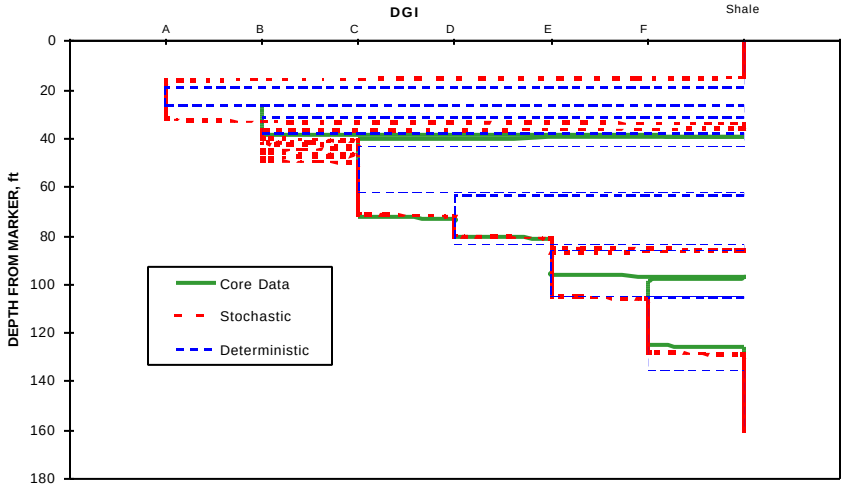

Figure 49b - DGI comparison at well no. 37 - DGI model

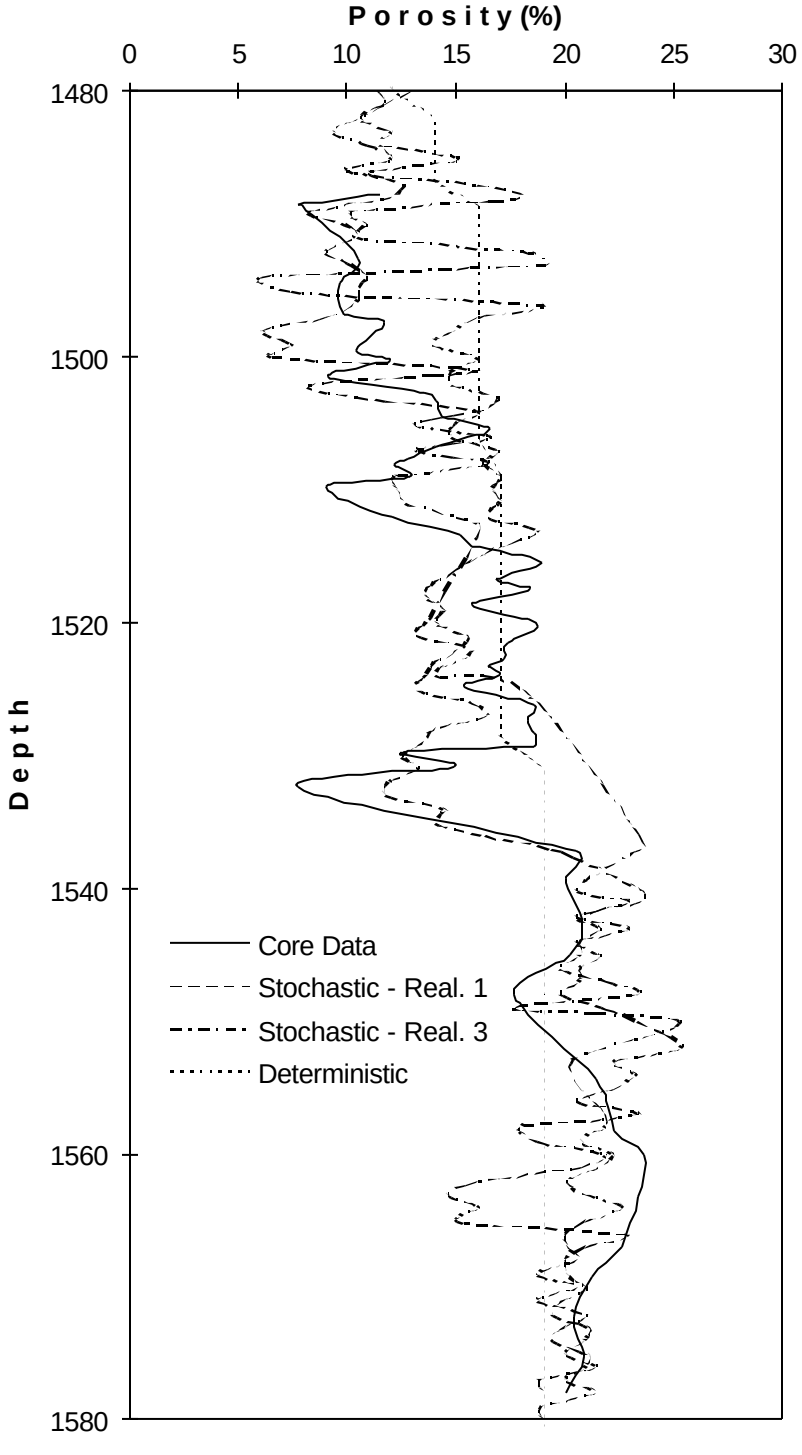

Figure 50 - Porosity comparison at Self-82 - DGI model

Permeability Description

After simulating the porosity values, permeability values were simulated using the relationship between log of permeability and porosity. A conditional distribution technique was used whereby for given porosity, permeability value was sampled from a given class. **Figure 51** shows a typical cross section of simulated permeability values.

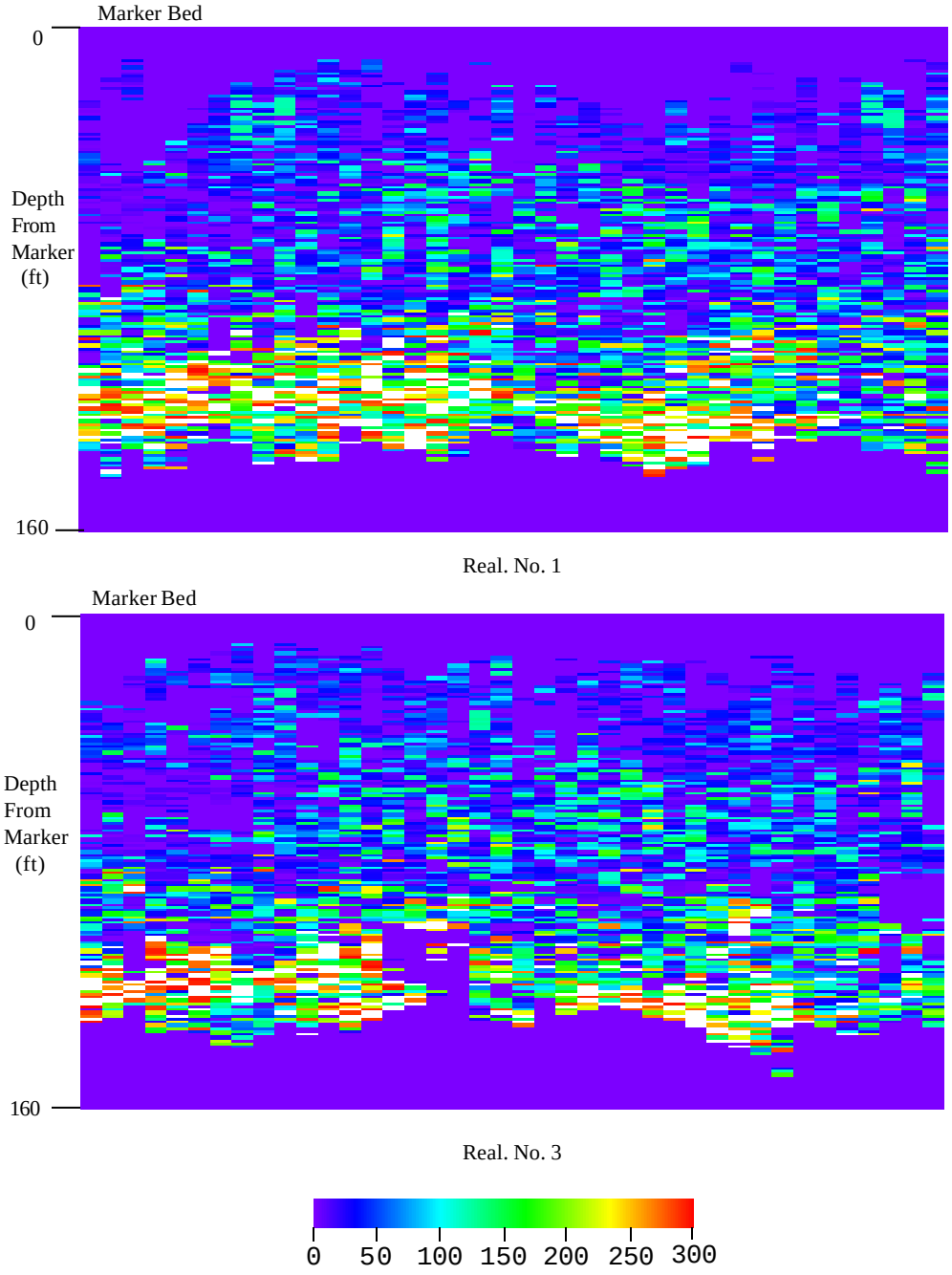

Figure 51 - Permeability distribution – north-south cross section - DGI model

Figure 52 shows the comparison between simulated permeability values and observed permeability values at Self-82. As can be seen, the permeability heterogeneity is better captured by stochastic model compared to deterministic model.

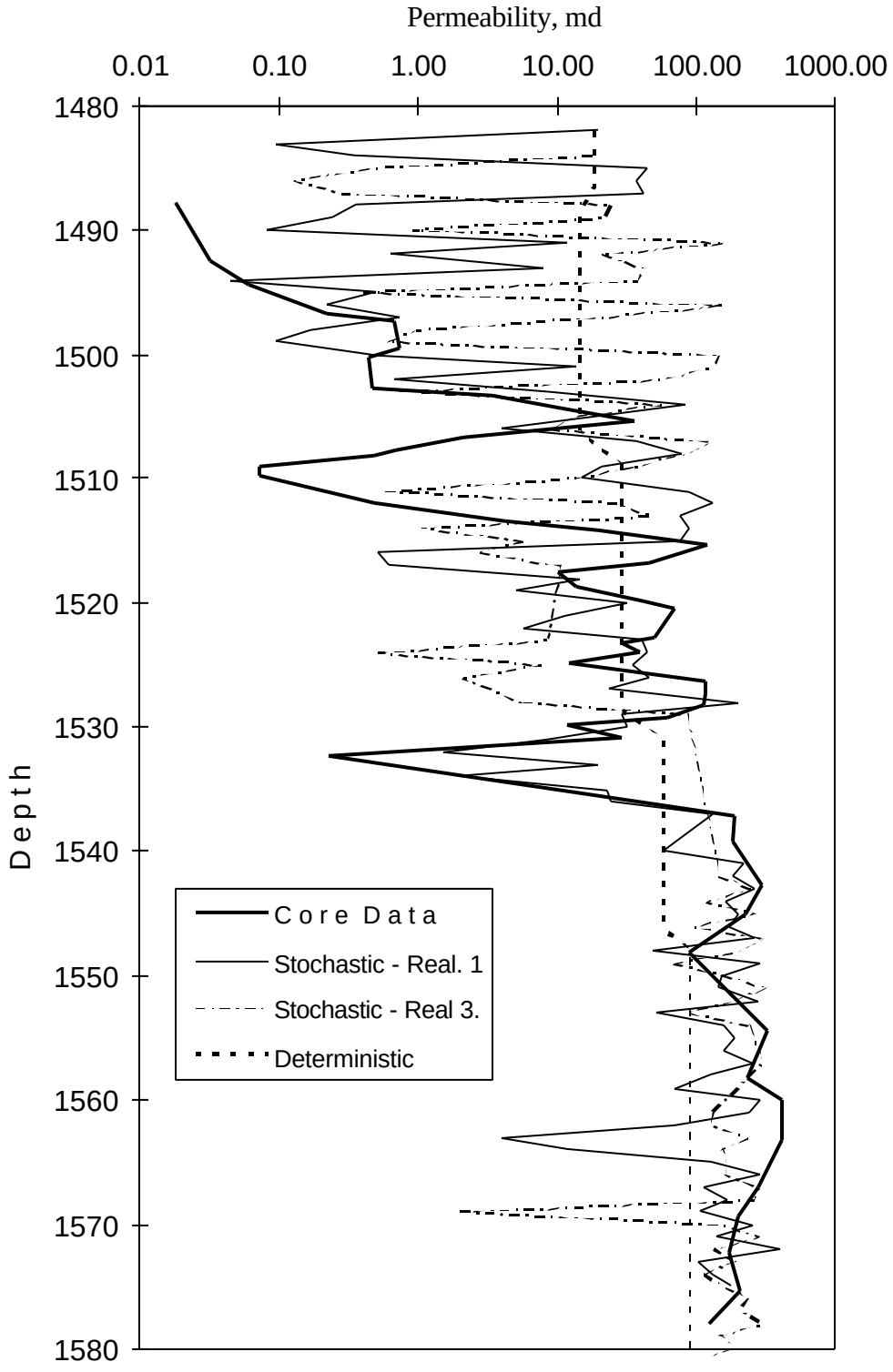

Figure 52 – Permeability comparison at Self-82 – stochastic model

To cross validate the result, the permeability-thickness product (kh) value from the model with the well test is compared. The comparison is shown in **Figure53**. Except for Well No. 61, where an anomaly was observed during the test, this figure clearly indicates that the stochastic model does a good job. The overestimated prediction of the deterministic model can be observed from the comparison presented in this figure.

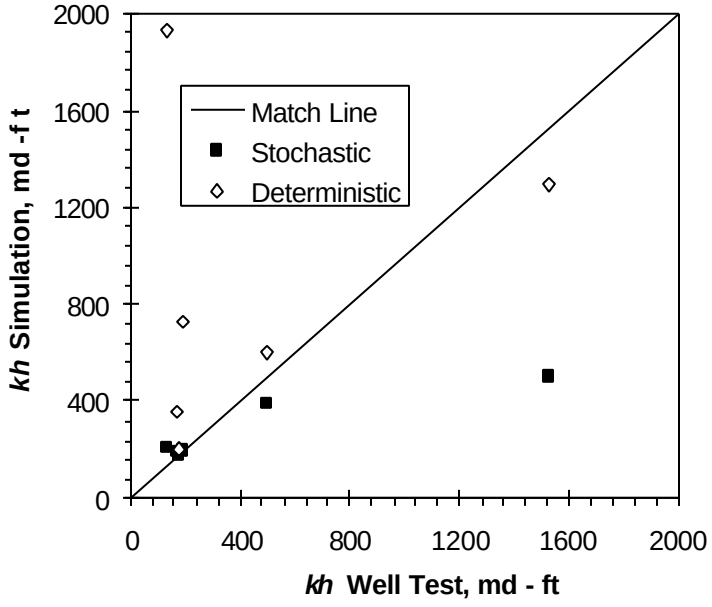

Figure 53 – Permeability – thickness (kh) comparison – stochastic model

Upscaling of Petrophysical Properties

The reservoir description generated in this model used 256,000 ($40 \times 40 \times 160$) grid blocks. This huge number of grid blocks can not be used in the flow simulation due to hardware (memory) limitations. The common number of simulator grid blocks used in the industry is in the range of 15,000 - 30,000 grid blocks. Unfortunately, the facility that was available for this study can handle only up to about 6,400 grid blocks. Thus, an upscaling process of the petrophysical properties is required before the simulation can be run. To get the total 6,400 grid blocks the configuration is reduced to $20 \times 20 \times 16$. This means that every 4 blocks in the horizontal plane have to become 1 super block, while for the

vertical direction average, every 10 blocks have to become 1 super block. All together, 40 blocks have to become 1 super block.

The upscaling of porosity was performed using a simple arithmetic average while the permeability is upscaled using the combination of arithmetic and harmonic average as follows.

1. Permeability average in either X or Y direction (Kx or Ky).

   •The permeability generated by the simulation was assumed to be the permeability in the horizontal direction ($Kx = Ky = Ksimulation$).

   •For blocks in the horizontal plane:

   -Two harmonic averages (kh_1 and kh_2) were calculated for 2 pair blocks in the direction of flow, as follows:

$$kh_i = \frac{2\,kx_1\,kx_2}{kx_1 + kx_2}$$

   -The super block average is calculated as the arithmetic average of kh_1 and kh_2, as follows:

$$k_x = k_y = \frac{kh_1 + kh_2}{2}$$

   -The arithmetic average is used to calculate the average for vertical blocks.

2. Permeability Average in Z direction (Kz)

   •Kz is assumed to be some percentage of Kx.

   •Harmonic average kh_i was calculated for blocks in the direction of flow (vertical direction).

   •The super block average for Kz is calculated as the arithmetic average of the 4-neighbor horizontal blocks.

Flow Simulation

The number of grid blocks to be used for the flow simulation as mentioned in the previous section was 6,400 ($20 \times 20 \times 16$) blocks. The dimension of each grid block in the horizontal directions (Δx and Δy) was chosen to be fixed at 132-ft. Several cases were run in the beginning of this study using a uniform size in z direction with Δz = 10-ft. It was observed that the results were not satisfactory. Thus, it was decided to run the simulation using a variable size in the vertical direction. This size is determined by observing the significant changes in the formation as given by the well log. The resulted size is as follows: 15, 15, 10, 5, 5, 5, 5, 5, 5, 5, 5, 10, 10, 20, 20, 20-ft. All of the simulation results presented below use this configuration.

The first result presented is the comparison of the initial potential of the reservoir between the simulation and the field data as shown in **Figure 54**. The bottom hole pressure used in this model is not a uniform value as was used in the deterministic model, but rather a variable value that is unique for each well. The result was derived using realization no. 1 of the reservoir description generated. It can be seen that the match is good.

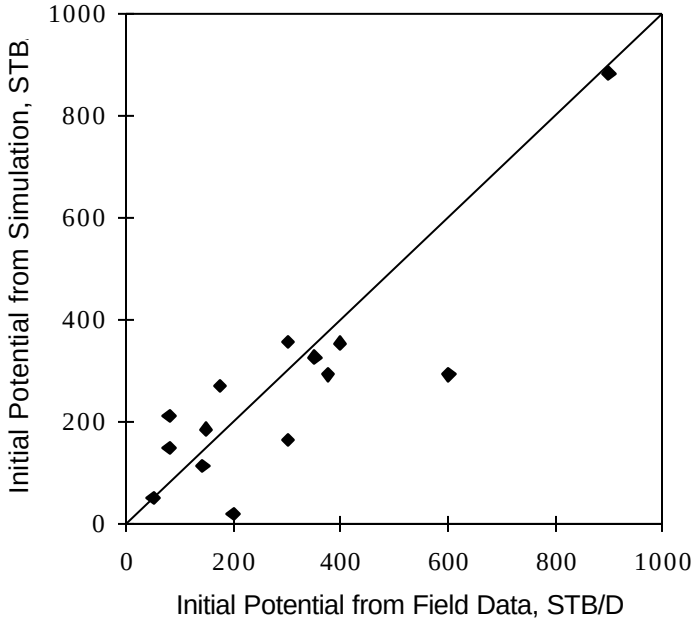

Figure 54 – Initial potential comparison – stochastic model

Figure 55 presents the field oil production rate for cases 1, 2 and 3. These cases represent use of different relative permeability curves. Similar results are observed for other realizations as well.

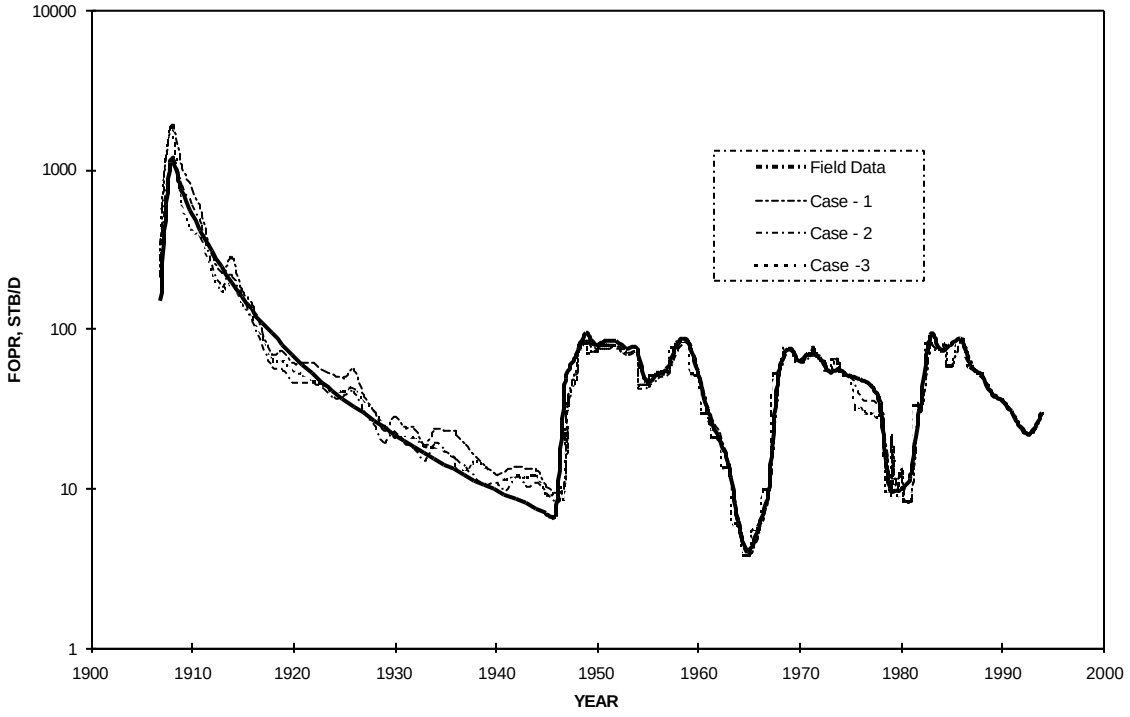

Figure 55 – Field oil production rate comparison – stochastic model

Figure 56 shows the results of OOIP and cumulative production at 1946 for different realizations and the deterministic model using case 4. The three realizations show a consistent result, even though some uncertainties can be observed. The mean value from these realizations is 11.77 MSTB, which is less than what is estimated by the deterministic model. Thus, this result shows that the deterministic model is more optimistic compared to stochastic models.

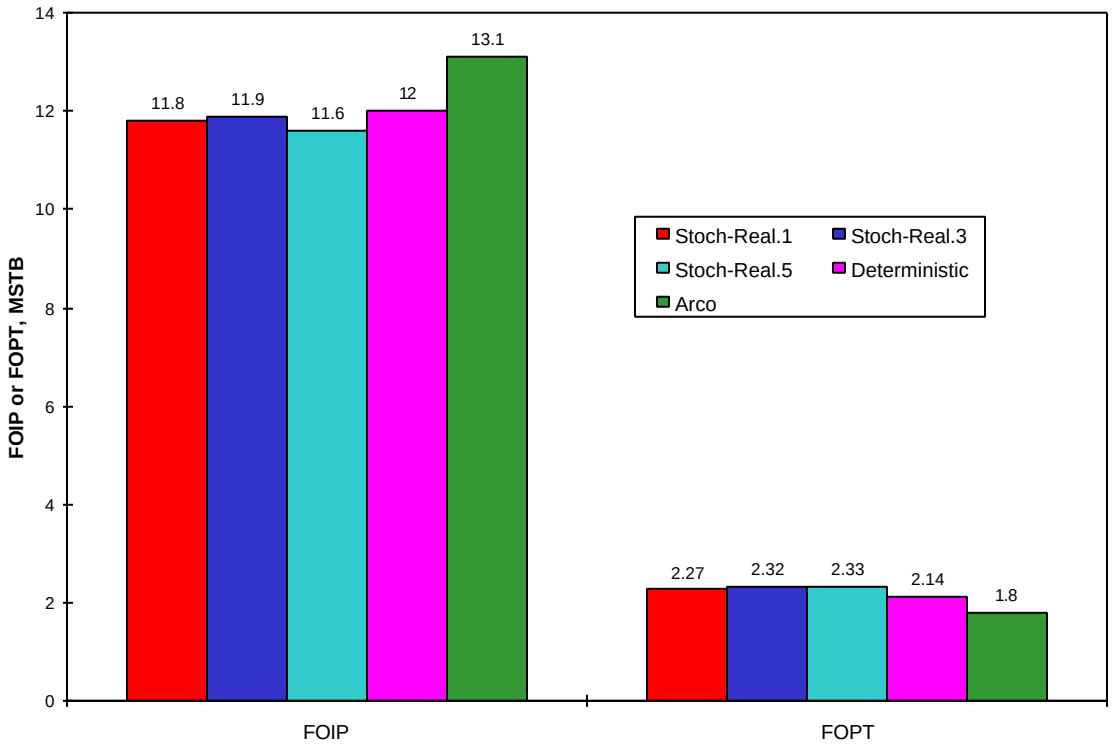

Figure 56 – Original oil in place (FOIP) and cumulative oil production (FOPT) at 1946 comparison – stochastic and deterministic models

Figure 57 shows the field water cut predicted by the simulation for different realizations. As in the deterministic model, the simulation does not match the field conditions very well. The comparison presented in Figure 57 once again supports the argument about the optimistic result of the deterministic model. Its water cut prediction is much lower (thus, the oil cut is much higher) than the ones that are predicted by the stochastic model.

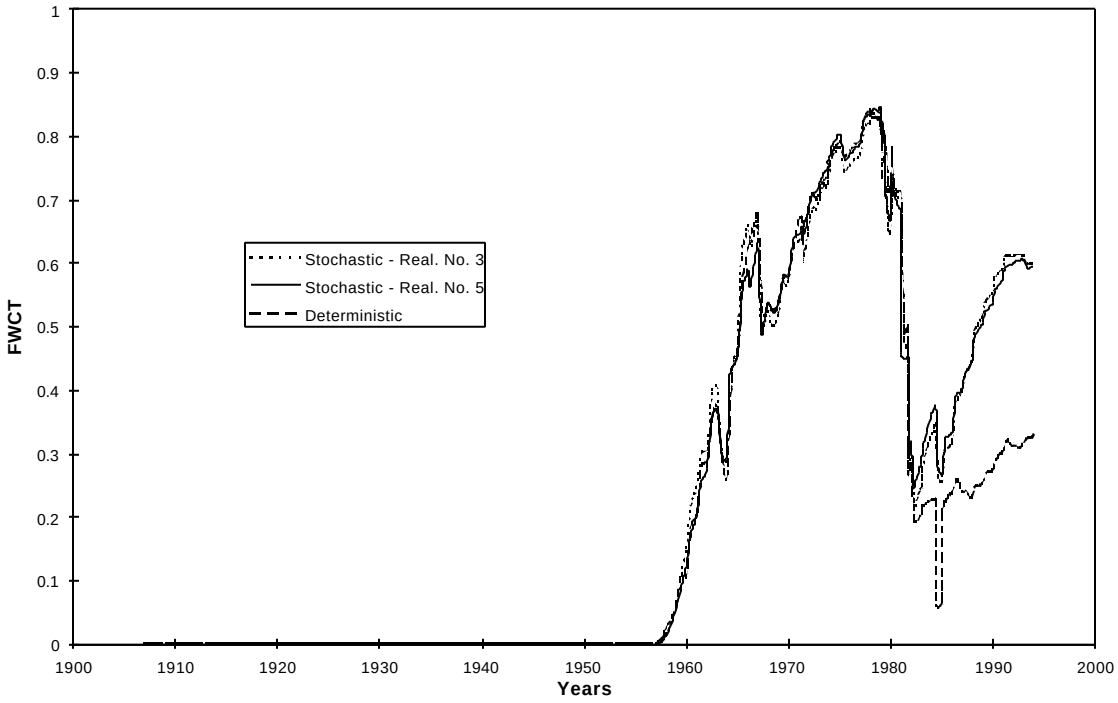

Figure 57 – Field water cut prediction for stochastic and deterministic models

The comparison of the simulation result with respect to the log data of Self-82 is presented in **Figure 58**. From this figure it can observed that the saturation heterogeneity of the reservoir was not really captured very well. This may be related to the grid resolution (number of grid blocks and its size at a particular location) that is very difficult to solve at the present condition.

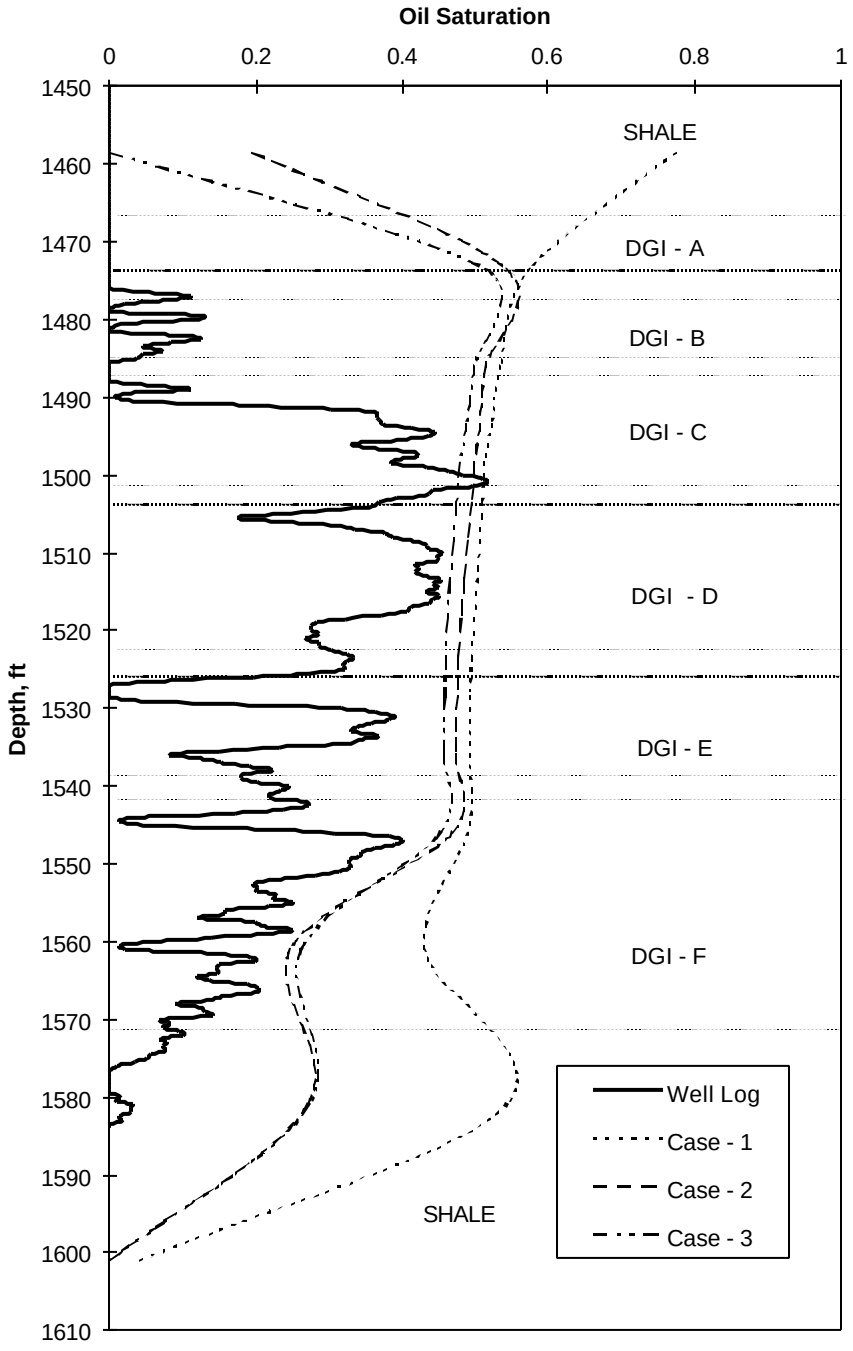

Figure 58 – Oil saturation comparison at Self-82 – stochastic and deterministic models

Summary

The stochastic model performed a very good job of capturing the reservoir description. It replicated the geological architecture very well. It matched the porosity as well as the permeability data at wells not used as conditional data and performed a reasonable job of matching the historical production performance.

Stochastic Model with Tomography Information

Porosity Description

This section presents the integration of the seismic data into reservoir description based on the stochastic model presented previously. The same geological model was used in this model but the porosity simulation contains extra information. Since the permeability description is related to the porosity distribution then the permeability distribution will also contain extra information. The term seismic in the above statement refers to the tomogram as interpreted from a series of cross well seismic field test surveys that were performed in the Self-unit between wells no. 82 - 63, 82 - 64, and 82 - 81 in January, 1994. Three tomogram panels were available for this study. The inversion of seismic data into velocity distributions at each panel was discussed in the previous section. The discussion presented here started from the assumption of known velocity distributions in each tomogram panel.

The use of velocity data in the reservoir description is related to the porosity distribution as given by the Wyllie Equation where the porosity is linearly related to the reciprocal of velocity, which is known as transit time. The main advantage of having these data is to get a better spatial relationship (variogram) in the interwell region, which is missing from the usage of log or core data alone. It was expected that the tomogram data would improve the variogram model with respect to the range of the model.

To superimpose the geology, the data were separated according to the type of the DGI at each location. In this case, the separation is not a straightforward process due to the differences in the grid block configuration. The velocity distribution had poor vertical resolution but better horizontal resolution compared to the simulated geological model. Horizontally, the changes of geology are known for every

66-ft whereas the changes of velocity are known for every 13-ft. Since the simulation of porosity follows the grid block configuration of the geological model, it was decided to take the average of 5 velocity data values before the conversion is done. On the other hand, in the vertical direction the geology is known on a one-foot interval whereas the velocity is only known for every 12-ft. For this case, no averaging process is required.

Figures 58 presents the porosity distribution at each tomogram panels after applying the correlation between porosity and transit time. It is assumed that the transit time and porosity are correlated using linear relationship. It can be observed that the layer of highest porosity occurs at the middle of the formation (DGI D). This result does not match with the observed field data where porosity increases with depth. There are two reasons that can be suggested for this result. The first one is related to the velocity distribution itself. The velocity distribution indicates that a layer of low velocity (high porosity) exists in the middle of the Glenn sand. The other reason may be that the correlation used in transforming the velocity into the porosity is not accurate. In spite of this concern, we decided to use this distribution since we wanted to preserve the information in the original form as much as possible.

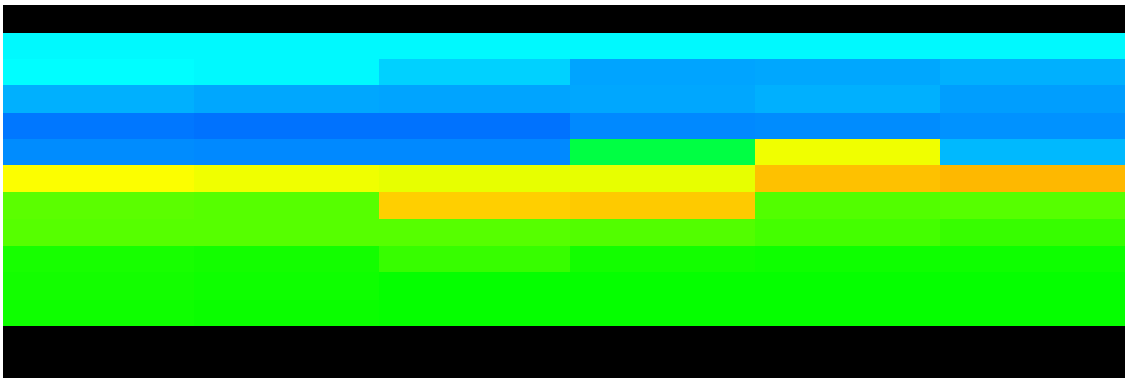

Wells 63 - 82

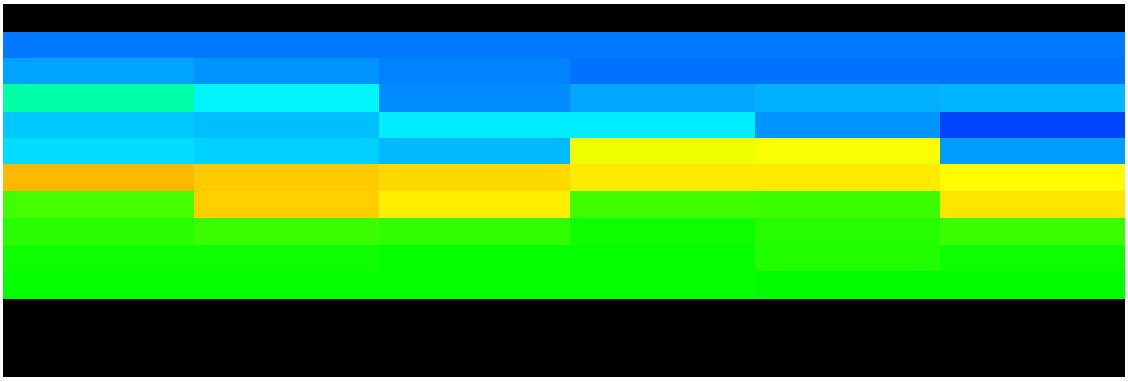

Wells 82 - 64

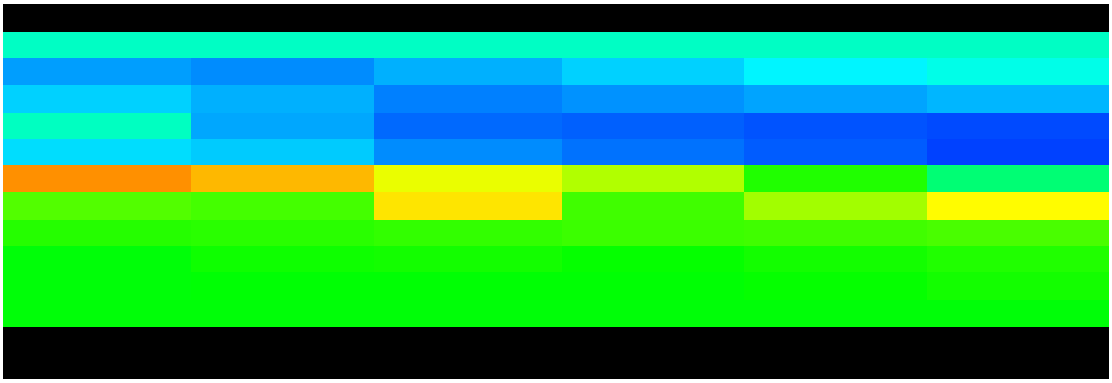

Wells 82 - 81

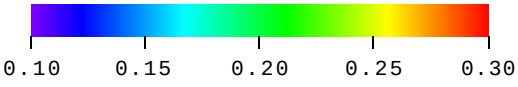

Figure 58 - Porosity distribution at tomogram panels after applying the correlations

The variograms for each DGI generated using the porosity distribution in each panel are shown in **Figure 59**. The separation of porosity of DGI's B and D from the other DGI's is due to the difference in the sill value in each DGI. It can be observed that in all DGI's the variogram of the conditional data can be represented by the spherical model. This observation is consistent with the assumed spherical model in the previous section where only limited data were used.

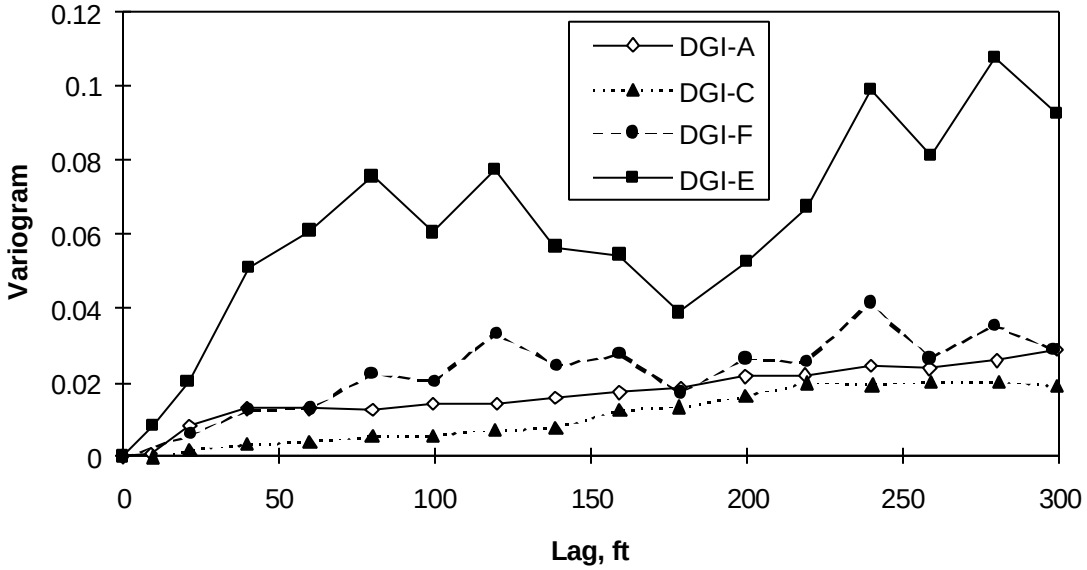

Figure 59a – Horizontal porosity variogram of the tomogram data (DGI's B and D)

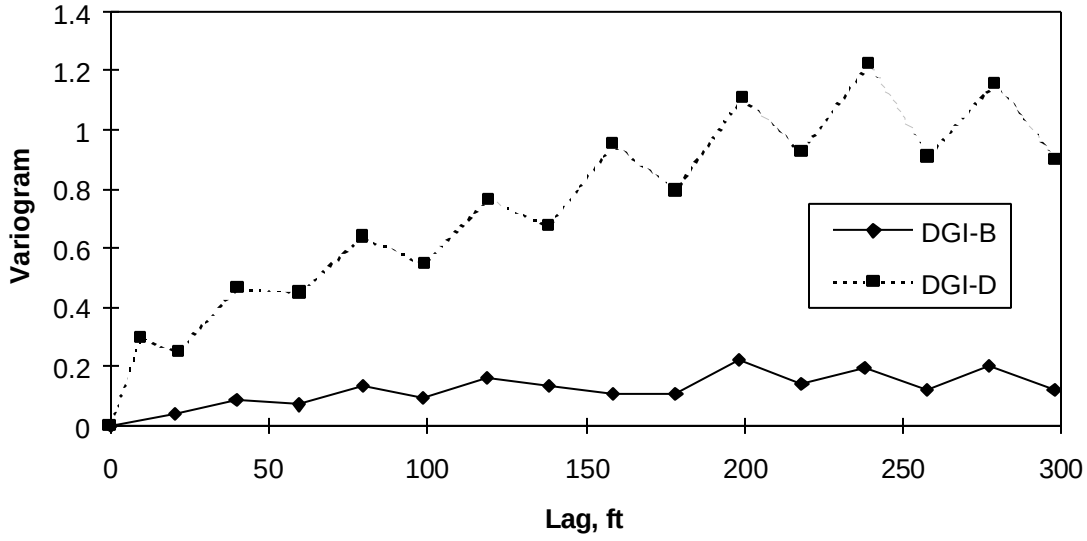

Figure 59b – Horizontal porosity variogram of the tomogram data (DGI's B and D)

The second observation that can be drawn from the variograms generated is related to the range parameter. It can be observed that the range of the porosity spatial relationship is at least the distance between two wells, i.e., about 300-ft. Thus, the assumption of using a range equal to the distance of the

closest well pair can also be justified. This assumption was used for DGI's B, E and F. The porosity variogram for DGI's A, C, D was modeled previously using soft geological information where the range is assumed to be a number that is greater than the distance between the wells and is related to length of the channel-fill in each DGI. Thus, this assumption can also be justified.

The simulation of the porosity distribution was conducted using the same method as discussed before. The only difference between this distribution and the previous one is in the conditioning data. The variogram models are the same since the assumptions used previously are justified.

The comparison of the porosity at Self-82 is presented in **Figure 60**. In general the match of porosity at Self-82 from this model can be considered good except in the zone of DGI D where two peaks occur. This discrepancy may be due to the high velocity region in the D zone found from the velocity distribution.

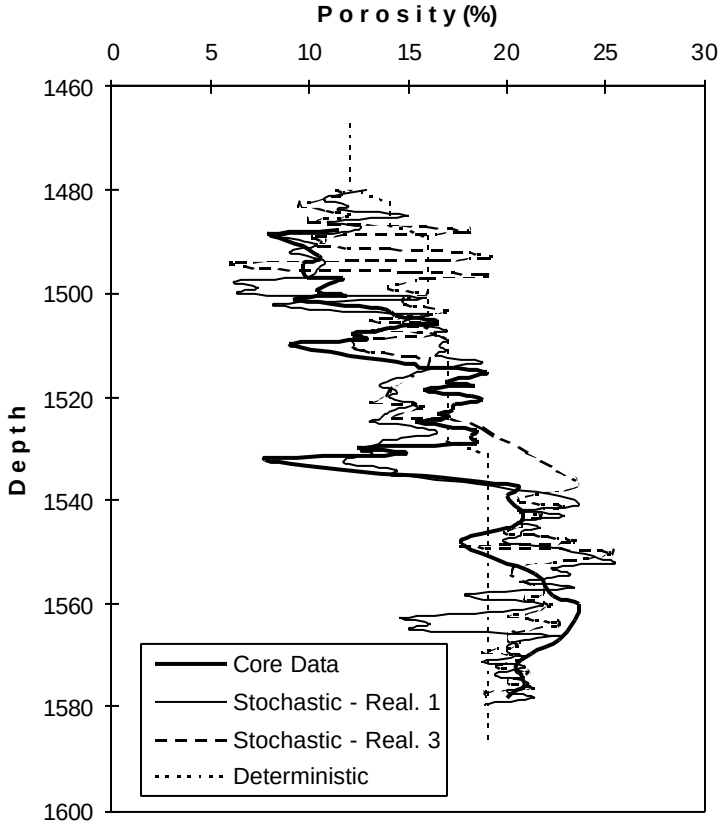

Figure 60 – Porosity comparison at Self-82

Permeability Description

Following the same method used previously, the permeability distribution was generated using the conditional distribution method where it is calculated using the distribution function of the permeability in a given porosity class.

The comparison of the permeability at Self-82 is presented in **Figure 61**. This figure shows that the model with tomogram data performed a better job than the model without the tomogram data. This statement can be verified by observing the top and bottom zones. In the top zone, the previous model (no tomogram) tends to give a higher value whereas the present model (with tomogram data) remains in the range 0.1 to 1 md. The core data show a very low value. At the bottom interval, the present model follows the core data consistently whereas the previous model predicted a layer with a lower permeability value. At the middle of the formation, both models give the same result.

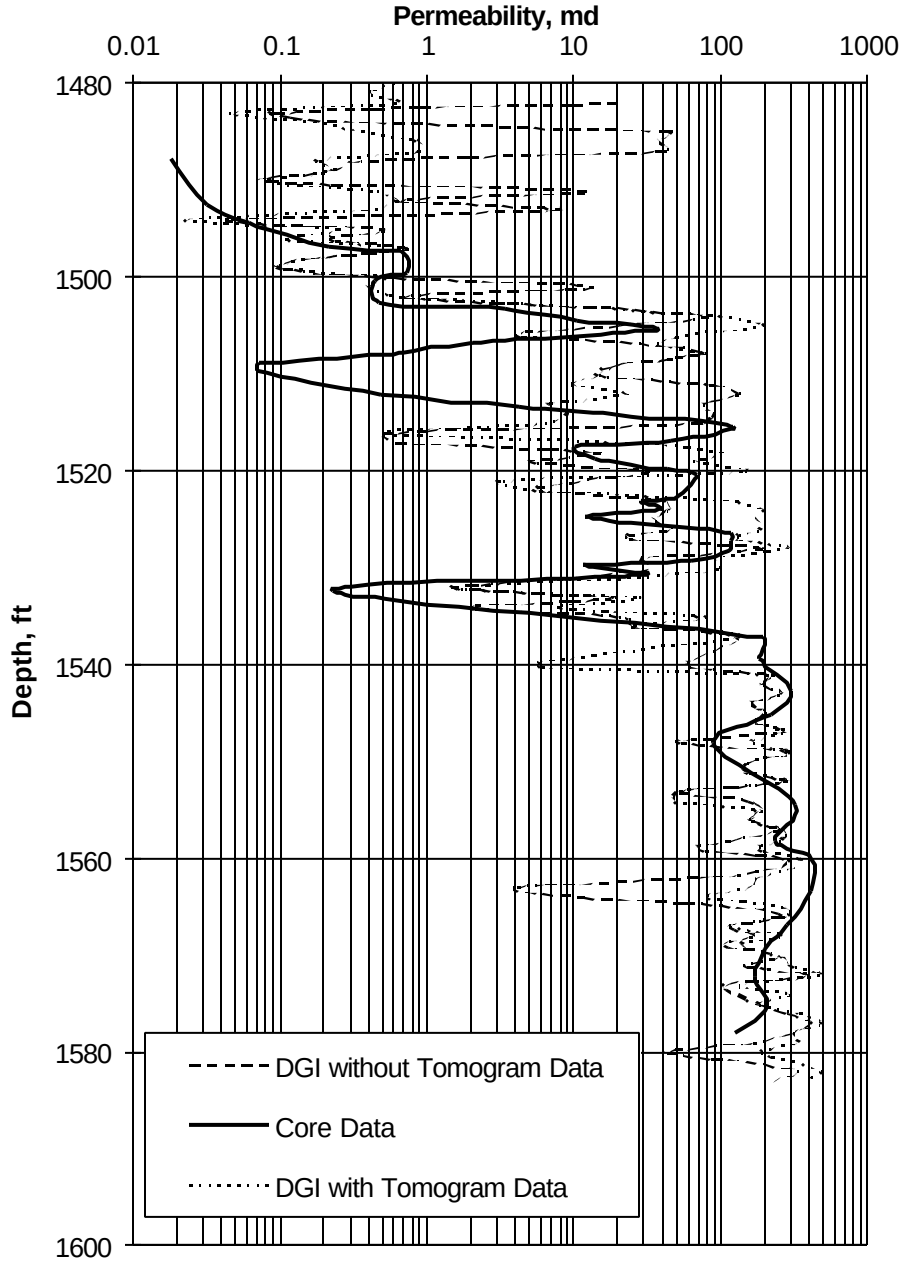

Figure 61 – Permeability comparison at Self-82

The validation of the permeability distribution generated using this model is done by comparing the product of permeability and thickness (kh) as was done for each model. This comparison is presented in **Figure 62**. This figure clearly indicates that the tomogram model performs an excellent job. The matches are good for all wells including the result of well No. 61 where a kh value of 1,530 md-ft was

calculated from the well test and the model predicted 1,405 md-ft. This figure is an important illustration of the principle that addition of different information reduces uncertainty in the reservoir description.

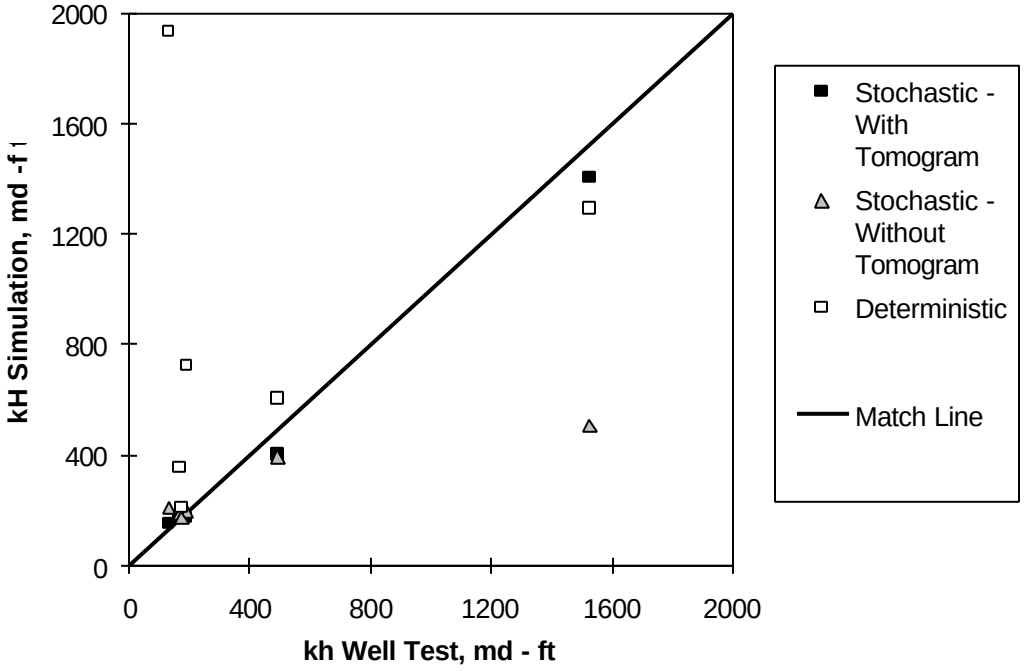

Figure 62 – Permeability – thickness (*kh*) product comparison – all models

Flow Simulation

Figure 63 presents the field oil production rate predicted by the simulation. For the early period, the tomogram model shows a slightly higher production rate compared to the non-tomogram model. The higher production rate for the same relative permeability curve may be due to the higher initial oil in place, which means a higher pore volume generated from the reservoir description. To see if this is the case, **Figure 64** compares the original oil in place calculated using several models. It can be seen that the tomogram model estimated the most optimistic original oil in place.

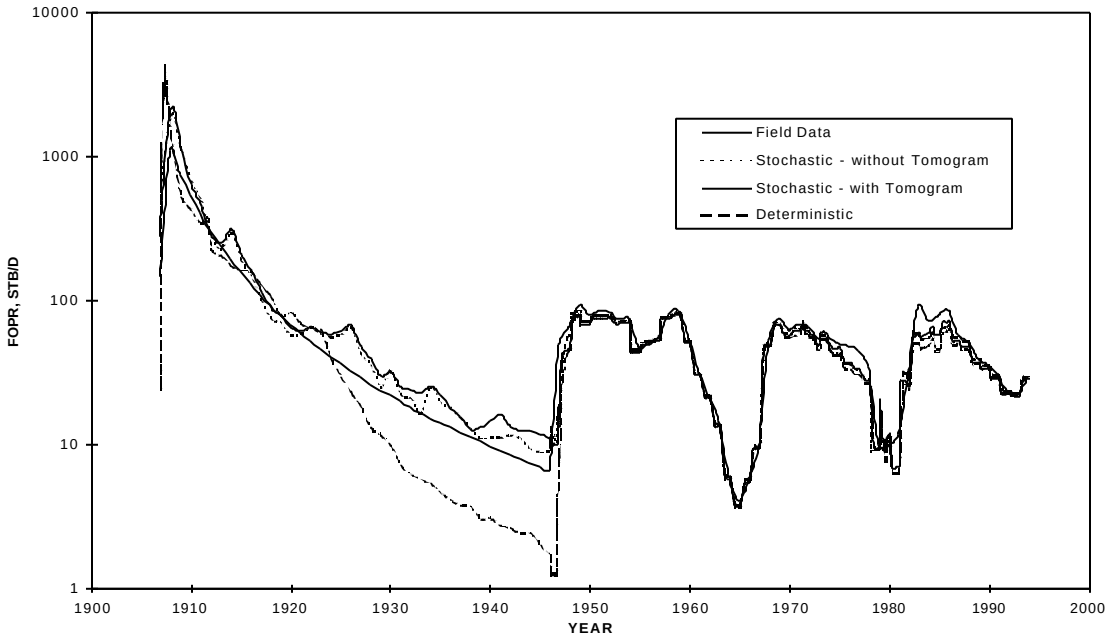

Figure 63 - Comparison of field oil production rate (FORP) – all models

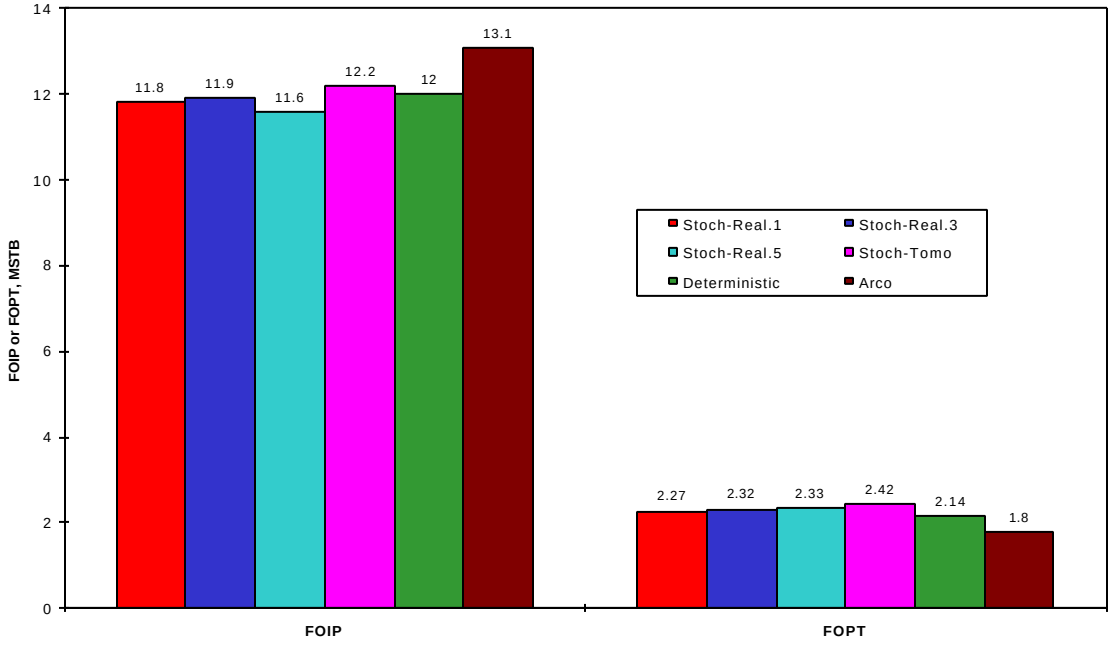

Figure 64 – Comparison of original oil production rate (FOIP) and cumulative production at 1946 for different models

Figure 65 compares the field water cut predicted using this model with respect to the other models. It can be seen that the two stochastic models give about the same prediction of water cut during the life of the reservoir even though it does not match very well with the field data. The deterministic model remains the optimistic model since it predicts the lowest water cut while the field was operated with a very high water cut.

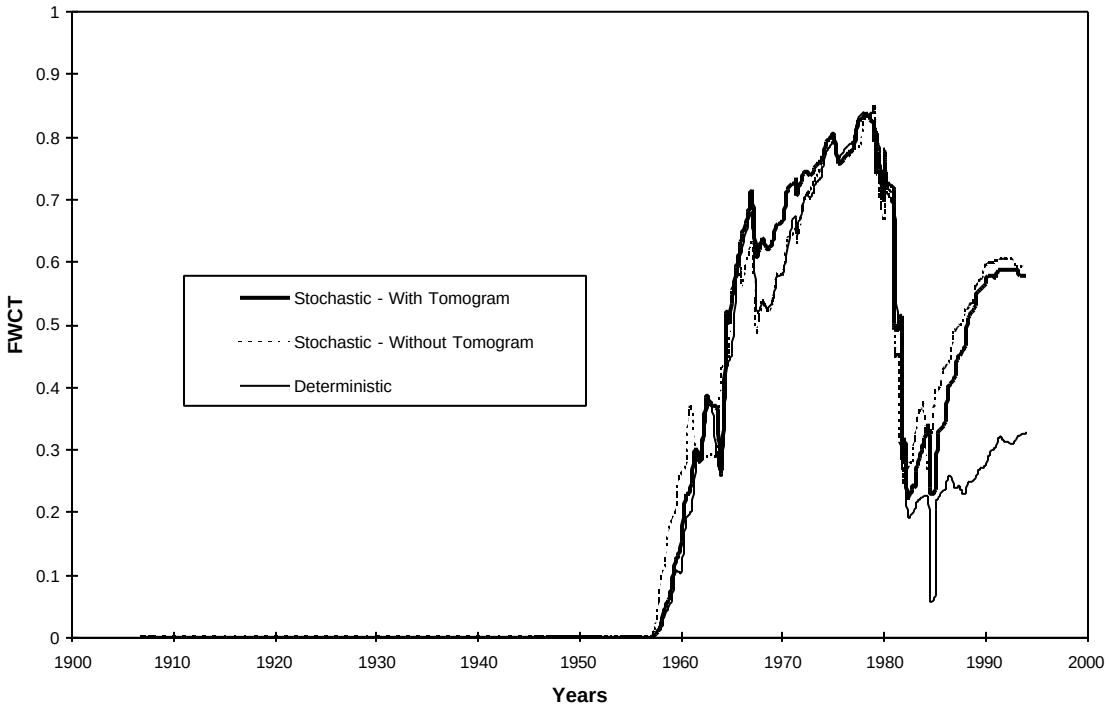

Figure 65 – Comparison of field water cut – all models

Finally, the comparison between the simulated and the measured oil saturation at Self-82 is presented in **Figure 66**. As it is shown in this figure, there is no significant difference among the models with respect to the oil saturation at Self-82. The three models do not follow very well the heterogeneity of the oil saturation profile. This is mainly due to the resolution of the grid blocks configuration.

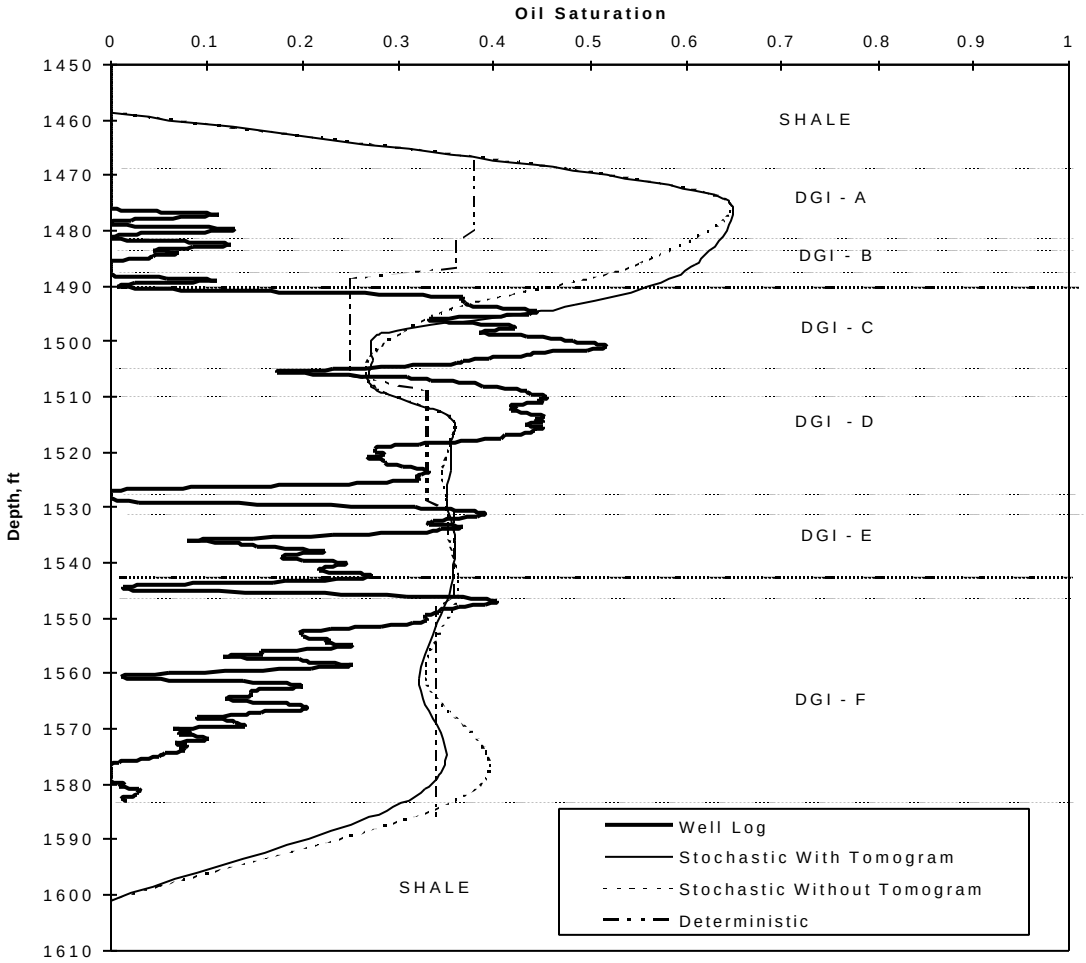

Figure 66 – Comparison of oil saturation at Self-82 – all models

Summary

To summarize the findings in this model, the tomogram data could be incorporated into the reservoir description through velocity porosity transformations. The main use of the tomogram data in this model was to estimate the variogram models used in the previous model. It was found that the spherical model was adequate for the modeling purposes and the range of the porosity variogram was not less than the distance between two wells. In general, the results were in good agreement with the other stochastic model except for the permeability distribution where the model with tomogram data performed a much better job. Especially, the dynamic reproduction of the well test permeability data was much improved

after incorporating the tomogram data. This indicates that additional information can improve the reservoir description.

Reservoir Management

The overall goal of the study is to improve the secondary recovery performance through the use of a better reservoir description and better reservoir management. This section presents the analysis that led to the reservoir management plan of the Self-unit for future production. The analysis started with the discussion of the future production forecast using three different scenarios for three reservoir description models discussed in the previous sections, i.e., the deterministic model, the stochastic-model without tomography information, and the stochastic model with tomography information. The three scenarios are:

1. Drilling no additional wells.
2. Drilling a horizontal well.
3. Drilling new vertical production wells.

Each scenario was related to the well completion and the water injection rate. To cover several possibilities of this configuration, several sub-scenarios were defined within each scenario. The flow simulation was run for each sub-scenario until the year 2000 and the increase of production (if any) was compared with the base case which is the simulation with current field conditions (based on 1993 data).

Following the flow simulation, an economic analysis was performed for several selected sub-scenarios that would give the best increase of production. The analysis was based on the data provided by Uplands Resources, Inc. Conservative estimates are used for the cost of production to avoid over optimistic forecasts of the profits. The best scenario was determined by the rate of return and the payout time as criteria based on a constant oil price at the current level of $17.00 per barrel.

Future Production Forecast

The definition of each sub-scenario (presented in **Table 4**) was determined based on the following two reasons: the Self-unit was completed very well at the middle to the bottom interval (DGI's D and E),

and it was feasible to increase the injection rate. Since the deterministic model predicted relatively high permeability and high oil saturation in DGI's A and B then these two DGI's cannot be ignored for this model. Thus, for the deterministic model the future forecast also include DGI's A and B in addition to DGI's D and E whereas for the stochastic model only DGI's D and E are to be considered for recompletion. The exclusion of DGI C is due to the relatively low permeability (in both models) and the fact that it has been opened within most of the Unit. The DGI F was excluded from any sub-scenario since it has been flushed by water as observed on the flow simulation runs.

Table 4 – Definition of sub-scenario used in future production forecast	
Name	Description
Scenario - 1A	Open well 82 as producer Convert well 81 as producer
Scenario - 1B	Reopen DGI's* at all wells Base Injection rate
Scenario - 1C	Current perforation Double injection rate
Scenario - 1D	Reopen DGI's* at all wells Double injection rate
Scenario - 1E	Reopen DGI's* at all wells Triple injection rate
Scenario - 2A	Horizontal injection well with injection rate of 1000 BWPD, Reopen DGI's*, double rate at old wells
Scenario - 2B	Horizontal injection well with injection rate of 2000 BWPD, Reopen DGI's*, double rate at old wells
Scenario - 2C	Horizontal injection well with injection rate of 3000 BWPD, Reopen DGI's*, double rate at old wells
Scenario - 2D	Horizontal injection well with injection rate of 3000 BWPD, Reopen DGI's*, base rate at old wells
Scenario - 2E	Horizontal producer well Reopen DGI's*, base rate at old wells
Scenario - 3A	4 new vertical wells (producer) Base rate at old wells
Scenario - 3B	4 new vertical wells (producer) Double rate at old wells

*Reopen DGI's means: Reopen DGI's A, B, D, and E for deterministic model and DGI's D and E for stochastic model

The possibility of increasing the injection rate was based on the data from 1992 and 1993 where the production increased 38% (from 21 BOPD to 29 BOPD) when the field was flooded with a 125% higher injection rate. This fact suggested that the field responded to an increase in the amount of water

injected. We expect that, in the future, by increasing the water injection rate, we can increase the oil production.

Scenario 1: Drilling No Additional Wells / Current Field Configuration

From Table 4, there are 5 sub-scenarios defined for scenario 1, i.e., scenario 1A through 1E. For each of these sub-scenarios, the results of the 4 case studies (defined in Table 3) of the stochastic model without the tomogram data are presented. For the purpose of comparison and also to evaluate the uncertainty of the result, case 4 is run using scenario 1D for other models, i.e., deterministic, stochastic description without tomogram for 3 realizations, and stochastic description with tomogram data. The result is presented at the end of this section.

Figures 67-71 present the result of scenario 1A through 1E respectively. The result of scenario 1A shows that there will be no increase of production if this scenario is applied in the Unit. Thus this scenario can be ignored. Figure 63.B shows that the range of additional oil production that can be expected by implementing scenario 1B is between 10 to 16 barrels of oil per day. In this scenario, case 4 shows almost a steady performance whereas the other cases seem to decline faster. In scenario 1C the first three cases predicted almost the same result, but case 4 is very pessimistic. A contrasting performance can be observed by comparing the result of case 4 between scenarios 1B and 1C. This result indicates that case 4 is more sensitive to the opening of new intervals (scenario 1B) than to increasing the injection rate (scenario 1C).

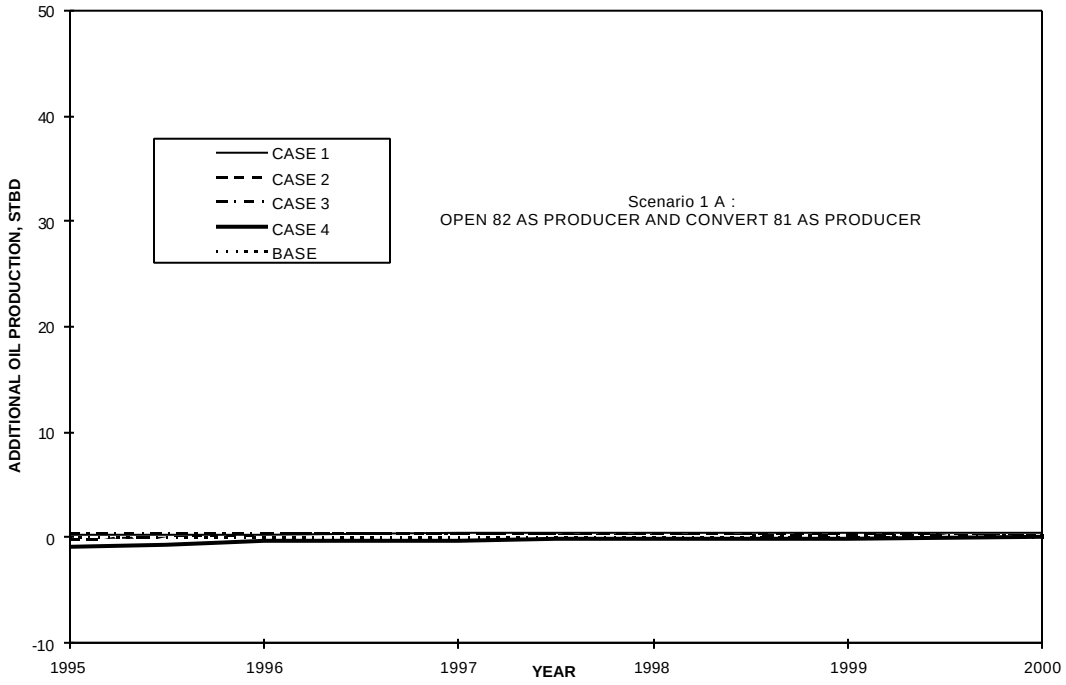

Figure 67 - Increase of oil production using scenario 1A

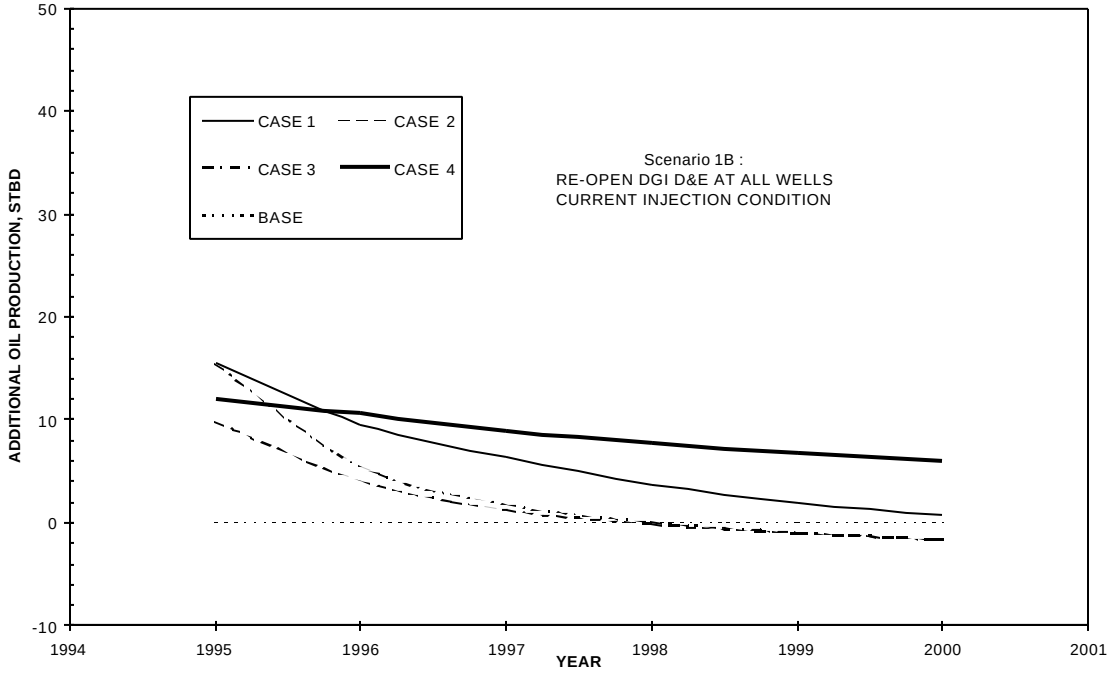

Figure 68 - Increase of oil production using scenario 1B

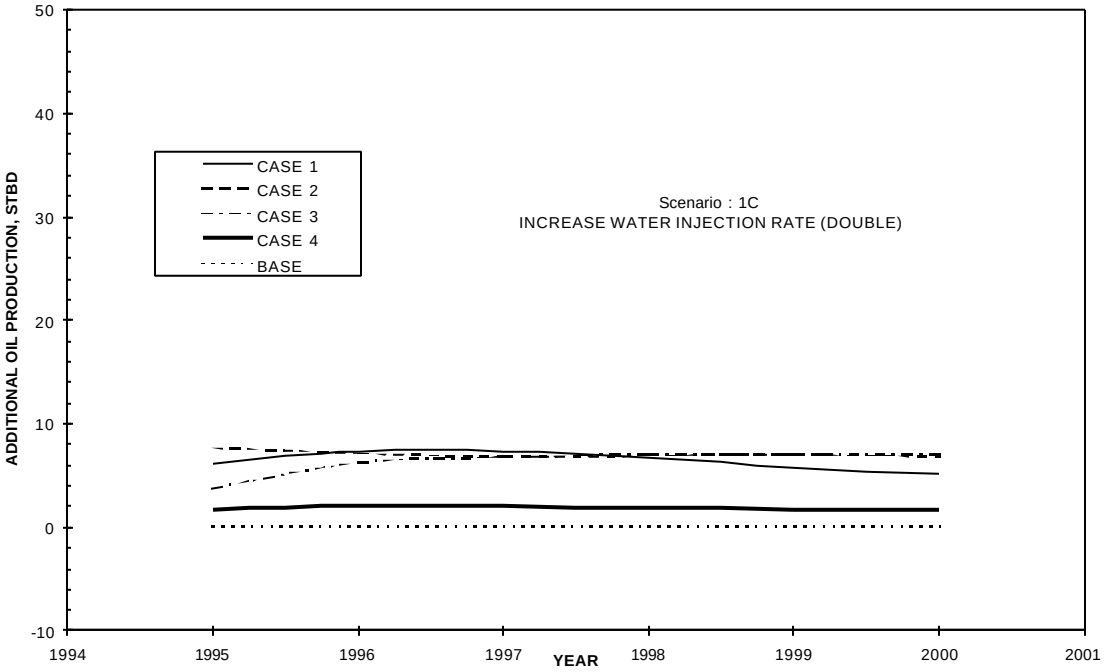

Figure 69 - Increase of oil production using scenario 1C

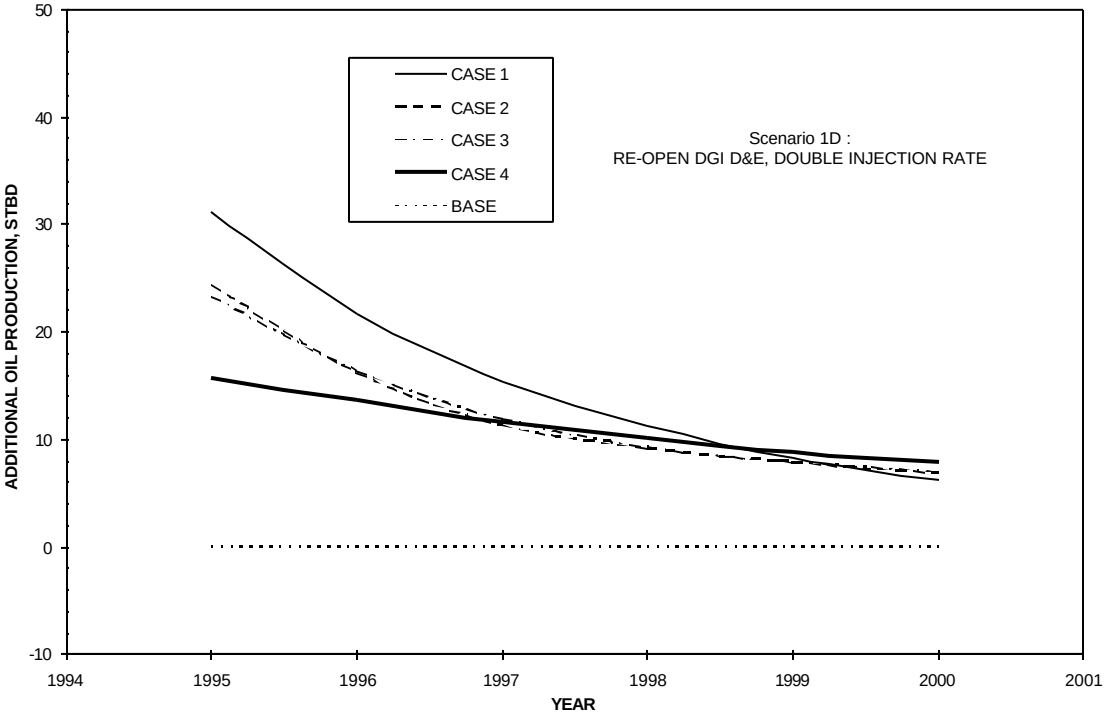

Figure 70 - Increase of oil production using scenario 1D

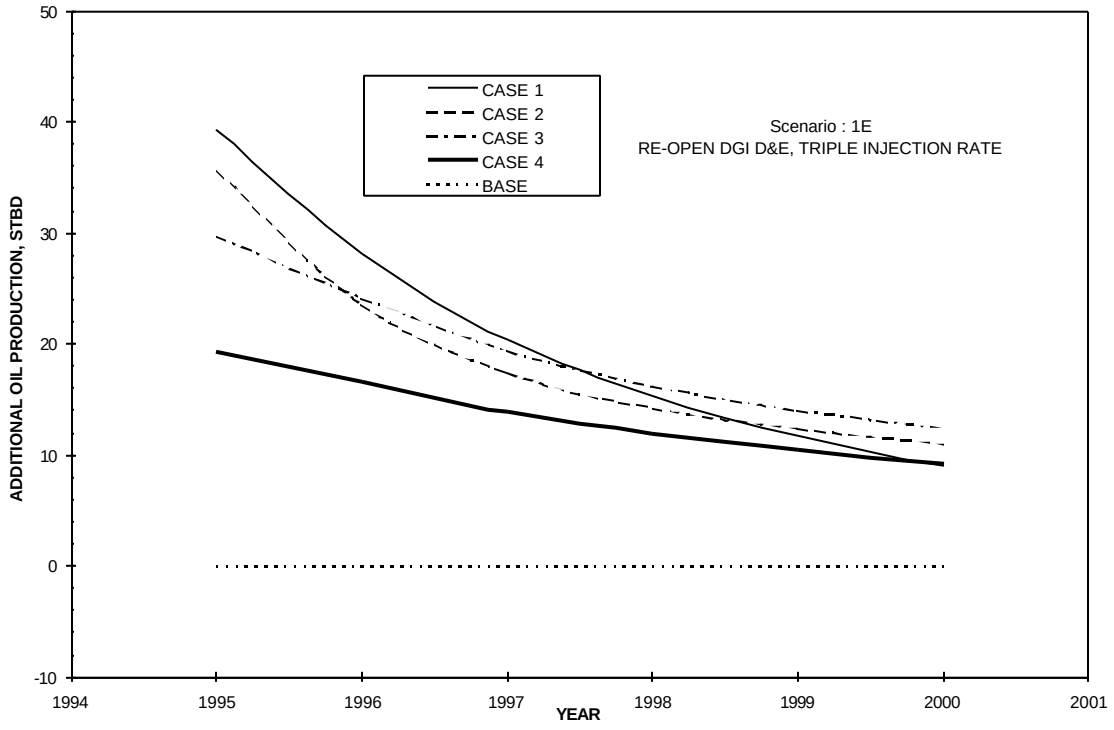

Figure 71 - Increase of oil production using scenario 1E

The result of scenario 1D, which is the combination of scenarios 1B and 1C, shows the combined effect of the previous two scenarios. It can be seen that more additional production can be expected from this scenario. Thus, by simultaneously opening DGI's D and E and increasing the injection rate, a better result will be achieved. Scenario 1E shows the effect of higher injection rate. Intuitively, the result should be better and this is proved from Figure 71. Overall, it was concluded that significant increase of oil production can be obtained if the formation is reopened at DGI's D and E and simultaneously the water injection rate is increased.

The comparison of the simulated future production for different models using scenario 1D - case 4 is presented in **Figure 72**. There are two important points that can be concluded from this figure. First, the stochastic model demonstrates its capability of giving an estimation of the uncertainty (for a given set of information) of the future production whereas the deterministic model predicts only one value. The increase of oil production from the stochastic model ranges from 18 - 21 barrels of oil per day in 1995

whereas from the deterministic model this value is 21 barrels of oil per day. Secondly, the deterministic model is more optimistic. It can be seen that at any time in future the deterministic model always provides a higher prediction.

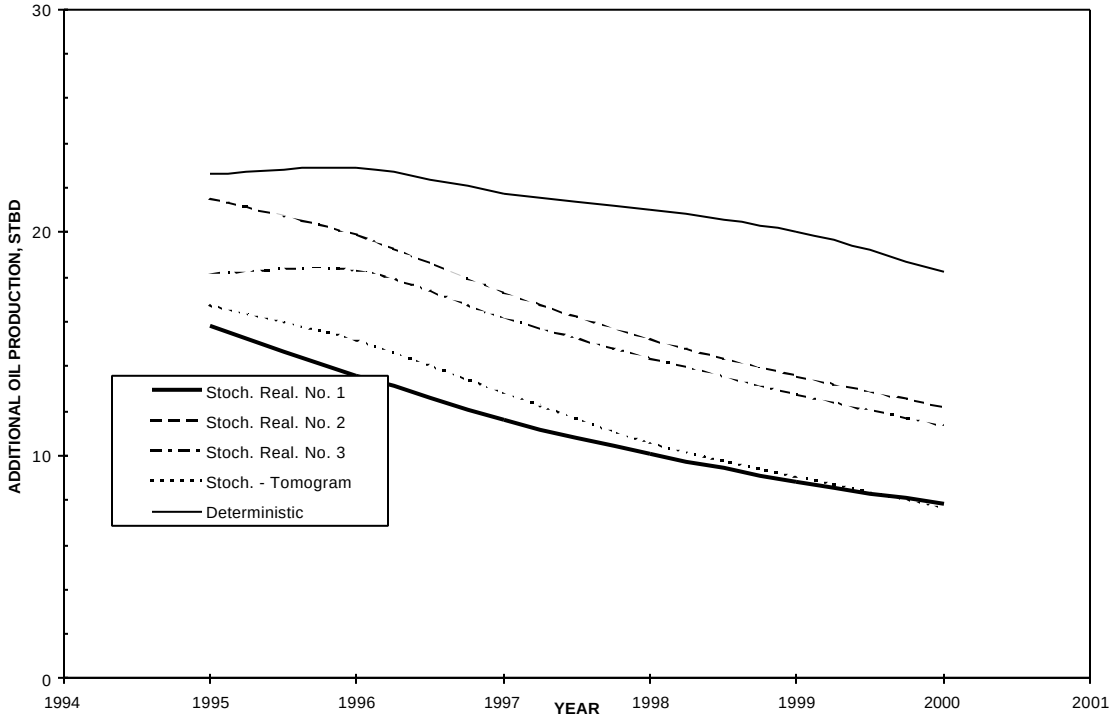

Figure 72 – Comparison of additional oil production – all models

Scenario 2: Drilling Horizontal Well

The purpose of this scenario was to explore the feasibility of drilling a horizontal well in the Self-unit. This prediction is very critical since the cost of drilling a horizontal well is very high (cost ~ $400,000). We investigated the effect of three sub-scenarios as defined in Table 5. The first one is related to the amount of injection rate either in the horizontal well or at other wells if this horizontal well is to be used as the injector. The second one is to see the effect of re-completing other old wells. The last one is to see whether the horizontal well should be an injector or producer.

The horizontal well investigated in this study is located in the vicinity of the Self-82. The simulation has been run for 3 different areal locations and 6 different vertical positions, but no significant difference in

the results is observed. **Figures 73-77** present the results of scenario 2A through 2E respectively. Figures 73-75 show the effect of injection rate in the horizontal well on the production performance. It can be observed that only a slight increase of additional production can be obtained. Figure 76 shows the effect of injection rate at the old wells. It can be observed that the result of case 4 almost remains the same. This result is also observed in scenario 1, where case 4 is more sensitive to reopening DGI's than increasing the injection rate. In addition, this result also shows the importance of opening DGI's simultaneously with increasing the injection rate. Finally, Figure 77 shows that an injector horizontal well is preferable to a producer horizontal well.

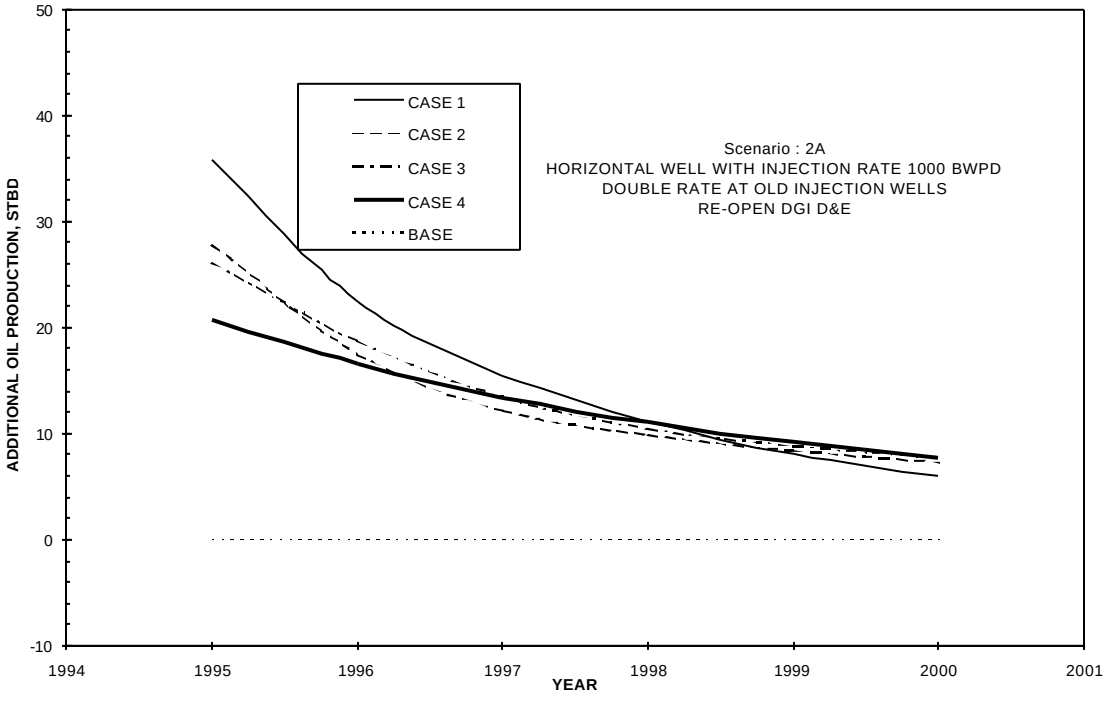

Figure 73 - Increase of oil production using scenario 2A

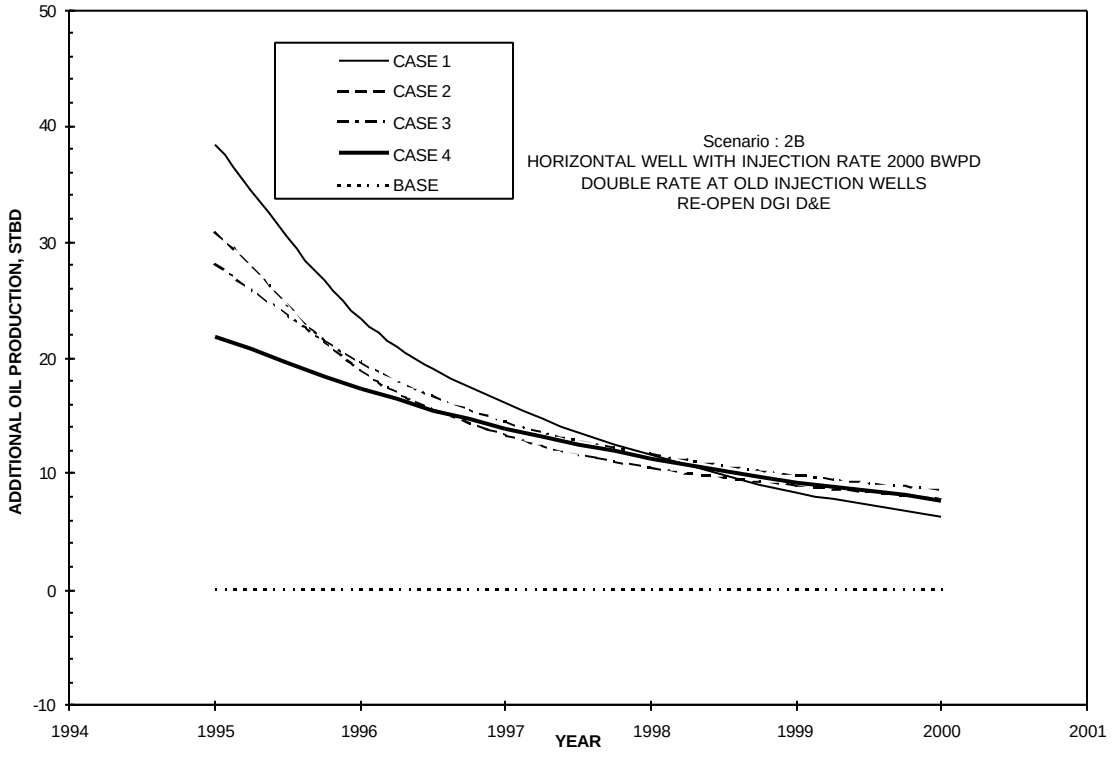

Figure 74 - Increase of oil production using scenario 2B

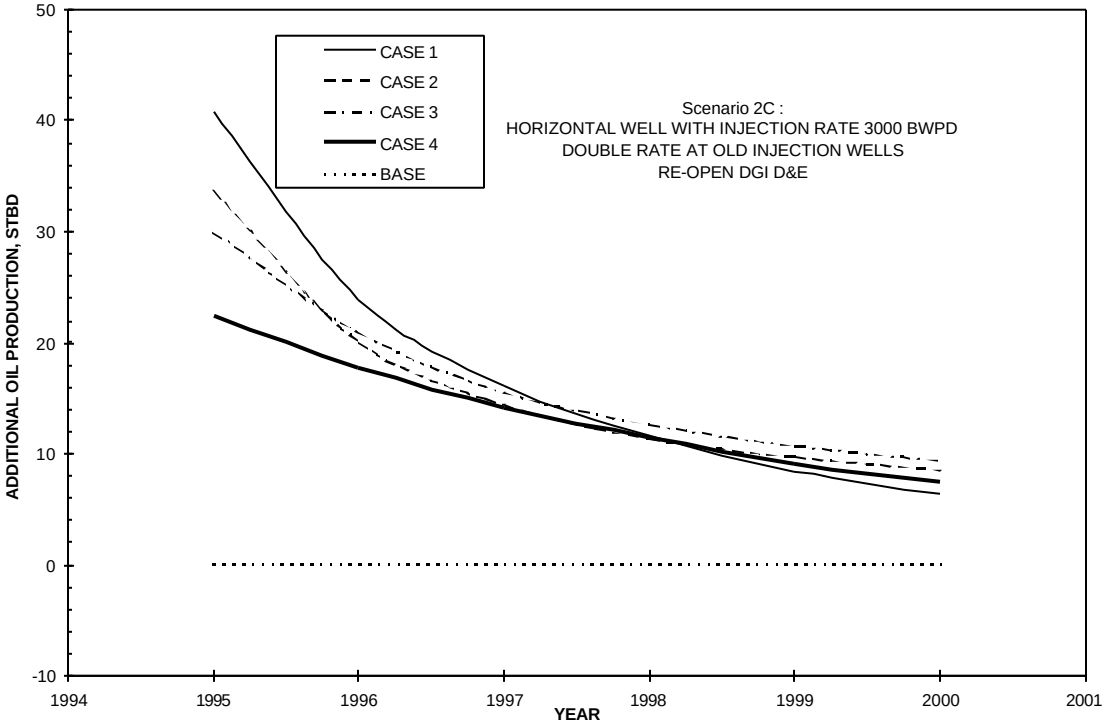

Figure 75 - Increase of oil production using scenario 2C

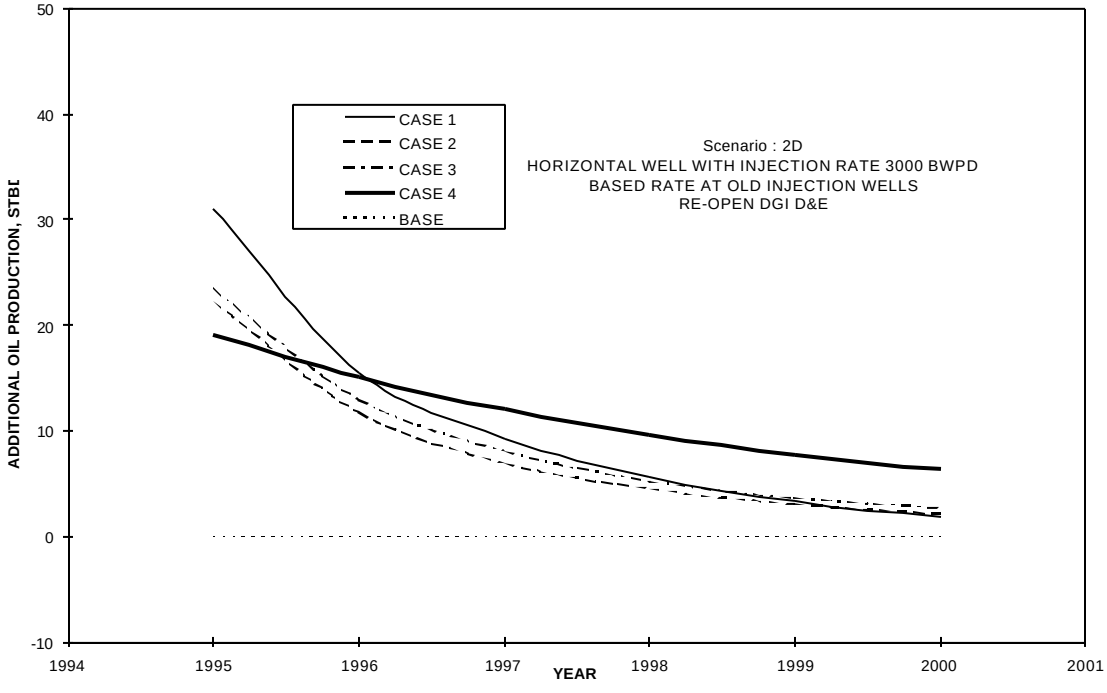

Figure 76 - Increase of oil production using scenario 2D

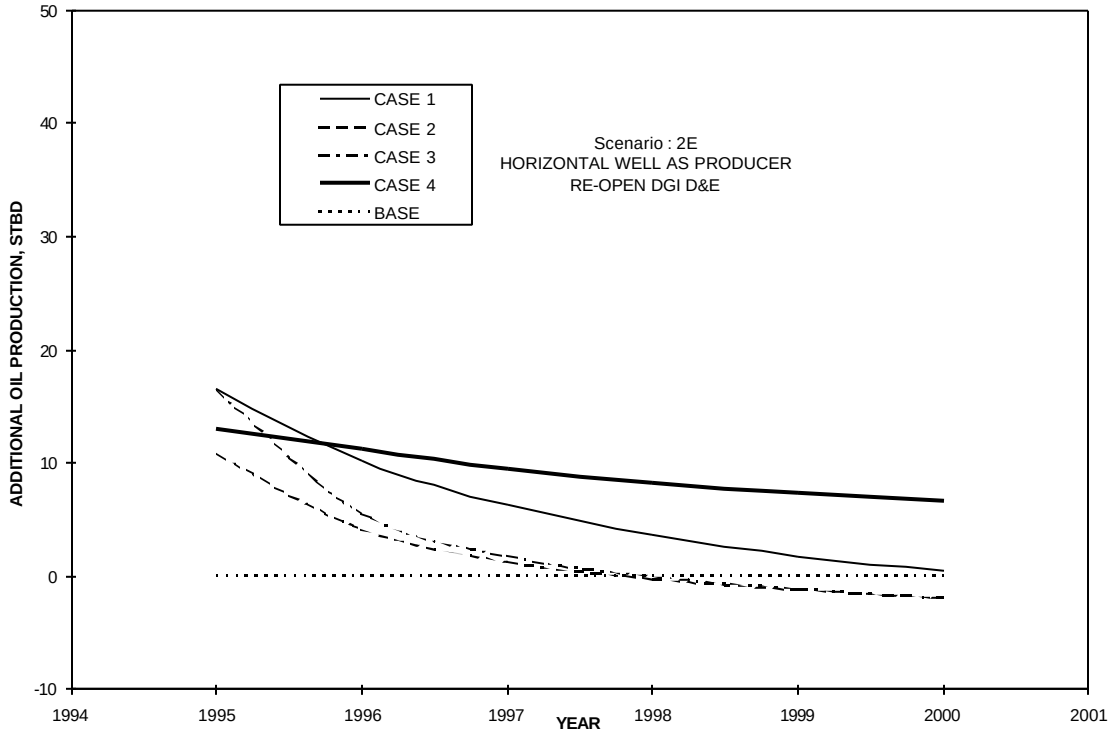

Figure 77 - Increase of oil production using scenario 2E

Overall, excluding scenarios 2D and 2E, the additional oil production from this scenario ranges between 21 - 41 BOPD whereas the range for the first scenario is 16 - 39 BOPD. It was evident that drilling horizontal well does not provide significantly better performance compared to the first scenario. Intuitively, this additional oil production would not have been able to cover the cost of drilling a horizontal well at the existing level of oil price.

Scenario 3: Drilling New Vertical Production Wells

An additional 4 vertical wells were used in this simulation. The locations were determined based on the oil saturation map and also by considering the vacant space that exists in the Self-unit. **Figures 78-79** show the simulation for this scenario. The conclusion about the importance of increasing injection rate as found from the previous scenarios could also be observed from this scenario by comparing the results of scenarios 3A and 3B. From Figure 78 it can be observed that the overall additional oil production using this scenario is about the same as for the previous scenarios, which ranges from 18 to 37 BOPD.

Thus, there is no significant increase in oil production after implementing this scenario. Comparing the results of the three scenarios, it was concluded that the best alternative from an economic standpoint is scenario 1 since there are no drilling costs associated with this scenario.

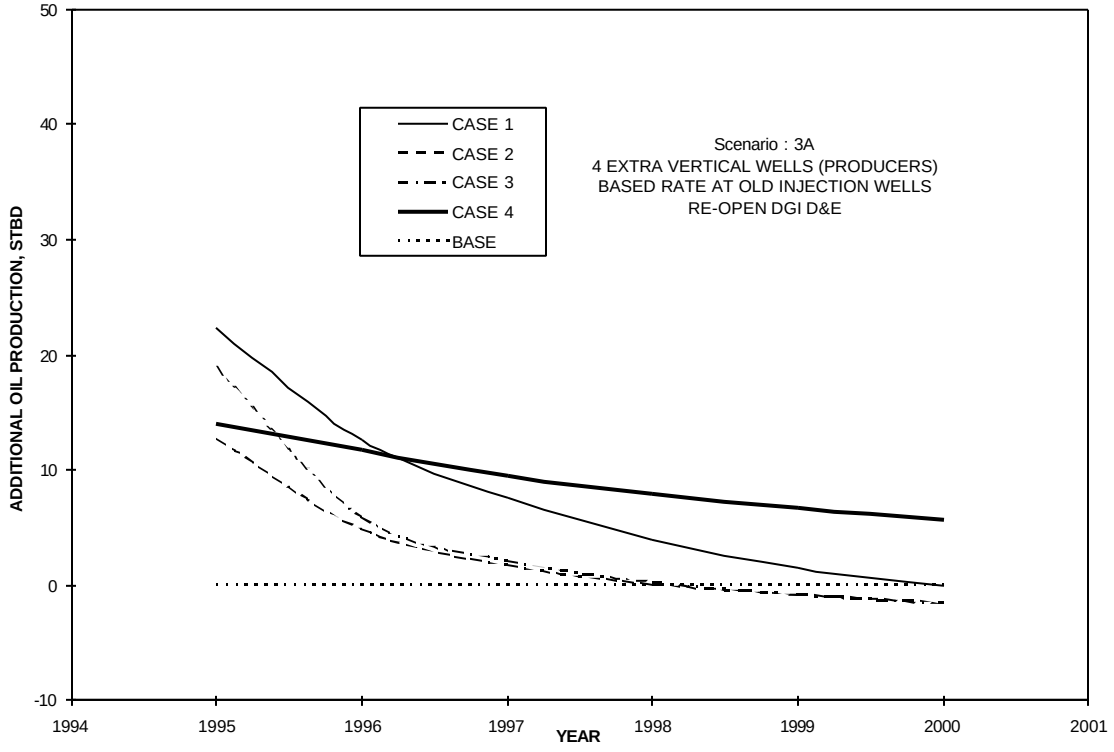

Figure 78 – Increase of oil production using scenario 3A

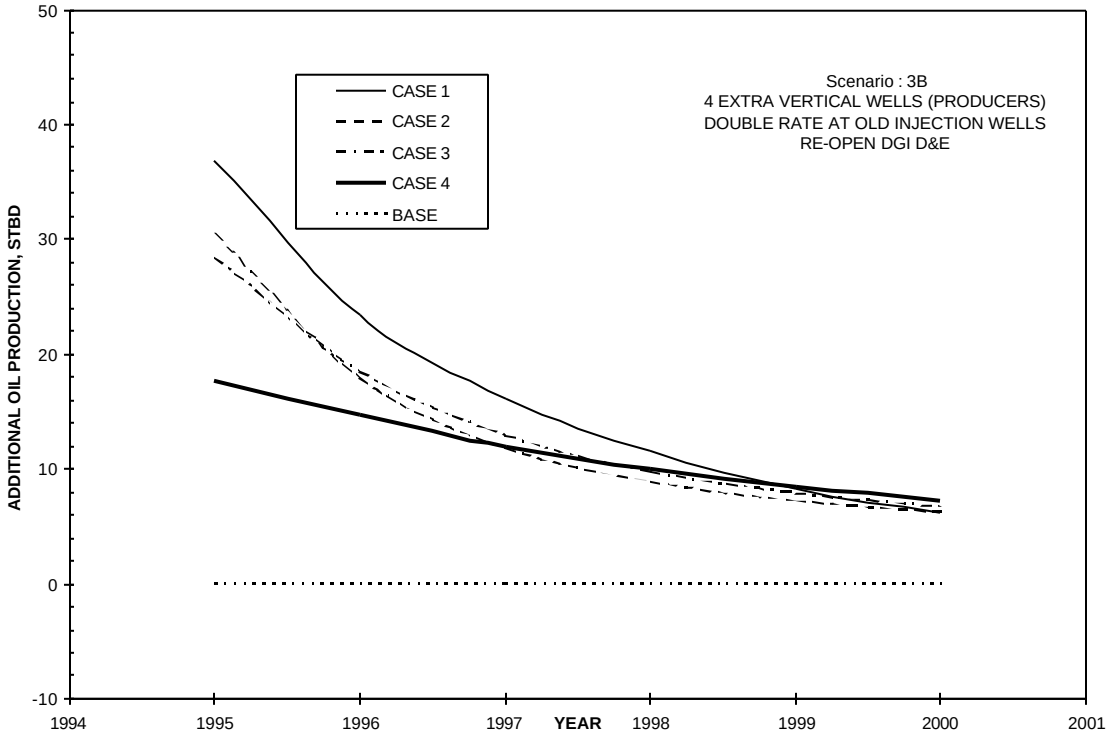

Figure 79 – Increase of oil production using scenario 3B

Economic Analysis

As mentioned previously, the criteria used in the economic analysis are the rate of return and the pay out time. These parameters were calculated using the first scenario (except scenario 1A) which was found to be the only scenario that is feasible for the Self-unit. Before this calculation is performed, the simulations were rerun for another 4 years so that a 10-year projection can be made. The revenue was calculated using the constant oil price of $17.00 per barrel. The capital and operating costs were provided by Uplands Resources, Inc. The capital cost includes the cost to improve the water injection system that is capable of doubling or tripling the injection rate and the cost that is related to opening new intervals (perforation, stimulation, etc.). The fixed cost to improve the water injection system is $87,495, whereas the cost to reperforate DGI's D and E is predicted as $61,600. The fixed cost provided is applicable to tripling the injection rate.

The operating cost is mainly due to chemical treatment of water, electrical, and maintenance costs. This cost varies significantly for the Self-unit. It ranged between $6 per bbl of oil to $9 per barrel of oil during 1993-1994. The value of $9.50 per barrel of the produced oil is considered to be a conservative estimate under current conditions. In this study, this value is used for the condition where no increase of injection rate is applied (scenario 1B). For the scenario where the injection rate is to be doubled (scenario 1C and 1D), the operating cost of $10.50 per barrel of produced oil is used. For scenario 1E (tripled injection rate) the operating cost is assumed as $11.50 per barrel of produced oil.

Figure 80 presents the different rates of return (ROR) estimated for the 4 case studies using 4 different scenarios (1B through 1E). The ROR shown in Figure 80 is the rate of return for the period where the production is still profitable (non-negative cash flow). **Figure 81** presents the result of pay out time predictions for the cases investigated.

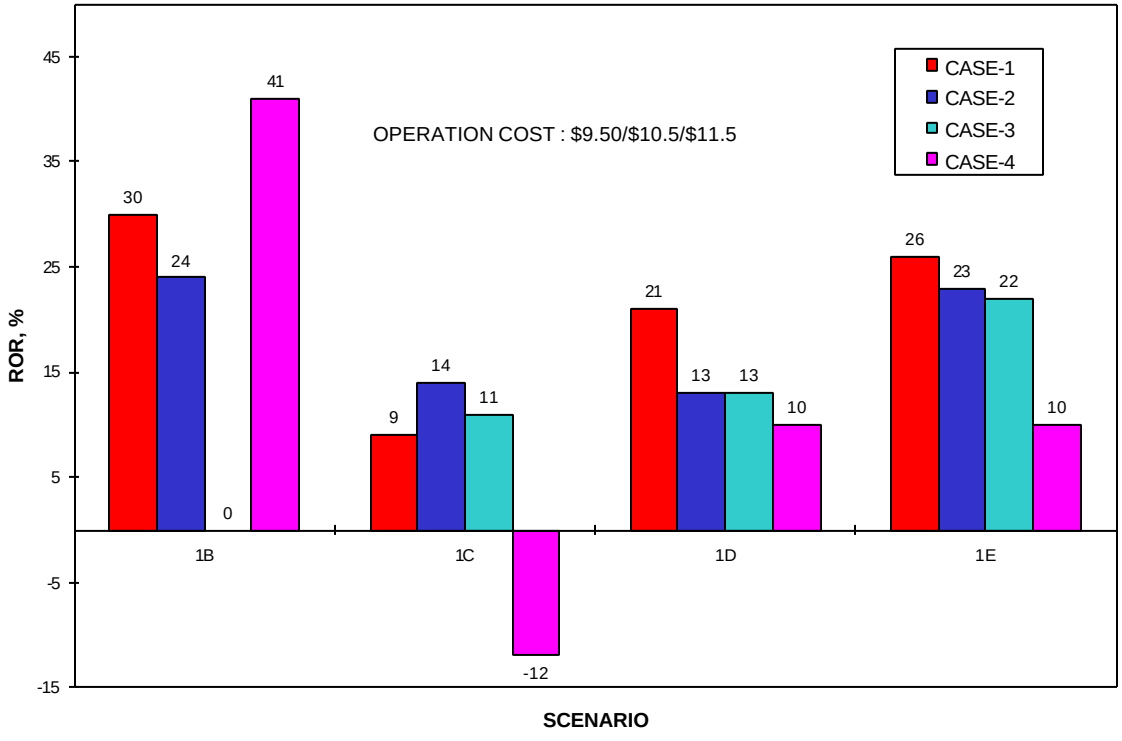

Figure 80 – Rate of return estimation for different case study stochastic model without tomography information

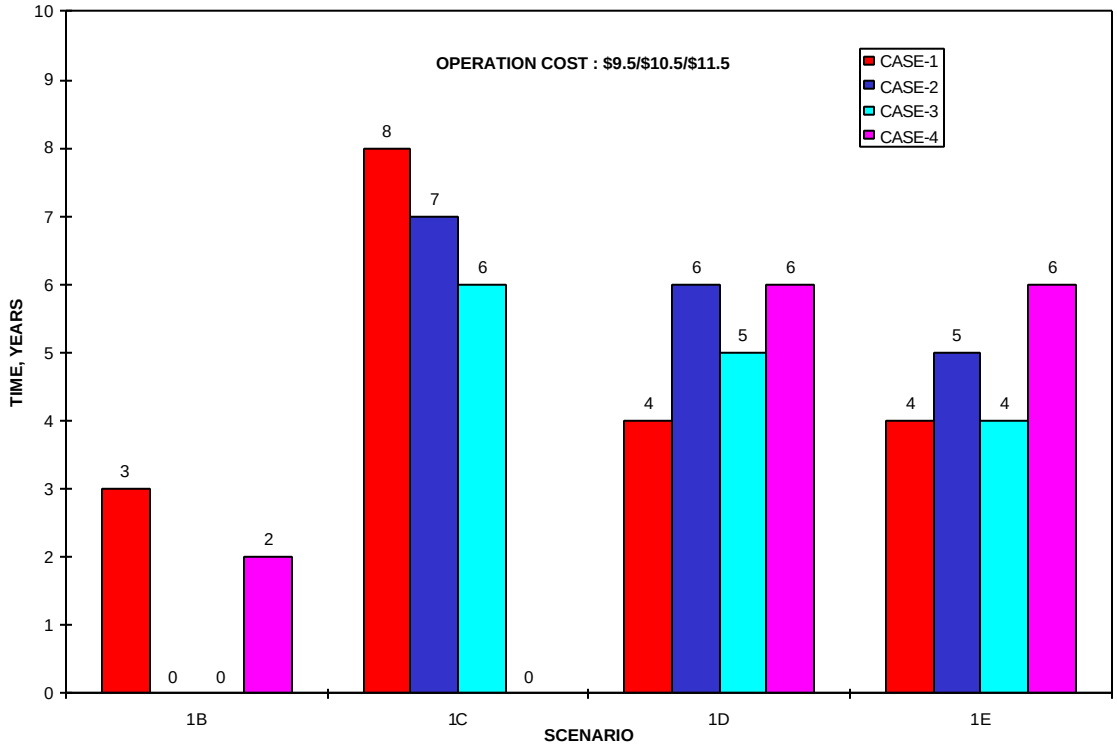

Figure 81 – Pay out time estimation for different cases stochastic model without tomography information

As Figure 80 indicates, the highest ROR is indicated from scenario 1B. This is mainly due to the lowest capital costs (equal to the cost of reopening DGI's D and E only). But the uncertainty among the four cases in this scenario was significant. To further examine the effect of the operating cost, a sensitivity study was conducted by increasing the operating cost by $1.00, so that it becomes $10.50 / $11.50 / $12.50 for no increase in injection rate, double injection rate, and triple injection rate respectively. The result is shown in **Figure 82**. It can be seen that scenario 1B is not very stable (negative ROR for case 2 and 3) and very sensitive to the operating cost. **Figure 83** presents the effect of oil price on the ROR prediction. It can be seen that in order for this scenario to work the oil price can not be lower than $15.00 per barrel.

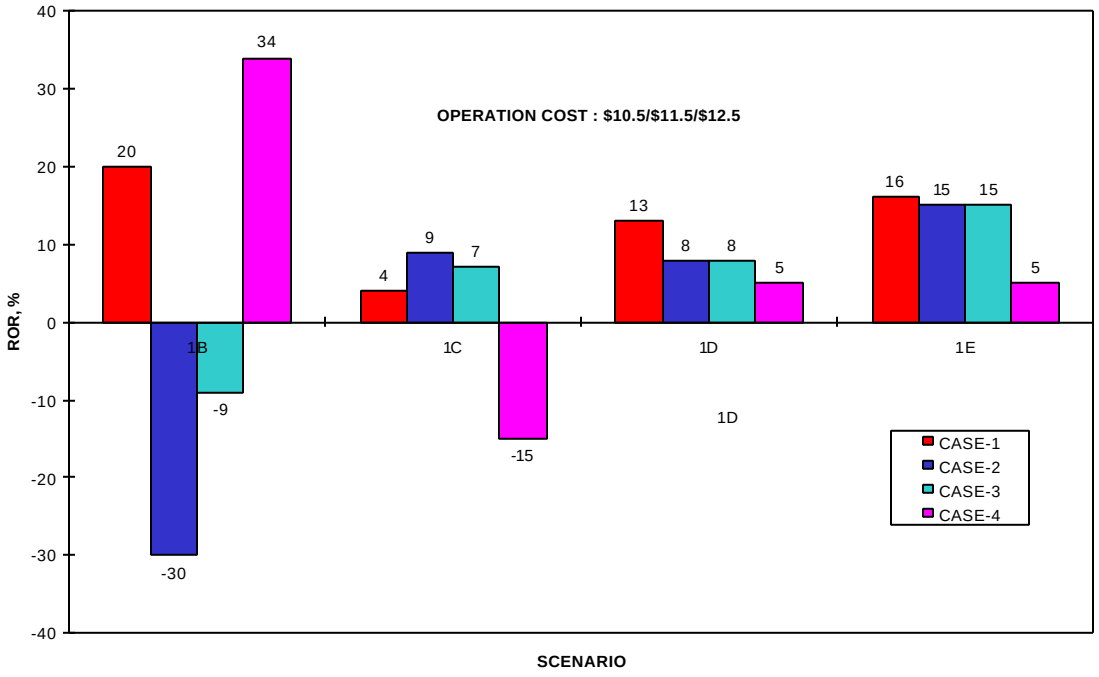

Figure 82 - Rate of return estimation for higher operating cost - DGI model

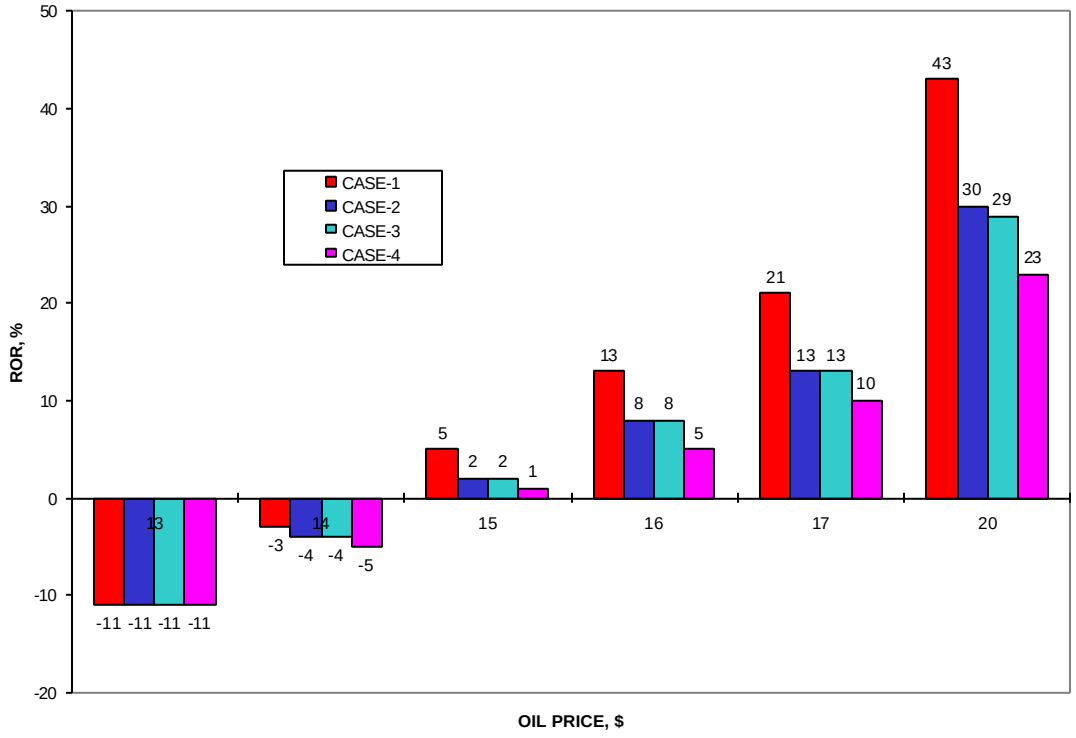

Figure 83 - The effect of oil price - scenario 1D - DGI model

Figure 84 presents the comparison of the ROR and pay out time estimated from the different models using scenario 1D of case 4. This figure shows one of the advantages of the stochastic model whereby it provides the estimation of uncertainty. In this case, the predicted ROR ranges from 10 to 22 percent and the pay out time varies between varies 4 to 6 years, whereas the deterministic model predicted one single value of 31% for ROR and 3 years for pay out time. This figure also confirms the optimistic nature of the deterministic model.

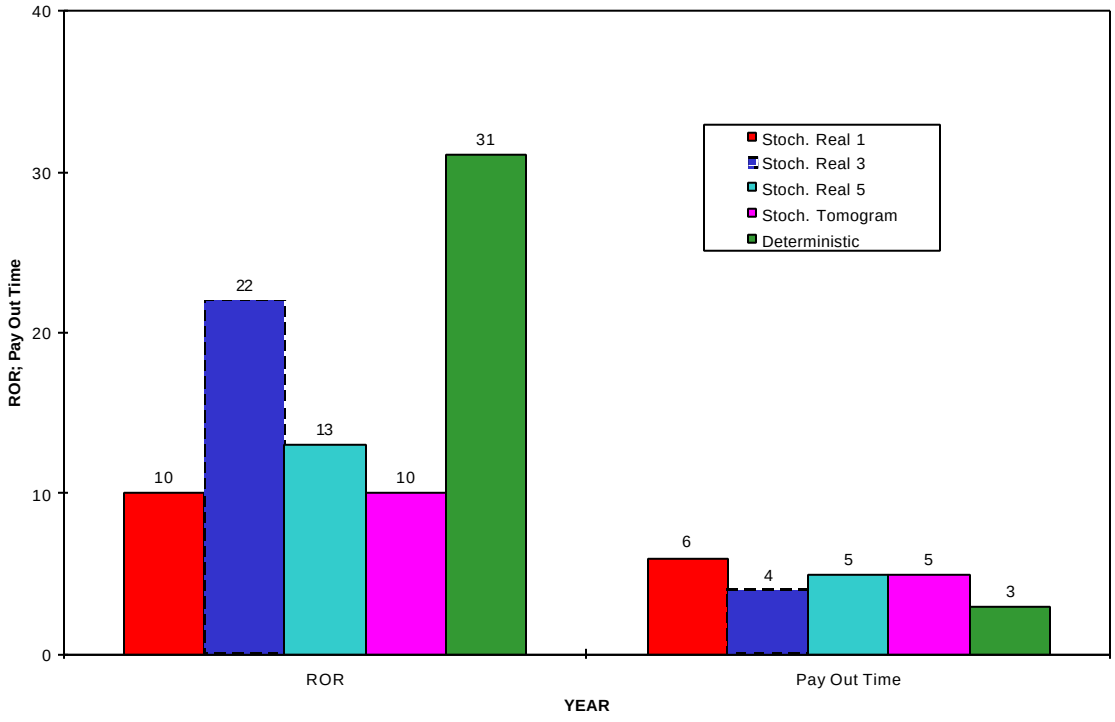

Figure 84 - ROR and pay out time comparison for different models

Summary

The flow simulation to forecast the future production was conducted. It was found that the additional oil production that can be expected from the Self-unit is in the range of 16 - 41 barrels per day depending on the specific scenario applied to the unit. The drilling of any extra wells, either one horizontal well or several vertical wells, was not feasible for the Self-unit at the current level of oil price since the increase of oil production can not justify the cost that was required to drill those wells. The scenario of reopening DGI's D and E and simultaneously increasing the injection rate was found to be the most feasible. The economic analysis was done for this scenario. A rate of return in the range of 10 - 25% was expected by applying this scenario. The deterministic model consistently predicted optimistic results compared to the stochastic model.

Implementation of Reservoir Management Plan

Based on the sensitivity analysis, we decided to implement our reservoir management plan. The details are discussed below.

Recommendations

Our evaluation of the reservoir and production data indicated that the DGI's A and B probably contain immovable oil, DGI F (lower unit) has already been flooded, and DGI's C, D and E had the most potential in terms of additional recovery. DGI C is already open in most of the existing wells. This left us with two possible DGI's for further exploitation, DGI's D and E. We also noticed that an increase in the injection rate had resulted in an increase in the oil rate in the past. Based on the well configuration, the injection wells are capable of taking a lot more water without any modifications.

Based on our understanding of the reservoir, we considered several strategies to improve the performance of the unit. These included: i) re-perforating selected intervals and stimulating them; ii) increasing the injection rate; iii) drilling a horizontal injection well; and iv) drilling additional vertical wells. We also considered combinations of these alternatives. Assuming an oil price of $17/bbl over the life of the project, we determined that the best alternative is to re-perforate some of the intervals and double the injection rate. Drilling of a horizontal injection well may have resulted in higher production rates; however, the cost of the horizontal well did not justify the additional production. Drilling of additional vertical wells did not result in any significant increase in production. The results of recompletion are already presented in the previous section. To repeat, our prediction was incremental oil recovery between 18 to 21 barrels per day without any increase in water injection. If we would increase the water injection rate, the predicted range was between 18 to 32 barrels per day.

Field Implementation - Problems and Solutions

Upon identification of the additional intervals to be perforated in each of the 28 wells on the Self-unit, a prognosis was developed for up-sizing the water injection station, and re-completing each of the wells. Several concerns were considered with regard to recompletions. These included the current integrity of

casing, condition of the injection well packers and tubing, and the actual increase of fluid volumes that would come from the producing wells after completion. Five producers and two injectors were selected for initial recompletion so that the operator can test the recompletion methodology and obtain actual production data to evaluate the economic viability of the project in stages. This also ensured that the lease continued to produce without undue loss of production.

The steps involved in recompletion are: i) pull all the equipment out of casing; ii) run the bit and scraper to clean casing; iii) re-perforate the desired intervals as indicated by the simulation results; iv) acidize both new and old perforations; and v) test wells. No substantial problems were encountered through the perforation process. However, acidization took longer than expected. The breakdown took longer because the formation needed to be pre-soaked with acid before acidizing. The pre-soaking helped reduce the time required for acidizing. Through a learning experience, the costs of recompletion for the last two wells were less than the AFE. The up sizing of the water plant was done without significant deviation from the construction plan.

All wells were initially swabbed back to recover the spent acid and flush, and the producers were swab tested. It became apparent that the fluid volumes being produced were substantially greater than expected. To measure the maximum possible rates, variable speed submersible pump was used. Both the volume and the oil cuts were monitored for three weeks for each well. The initial production from the wells was essentially all water. However, as the time progressed, the oil cut from the well increased gradually. At present, the oil cut varies between 1 to 1.5%. This was an improvement over previous observations.

Results

Based on the implementation of the reservoir management plan, we observed an increase in the oil production. As can be seen in **Figure 85**, the oil production increased from initial value of 17 to 18 barrels per day to about 42 barrels per day. This increase of about 24 barrels per day was consistent with our original model observation. In addition to recompleting the wells, we also increased the injection rate. Currently (1999), the unit is producing about 28 barrels per day. This is an increment of

10 barrels per day. This is also consistent with our prediction (see Figure 70). Currently, only make-up water is injected. This change is due to a significant reduction in oil price.

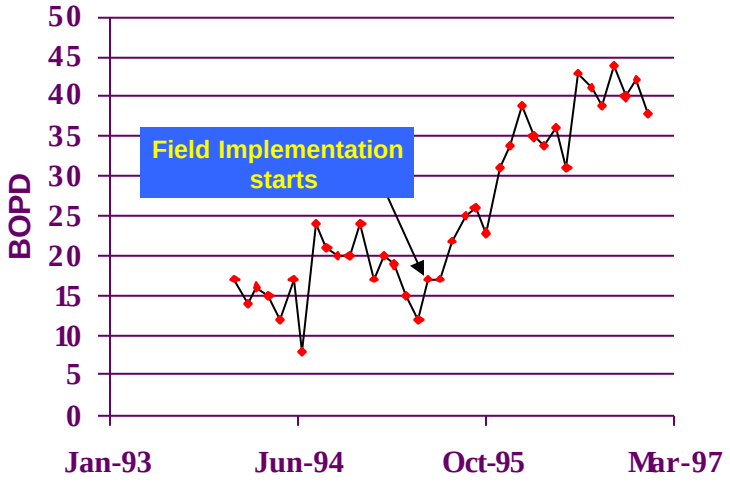

Figure 85 – Results of field implementation

Economic Evaluation

One of the important goals of this project was to investigate the economic feasibility of the implemented strategies. For an effective transfer of technology, it is critical that the technology be cost effective.

By assuming that the production will decline at 6% per year, we estimated the range of additional oil that can be recovered from the unit in the next 15 years. This amount ranged between 200,000 barrels to 250,000 barrels. The anticipated cost of this project is approximately $1.2 million. This translates into finding cost per barrel of $4.80 to $6. This number may be unattractive. However, we can also calculate the finding cost based on the knowledge gained in this project. Some technologies in this project were either proven to be ineffective or marginal. If we assume the same field costs and further assume that a typical consultant in the oil patch can apply the methodology proposed in this project, the overall cost of the project will be in the range of $500,000 to $600,000. This translates into finding cost of $2 to $3 per barrel. This is significantly less than the present acquisition cost used in the market. This reduction in the cost, although dramatic, is not unrealistic. For example, the cost associated with cross borehole seismic data acquisition and analysis was $250,000. The cost of drilling a new well and

acquiring the modern suite of logs was $120,000. Additional costs associated with the administration of the project as well as technology transfer costs can be paired down substantially as well.

It is also worth remembering that the Glenn Pool field is one of the oldest fields in the United States. Most of the fields are much younger than this field. If we can apply better reservoir management techniques to improve the performance of this field in an economically viable manner, we sure will be able to do the same for other fields, which are much younger.

Evaluation of Various Technologies

In this budget period, we used several modern technologies. In this section, we briefly describe the technologies and their value to the project.

Integrated Approach

We made a concerted effort to integrate information from various sources to better understand the reservoir. Geophysical, geological, and engineering data were used to better describe the reservoir properties. In addition to interdisciplinary nature of the project, this project also involved active participation from government, the university, a small oil company and a major oil company. The biggest benefit of working together among such a diverse group of people is understanding and appreciating each other's language and perspective on the issues at hand. Communication between different disciplines helped us better understand what each discipline considers to be an important part of the reservoir description. We tried to create a good balance between the form of the reservoir (architecture) and the function of the reservoir (production performance). Interaction among various entities during the project made us aware of each other's priorities and each other's objectives. Although the objectives of each organization did not always coincide, we learned to appreciate and respect each other's objectives. This helped us in proceeding in the project in an optimal way.

Cross Borehole Tomography

Cross borehole tomography is a method by which an interwell image of reservoir characteristics is constructed by using an acoustic source in one well and receivers in another well. We conducted three

such surveys with the help of Amoco Production Company and Conoco. The surveys were conducted between well pairs 82-63, 82-64 and 82-81. The collected data were processed by Amoco, using public domain software and by Memorial University in Newfoundland, Canada. In addition, data were also provided to a group of scientists from Imperial College. Depending on the assumptions involved in the software, the results obtained from the three methods were significantly different. The results are in the form of sonic velocity distribution across the well pair. We used this information by relating the velocity to the porosity and the facies at the well location. The use of these data slightly improved our reservoir description. Because of the high cost of acquisition and significant uncertainty in the interpretation, the use of cross borehole data was limited.

Formation Micro-Resistivity Borehole Imaging

We used this tool in the newly drilled Self-82. Along with the resistivity imaging, we also cored the desired interval. Formation micro-resistivity imaging tool produces a high-resolution resistivity of the wellbore. Analysis of the image provides spatial orientation of architectural elements in the vicinity of the wellbore. By combining the information from the core data and the imaging tool, we were able to describe the geological heterogeneties at higher resolution level than otherwise possible with conventional well logs. Unfortunately, we were not able to use this detailed information in an effective way in flow simulations due to computer memory limitations. For a mature, shallow, oil field with marginal oil production, the detailed knowledge of geological structure may not be important in predicting unswept reservoir and preferential flow paths. The cost benefit analysis of using micro resistivity log versus taking an oriented core needs to be evaluated further before reaching the final conclusion on the utility of these type of logs. The preliminary analysis indicates that micro-imaging log may not be very valuable in terms of adding incremental value compared to taking a core sample.

Discrete Genetic Interval (DGI) Evaluation

Using the data collected from all the wells, we were able to construct a detailed description of geologically distinct units deposited during a limited time interval. This information was extremely valuable in understanding the vertical as well as areal heterogeneties. Previously, Glenn sand was

divided into three basic units - upper, middle, and lower. With the help of DGI approach, we were able to divide the sand in six geological units. This detailed geological description helped us in flow simulation as well as in our overall reservoir management planning.

Geostatistics

Geostatistics is a procedure by which interwell properties are described using all the available information. Geostatistics assumes that the reservoir properties are spatially correlated, and this correlation can be quantified by a method called variogram analysis. Geostatistics further allows us to quantify uncertainties in describing these properties. Using geostatistics as a tool, we were able to describe the spatial relationships for geological facies as well as the petrophysical properties. By using the relationship between the seismic velocity and the porosity, we were able to use the cross borehole data to improve the spatial relationship for porosity at interwell distances. Using a geostatistical technique called conditional simulation; we generated geological facies image. The comparison between the simulated image and the geologist's view of the reservoir indicated good results. This provided us the confidence that the architecture of the reservoir is preserved. Using the geological description as a starting point, alternate images of the petrophysical properties (permeability and porosity) are constructed by further integrating engineering and geophysical information. Overall, geostatistics was a valuable tool in constructing realistic reservoir descriptions.

Flow Simulation

Once the reservoir description was constructed, we used the ECLIPSE commercial simulator to simulate the reservoir performance. We used both the deterministic (conventional, "layer-cake") as well as geostatistical reservoir descriptions for simulation purposes. Typically, the number of grid blocks in the simulator is less than the number of grid blocks in geostatistical simulation. As a result, appropriate up scaling procedure is used to scale the petrophysical properties suitable for simulation purposes. Since the performance data from individual wells were not available, we could only match overall unit performance. After matching the historical oil production performance, we projected the future oil

production performance under various scenarios to understand the benefits and the drawbacks of various alternatives.

With increasing speed of computers, flow simulation technology is becoming increasingly viable for small operators. Field simulations can be conducted on personal computers without much difficulty. We believe that flow simulation will be an integral part of future reservoir evaluation procedures.

BUDGET PERIOD II

Introduction

In the second budget period, we extended our efforts to other parts of the Glenn Pool field (see Figure 1). This part of the Glenn Pool field was also operated by Uplands Resources. The main idea behind the second budget period was to apply conventional technology to develop reservoir management plan. Unlike the first budget period, where modern technologies such as micro-resistivity logs and cross borehole tomography data were collected, in the second budget period, the analysis relied on more conventional data. Any use of modern technology was restricted to the analysis and interpretation of the data.

Data Collection

During the second budget period of the project, we intended to concentrate on tract 7 and surrounding areas. Tract 7, another 160-acre unit in southern Glenn Pool field, is located about 1 mile north of the Self-unit. The emphasis of second budget period is to use conventional technology and knowledge gained from advanced technology in budget period one (FMI, cross-well tomography etc.) in developing an effective reservoir management plan.

Study of tract 7 and adjacent area involved data compilation, well log correlation of DGI's, and facies architecture reconstruction. For a better and more complete description of tract 7, its adjacent areas including tract 6, tract 10, tract 12, tract 13, tract 11, part of tract 3, tract 4, tract 33, and Corbray unit are included into the mapping area (**Figure 86**), with total area about 1.6 square miles. Subsequently, the area of coverage was expanded to include additional areas in the southern part of the Glenn Pool field including tract 9 and Chevron miceller-polymer unit which is directly north of tract 9, and is directly west of tract 6. See **Figure 87.** Figure 87 shows the area of concentration, whereas, **Figure 88** shows the areas from where additional log and core data were collected. In addition to the existing logs, six new Gamma Ray logs were acquired to compliment the existing data. Five of them are in the tract 7 unit (well numbers: 7-97, 7-99, 7-100, 7-103, and 7-107), and the other one (11-82) is in the

tract 11 unit. There is a suspicion that upper part of the Bartlesville sandstone in tract 7 area may contain a gas cap. Thus cased-hole neutron logging (TDT) was also performed for three wells (well numbers: 7-97, 7-103, 7-107). These TDT logs do not show any evidence of gas.

In addition to the data available from Uplands Resources, Inc. data were also collected from Hyperion Oil Company's office. Data from 23 cores (which includes oil saturation information), well logs and many other materials regarding the micellar-polymer project were collected.

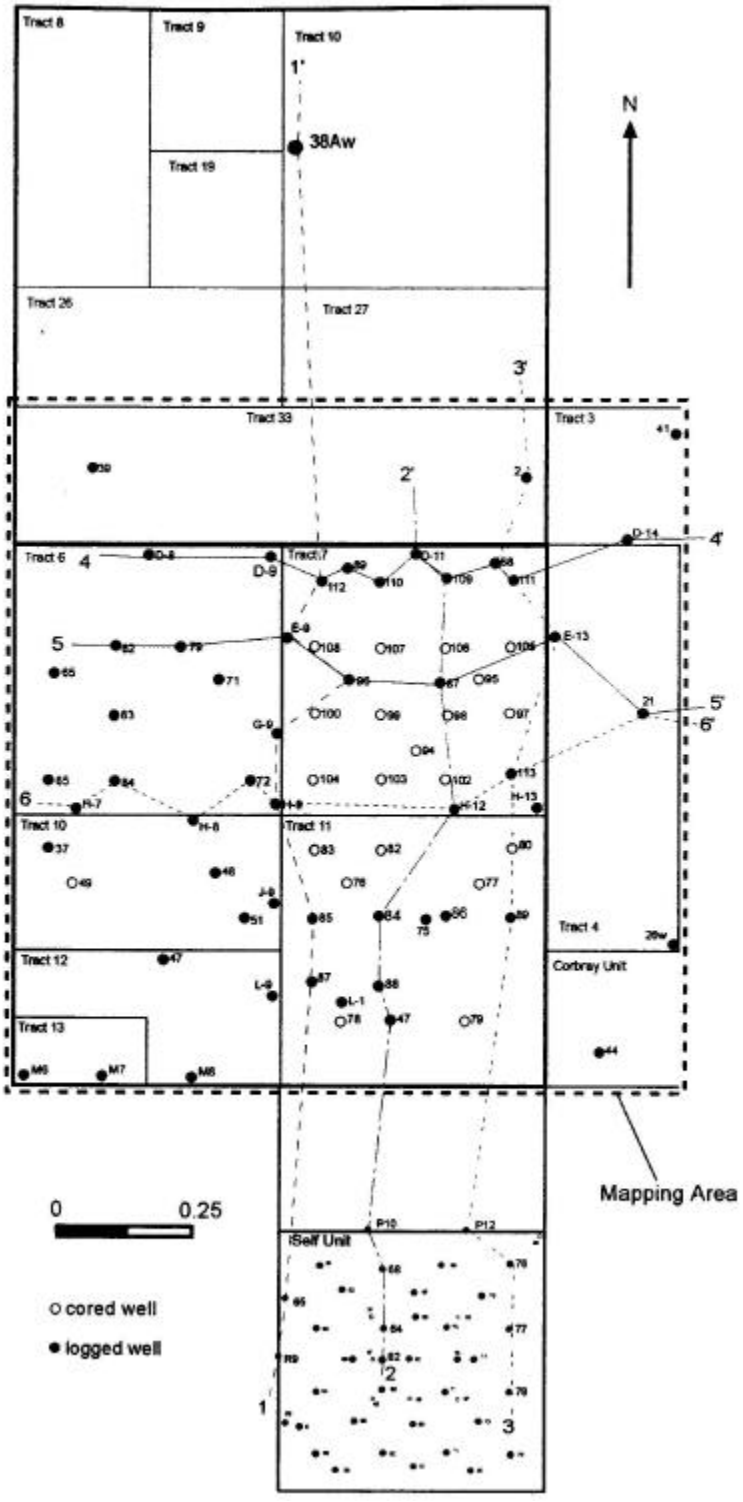

Figure 86 – Index map showing the locations of six cross sections constructed

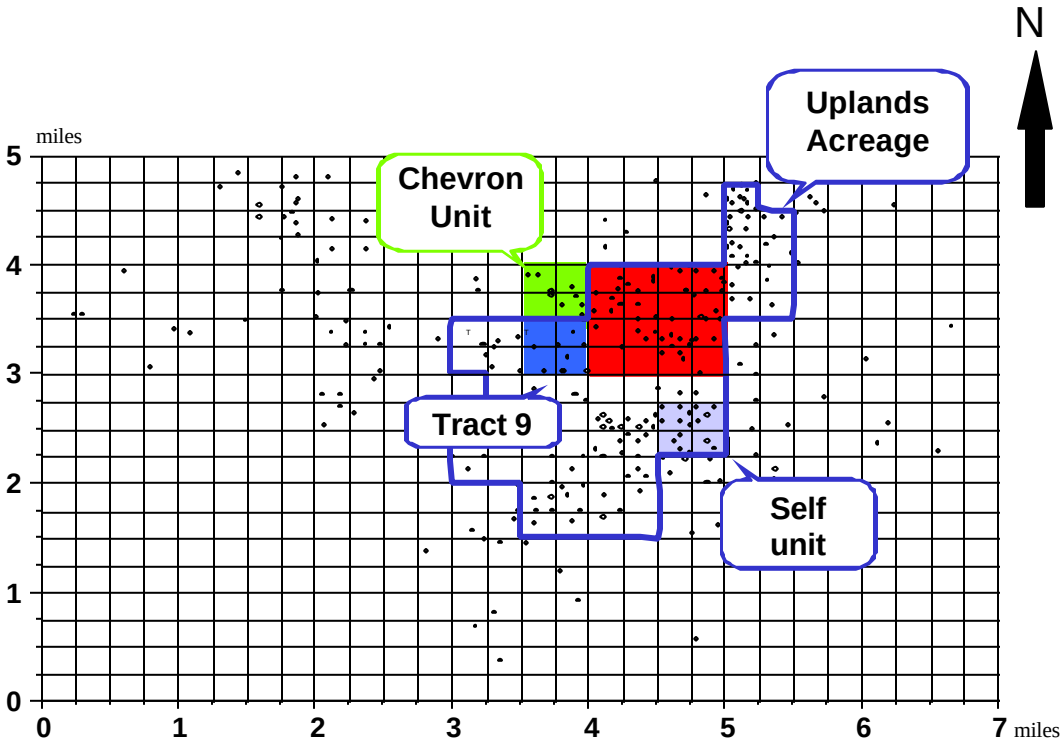

Figure 87 - Area of concentration

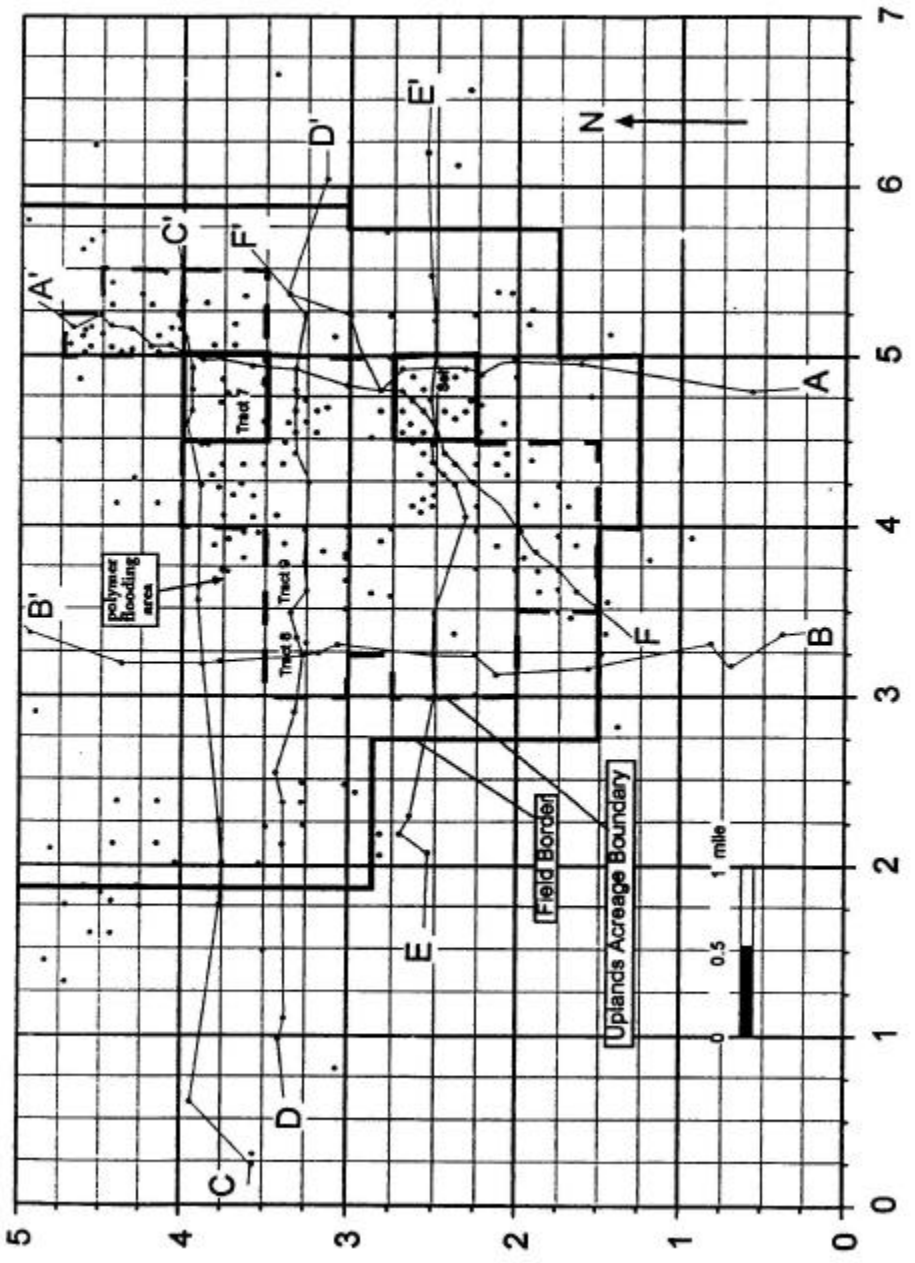

Figure 88 - Expanded coverage of core and log data

Data compilation included collecting all logs and core data available in the office of Uplands Resources and Oklahoma Well Log Library and constructing the well location map (**Figure 88 and 89**).

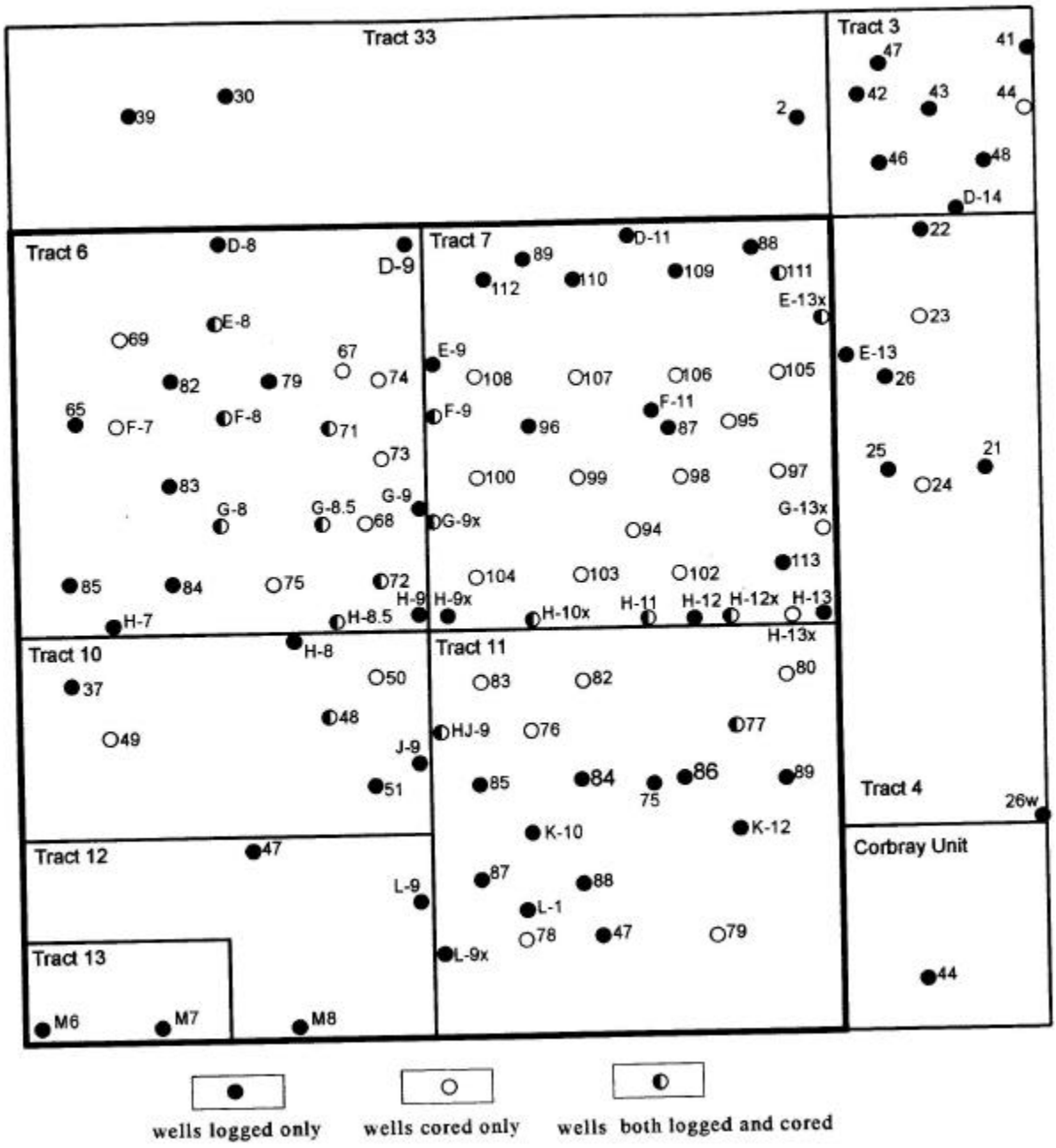

Figure 89 – Data availability within section 16 and surrounding areas

Tract 7 includes 36 wells which have some sort of data available to use: 14 wells were logged (8 open-hole logs and 6 cased-hole logs) but not cored; 9 wells were both cored and logged (8 cased-hole logs and 1 open-hole log); and 13 wells were cored but not logged.

In areas adjacent to tract 7, information from 80 wells were collected and used for the study. Of these 80 wells, 9 wells were both logged and cored (in some intervals), 18 wells were cored but not logged, and the remaining 53 wells have log data only. In total, core and/or log data from 116 wells were collected and used for the mapping area. Unfortunately, the 23 wells with logs in tract 7 are not uniformly distributed across the unit but mainly concentrated along the edge of the unit (Figure 89), cores of this unit are from the lowest part (DGI F & G) of the Glenn sand only. In addition, all cores within tract 7 have been physically missing and are likely not to be found.

In addition to the area of concentration, additional core and log data were collected within a 25-sqaure mile area (see Figure 88). This covers Glenn Pool acreage of several independent oil companies, including Uplands Resources, Producers, ELS, Hyperion, Reddy and part of Bazneet.

320 logs were available in the public domain within the area; 280 of them cover the whole Bartlesville interval. Correlation was completed to the DGI level for all these logs, with reference to the Pink lime, Inola lime, and Brown lime markers. Six cross sections, showing the interval from the Pink lime to the Brown lime, were constructed (see Figure 88 for cross section locations, designated as A-A' to F-F'').

Geological Analysis

The geological analysis concentrated on developing DGI relationships for the expanded area. We started with well log correlation. Well log correlation aims at investigating the stratal relationship between Self-unit and tract 7. Detailed correlation at a level of individual DGI's was performed and six cross sections were constructed, three of them are in north-south direction connecting the Self-unit and tract 7 (Figure 86). Correlation results show that the Glenn sand interval thickens from Self-unit to tract 7 (160-ft to about 200-ft). In Self-unit, six DGI's (DGI A to F) are recognized, but seven DGI's (DGI A to G) in tract 11 and eight DGI's (DGI A to H) in north-central part of tract 7 are recognized. DGI G and H are equivalent to the lower Glenn sand of Kuykendall and Matson.[1] Thus, the lower Glenn sand (DGI G and H) is absent in Self-unit, and DGI H is absent in tract 11. **Figure 90** shows schematically the stratal relationship from Self-unit to tract 7.

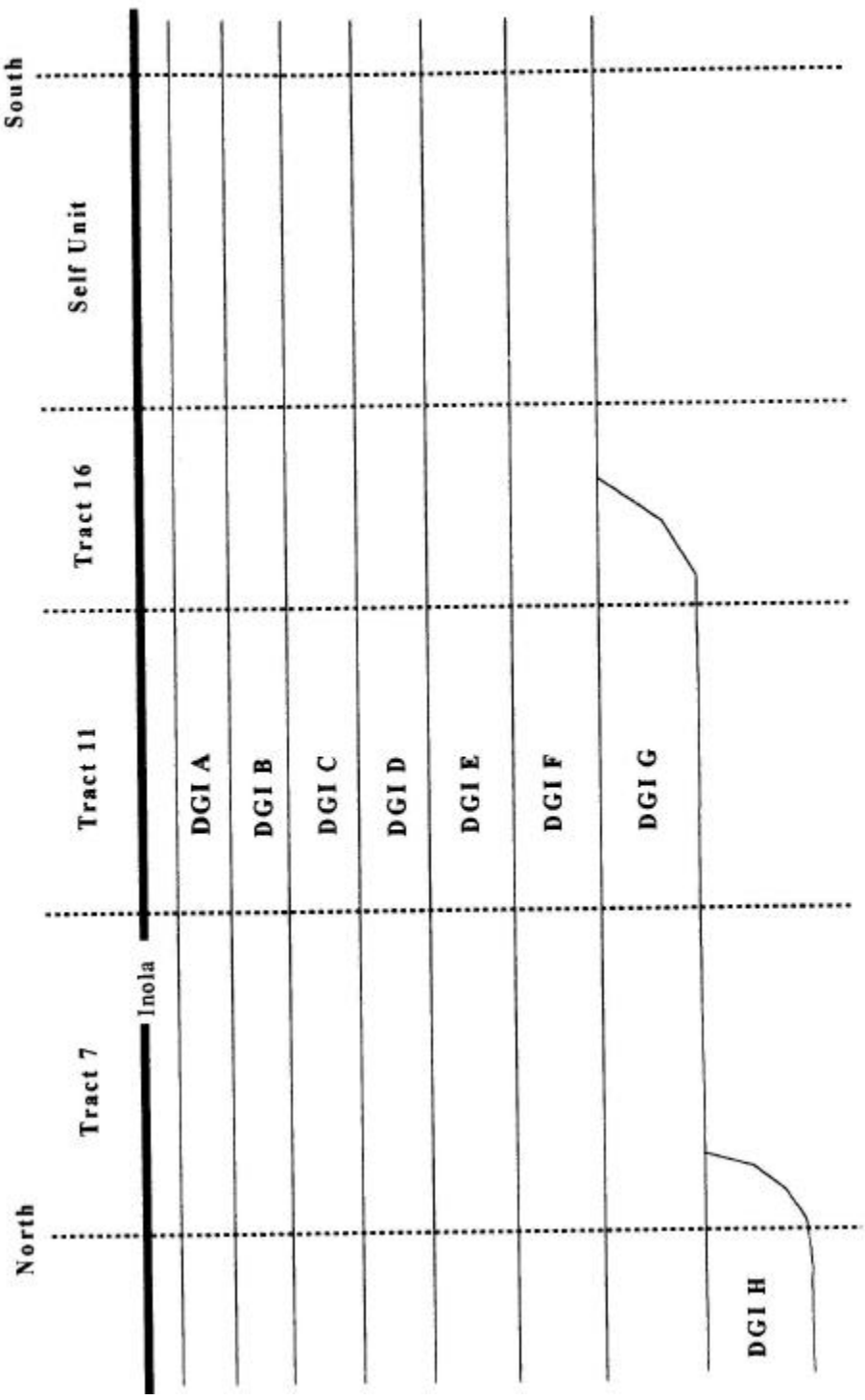

Figure 90 – A sketch map showing the general stratal relationship from Self-unit to tract 7 (figure not drawn to scale; thickness variation of each DGI is not shown)

Based on the correlation results, tables of sandstone depth intervals for each DGI at each well used were developed, which served as an important database for further mapping and reservoir simulation.

One important aspect of the tract 7 study had focused on the revision of sand isopach and facies maps constructed for each DGI in the area (1.6 square miles). This revision was deemed necessary after the acquisition of additional well data. Also insights into the reservoir architecture of the Bartlesville sandstone gained from outcrop studies benefited this revision greatly. In this version of the facies architecture reconstruction, the Bartlesville sandstone (especially intervals DGI A-C) is less layer-caked than earlier believed. It was observed that a thick and blocky sandstone, if it exists, is within the top part of the Bartlesville sandstone. It is more likely to be placed into one DGI rather than divided into more multiple DGI's. This resulted in the interpretation that sandstones of DGI A to C are more channelized than described in the earlier interpretation.

Also the outcrop study resulted in a new facies interpretation for the DGI F sandstone (about 40-50 ft thick). DGI F was interpreted as channel mouth bar deposits based on the Self-82 core characteristics and persistent blocky log shapes. Similar rocks have been observed in the lower part of Bartlesville sandstone outcrops in the Eufaula Dam area. These "massive" thick sandstones may laterally transition to cross-stratified and/or parallel-bedded thick sandstone. They are highly channelized, showing unidirectional paleoflow; vary greatly in thickness according to their position relative to the channel thalwegs; and are made of many small individual channels which are stacked together and cut each other horizontally and vertically, resulting in a widespread distribution.

Thus, while the facies interpretation of DGI A to E was kept unchanged, DGI F was re-interpreted as braided-stream deposits. Facies interpretation for DGI G was undertaken on the only available core from Crow 9-43, which is on the property of Gemini Oil Company. Observation of this core indicated that the DGI G sandstone is analogous to the DGI F sandstone, except that the DGI G is often more shaly than the DGI F because of a higher rip-up class content.

As has been done for the Self-unit study, several maps showing the shale thickness between DGI's were constructed for investigating the vertical separation of the reservoirs. As an example, **Figure 91**

shows the shale thickness between DGI D and E. Generally speaking, Bartlesville sandstone has a good vertical separation between DGI's. **Table 5** presents the separation between different DGI's in terms of shale thickness and the number of wells which show no shale break. This indicates that the reservoirs of the upper part of the Bartlesville sandstone (DGI A to C) have a worse vertical separation than those of lower part (DGI D to G).

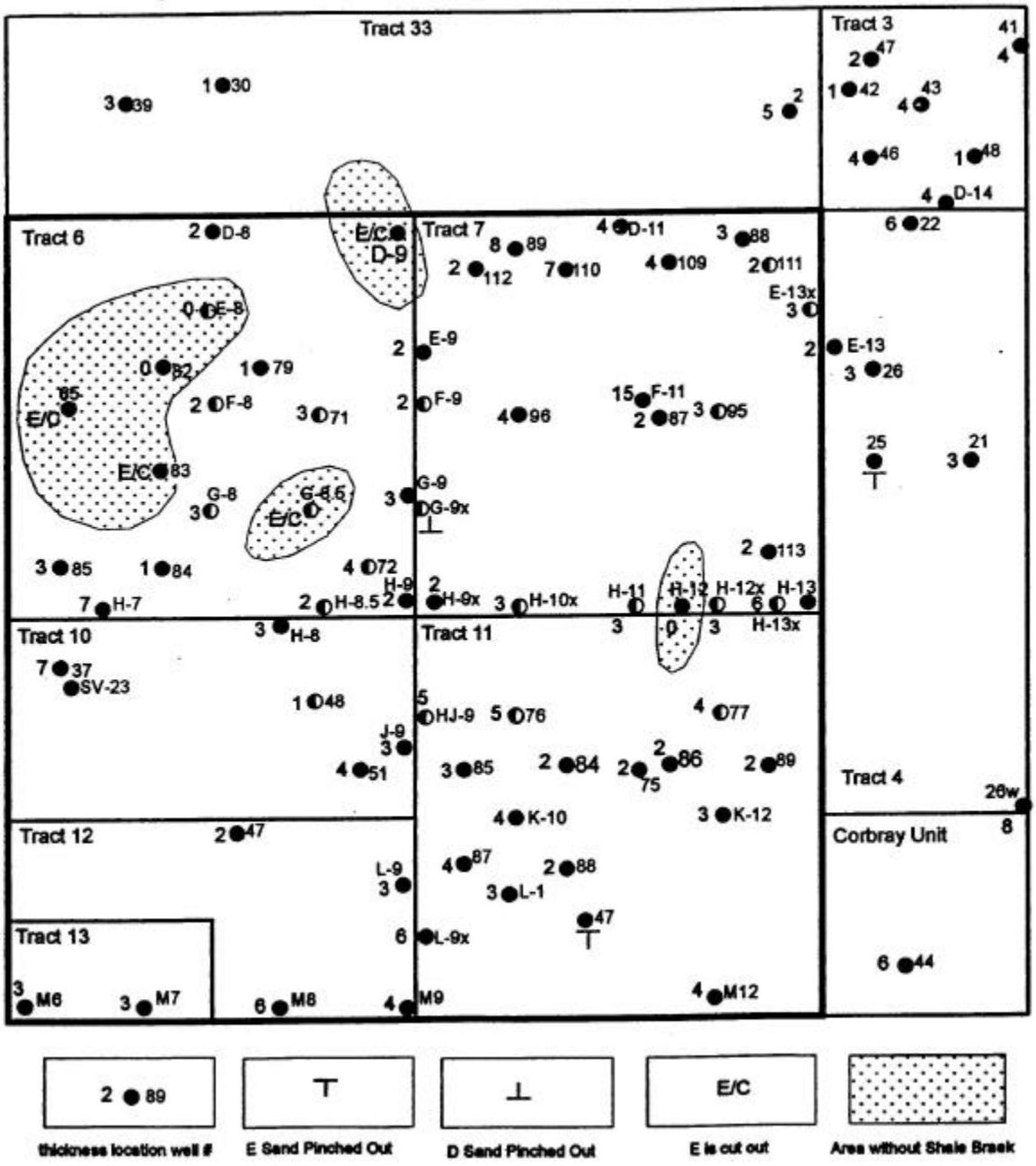

Figure 91 – Shale thickness between DGI D and E

Table 5 - Vertical separation condition, tract 7 and adjacent area

Shale Break	Typical Thickness Range (Ft)	NWI*	NWWNS*	PWWNS*
A vs. B	1 to 3	89	27	30
B vs. C	2 to 4	89	19	21
C vs. D	2 to 6	89	7	8
D vs. E	2 to 6	89	7	8
E vs. F	2 to 6	89	9	10
F vs. G	3 to 8	116	4	3

Note: NWI* = number of wells investigated

NWWNS* = number of wells which shows no shale break

PWWNS* = percentage of wells which shows no shale break

It is difficult to evaluate the petrophysical properties for reservoirs in tract 7, because all cores (20 in total) were cut for DGI F and G only. Fortunately, there are three longer cores cut in nearby area of tract 7 (i.e., well 6-F8, 10-49, 4-24), data of which can be used as a reference for tract 7. **Table 6** shows core porosity and permeability data for these three wells, as well as some core data for DGI F and G in tract 7, in comparison to the data of Self-82 core.

The data presented in Table 6 indicates that for DGI E to F (or G if present), the tract 7 area and Self-unit have comparable porosity and permeability. However, for DGI B to D, the tract 7 area has a much higher porosity and permeability than that of the Self-unit. There is no core sample for DGI A in tract 7 area, however well logs show good reservoir quality for DGI A sandstone in the tract. This implies that the upper part of Bartlesville sandstone in tract 7 area could have very good potential for further development.

Table 6 - Comparison of core porosity and permeability between Self-unit and tract 7 area

	Well Self 82			Well 6-F8			Well 10-49			Well 4-24		
DGI	Phi (%)	K (md)	Facies	Phi (%)	K (md)	Facies	Phi (%)	K (md)	Facies	Phi (%)	K (md)	Facies
A	NS	NS	CH	NC	NC	FP	NC	NC	FP	NC	NC	FP
B	9.1 (3)	0.018 (1)	CH	11.5 (2)	1.6 (2)	CH	0.1 (1)	13.3 (1)	FP	NS	NS	FP
C	11.8 (16)	0.57 (15)	CH	22.3 (19)	397 (19)	SP	20.6 (17)	148 (17)	CH	5.1 (22)	2.3 (22)	CH
D	16.5 (20)	26.4 (19)	SP	20.7 (17)	237 (17)	SP	17.8 (12)	105 (12)	SP	11.9 (4)	18.2 (4)	SP
E	19.9 (5)	181.8 (5)	SP	19.3 (20)	151 (20)	CH	18.1 (26)	77.6 (26)	CH	15.7 (8)	66.9 (8)	SP
F	21.8 (9)	246 (9)	BS	20.5 (56)	137 (56)	BS	22.2 (24)	217 (24)	BS	18.5 (43)	146 (43)	BS
G		Not developed		17.9 (34)	30 (34)	BS	16.2 (49)	18.2 (49)	BS	19.4 (36)	91.4 (36)	BS

	Well 7-100			Well 7-102			Well 7-103		
DGI	Phi (%)	K (md)	Facies	Phi (%)	K (md)	Facies	Phi (%)	K (md)	Facies
A-E	NC	NC		NC	NC		NC	NC	
F	21.2 (22)	162.3 (22)	BS	15.4 (4)	32 (4)	BS	20.2 (20)	141.3 (20)	BS
G	15 (40)	35.5 (40)	BS	17.8 (50)	14.9 (50)	BS	17.2 (36)	29.5 (36)	BS

Note: The number within parenthesis is the number of samples.

NC = not cored

NS = not sampled

CH = channel-fill sandstone

FP = flood plain mudstone

SP = splay sandstone

BS = braided stream sandstone

The geological analysis of tract 16, based on the limited data available, showed that the DGI G sandstone is absent in the southern two-thirds part of the unit. DGI A to C has the most likely potential for further oil recovery.

56 wells have been drilled on tract 9, however, only 11 logs were available for geological interpretation. As was done in other tracts, the Bartlesville sandstone was subdivided based on the correlation of these 11 logs and logs in other tracts. DGI A to DGI G was recognized. Log facies interpretation was performed for each well, and each DGI facies map was completed for each DGI in conjunction with other tracts. Characteristics of the vertical profiles are very similar and correlatable to what was observed in tract 7 area.

Chevron's miceller-polymer flooding acreage, also a 160-acre unit, is located in the northeast quarter of section 17-17N-12E, i.e., immediately north of tract 9 and west of tract 6 (Figure 87). The miceller-polymer flooding project was conducted during the early 1980's and is considered to be very successful in terms of oil production increase. Currently this unit is operated by Hyperion Oil Company.

An investigation of the factors leading to this success was intended, in the hope of gaining insight into our proposed reservoir management planning. Fourteen logs were collected from public domain in Tulsa. Correlation to DGI level and sandstone classification for each DGI was made for each of these wells. Facies maps for each DGI were constructed for this unit in conjunction with other reservoir units.

In addition to conventional logs, we also had detailed log descriptions from micellar-polymer unit. This included information about saturation (see **Figure 92**). As can be seen from this figure, oil saturation tends to be much higher in the upper part of the Glenn sand than the lower part. This is an indication that more potential for recovering additional oil existed in the upper part of the Glenn sand.

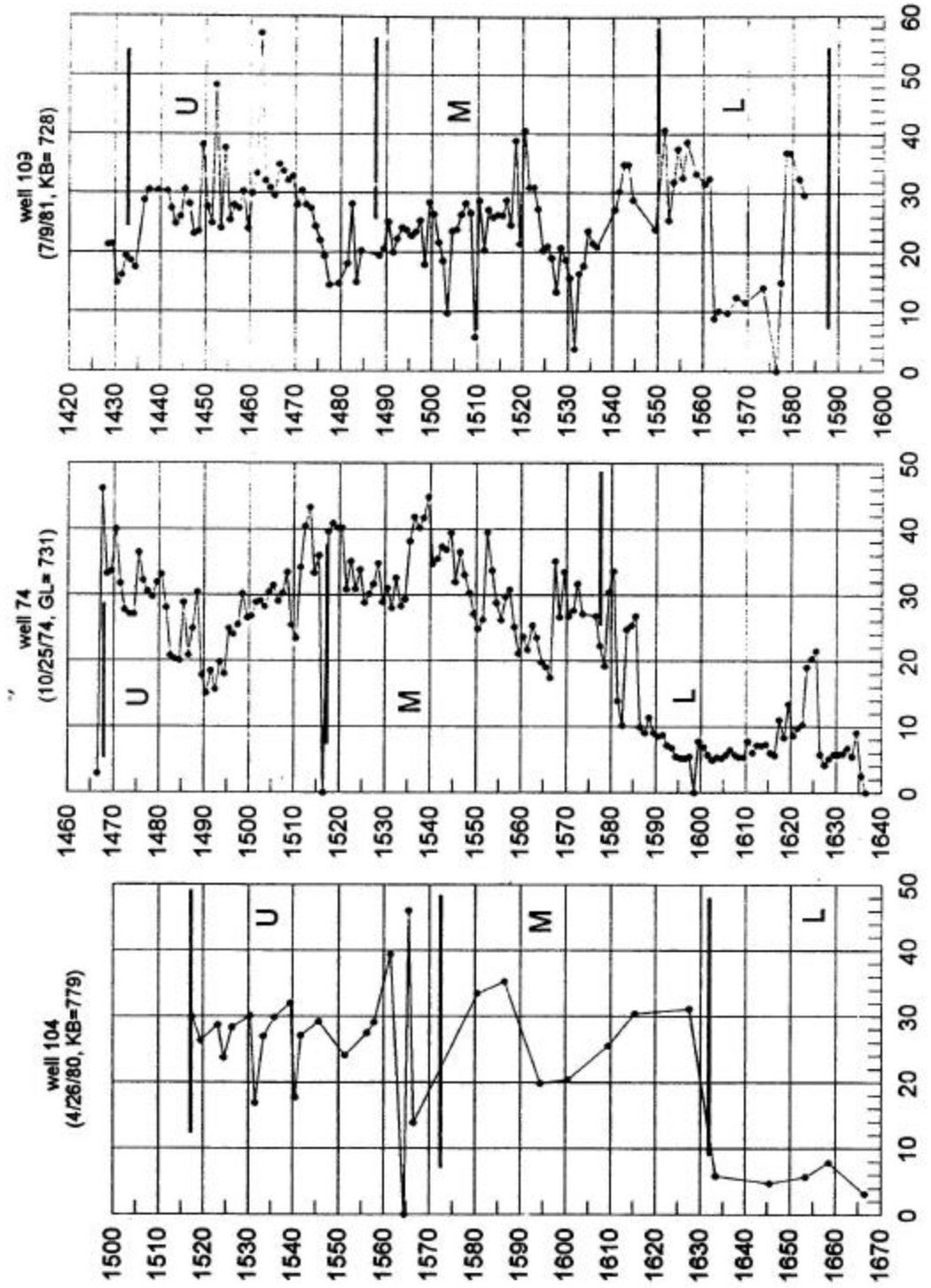

Figure 92 – Core oil saturation (%) profile (Chevron's micellar-polymer unit)

With inclusion of tract 16, tract 9, and the Chevron miceller-polymer flooding acreage, the area mapped for detailed facies architecture over the course of the project was about 1,500 acres. It was helpful to construct a unified facies map for entire area including the Self-unit, and tracts 3, 4, 6,

7, 9, 10, 11, 12, 13, 16, and the Chevron miceller-polymer flooding acreage. The unified facies map was completed for each DGI and shows the depositional relationship among different tracts very clearly. **Figure 93,** as an example, shows the unified facies map of DGI A for the entire area.

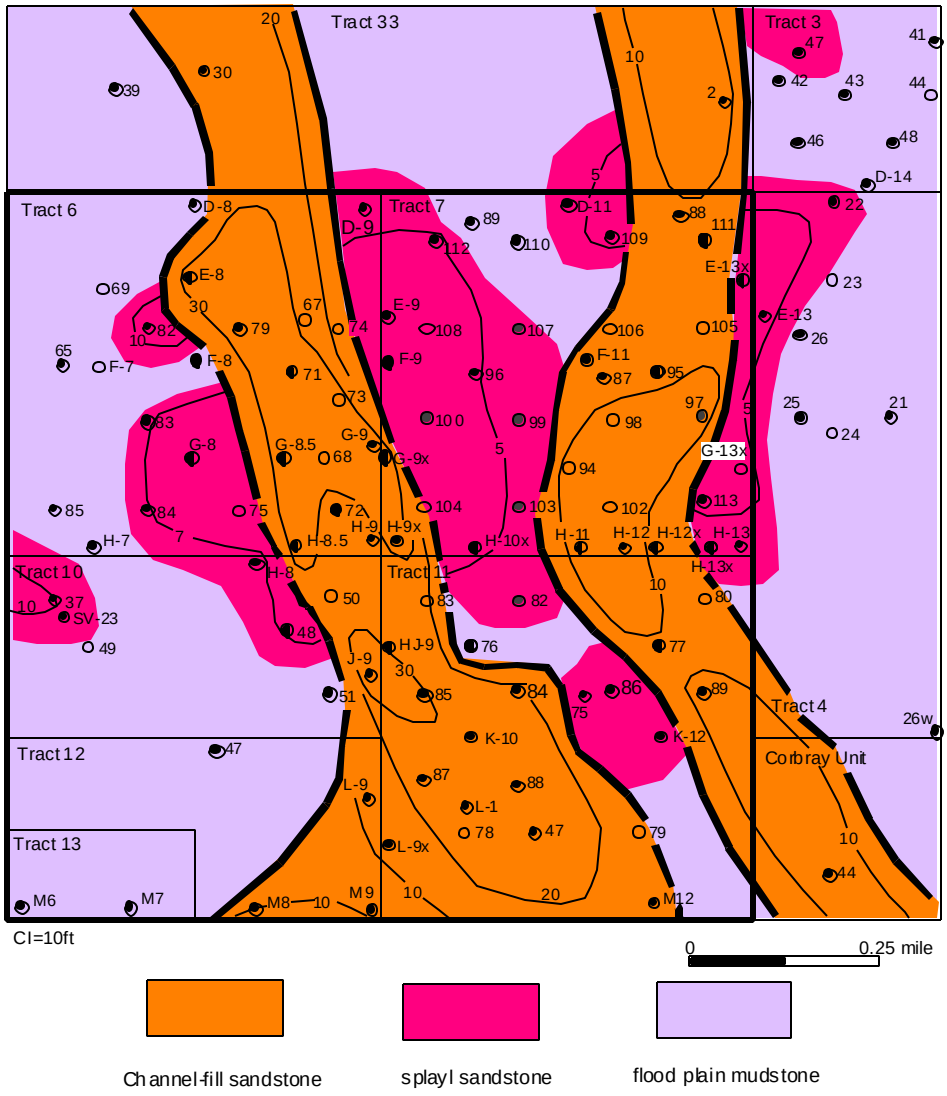

Figure 93 – DGI A map for the area of interest

To form a more accurate estimate of oil reserves in tracts 6, 7, 9, 10, 11, 12, 13, 16 and the Chevron miceller-polymer flooding acreage, net sand thickness was evaluated by using well logs. The "50% method" was adopted for determining the net sand thickness, which is the portion of sandstone with reservoir quality. About 120 logs were analyzed for this purpose.

Figure 94 displays the ratio of net sand thickness to gross sand thickness (i.e., the interval thickness from sandstone top to sandstone bottom within a DGI) for each DGI. The ratio displayed is the average value calculated from all 120 logs. From this figure we can see that the ratios for DGI A and DGI G are slightly smaller than those for other DGI's. This implies that at least in these tracts, DGI A and G are more muddy or shaly than other DGI's. As was mentioned earlier, the Bartlesville sandstone was deposited in a regressive manner, thus it is easy to understand why DGI A is shalier than the lower DGI's. But why is DGI G different? One possible explanation is that the lower part of Bartlesville sandstone contains more rip-up class shale originated from the erosion of underlying Savanna shale.

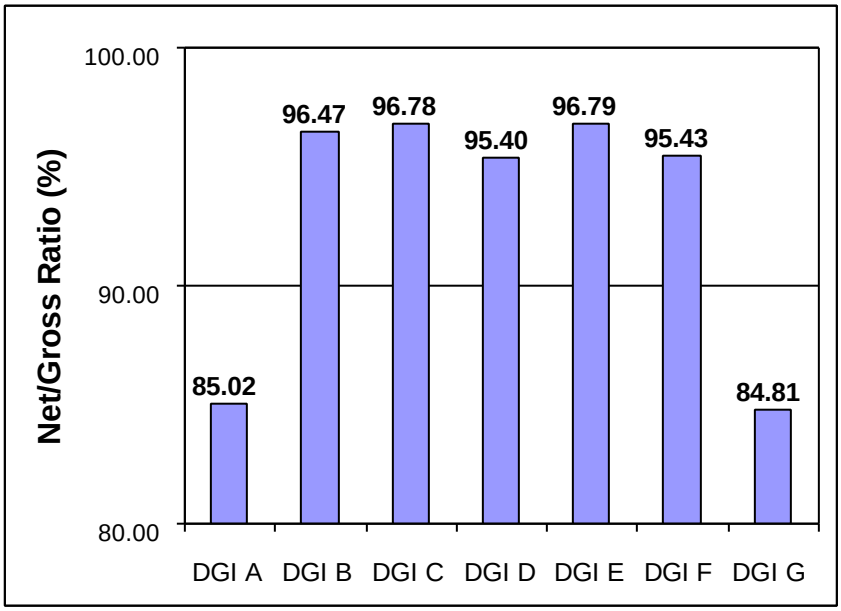

Figure 94 – Average net/gross ratio determined from 120 logs

Using this geological analysis as input, a detailed engineering evaluation was conducted as discussed in the next section. No geophysical component was involved in this budget period.

Engineering Evaluation

Introduction

This section discusses the engineering evaluation of the Glenn Pool field, which was the subject of interest in the second budget period. In addition to the part of the field operated by Uplands

Resources, we also investigated the Chevron's miceller-polymer flood. This flood was very successful in recovering significant additional oil.

A database of all the wells that have been drilled was compiled detailing information pertaining to the location of the well and the perforation depths. A total of 280 wells were included in this database, including both producers and injectors. Perforation maps were generated for each DGI displaying only those wells that have been completed in that DGI with an estimate of the interval that has been completed out of the thickness of the DGI under consideration. The conclusion derived from these maps was that the upper zones were not perforated as densely as the lower zones. Since most of the available completion data are skewed towards the years 1942-1995 this conclusion is appropriate during the course of secondary flooding implementation in the field.

Perforation interval maps were plotted for the Chevron lease to understand the completion practices before and after the miceller-polymer flood implementation in l980. These maps showed that Chevron had concentrated its completions in the upper intervals. There was very little activity in the lower DGI's especially DGI G. We believe that the rationale used was upper zones have a lot of potential owing to ineffective flooding practices. This is supported by the TDT logs in tract 7, which shows clean sands with high oil saturations in the upper regions.

Screening Test for High Potential Areas

It was difficult to determine which part of the study area we need to concentrate further. A screening procedure needed to be developed so that we can high-grade and low-grade some of the areas. A procedure was developed as a screening test to identify the areas with high potential for oil recovery in terms of the petrophysical properties.

The investigation area was divided into 60-ft $\times$ 60-ft grid blocks. The area of interest spans 7,920-ft in the x direction and 5,820-ft in the y direction and 5 DGI's (A-E) in the z direction. DGI's F and G were not included in this analysis since it was believed that they have already been effectively flooded by previous water floods. This results in a 3-dimensional grid block setup of $132 \times 88 \times 5$ (x, y, z) respectively. Each DGI was represented as a slice independent of a physical magnitude associated with it.

Mapping of Petrophysical Properties

(a) Porosity

Logs were collected and digitized wherein the combination of logs for a particular well is sufficient to make a reasonable estimation of porosity and saturation. The number of such wells is extremely small. Typically a combination of Spontaneous potential, Gamma ray, Density and Neutron logs is used to compute porosity. The computation validity is then established by comparing it with the core porosity data for the lower intervals since the upper intervals are predominantly uncored. The porosity values at the well locations are averaged for each DGI. These average values are kriged to estimate porosity values at all other grid blocks for a particular DGI. The result is seven areal slices (DGI A-G); each slice represents a particular DGI.

(b) Permeability

Log permeability versus porosity relationships is established for each DGI individually by combining all available core data. Permeabilities are evaluated based on the above relationships for all wells where porosity is computed. The permeability values at the well locations are averaged for each DGI. Precautions are taken to strip any unreasonable permeability value. These average values are kriged to estimate permeability values at all other grid blocks for a particular DGI.

(c) Saturation

Typically a combination of porosity, induction or resistivity logs is used to compute saturation. The saturation values at the well locations are averaged for each DGI. The computation validity is then established by,

- Comparing the log derived profile with the core profile.
- Comparing S_w averaged for each DGI with TDT saturations using compatible R_w and s_w values.

The average values are kriged to estimate saturation values at all other grid blocks for a particular DGI.

Potential Index Estimation

The potential for a particular location is a cumulative effect of the production capacity, storage capacity and access to the existing wells. The potential should be directly related to the production, storage capacities and inversely proportional to the access by existing wells.

(a) Conductivity Index (CI)

This index quantifies the production capacity and is related to the product of permeability and thickness $(k \times h)$. Since k and h are defined at all grid blocks in all the seven DGI slices (A-G) the productivity can be estimated at each grid block. Since F and G have been drained considerably, further indexing is done only from DGI's A-E. The productivity data for the DGI's A-E are then combined to establish quartiles X_{25}, X_{50} and X_{75}. Ranks are then assigned from 1-4 by comparing data points at each grid block with the quartiles. For instance if the productivity for a particular grid block is less than X_{25} then it is assigned a rank 1. If it is between X_{25} and X_{50} then the grid block is assigned a rank 2. If it is between X_{50} and X_{75} then the grid block is assigned a rank 3 and if the value is greater than X_{75}, it is assigned a rank 4.

(b) Storativity Index (SI)

This index quantifies the storage capacity, and is related to the product of porosity, oil saturation and thickness $(f \times S_o \times h)$. Since porosity, saturation and thickness are known at all grid blocks in all the five DGI slices (A-E), the storativity can be estimated at each grid block. The storativity data for the DGI's A-E are then combined to establish quartiles X_{25}, X_{50} and X_{75}. Ranks are then assigned from 1-4 by comparing data points at each grid block with the quartiles as was done for the conductivity index.

(c) Accessibility Index (AI)

This index defines the access to a particular area by drilled wells. It is assumed that a fully penetrated well in a particular DGI contacts 10 acres. Although arbitrary, this assumption is consistent with the overall observations in the field that indicate low areal continuity. If partially

penetrated, the area is proportionately reduced. The area contacted by a well is assumed to be proportional to the square of the ratio of perforated interval to the total thickness for each DGI. If a grid block is contacted by a drilled well (i.e., it falls within the assigned drainage area), the accessibility index is assigned 0 and if grid block is not contacted, the accessibility index is assigned 1.

(d) Potential Index (PI)

The productivity and storativity indexes are combined by summing up their individual ranks at all grid blocks. The maximum value of the sum is 8 denoting that the area has the highest potential both in terms of its productivity and storativity. Conversely, the least value of the sum is 2 denoting low potential. Since the essence of the procedure is to identify areas of high potential it was decided to use a combined sum of 4 as the index of demarcation between high and low potential areas. Hence if the sum is greater than 4, the grid block is categorized as 1 (high potential) and if sum is less than 4, the grid block is categorized as 0 (low potential). The category value is then multiplied by accessibility index to calculate the final potential index as,

$$PI = (CI + SI) \times AI \tag{2}$$

Irrespective of a grid block having a high or low potential, if the area is being contacted by a well, its accessibility is 0, which also reduces the PI value to a 0. By including the accessibility, we essentially mask all the regions that are being drained and treat them as being equivalent to areas having zero potential (see **Figure 95**).

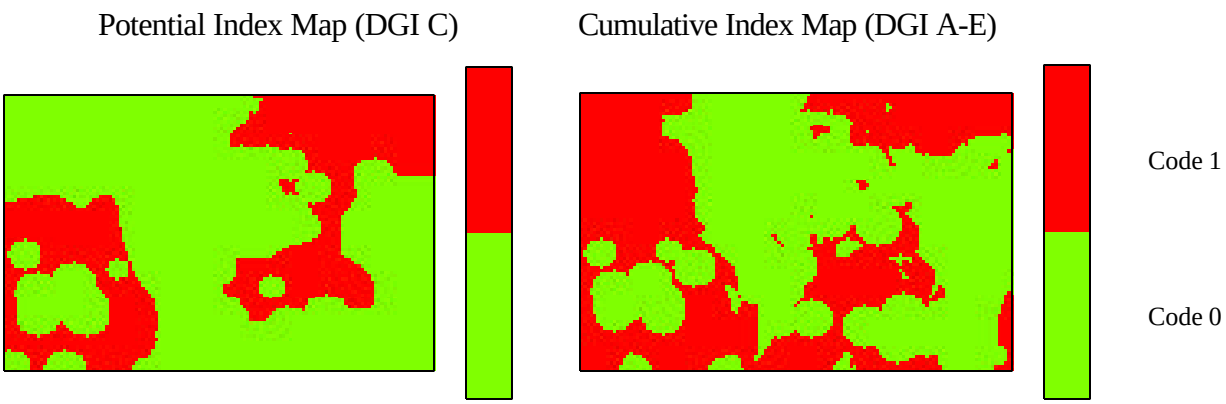

Figure 95 – Potential index map for DGI C and cumulative index map for DGI A-E

Cumulative index is estimated by adding the PI values at corresponding grid blocks for all DGI's A-E. For each areal location, 5 indices are added corresponding to each DGI. By collapsing all the DGI's into one unit we can examine which areas have the highest potential both areally and vertically. (see Figure 95). In Figure 95, code 1 represents high potential, whereas, code 0 represents low potential.

Evaluation of Production Information

In addition to generating the Production Index maps, the cumulative production data from the individual tracts was evaluated to assess the relative success of secondary recovery to primary recovery. The specific objectives were,

- To make a comparative analysis of the primary production and incremental secondary recovery production for tracts numbering 1 - 18.
- Estimate original oil in place (OOIP) and total recovery as a percentage of the OOIP in tracts 1-18.

Tracts 1-18 cover the areal expanse where the Berryhill Glenn Sand Unit (BGSU) has been identified. We also included Chevron miceller-polymer unit for comparison purposes.

Analysis of Primary Production and Secondary Recovery

Primary and secondary recovery production data were obtained from Reference 50. The report lists year wise production data from the field inception time in 1908 through 1988. It also lists the contribution from each tract provided the tract was in commercial operation in the year of question. The field wide production history can be summarized as follows,

1908- 1955-60:	Primary Depletion
1940- 1961-66:	Gas Injection
1965 - 1985-95:	Waterflooding

The production data for each tract is plotted as a function of time. Then the area under the curve is estimated to obtain the cumulative primary production and incremental recoveries due to 1) gas injection and 2) waterflooding.

A typical example is shown in **Figure 96.** It can be noted from the production response that the data compares well with the field wide history mentioned above. The production data was extrapolated as in decline curve analysis for the cumulative production estimates and the area under the curve was adjusted accordingly during the time spans when two processes are in effect simultaneously. For instance, in Figure 96 during 1940-52 primary depletion and production due to gas injection are occurring simultaneously. The following ratios were then estimated and the values were compared for all tracts under consideration

G/P = Incremental cumulative production due to gas injection (G) / cumulative production due to primary depletion (P)

W/P = Incremental cumulative production due to injection of water or other fluids (except gas) (W) / cumulative production due to primary depletion (P)

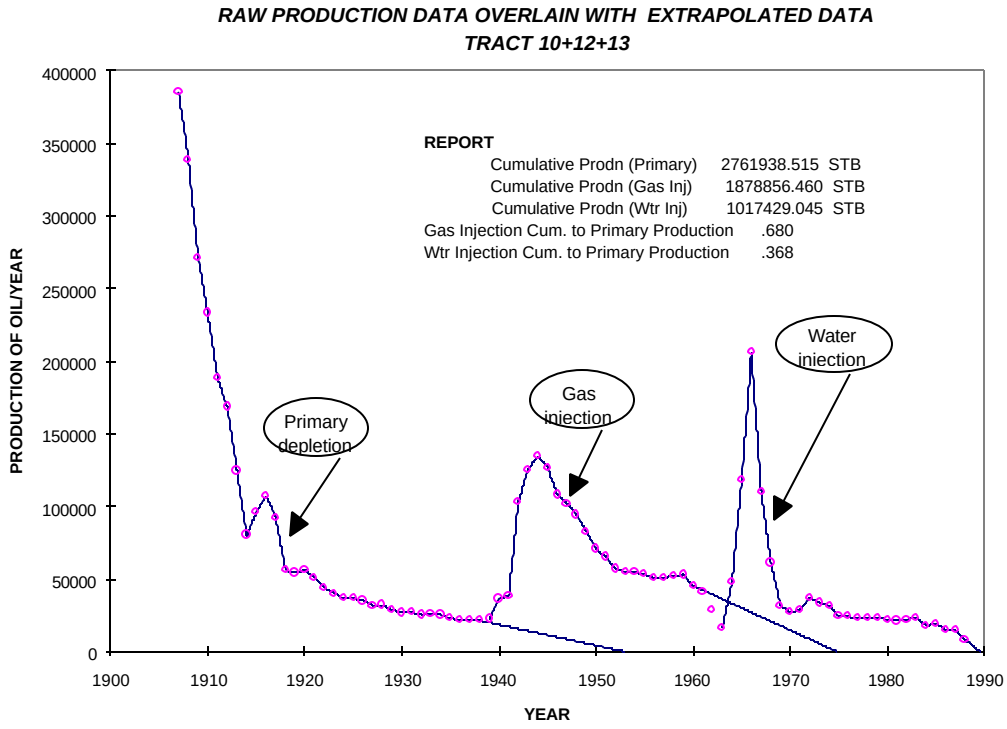

Figure 96 – Raw production data overlain with extrapolated data

Figure 97 is a representation of this information. In Figure 97, tract 10 represents the combined area of tracts 10, 12 and 13. It was obvious that gas injection response is poor over the entire field with the exception of tracts 7, 6 and 3. The most interesting feature of the plot was the W/P value for the micellar-polymer unit. It stands out in comparison to other tracts demonstrating the success of the Chevron miceller-polymer unit.

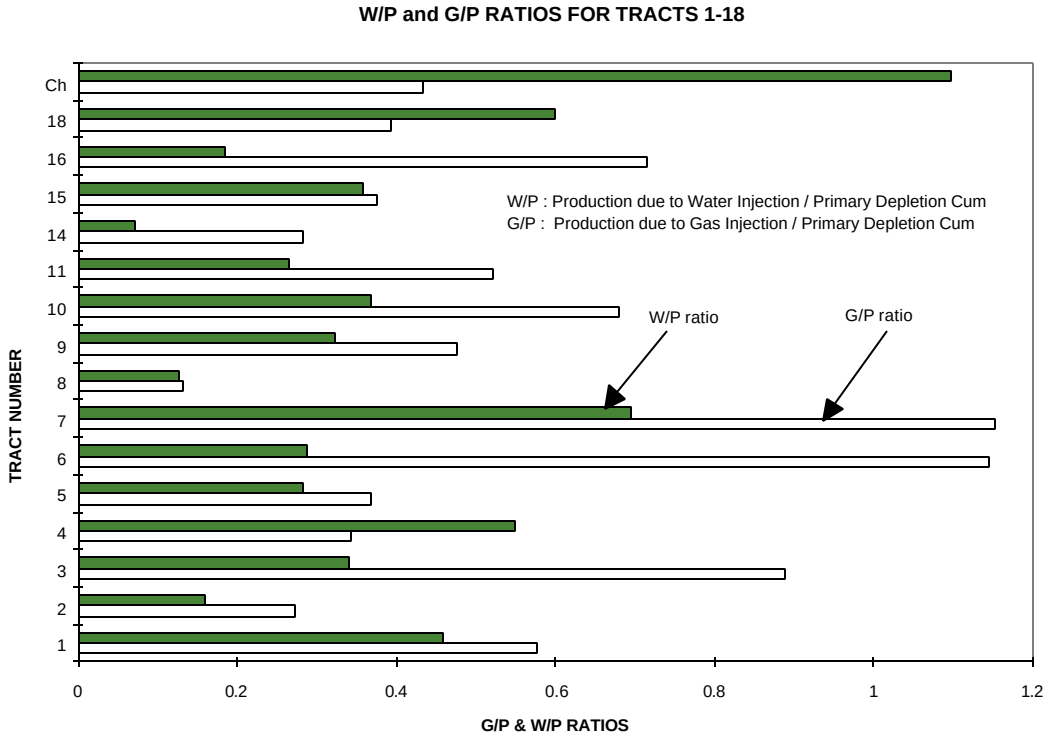

Figure 97 – W/P and G/P ratios for tracts 1-18 and micellar-polymer unit

Original Oil in Place (OOIP) Estimations

The net sand volume figures as quoted in Reference 50 for the upper, middle and lower Glenn sands were summed to get the total sand volume. This was then multiplied by an assumed constant field wide initial oil saturation of 0.78 and formation volume factor of 1.15 RB/STB to get the original oil in place. The calculated values are shown in **Table 7**.

Table 7 - Oil in place estimates

Tract	OOIP MMstb	Tract	OOIP MMstb
Chevron	9.745	10	6.003
1	8.148	11	12.388
2	1.739	12	4.717
3	9.216	13	1.792
4	6.026	14	2.494
5	4.403	15	9.940
6	14.660	16	7.320
7	14.717	17	2.071
8	6.794	18	3.809
9	13.428		

The OOIP estimates were also used to calculate the total recovery of each tract from primary and incremental production from secondary methods. **Figure 98** shows the result. It can be seen that tract 7 has a lot of potential that can still be tapped. Tract 7 is a good candidate for secondary process implementation since the OOIP is large. Tract 9 is also attractive for the same reason coupled with the fact that it has an extremely low well density in terms of number of wells drilled.

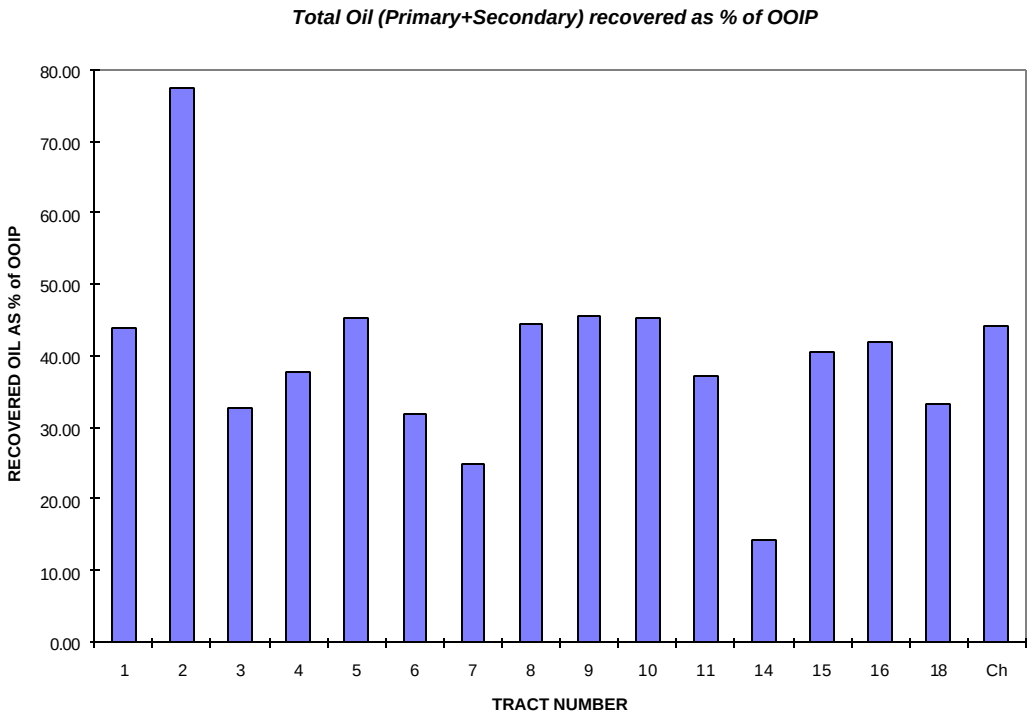

Figure 98 – Total oil (primary + secondary) recovered as % of OOIP (all tracts + Chevron's micellar-polymer unit)

Summary

Using our screening criteria, the areas with the highest potential for additional recovery were identified. The areas with the highest potential for recompletions were identified as tracts 9 and 7. These tracts were investigated in more detail as discussed below. In addition, Chevron's micellar-polymer unit was studied further to understand why the micellar-polymer flood was successful in that unit.

Chevron's Micellar-Polymer Unit

The area of analysis was the Chevron micellar-polymer unit, which is north of tract 9. Chevron implemented a micellar-polymer flood pilot from 1979-1983, which was based on selective isolation of the upper zones. Chevron initiated field-wide implementation in 1983-1984 that resulted in a remarkable increase in oil production, which will be discussed later in more detail. The obvious success of the Chevron micellar-polymer flood prompted us to analyze the unit in more

detail. Further, the performance and the completion strategies in this unit could be used as a focal point to compare and contrast it against tract 9 which is a geologically similar unit with comparable oil saturation profiles.

Perforation Strategies

Chevron used the prevalent upper Glenn, middle Glenn and lower Glenn divisions of the Bartlesville sandstone to describe the reservoir. Chevron believed that the upper and middle Glenn layers were separated by a continuous shale barrier and implemented the pilot flood by isolating the perforations in the upper zones. This was later proved to be untrue. The strategy during the field-wide implementation was to complete the wells both in the upper and middle Glenn layers. **Figure 99a** shows the contrast in completion strategies during the pilot and field implementation. The lower Glenn was avoided since it is known to be water bearing. This is in sharp contrast to the completion practices in section 16 and tract 9 wherein the completion density increases as we progress down to the lower intervals. **Figure 99b** shows this in graphical form.

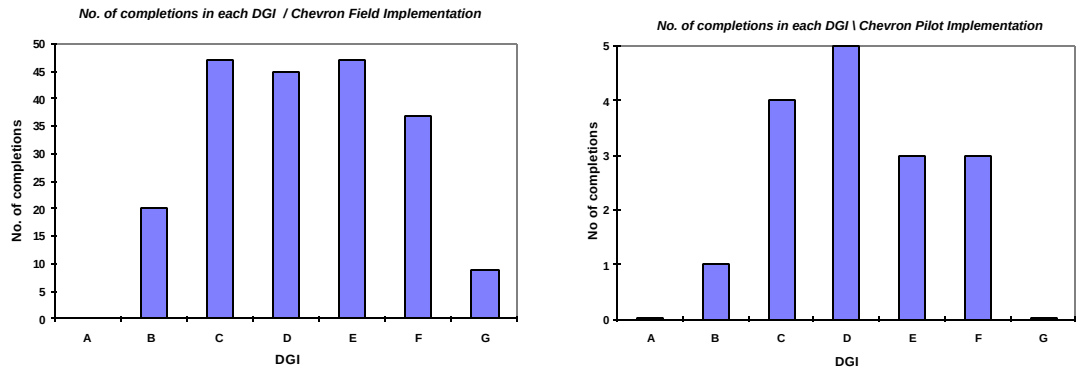

a

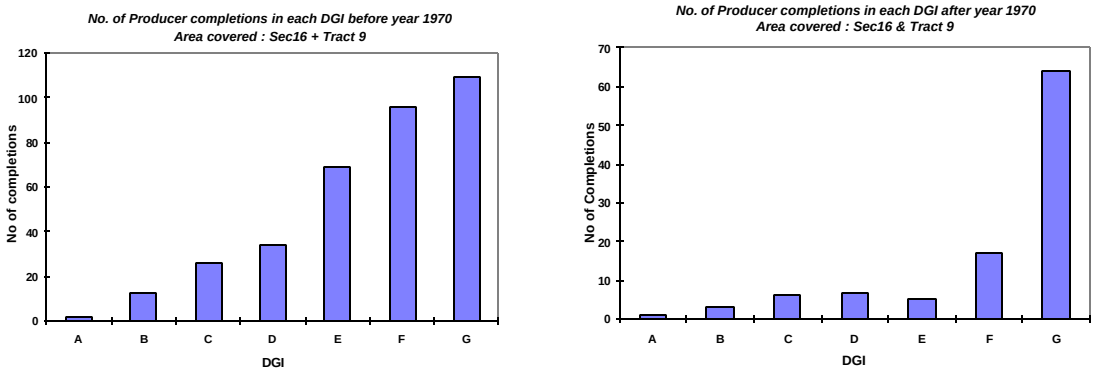

b

Figure 99 - (a) Completion practices in the Chevron unit. (b) Completion practices in section 16 and tract 9

Effects of the Micellar-Polymer Flood

The micellar-polymer flood implementation resulted in 52-times increase in oil production and a WOR decrease of almost 10 times as shown in **Figure 100**. Chevron increased the number of completions dramatically in 1982-83 prior to micellar-polymer flood field implementation. We believed that at least part of the additional oil response could be attributed to better completion practices. Hence it was decided to conduct a flow simulation to study the effect of additional completions by waterflooding the reservoir as opposed to a micellar-polymer flooding effort. This enabled us to quantify the additional recovery that could be expected out of a similar program in tract 9.

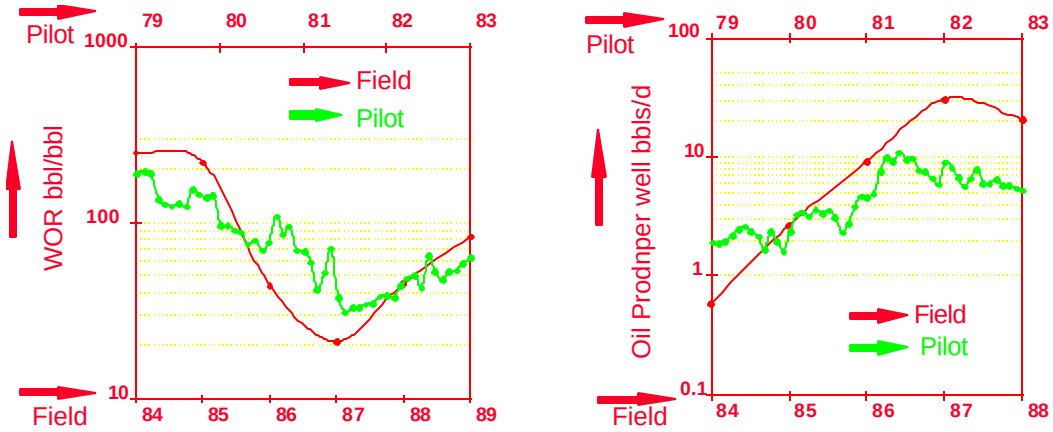

Figure 100 – WOR and oil production response of the Chevron unit

Chevron Unit Flow Simulation

The following data were collected for the area courtesy of Hyperion Energy Resources, the current operator for the lease. In general the porosity in the Chevron area is higher as compared to section 16 although this is not true for permeability.

- Core and log data
- Production data as a function of time
- Perforation/completion data

The core data at each well location was averaged for each DGI. The average values were then interpolated at interwell locations to create areal maps of porosity and permeability (**Figure 101**) for each DGI. The shale barriers between the DGI's were assumed to be continuous since the vertical permeability is observed to be negligible as compared to the horizontal permeability.

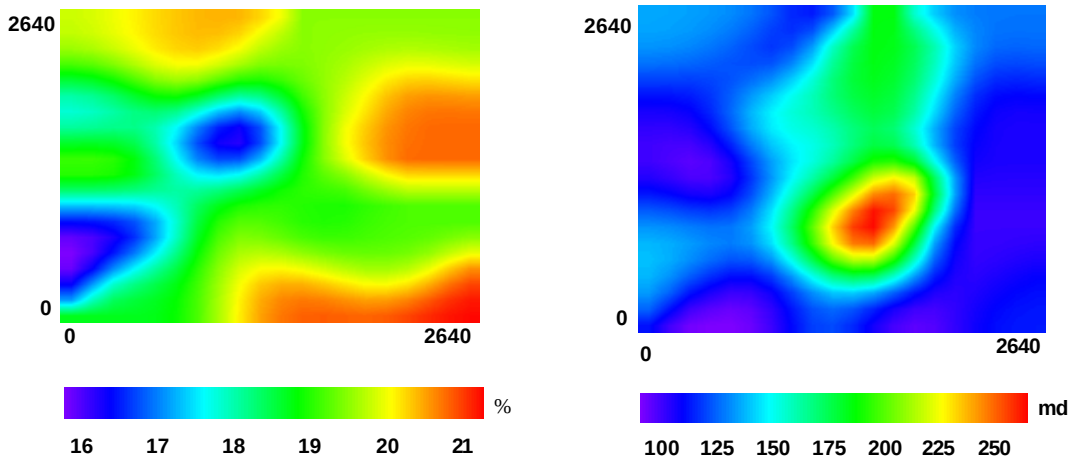

Figure 101 – Sample porosity and permeability areal profiles

The PVT properties input requires oil and gas properties as a function of pressure. The minimum bottom hole pressure is known to be around 20 psi and the initial pressure of the reservoir was around 900 psi. Therefore the working range of pressure is 20-900 psi. All the properties were generated using standard black oil model correlations for the above working range in discrete increments of pressure.

The parameterization of the relative permeabilities was done using the power law model with reasonable end point permeabilities suggested by the Kuykendall.[2] The exponents of the oil and water curves were varied as a function of time.

A commercial simulator, ECLIPSE, was used for simulation purposes. The primary depletion stage simulation was carried out so as to approximate the field oil production response by standard hyperbolic decline with a reasonable guess value of initial oil production. The secondary recovery stages of the simulation were constrained to match the oil rates. The relative permeabilities were fine-tuned as a function of time to get the observed water cuts. Every effort was made to closely monitor the number of active wells and the average reservoir pressure at any time to get a reasonable forecast.

The areal expanse of the Chevron unit is 160 acres. It was decided to divide the area into 132-ft x 132-ft grid blocks so that any layer is split in 400 grid blocks. The thickness of each grid block is assigned to be the thickness of the layer itself, which is obtained by interpolating at interwell

locations. The system has 11 layers, which is the sum of all DGI's B through G and the intermediate shale layers between any two DGI's.

The results are as shown in **Figure 102**. The simulated water flooding response shows a much lower kick in the field oil production (FOPR) as compared to the actual micellar-polymer flood response. Similarly the WOR plot shows decrease by a larger factor for the actual micellar-polymer flood response as compared to the simulated water flooding response. **Table 8** quantifies the responses observed.

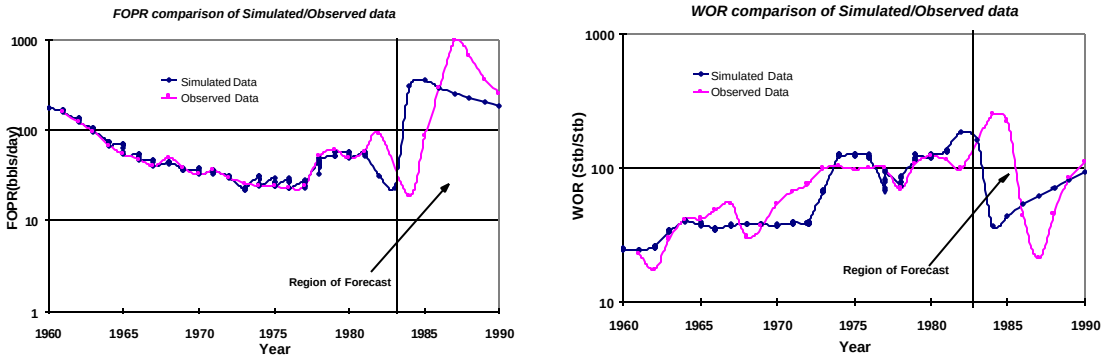

Figure 102 – WOR and field oil production plots for the Chevron unit

Table 8 – Comparison of miceller-polymer versus conventional waterflood

Response	Miceller-Polymer	Waterflood
Field oil production (bbl/d)	51 times increase	15 times increase
WOR (bbl/bbl)	10 times decrease	4 times decrease

Summary of Simulation of Chevron's Unit

Based on the simulation results from Chevron's unit, it was clear that the favorable response observed during the miceller-polymer flood was partly due to better completion strategies and partly due to the addition of chemicals. Conservatively, if only water flooding would have been used in the Chevron unit, the oil production would have increased by 15 times as compared to 51 times. The WOR would have decreased from 200 to 50 instead from 200 to 20. Although not as impressive, re-completion of upper zones would have added significant oil production. This type of completion

strategy is relatively cheap as compared to injecting expensive chemicals. We evaluated the usefulness of these strategies for tracts 9 and 7 in the following two sub-sections.

Tract 9 Evaluation

Tract 9 is located south of the Chevron unit and has an areal expanse of 160-acres (see Figure 87). The unit is operated by Uplands Resources Incorporated and has very similar reservoir conditions to the Chevron unit. The well schedule information was very difficult to reconstruct. It is known with a fair degree of certainty that number of wells that have been drilled so far from the time of discovery is close to 65. The unit currently has six active producers and ten active injectors providing pressure support. Tract 9 is one of the units that rank high with respect to the original oil in place (15 MMStb). From the report compiled by Welch[50] it was observed that tract 9 had produced cumulatively 6.058 MMStb of oil through primary depletion and secondary recovery operations as shown in **Figure 103**. This amounts to a recovery of 40% of the original oil in place.

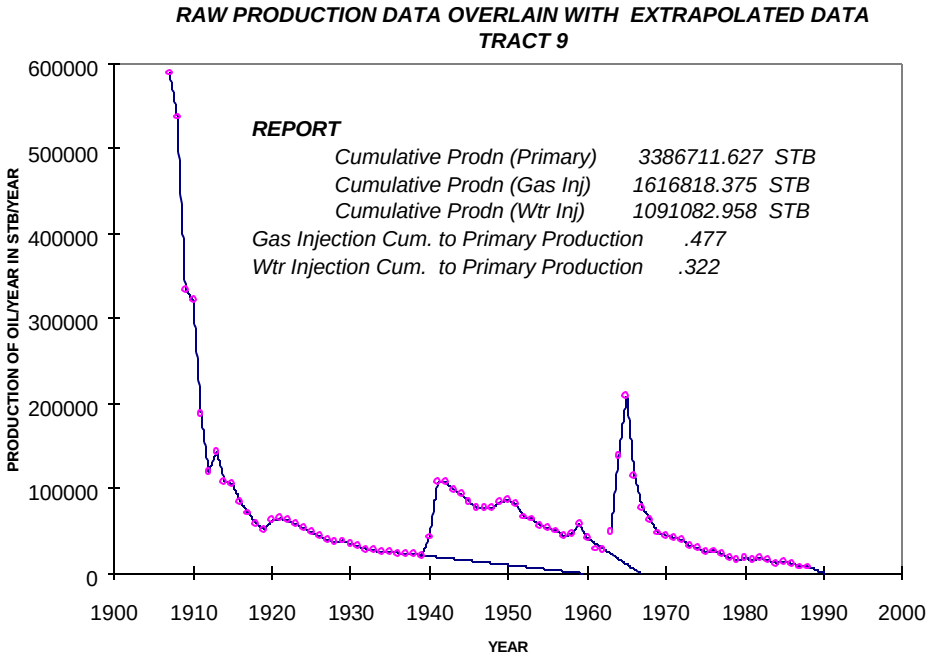

Figure 103 – Production analysis plot for tract 9 showing the primary gas injection and water flooding stages of depletion

Geostatistical Estimation of Petrophysical Properties[51]

The A-G DGI model provided by the geologist was directly used as input for a thirteen layer system into the simulator with each DGI constituting one layer with shale interbedding between successive DGI's. The facies divisions used within each DGI are channel sand, splay sand and flood plain mudstone as provided by the geologist.

A well base map for each DGI was constructed with the facies code assigned at the well locations. The facies type was determined by the type of SP or Gamma ray log response observed at the well. The facies code was assigned based on the following convention:

- Channel sand
- Splay sand
- Flood plain mudstone, shale

Indicator variograms were then generated for each facies, which were then input into the indicator simulation program-Sisimpdf[52] for constructing the areal facies map. The Sisimpdf program honors the input proportion of each facies. In this study a multi-layered model was used which compromised the variability of the petrophysical properties to a certain degree but the depositional hierarchy was strictly honored. Unlike the Chevron unit study an attempt was made to simulate the shale layers between successive DGI layers to identify areas where the shale barrier is discontinuous permitting sand upon sand stacking.

The thickness of sand in each DGI at well locations was estimated from the data provided by the geologist. These estimates were then kriged at interwell locations using the ordinary kriging procedure to generate thickness maps for each DGI. It should be noted that the thickness of sand is explicitly forced to zero for interwell locations where the simulated facies is known to be shale.

The porosity at each well location was estimated based on the gamma ray logs due to insufficient density-neutron or sonic logs. A gamma ray to core porosity regression relationship was established based on data from the Self-82 well located in the Self-unit (**Figure 104**). This was the only physical core situated proximal to the study area. The gamma ray values were then averaged

within each DGI and then kriged at interwell locations to produce gamma ray maps for all DGI's. The kriging was performed with the previously simulated facies maps as external drift.[52] The regression relationship was then used to translate this to a porosity map.

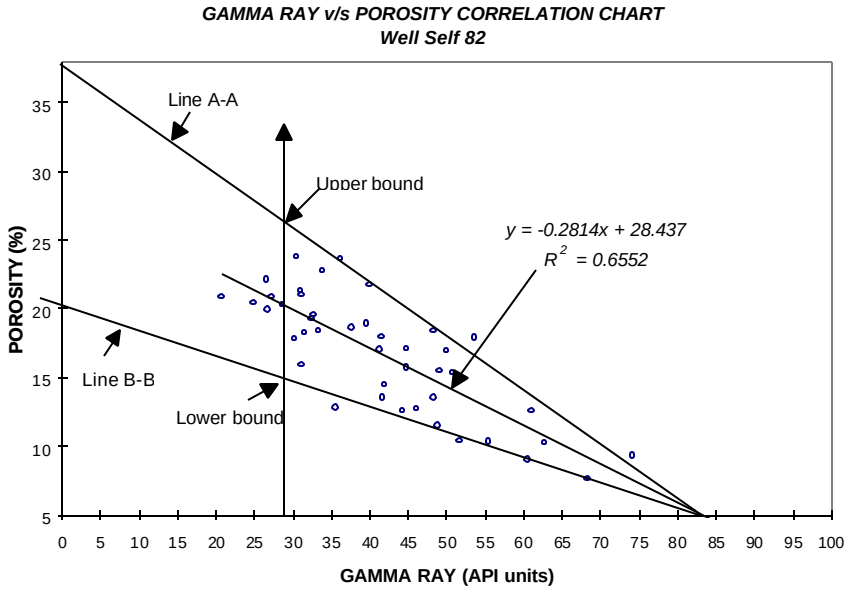

Figure 104 – Gamma ray versus core porosity correlation developed from the data compiled from Self-82

Gamma-ray values have a direct dependence on the shale content of the reservoir, which is inversely proportional to the porosity of section. Since gamma-ray logs show a pulsating response as opposed to the blocky response shown by SP logs, foot by foot measurements of gamma ray logs may be misleading. When they are averaged over the thickness of the DGI itself the value should be representative of the shale content and in turn porosity at a particular location.

Figure 104 shows a large scatter identified by the lines A-A and B-B around the trendline for which the equation is provided. Hence it was proposed to feed the straight-line equations of A-A and B-B and use a random number generator for determining the porosity value for a given gamma ray measurement. For example a gamma ray measurement of 30 API units could be representative of a porosity value between 15% and 26% marked on the plot as Lower and Upper bounds respectively. It should be noted that the lower the gamma ray value, the higher the uncertainty in the correlation.

Even though the correlations between $\ln(k)$ and porosity are quite good it was not used since the regression relationship may yield unreasonable values when extrapolated beyond the input porosity range used to construct the correlation. Once the porosity maps were generated for all DGI's the values in each DGI were transformed into a standard normal Gaussian distribution. It is known that the porosity values are related to permeability without a large scatter. So the values in the Gaussian domain obtained from porosity are back transformed into permeability (real space) using the cumulative distribution function (cdf) from Chevron unit data as input. This is done DGI by DGI with the input cdf for the corresponding DGI generated from the Chevron unit.

Figure 105 presents a composite diagram of the facies, thickness, porosity and permeability map. It can be observed that the thickness and the petrophysical property maps carry the geological facies imprint.

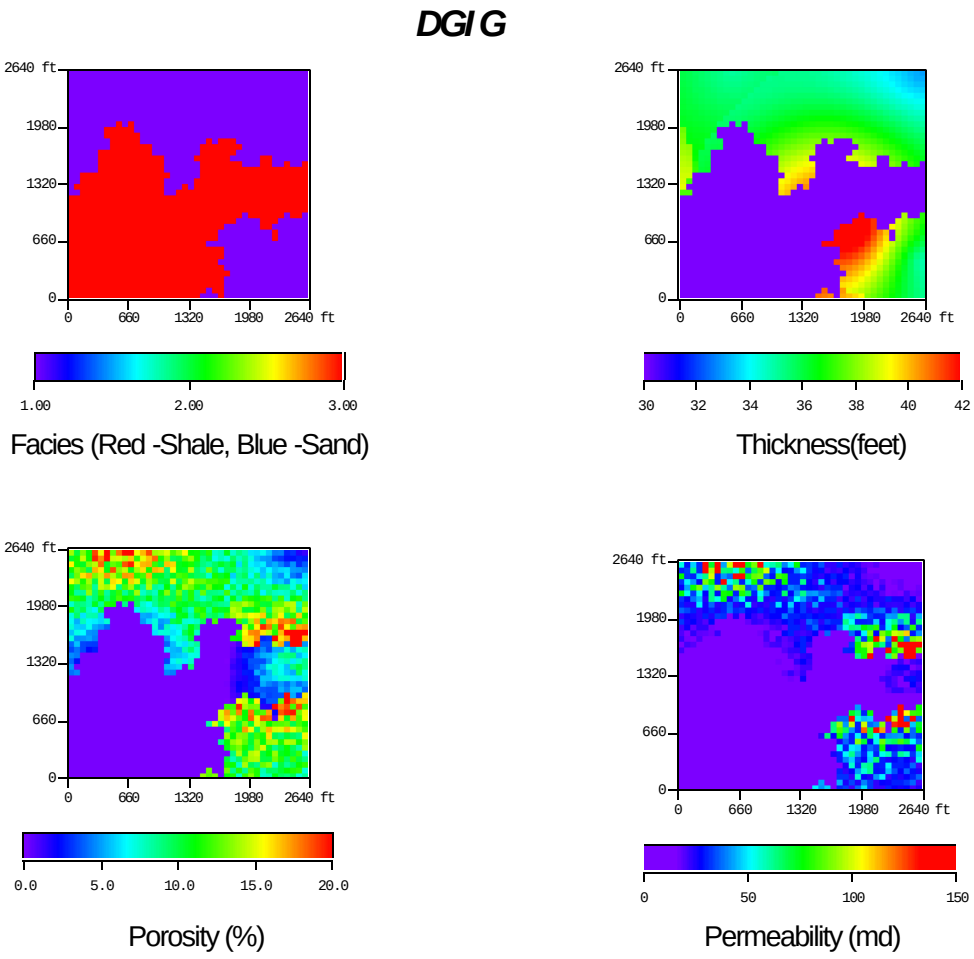

Figure 105 – Composite diagram showing areal maps of porosity, permeability and thickness honoring the facies distribution

Flow Simulation Procedure

Tract 9 simulation study used total liquid production as the flow constraint instead of oil production. The rationale used was that if the total liquid production were matched, discrepancies in simulated water cuts compared to the actual field values would result in unacceptable errors in simulated oil production. This should be understood in light of the fact that typical water cuts in producing wells are 99%. If a small difference in simulated versus observed water cut is observed it results in significant difference in water production. It would have happened if we had used oil rate as a constraint.

Another difference from conventional history matching procedure was the entire history of tract 9 was not matched. Significant uncertainty exists as to the well locations during the early life of tract 9. Further data on individual wells – production, completion, and abandonment – was not available. Even the total production on tractwide basis was missing for many years. This made it very difficult to simulate the historical performance. Instead of trying to match an "estimated" historical performance, it was decided to concentrate on the last five years of production history for which better quality data were available. We initialized the model in 1992, and estimated the prevalent conditions at that time using available data as described below.

The areal expanse of the tract 9 is 160-acres. It was decided to divide the area into 66 × 66-ft grid blocks so that any DGI is divided in 1,600 gridblocks. The thickness of each gridblock was assigned to be the thickness of the DGI itself, which was obtained by interpolating the values at interwell locations. The system had 13 layers, which is the sum of all DGI's A through G and the intermediate shale layers between successive DGI's.

The PVT properties input requires oil and gas properties as a function of pressure. The minimum bottom hole pressure is known to be around 20 psi and the initial pressure of the reservoir was around 900 psi. Therefore the working range of pressure is 20-900 psi. All the properties were generated using standard black oil model correlations for the above working range in discrete increments of pressure.

The well test data provided an estimate of the average reservoir pressure around the well. Four well tests were conducted within tract 9. These average pressures were gridded using the kernel smoothing technique to generate an areal base map of pressure for the year 1992. Since all the DGI's are in vertical communication with the exception of DGI's A and B vertical equilibrium was assumed to calculate the areal pressure profile for each DGI. It should be noted that the base pressure map is tied to DGI E since this layer represents a median depth in the vertical structure of Glenn sand. All other DGI pressure profiles were determined based on the hydrostatic pressure difference. **Figure 106** shows the base pressure map that is tied to DGI E. It can be seen that the southwestern corner pressures are lower as compared to other areas. This might be an indication of lack of support to the existing producers from the current injectors.

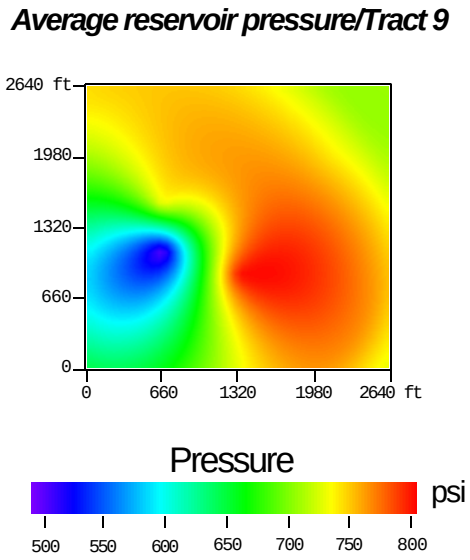

Figure 106 – Areal reservoir pressure map that is tied to DGI E in psi

The saturation profile was derived from resistivity logs. It was then scaled using a multiplier to make it representative of the year 1992. The methodology used to determine the multiplier is as follows. The effective permeability (product of relative permeability and absolute permeability) was estimated from the model at all wells where well testing was carried out. The effective permeability, which is a function of saturation, was then compared with the observed effective permeability derived from the well test. Since the effective permeability has a direct dependence on saturation, the saturation was scaled so as to bring the model derived effective permeability closer to the well test derived effective permeability at all the wells. Using this method, the multiplier selected was 1.4.

Flow Simulation Results

The well map is presented in **Figure 107**. It shows only the active wells for clarity and does not include all the wells that have been drilled in this unit. Initially it was proposed to restrict the recompletion/redrilling program to the area marked by dotted lines in the well base map. In accordance, the following scenarios were proposed.

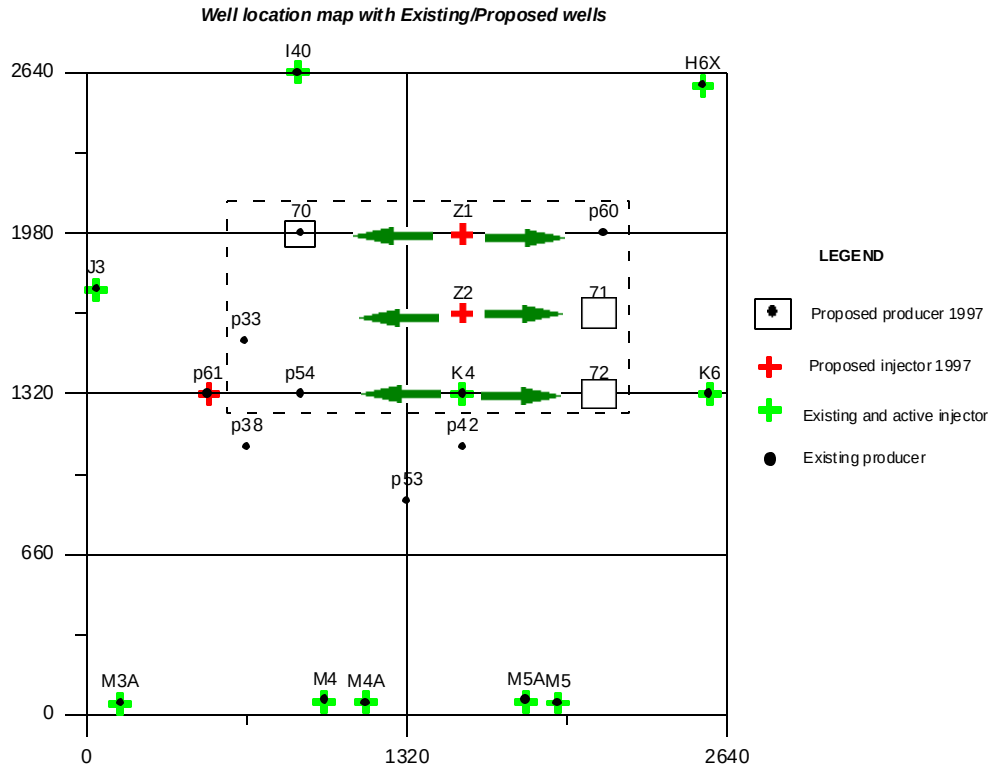

Figure 107 – Well base map of existing/proposed wells for tract 9

Scenario Base

It was proposed to plug the lower DGI's (E, F, G) and then complete upper DGI's (A, B, C, D) for all existing wells within dotted area namely p33, p54, p60 and K4. Two new injectors and three new producers 70, 71 and 72 were proposed. It was intended that the injectors Z1, Z2 and K4 would form a water bank and sweep the oil east and west of the line of injectors toward the producers as shown by the green arrows in Figure 107.

Anisotropy Favorable/Unfavorable

It was proposed to investigate the effect of anisotropy $K_{N-S} = 3 \times K_{E-W}$ for the base case. This would be favorable for the proposed intent since the water bank formation is promoted owing to the North-South permeability being higher. It was also decided to consider the adverse case where $K_{N-S} = (1/3) \times K_{E-W}$ to get an idea of the possible downside if the truth is an exact converse to the favorable case.

The history matching for all the cases was done from the year 1992-1997. The forecasting was done from May 1997. It should be noted that the history matching was done with total liquid production as the flow constraint. Hence the oil production curve during the history matching stage would be case dependent because of variations in the oil cuts.

Scenario Plug/Recomplete All Wells

Scenario base did not yield a good response. Hence it was decided not to restrict the scope of operations to the dotted area mentioned in the base scenario. It was proposed to plug all injectors and producers in the lower DGI's (E, F, G) and complete them in the upper DGI's (A, B, C, and D) without redrilling new wells.

The proposal did not look attractive at first glance (**Figure 108**) since the incremental oil production on implementation of recompletion/redrilling program was not significantly higher as compared to the case in which existing conditions were allowed to prevail. This was indicated by the closeness of the two curves in the oil production plot. The water cut plot showed a decrease of 98.7% to 97.3% that translates into a considerable reduction in water production. Hence despite the fact that incremental oil production was not encouraging the proposal was economically viable since the water production was cut drastically resulting in a remarkable reduction in operating costs.

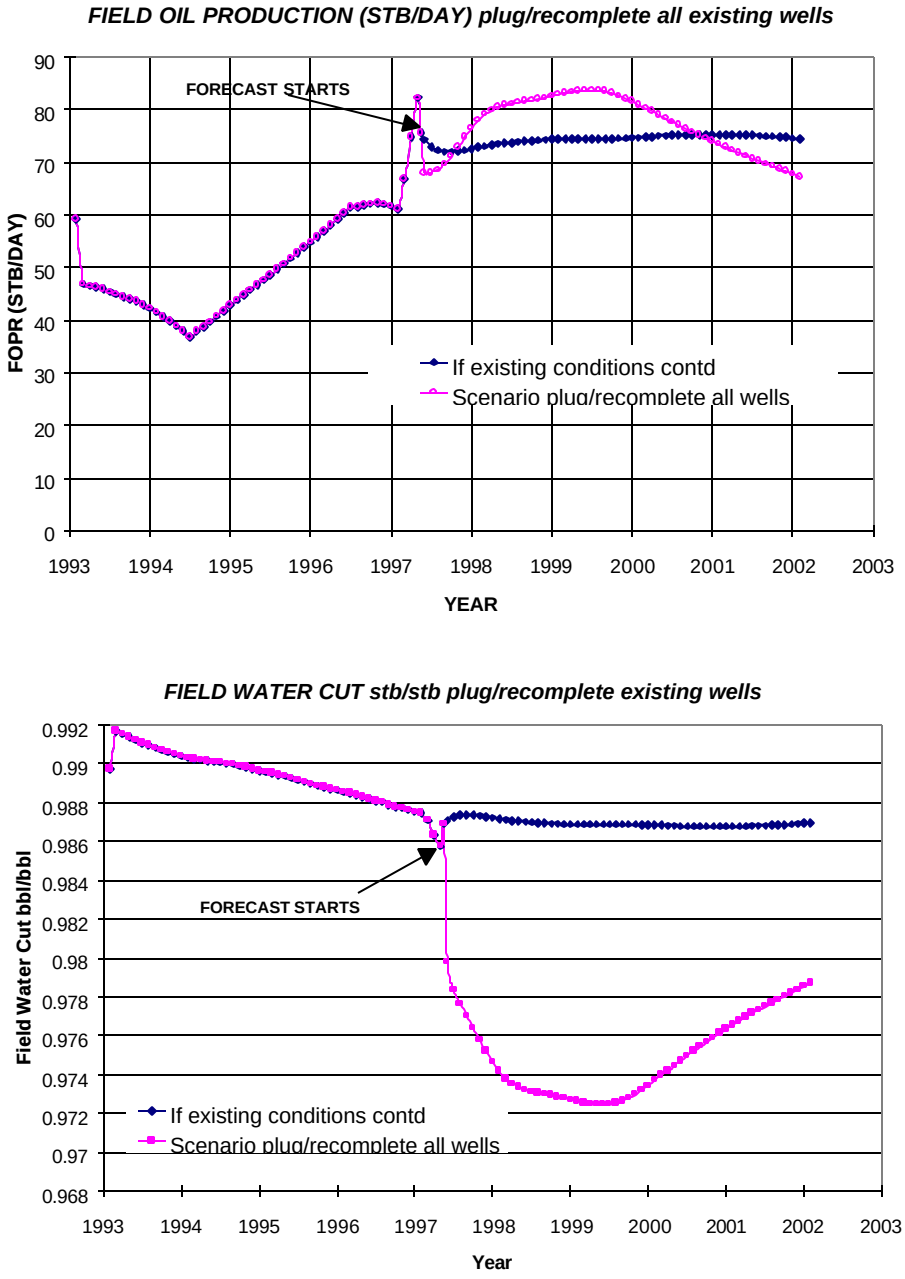

Figure 108 – Oil production and water cut plot for scenario plug/recomplete all wells

Scenario Plug/Recomplete Old Well and Drill New Vertical Wells

This scenario was a combination of the base case and the scenario detailed in the previous section. The proposal for new wells was not changed. Hence in this scenario the new wells are p70, p71 and p72 as producers and Z1, Z2 as injectors. The intention was to capture the advantages of

plugging the lower intervals in terms of reduction in water cut and still gain incremental oil production by virtue of the new wells drilled.

The incremental oil production, after implementation of the proposal over the existing condition case, was at best about 35 bbls/d. The water cut goes down from a value of 98.7% before implementation to a low of 97.8% which was a reduction of 0.9% as compared to a cut of 1.4% brought about by the plug/recomplete program.

Scenario Plug/Recomplete Old Wells and Drill New Multilaterals

It was proposed to drill multilateral wells (**Figure 109**) with lateral sections penetrating each of the upper DGIs A, B, C, D. The well would penetrate the formation in the North-South direction. Well Z1 would be a multilateral injector and well 71 would be a multilateral producer. The intention was to gain advantage of the horizontal sections of the multilateral wells. It was hoped that multilateral injector would provide good sweep and that the multilateral producer would yield more incremental oil production as compared to vertical wells.

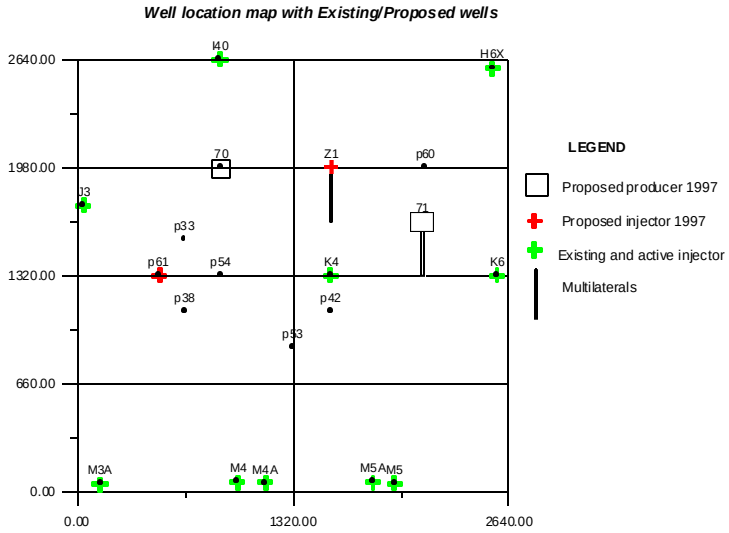

Figure 109- Proposed well base map with multilateral well locations

The incremental oil production after implementation of the proposal over the existing condition case was at best about 70 bbls/d which was considerably larger than the vertical well scenario (35 bbls/d). The maximum reduction in water cut was about 1%.

Scenario Plug/Recomplete Old Wells and Drill Deviated Wells

Since the multilaterals proved not to be cost ineffective it was proposed to investigate a scenario wherein the multilateral wells were substituted by deviated wells. The idea was drill at an angle of 80 degrees to the vertical (almost horizontal) and penetrate all upper DGI's namely A, B, C, D with an approximate span of 80 feet in each layer. The principal direction of penetration would be North-South.

The incremental oil production after implementation of the proposal over the existing condition case was at best about 70 bbls/d, which was lower as compared to the scenario in which multilaterals were proposed. The maximum reduction in water cut was once again about 1%. Since the cost of drilling a deviated well is a cheaper proposition as compared to the cost for a multilateral well, it was economically more attractive.

Ancillary Scenarios

In addition to the above scenarios, we also considered scenarios that were based on our understanding of potential index mapping of tract 9. Based on the mapping of potential index, we had noted that all the areas of tract 9 were not equally explored. Based on the potential maps, we investigated three additional scenarios that involved either drilling vertical producing wells, or either drilling deviated injection or production wells. These scenarios are shown in **Figure 110**.

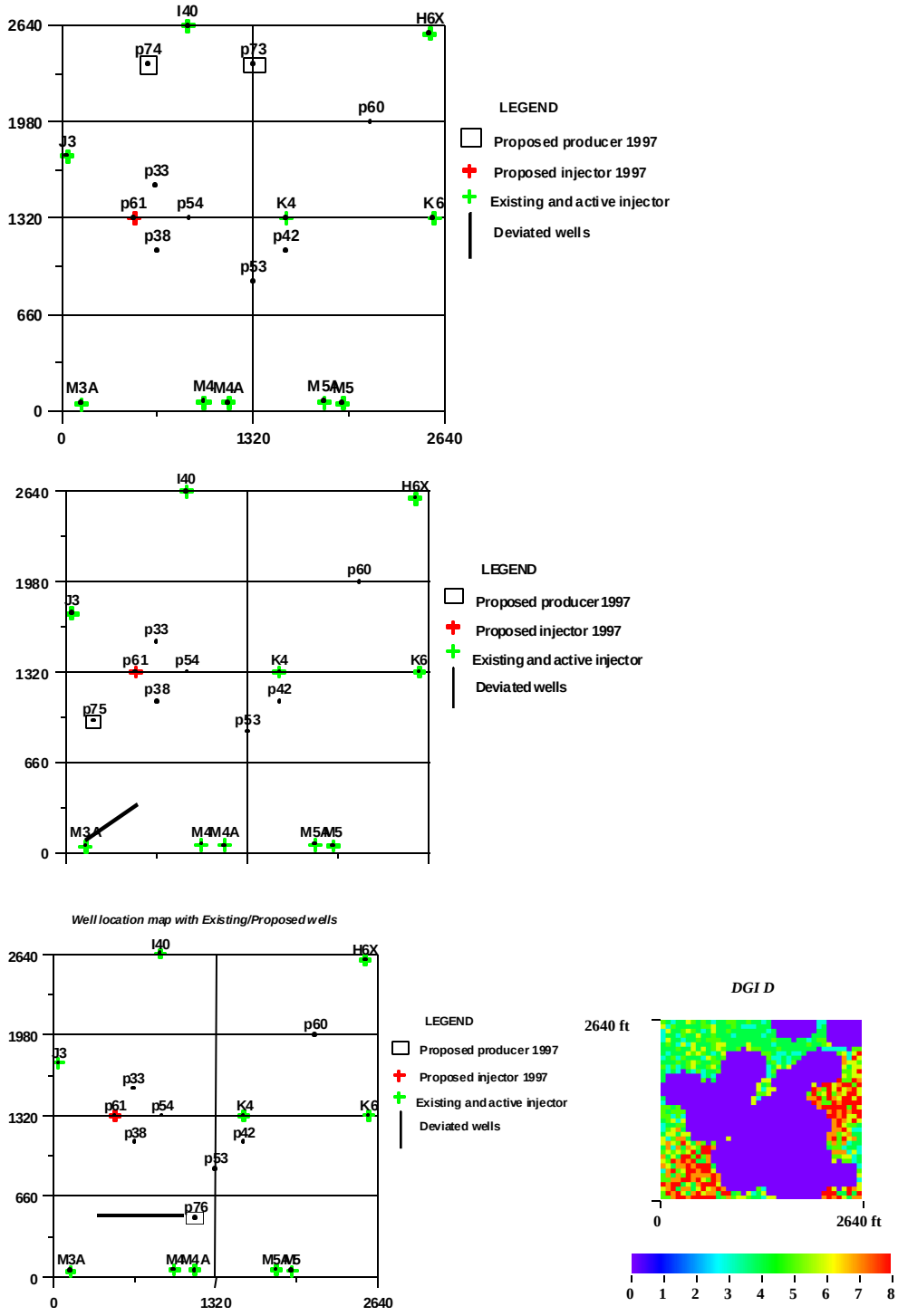

Figure 110 – Well locations of the existing/proposed wells along with a sample potential index map

The response from these scenarios is shown in **Figure 111**. The results are compared with the base line where existing conditions are allowed to prevail. The best response is given by drilling a

deviated producing well – P76, and is second only to the scenario when all the individual scenarios are implemented simultaneously.

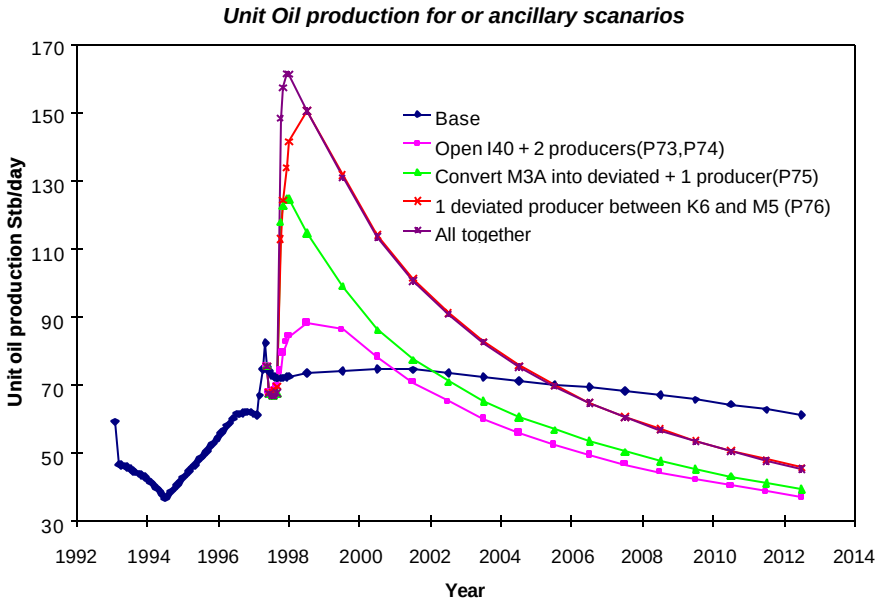

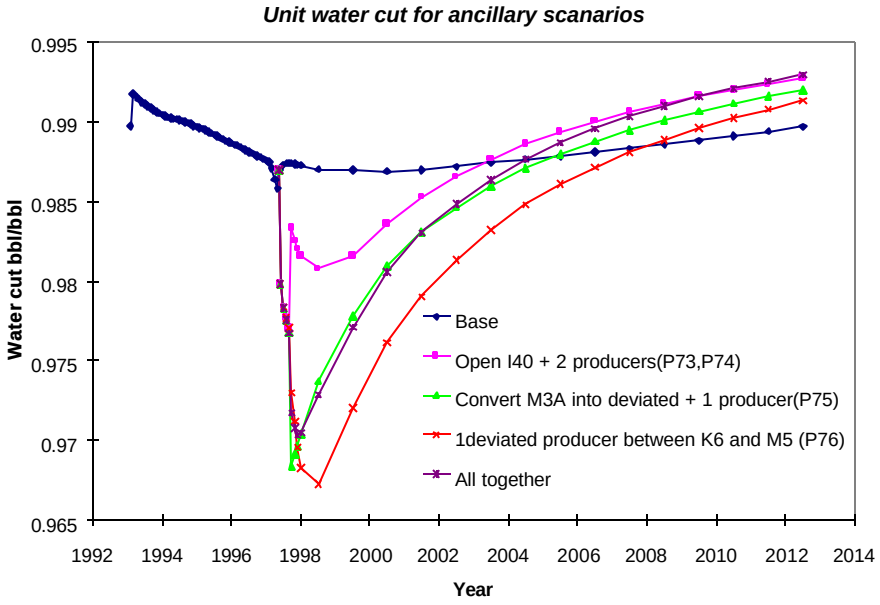

Figure 111 – Oil production and the water cut plot for ancillary scenarios

Economic Evaluation

A simple economic evaluation was conducted to identify the most favorable scenarios.[51] The rate of return histogram is presented which is a compilation of all scenarios (with the exception of ancillary

scenarios) together arranged in ascending order. It was decided to incorporate sensitivity analysis on the oil price with variations as shown in **Figure 112**. The ROR figures do not show a large variation for any given scenario. It can be noted that the plug lower DGI's/ recomplete upper DGI's flow scenario stands out among all the proposals. However, it should be noted that the production increase in plug/recompletion scenario was not significant. Most of the cost savings were achieved by reducing the water cut, and hence cost of lifting.

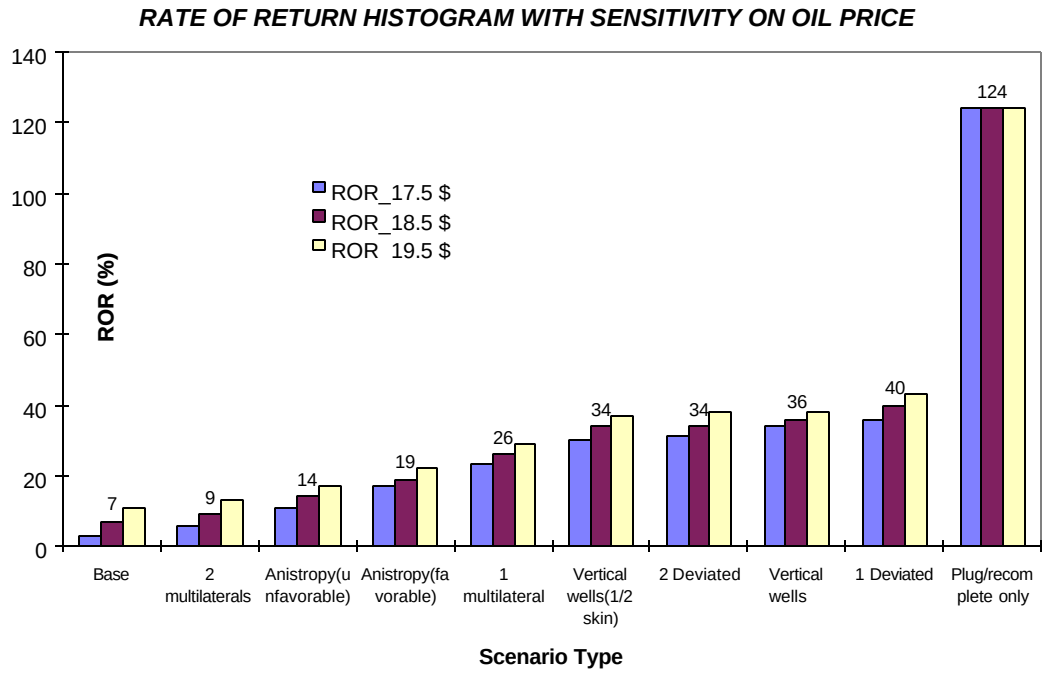

Figure 112 – ROR histogram with sensitivity on oil price

The ancillary scenarios were investigated separately because of the method with which locations of the wells were selected. The results of the economic analysis are presented in **Figure 113**. The deviated producer resulted in an impressive ROR with a positive NPV at both 15 % and 25 % interest rate. In these scenarios, we have assumed that the existing wells were selectively plugged/recompleted for three months, and the new wells were drilled following the three-month observation period.

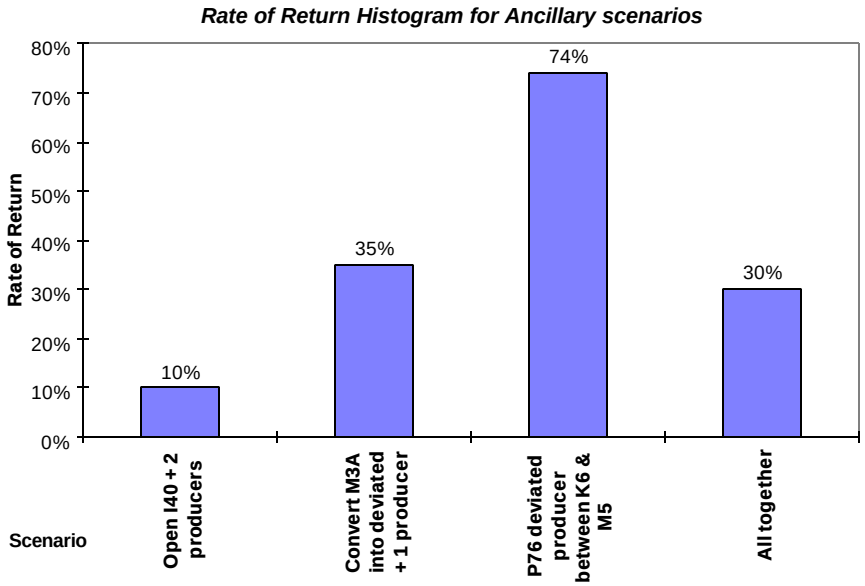

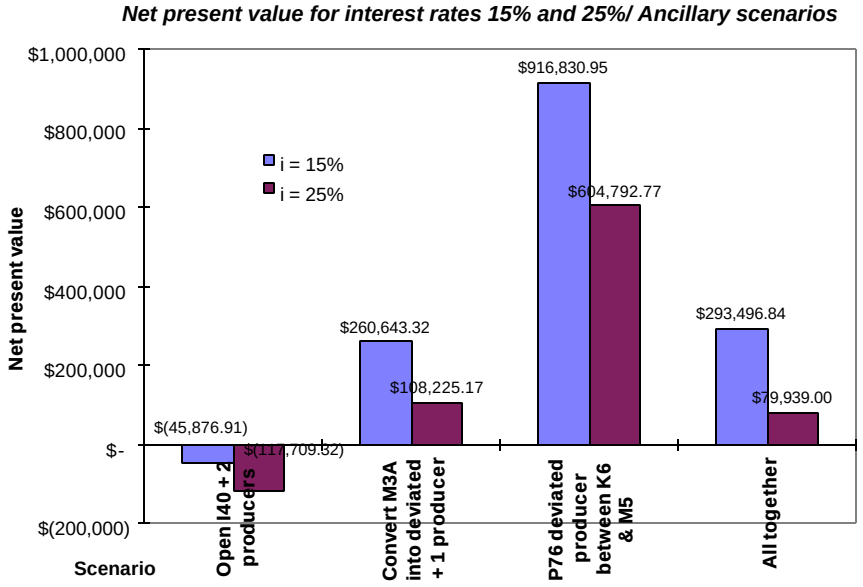

Figure 113 – Rate of return and net present value charts for ancillary scenarios

Summary from Tract 9 Simulation

Based on the evaluation of several scenarios, we observed that the most feasible scenario was drilling of a deviated well, p76. This well would result in most incremental oil production with a significant reduction in water cut.

Tract 7 Evaluation

Tract 7 is located north and east of tract 9 and is also operated by Uplands Resources, Inc. The well density is higher as compared to tract 9, and the unit has a history of good response to water flooding. The present well locations are shown in **Figure 114**. It is estimated that tract 7 has close to 15 MMStb of Original Oil in place (OOIP). From Welch[50] it was noted that tract 7 has produced about 3.9 MMStb through primary depletion and secondary recovery operations. This means that the total recovery is about 26% of the OOIP, implying there is still a lot of untapped potential in the reservoir as compared to tract 9 which has a cumulative recovery closer to 40%. The well density being high, it was not advisable to drill new wells, but a plugging/recompletion program to exploit the upper zones may yield significant additional oil recovery.

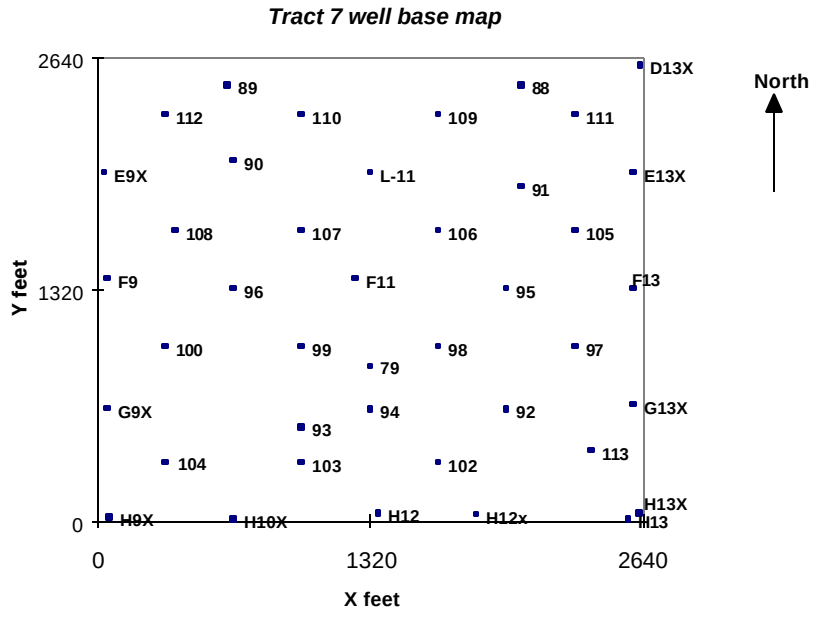

Figure 114 – Well map for tract 7

Data Input and Flow Simulation Technique

The facies maps for all DGI's were generated using similar methodology as discussed in the previous sub-section. Several realizations were performed, and the realization which closely matches the map generated by the geologist, was chosen for petrophysical property estimation. In this work, this selection was done by visual observation.

As discussed in the previous sub-section, we used gamma ray values to estimate the porosity data. Although gamma ray logs are common in the field, one of the major drawbacks of estimating porosity from gamma ray logs in mature fields is as follows. The engineer has to contend with the fact that calibration of the gamma ray tool is not uniform since the logs are performed by different service companies.

Open hole logs always give a higher gamma ray reading as compared to cased hole logs. Since gamma ray logs measure the natural radioactivity of the formation, cased hole logs are affected by the presence of the casing between the recording tool and the formation. Conceptually, if two different wells are logged with the same tool, a pure shale interval in the two wells would have the same reading of gamma ray API units. This is not observed in practice since the shale found at two different vertical sections may have different sand content, varying organic material content, contrasting compaction levels, all of which affect the value of the gamma ray readings.

If the raw values of gamma ray readings from different wells are translated to porosity without accounting for the facts mentioned above, it would lead to under or over estimation of porosity. It should be noted that the gamma ray to porosity regression correlation is one single relationship and the same relationship is used for all the wells uniformly. By itself, the correlation does not take into account the variations in the gamma ray readings between the wells. To overcome this problem, we used a procedure of multiwell normalization.

The objective of the procedure is to bring the shale base line for different logs in alignment so that all deviations from this base line, which are indicative of sand, are referenced from a common base datum, thus making the use of gamma ray-porosity relationship more reliable. It is observed that most of the wells in this study area are cored in the lower interval. Gamma-ray logs are transformed into porosity values for wells, which are cored in the lower intervals. Then the gamma ray derived porosity is compared with the core porosity. Only those gamma-ray logs are selected which demonstrate a good comparison. Foot by foot gamma-ray readings for such logs are pooled together to construct a probability density function (pdf) and this pdf is termed as the standard distribution. Individual well gamma-ray logs are then used to construct pdf(s) for the respective

wells. The well pdf is then plotted against the standard distribution to determine the amount of linear shift in gamma-ray absolute value required to bring the shale base lines in alignment.

Figure 115 graphically exhibits the procedure. It can be observed that pdf curves exhibit two peaks, one for a range of gamma ray values between 15-60 units and the other centered around 90 API units. The first peak represents the range of possible gamma ray values representative of sand and splay. The range of values exhibited by the second peak is representative of shale. The underlying principle in shifting individual well pdf's is that even though the probability of occurrence of a gamma ray value representative of shale may not be the same in two different wells, the range of gamma-ray values which represent shale should be centered approximately around the same gamma ray reading. For well E-9 it was determined that a linear correction of -25 API units is appropriate. It can be seen that originally the centerline of the shale peak, which was 125 API units, after adjustment is about 100 units. This was done for all the wells other than those that were used to generate the standard distribution.

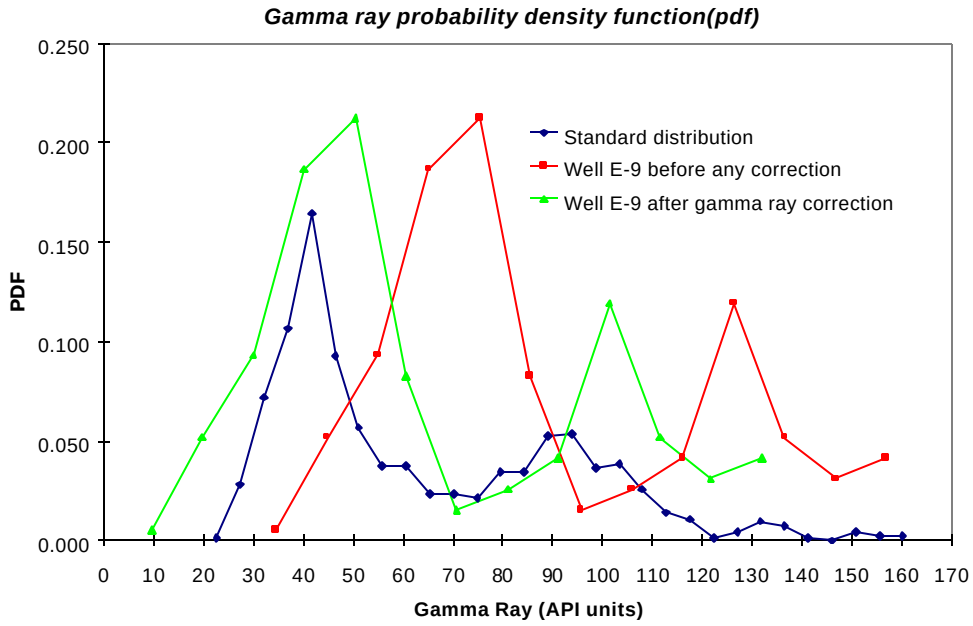

Figure 115 – Shift in pdf to align gamma ray probability distribution functions

Once the normalization procedure was completed the gamma ray values were averaged within each DGI at all wells. These average values were then kriged at all interwell locations DGI by DGI to produce areal maps of gamma ray readings with the simulated facies maps as external drift.

The areal gamma ray maps were transformed into porosity maps by using the gamma ray-porosity relationships with the use of a random number to aid the reproduction of the scatter seen in the gamma-ray vs. porosity plots (**Figure 116**). The correlations were generated with the use of digitized gamma ray values and density-neutron log porosity values. It can be observed that the wells show a fairly consistent relationship. In this study a cutoff was used with respect to the gamma ray values beyond which transformation of gamma ray values to porosity is meaningless. The cutoff in this case was fixed as 140 API units. Beyond this range, the porosity was fixed as 1%.

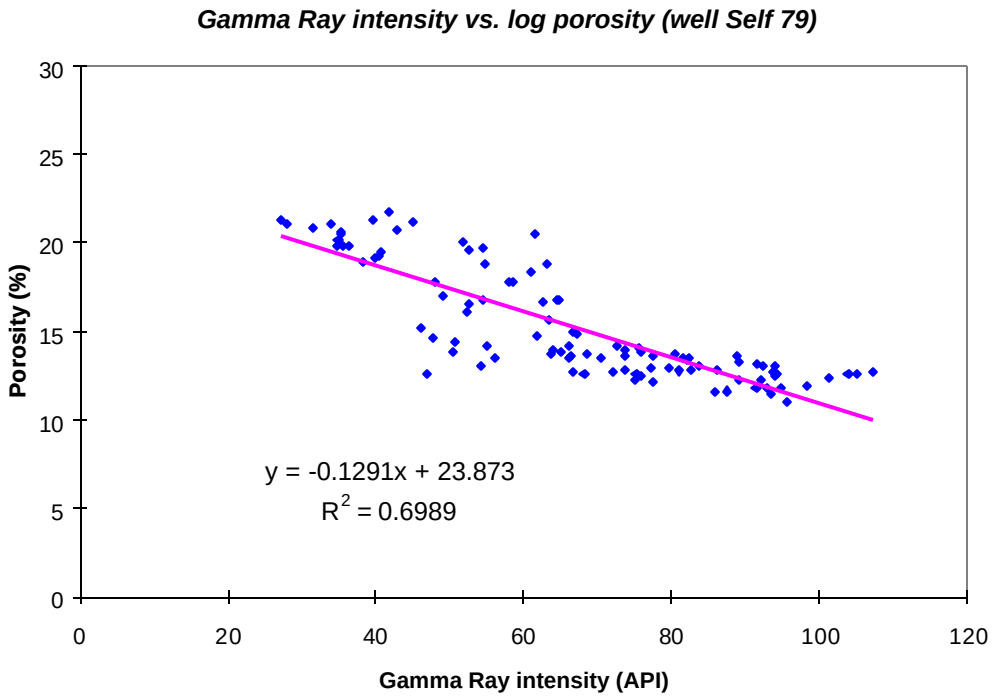

Figure 116 – Gamma ray versus porosity relationship

Regression relationships between *log(k)* and porosity were used to generate the permeability distribution from the porosity maps.

The thickness maps for all DGI's were generated by using the ordinary kriging procedure at interwell locations. The thickness of all gridblocks for which the facies type is known as shale/flood plain mudstone was forced to zero. Since thickness is a continuous variable as opposed to facies which is a discrete variable kriging on thickness even with zero thickness points need not necessarily capture the facies boundary between sand and shale. It was therefore necessary to use explicit procedures to make the simulated facies and kriged thickness maps consistent with each other.

Flow Simulation Process

The conventional history matching procedure involves reconstructing the well history from inception time to present time. A deterministic initial pressure and saturation profile is mapped, and then field flow performance is matched by tuning the input parameters. In this case study the saturation and pressure profiles were derived for the year 1993 and history matching is initiated at this time. This eliminates the need for reconstructing the well schedule history from inception time of the field. The history matching was performed for a short segment of time 1993-1997, during the course of which the input model was calibrated. It should be noted that the production and injection data were provided by the operator for this unit and is far more reliable than public sources of data.

The areal expanse of the tract 7 is 160 acres. It was decided to divide the area into 66 $\times$ 66-ft grid blocks so that any DGI is split in 1600 grid blocks. The thickness of each grid block was assigned to be the thickness of the DGI itself, which was obtained by kriging at interwell locations. The system has 13 layers, which is the sum of all DGI's A through G and the intermediate shale layers between successive DGI's.

The PVT properties used for this case study are essentially the same as those used for the Chevron unit study. The saturation profile derived from the resistivity logs was scaled up so as to match the water cuts. It can be recalled that the tract 9 case study uses well test data to match the effective permeability calculated from the model with the effective permeability derived from the well test. In this simulation study, this approach could not be realized since only a single well was tested within this study area. Hence the reserves in place and the saturation multiplier used for tract 9 were used as a guidelines for estimating the possible range of scaling coefficients of saturation. Recall that

saturation multiplier was necessary because we did not begin the simulation right from the beginning of production. Since our well log data were collected earlier compared to when we began the simulation, we needed to adjust the well log derived saturation so as to match the initial oil production as well as water cut. This was done by adjusting initial water saturations. The saturation multiplier represents the increase in water saturation required to match the observed production as well as water cut at the beginning of simulation period.

First, a multiplier of 1.4, which was used for tract 9, was used for this study also. The ratio of oil phase effective permeability to water phase effective permeability was similar in both the study areas justifying use of the same multiplier.

Second, a multiplier of 1.2 was chosen based on the fact that it is the lowest possible multiplier that would still yield a good history match with regard to the accuracy necessary in simulated water cuts.

It was known that reserves in place at the time when history matching is started (1993) is around 11.1 MMstb. Based on the use two multiplier coefficients 1.2 and 1.4 on the water phase saturation S_w, the reserves in place were calculated as 10.653 and 9.43 MMstb respectively. These numbers are consistent with the estimated reserves (11.1 MMStb) which were based on initial oil in place and cumulative oil production so far. The objective is to get an idea of the incremental oil production obtainable with a worst case $(S_w \times 1.4)$ and best case $(S_w \times 1.2)$ scenarios.

The pressure profile was guessed for DGI E, based on which all the other DGI pressure maps were generated assuming that the pressure difference between DGI's is equal to the hydrostatic head. The guess profile was then input into the simulator and the performance of this profile was gauged by determining if it satisfies the field injection and production rates. If not, the pressure data were altered so as to be able to match the production and injection data. It should be noted that the BHP for producers (pumping wells) is about 20 psi and the BHP for the injectors is known to be 1,250 psi. Hence there is only a certain range of input average reservoir pressure (year 1993) for which the production data/injection data can be matched. This obviously assumes that there is no leverage with regard to alteration of the petrophysical property fields. If a typical fracture gradient of

0.75psi/ft is assumed, the formation fracture pressure is calculated as 1,163 psi. It was found that the BHP of injectors is very close and sometimes above the fracture pressure. This is taken into account in the simulator by multiplying well transmissibility based on the instantaneous pressure difference between BHP and the calculated fracture pressure.

It should be noted that the single well test (well 7-111) that was performed in this study area demonstrated an average reservoir pressure of 1,050 psi. It was also known that the row of injectors located in the southern part of the study area take in water at very high pressures only. Considering these facts there was enough reason to believe that the average reservoir pressure is high and close to about 1,000 psi. Well 7-111 produces the highest volume of fluid and contributes one half of the total liquid production at any given time.

Flow Simulation Results

The completion density in this study area is largely skewed towards DGI G (**Figure 117**). Considering the well density in tract 7, it was decided that a plugging/recompletion program is the most appropriate future implementation. All perforations in DGI G are plugged, and then DGI's B-F are recompleted. Recompletion of DGI A is avoided since the permeability for this layer is observed to be smaller as compared to all other DGI's. Independent simulations were conducted with two different S_w scaling factors mentioned before.

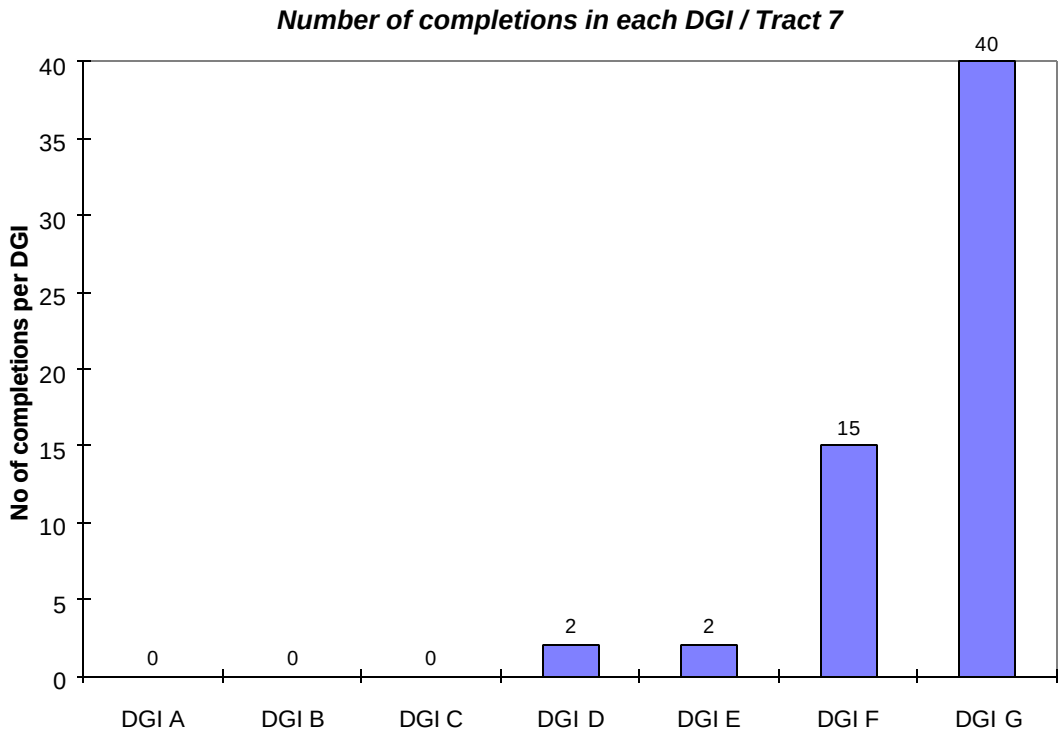

Figure 117 – Histogram of perforations in tract 7

Scenario $(S_w \times 1.2)$

This is the optimistic scenario wherein it is deemed sufficient that the resistivity log derived saturation profile, when scaled up by a factor 1.2, is adequate to bring it in tune with the initial time of history matching (1993). It should be noted that the saturation profile captures the global profile of the reservoir but the relative highs and lows predicted in this profile need not necessarily be valid. Extending this logic, it could be said that when the unit is considered as one unified system, the flow simulation gives an approximate idea of how the system would behave in response to a stimulus, but there is no guarantee that wells at selected locations will honor the simulated performance in truth. The reduction in water cut for this scenario was about 2%, and the incremental production obtainable after implementation of the plug/recompletion program was about 375 bbl/d. The simulated response is shown in **Figure 118**.

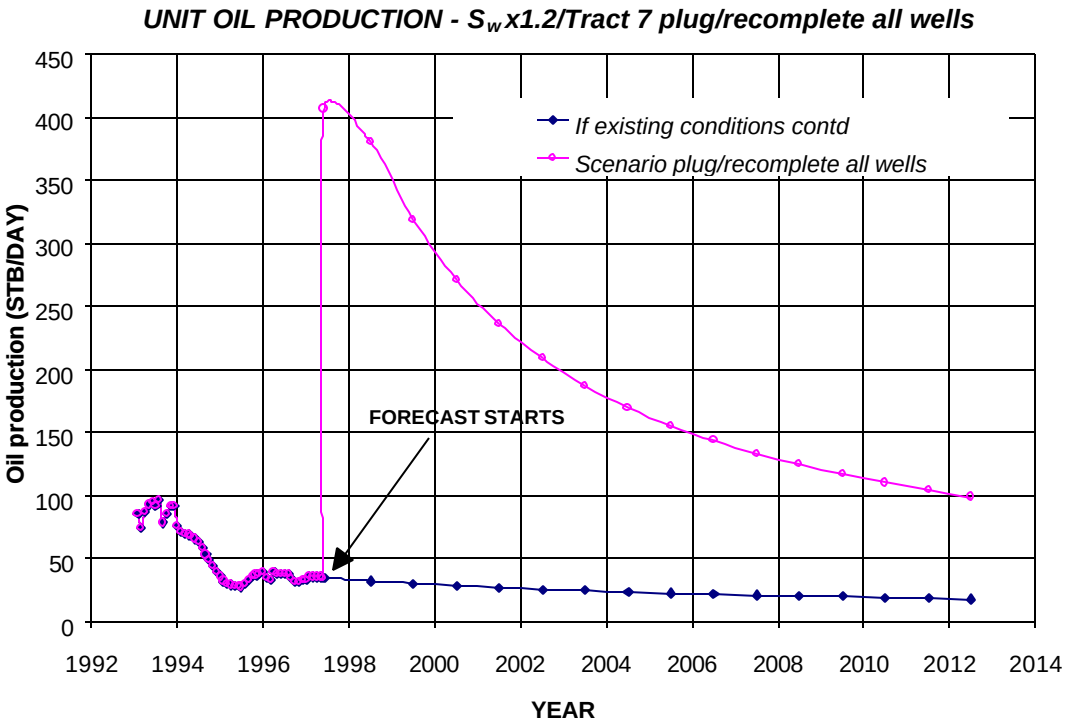

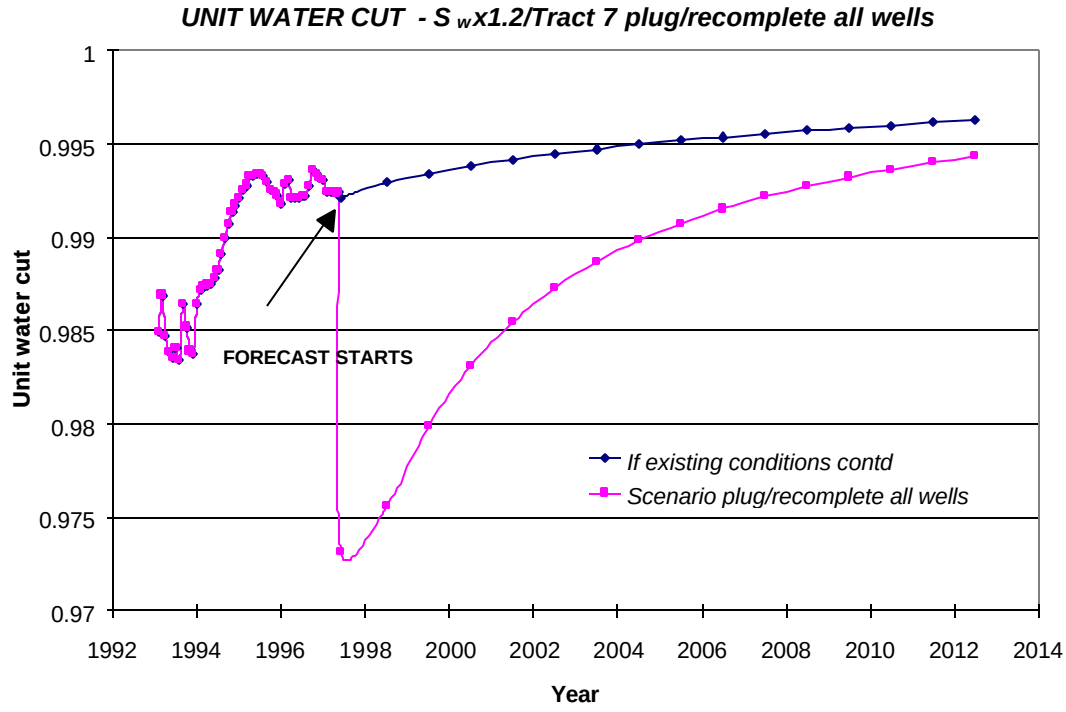

Figure 118 – Oil production and water cut plot for scenario with $S_w \times 1.2$

Scenario $(S_w \times 1.4)$

This is the pessimistic scenario, wherein the effect of a very large multiplying coefficient for the S_w profile at 1993 is simulated, and is contrasted against the previous case. It can be observed that the incremental oil production is still quite high but the reduction in water cut is small after implementation of the plug/recompletion program. The governing factor for a proposal to be viable or not, is the possible reduction in water cut coupled with the incremental oil production that could be obtained. In this case, oil production increases since more total fluid (oil+water) is being withdrawn. The high rates of total liquid withdrawal also result in increase of lifting or operating costs. It should be noted that, before implementation of the recompletion program, the wells were primarily producing from one DGI. But after implementation of the program fluid is withdrawn from DGI's B-F yielding more total liquid production.

It can be observed from **Figure 119** that the water cut shows a decrease of about 0.2% at best. It will be shown below in the economic analysis section that the incremental oil production does not generate enough revenue to offset the increase in lifting costs. If the saturation profile in reality is close to the saturation profile estimated in this scenario, then it can be concluded that a plug/recompletion program is not economically viable.

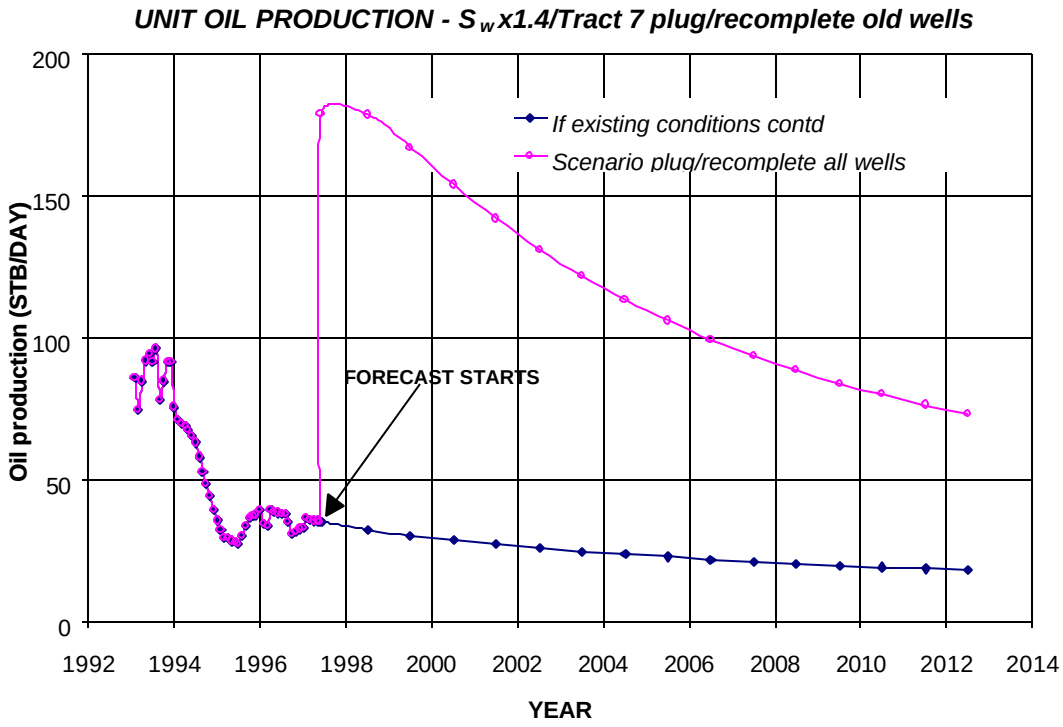

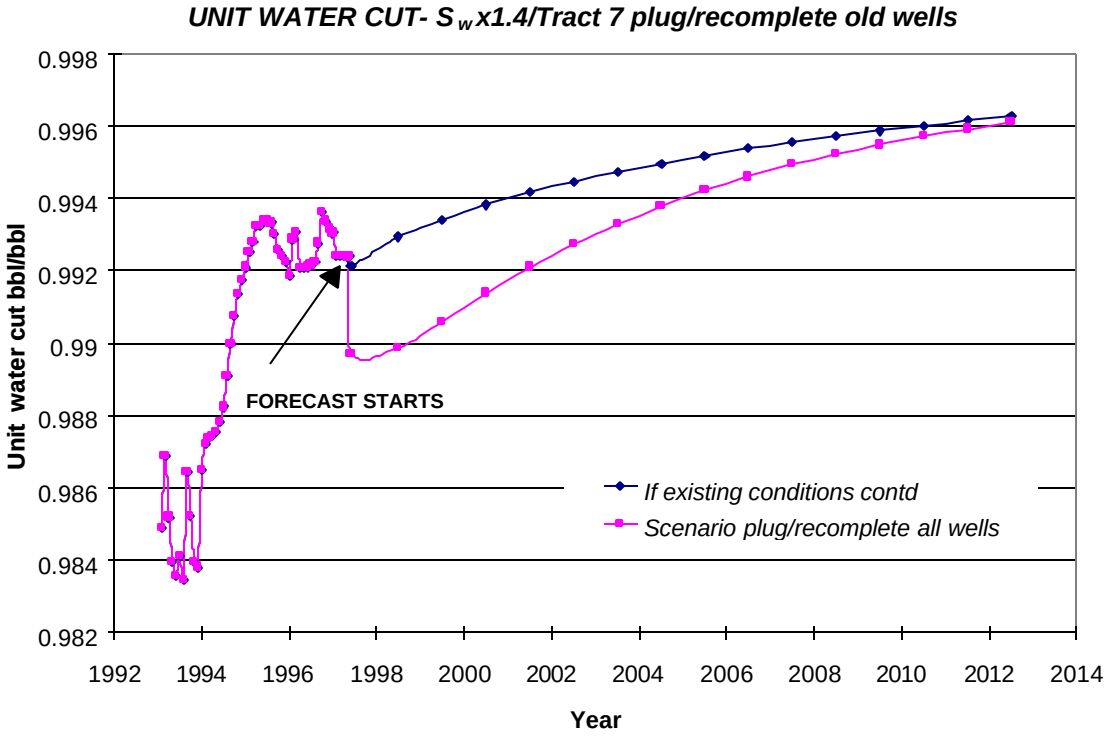

Figure 119 – Oil production and water cut for scenario with $S_w \times 1.4$

Economic Analysis of Tract 7

Only two scenarios were incorporated in the analysis of tract 7. The forecasting was performed for observing the response of plug/recompletion program but the simulation itself was initiated with two different base maps of resistivity log derived water saturation maps. This was accomplished by using two scaling coefficients for saturation namely $S_w \times 1.2$ and $S_w \times 1.4$. **Figure 120** presents the rate of return and the net present value charts for the two scenarios. The unit has 37 active wells for which the approximate plug/recompletion cost is $500,000. It can be observed that if the water saturation profile is scaled up by a factor of 1.4, the plug/recompletion program was unfeasible as indicated by the zero rate of return and negative net present value. Conversely, if in reality the saturation profile corresponds to the resistivity log derived profile scaled up by a factor of 1.2, the implementation of the plug/recompletion program would have been largely successful. These two extremes could be considered as the bounding cases for actual field implementation.

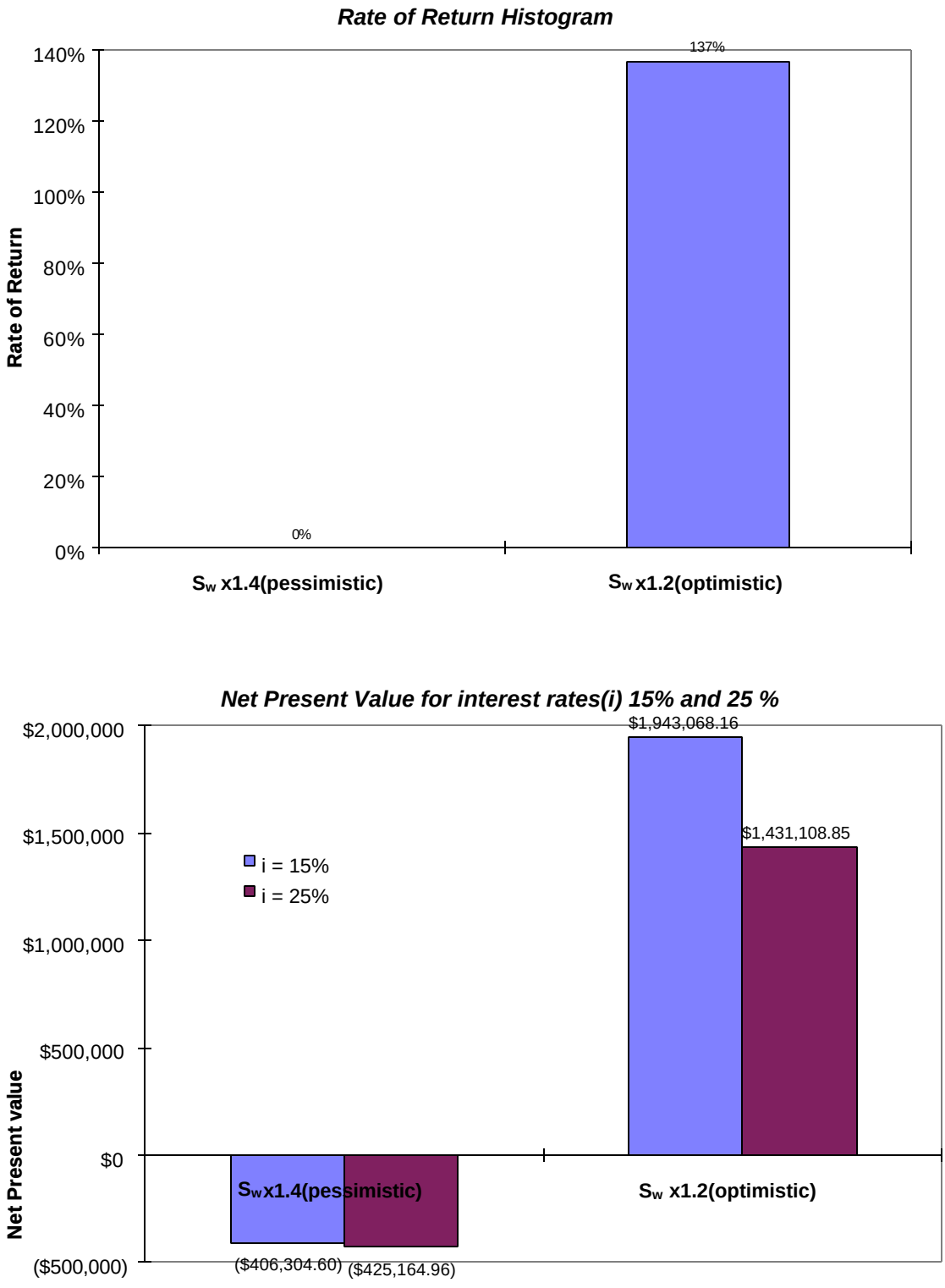

Figure 120 – Rate of return and net present value charts for tract 7

Summary of Tract 7 Simulation

Owing to the high well density and completion skewed towards the lower zones in tract 7, the most appropriate program is plug/recompletion. Most likely, the procedure would result in successful recovery of additional oil. The bounding extremes, discussed above, have been defined by performing simulations with different saturation profiles for the time instant when history matching is started.

Field Implementation

In the previous section, we discussed various detailed field implementation plans for tracts 7 and 9. We decided to concentrate on tract 9 because of the limited number of wells producing in that tract. Also, more economic uncertainty existed with respect to field implementation plan for tract 7. Initially, our plan was to re-complete the existing wells in the upper portion (DGI's A, B, C and D) of the reservoir and shut in the lower portions of the reservoir in the same wells. Unfortunately, these old wells were treated with nitroglycerine. As a result, we were not confident about the formation of caverns, which may have been left behind in these wells. After receiving several bids from various contractors, it became apparent that completing the lower portions of the existing wells is not an easy task. The amount of cement required cannot be known unless we start completing these wells, and it was possible that the cost would exceed the cost of drilling a new well. With this scenario in mind, we decided not to re-complete the old producing wells.

In addition to concern about the existing wells, we were also concerned with the possibility of a gas cap in tract 9. Earlier reports had indicated that there is a possibility of a gas cap in other parts of the reservoir. Although TDT logs in tract 7 had indicated an absence of a gas cap; we did not have any direct proof of presence of oil in the upper zones in tract 9. To test the presence or absence of gas, we completed well 9-60. The well was selectively completed in the upper intervals, and a bridge plug was placed to separate the bottom zones from the top zone. After the well was re-completed, there was no indication of the presence of gas – this is consistent with our model, and the well showed a slight improvement in the oil cut – also consistent with our model. We were

encouraged by this result which indicated that the oil saturation is higher in the upper zone, and there is no free gas present in the top zones.

Armed with all the information in the previous studies, as well as the information from well 9-60, we designed a deviated production well to be selectively completed in the upper four zones (A, B, C and D). The location is shown in **Figure 121**. This overall implementation includes converting well no 61 into an injector, reperforating wells M-3A and M-4A, and drilling a deviated production well between 61 and M-3A/M-4A in an east-west direction. The total length is expected to be about 500-ft, and the well would be completed in zones A through D. **Figure 122** shows the well plan proposed for the deviated hole and **Figure 123** shows the direction in which the well is to be drilled. With this configuration, we can take advantage of the portion of the tract 9 that has not been drained, and also support the production through three injectors that are completed in the same zone. In addition to testing the concept of a deviated hole, we also decided to test the concept of drilling a vertical well using air drilling.

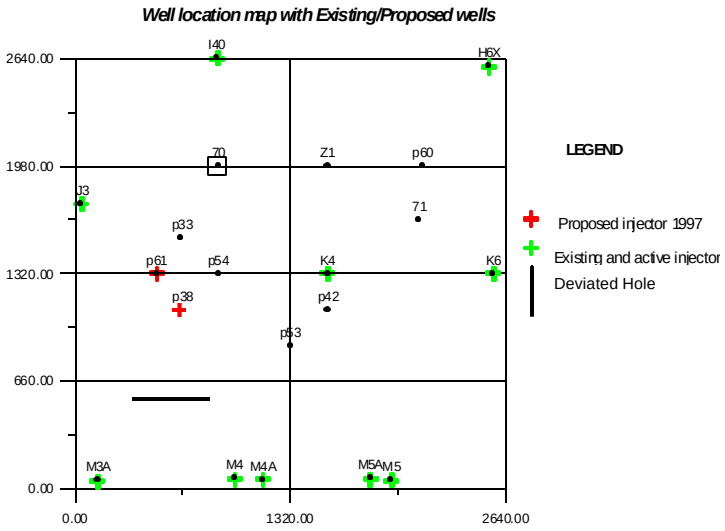

Figure 121 - Proposed management plan for tract 9

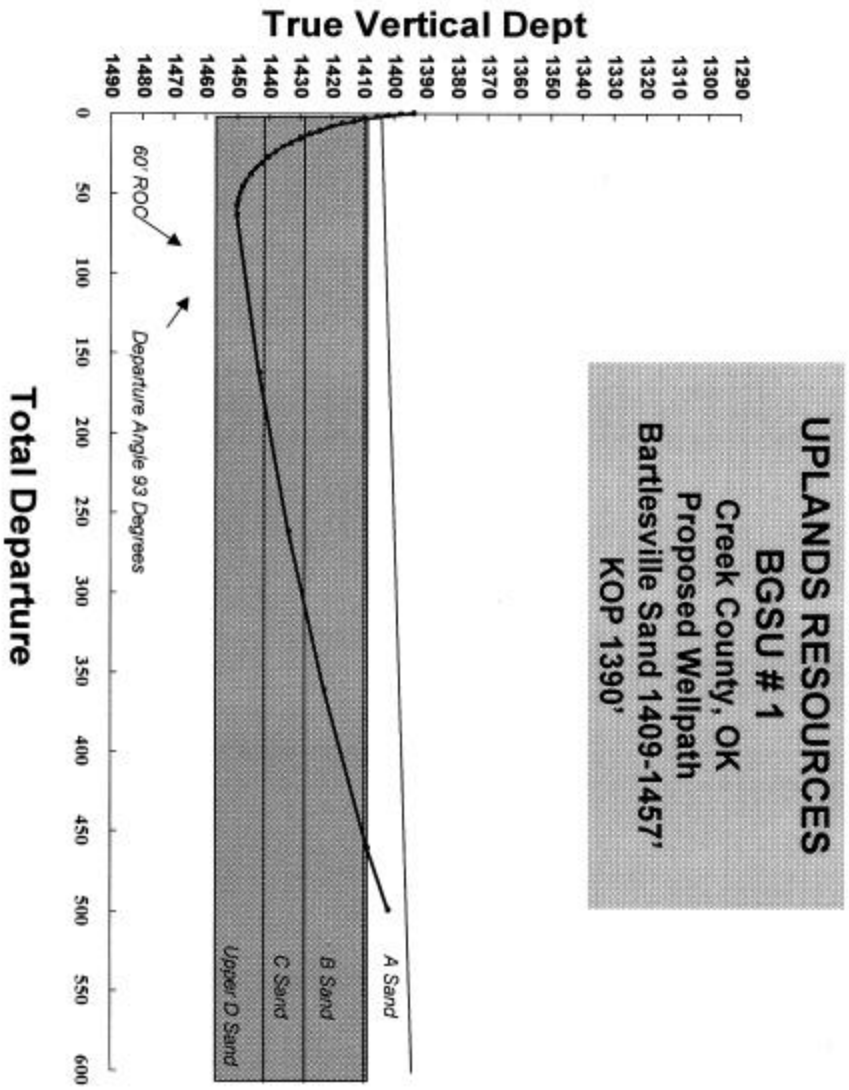

Figure 122 - Profile of a deviated hole

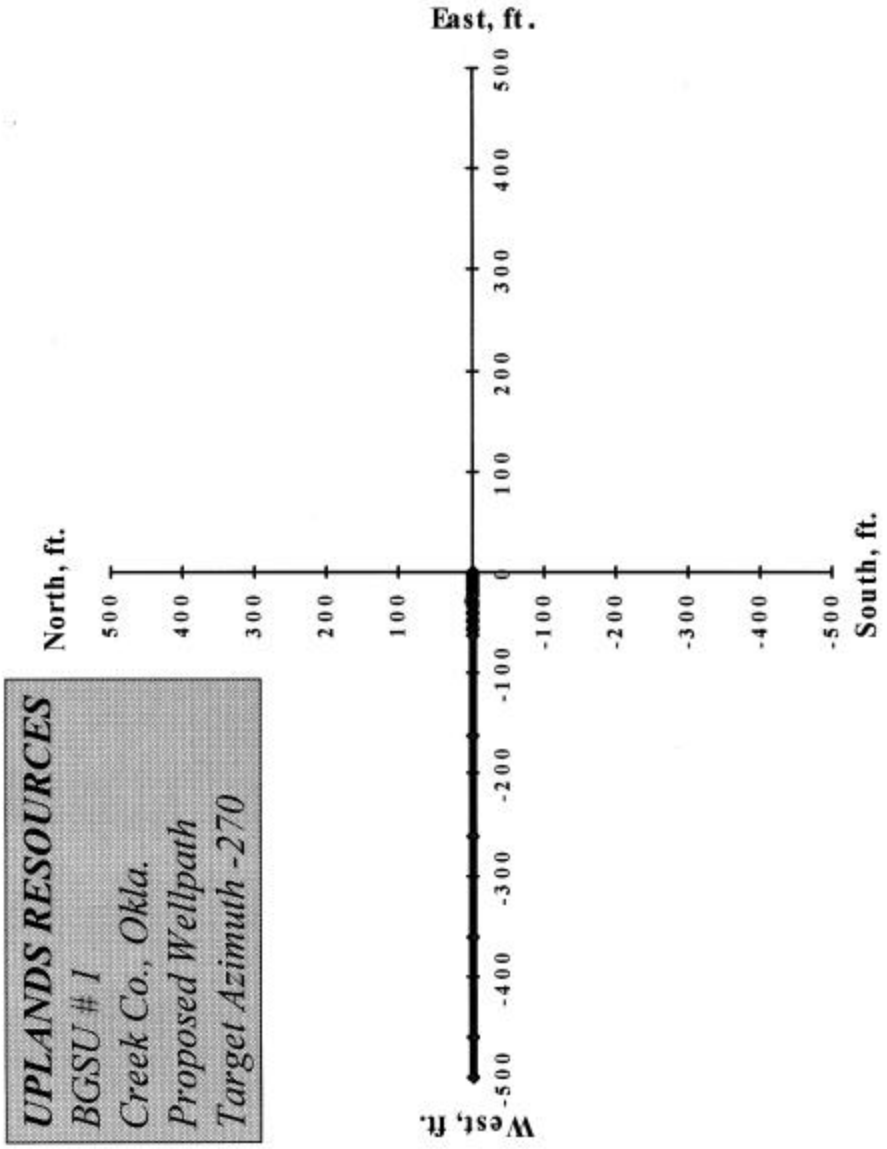

Figure 123 - Direction of a deviated hole

The drilling of the vertical portion of the well was initiated at the end of November 1998. The drilling encountered no problem, and we completed the vertical portion in the allocated time within our budget. For drilling the deviated hole portion, we gave a contract to Integrated Directional Resources (IDR), a company specializing in drilling directional wells through use of surface rotary equipment. The drill bit is steered from the surface rather than using mud motors. This is a relatively

new technology, and, if successful, can result in substantial savings in drilling horizontal holes in the future.

The drilling of the deviated hole was initiated on December 1, 1998. The bottom hole tool assembly included 6" PDC bit, CDA double joint, 2 Monel collars followed by 6 joints of drill pipe (PH6). The initial attempt to drill the well failed, because after drilling the well up to a depth of 1,363-ft, it was realized that the tool was not building any curve. Instead it was drilling a straight hole. The possible cause for this was assumed to be the double joint, and the decision was made to use a single knuckle tool. The well was plugged back using cement on December 2nd. On December 3rd, the drilling resumed with a slightly different assembly. Instead of double joint, a single knuckle tool was used. To control the direction, a gyro tool was used. From the surface, after drilling of 1-ft, the gyro was run and seated, a tool face was marked at the surface, and then gyro tool was pooled back and the rig resumed drilling. The drilling went smoothly with the angle being built according to the expectations. On December 5th, the gyro tool broke. The possible cause was determined to be high torque and high dogleg severity. After changing the tool, the drilling resumed at a very slow rate. After drilling a few more feet, the up hole Monel collar failed. The steel drill pipe failed at the pin due to high stress exerted by the Monel collar. A fishing operation was initiated and the fish was successfully brought to the surface with 3.5" basket grapple. To avoid a repeat, the decision was made to run with only one Monel collar.

After drilling another 24-ft on December 6th, the Monel collar failed at the connection on top of the non-magnetic cross over. The pipe was pulled and numerous fishing attempts were made over the next two days. The fish could not be caught. Because of significant cost over-runs, a decision was made to abandon the well by plugging back inside the casing.

An attempt was made to reinitiate the drilling in the first quarter of 1999. However, we were not able to come up with a successful cost effective strategy to re-drill the hole. Hence, the plan to complete the well was abandoned and the site was restored. It was an unfortunate end to the budget period two considering the fact that a significant effort was vested in developing a detailed reservoir management plan. In addition, with our ability to predict the performance of the reservoir, as evidenced in budget period one, gave us a lot of confidence in proposing a plan for budget

period two. We still believe that, with cost-effective technology to drill a deviated hole, we would be able to recover additional oil from the Glenn Pool field. However, this effort will have to be carried out by private oil companies.

TECHNOLOGY TRANSFER ACTIVITIES

During this project, several technology transfer activities were conducted. These activities can be broadly divided into two three categories – publications and presentations, technology transfer workshops and newsletters. These three activities are discussed below.

Publications and Presentations

Kerr, D.R., Martinez, G., Azof, I. and Kelkar, M.: "Integrated Reservoir Description Using Outcrop Studies: Example from Bartlesville Sandstone Northeast Oklahoma," presented at the Deltaic Reservoirs Workshop, Norman, Oklahoma (March 23-24, 1993).

Liner, C.L. and Lines, L.R.: "Simple Prestack Migration of Crosswell Seismic Data," Expanded Abstract, 63rd Annual International Meeting of the Society of Exploration Geophysicists (1993) pp 308-312.

Ahuja, B.: "Integration of Geological and Petrophysical Information Using Geostatistical Methods – "Self-Unit" Study," Thesis, The University of Tulsa, Tulsa, Oklahoma (1993).

Liner, C.L. *et al.*: "Glenn Pool Project: Initial Tomographic Results," Expanded Abstract, 64th Annual International Meeting of the Society of Exploration Geophysicists (1994) pp 302.

Ahuja, B.K., Bahar, A., Kerr, D.R. and Kelkar, M.: "Integrated Reservoir Description and Flow Performance Evaluation of Self-Unit, Glenn Pool Field," paper SPE 27748, presented at the Improved Oil Recovery Symposium, Tulsa, Oklahoma (April 17-20, 1994).

Kelkar, M.: "Integration of Interdisciplinary Information for Reservoir Characterization," presented at the Symposium on Multidisciplinary Approaches to Reservoir Characterization, The University of Tulsa, Tulsa, Oklahoma (May 9-12, 1994).

Bahar, A.: "Integrated Reservoir Description and Flow Performance Evaluation: Glenn Pool Field – Self-Unit Study," M.S. Thesis, The University of Tulsa, Tulsa, Oklahoma (1994).

Liner, C.L. and Lines, L.R.: "Simple Prestack Migration of Crosswell Seismic Data," Journal of Seismic Exploration, 3, (1994) pp 101-112.

Bozkurt, G. and Liner, C.L.: "Straight Ray Tomography: Synthetic and Real Data Examples," Expanded Abstract, 64th Annual International Meeting of the Society of Exploration Geophysicists (1994) pp 174-177.

Liner, C.L. *et al.*: "Glenn Pool Project: Crosswell Seismic Data Acquisition Overview," Expanded Abstract, 64th Annual International Meeting of the Society of Exploration Geophysicists (1994) 298-302.

Liner, C.L.: "Crosswell Seismic Research at the Glenn Pool Field," presentation to Geophysical Society of Tulsa, Tulsa, Oklahoma (April 1994).

Liner, C.L.: "Crosswell Seismic: Overview and Glenn Pool Project," presentation at the TGS/GST/AAPG/SPWLA Spring Symposium on Multidisciplinary Approaches to Reservoir Characterization, Tulsa, Oklahoma (May 1994).

Bahar, A., Kelkar, M. and Thompson, L.G.: "Integrated Reservoir Description and Flow Performance Evaluation - Glenn Pool Study," paper SPE 30622, presented at the Annual SPE Meeting, Dallas, Texas (October 22-25, 1995); also presented at the AAPG Mid-Continent Section Meeting, Tulsa, Oklahoma (October 8-10, 1995).

Ye, L. and Kerr, D.R.: "Characterization of Fluvial-Dominated Deltaic Reservoirs in a Mature Oil Field: Glenn Pool Field, Northeastern Oklahoma," Abstract, American Association of Petroleum Geologists Annual Convention, Houston, Texas (1995)

Kelkar, M. and Richmond, D.: "Implementation of Reservoir Management Plan - Self Unit, Glenn Pool Field," paper SPE 35407 presented at the 1996 SPE/DOE Tenth Symposium on Improved Oil Recovery, Tulsa, Oklahoma (April 21-24, 1996).

Liner, C.L., Bozkurt, G. and Cox, V.D.: "Shooting Direction and Crosswell Seismic Data Acquisition," Geophysics, 61, No. 5 (1996) 1489-1498.

Ye, L. and Kerr, D.R.: "Use of Microresistivity Image Logs in Detailed Reservoir Architecture Reconstruction of Glenn Sandstone, Glenn Pool Field, Northeastern, Oklahoma," Transactions of the 1995 AAPG Mid-Continent Section Meeting, Tulsa, Oklahoma (1996) pp 203-213.

Kelkar, M. and Richmond, D.: "Reservoir Management Plan Implemented in Glenn Pool Field," *Petroleum Engineer International* (July 1996) pp 45.

Kerr, D.R., Ye, L., Kelkar, M. and Bahar, A.: "Reservoir Characterization and Improved Waterflood Performance in Glenn Pool Field: A DOE Class I Project," presented at the American Association of Petroleum Geologists Annual Convention, Dallas, Texas (1997).

Ye, L., Kerr, D.R. and Yang, K.: "Facies Architecture of the Bluejacket Sandstone in the Eufaula Lake Area, Oklahoma: Implications for the Reservoir Characterization of the Bartlesville Sandstone, presented at the Fourth International Reservoir Characterization Technical Conference, Houston, Texas (1997).

Paranji, S.: "Integrated Reservoir Description and Flow Simulation Case Study: Glenn Pool Field," Thesis, The University of Tulsa, Tulsa, Oklahoma (1997).

Bahar, A. and Kelkar, M.: "Integrated Lithofacies and Petrophysical Properties Simulation," paper SPE 38261, presented at the Western Regional Meeting, Long Beach, California (June 25-27, 1997).

Bahar, A. and Kelkar, M.: "Journey from Well Logs/Cores to Integrated Geological and Petrophysical Properties Simulation: A Methodology and Application," paper SPE 39565, presented at the 1998 SPE India Oil and Gas Conference and Exhibition, New Delhi, India (February 10-12, 1998).

Ye, L., Kerr, D. R., and Yang, K.: "Facies Architecture of the Bluejacket Sandstone in the Eufaula Lake Area, Oklahoma: Implications for Reservoir Characterization of the Subsurface Bartlesville Sandstone," in Jordan, J. F. and Schatzinger, R., eds., Recent Advances in Reservoir Characterization (selected contributions from the Fourth

International Reservoir Characterization Conference), American Association of Petroleum Geologists Memoir Series, in press, scheduled for release for Spring, 1999.

Kerr, D. R., Ye, L., Bahar, A. and Kelkar, M.: "Glenn Pool Field, Oklahoma: A Case of Improved Production from a Mature Reservoir," American Association of Petroleum Geologists Bulletin, v. 83 (January 1999) pp 1-18.

Ye, L. and Kerr, D.R.: "Sequence Stratigraphy of the Middle Pennsylvanian Bartlesville Sandstone, Northeastern Oklahoma: A Case of an Underfilled Incised Valley," American Association of Petroleum Geologists Bulletin. Accepted, anticipated publication January, 2000.

Kerr, D.R., Ye, L., Aviantara, A. and Martinez. G.: "Application of Borehole Imaging for Meandering Fluvial Facies Architecture: Examples from the Bartlesville Sandstone, Oklahoma," American Association of Petroleum Geologists Bulletin, in preparation.

Technology Transfer Workshops

As part of the technology transfer program, Mohan Kelkar and Dan Richmond participated in a traveling workshop series organized by BDM-Oklahoma, Inc. The purpose of the workshop series is to make small operators aware of the technologies used in the Class I projects. The workshop included four Class I projects including this project. A total of six workshops were held at the following locations: Bartlesville, Oklahoma; Wichita, Kansas; Denver, Colorado; Billings, Montana; Oklahoma City, Oklahoma; and Grayville, Illinois. The average attendance for these workshops was 30 or more people. The response was extremely favorable and a lot of positive feedback was received from the attendees.

As the most important part of the technology transfer program, one-day-workshops regarding this DOE Glenn Pool project were offered in Tulsa, Denver, and Houston in October 1996. In addition, a workshop was also conducted in April 1997 in Fort Worth, Texas at the invitation of local SPE chapter. Workshop preparation included preparing materials for the workbook, poster exhibit, and slide presentation. This effort resulted in a notebook summary and more than 250 slides and photos for the workshop. Participants were provided with workshop materials and computer software to

generate the reservoir description. The response to the workshop was good. The average attendance to the workshop was 27. The audience represented a wide cross section of small and large operators, service companies and consultants.

Newsletters

As part of the technology transfer activities, two newsletters were prepared and were mailed to approximately 300 operators and independent producers. The newsletters contained progress about the project, and provided operators practical information regarding the implementation of reservoir management plan.

REFERENCES

1. Kuykendall, M. D., and Matson, T. E.: "Glenn Pool Oil Field, Northeast Oklahoma Platform," American Association of Petroleum Geology - Treatise of Petroleum Geology Atlas of Oil and Gas Fields: Stratigraphic Traps III (1992) pp 155-188.

2. Visher, G. S., Saitta, B. S., and Phares, R. S.: "Pennsylvanian Delta Patterns and Petroleum occurrences in Eastern Oklahoma," *American Association of Petroleum Geology Bulletin*, V.55, pp 916-926.

3. Johnson, K.S., Amsden, T.W., Denison, R.E., Dutton, S.P., Goldstein, R.B., Sutherland, P.K., and Thompson, D.M.: "Geology of the Southern Mid-Continent," Oklahoma Geological Survey Special Publication 89-2 (1989) pp 53.

4. Roberts, M.T.: "Geologic Relations along a Regional Cross Section from Spavinaw to Broken Bow, Eastern Oklahoma," (Suneson, N.H., and Hemish, L.A., eds.) Geology and Resources of the Eastern Ouachita Mountains Frontal Belt and Southeastern Arkoma Basin, Oklahoma: Oklahoma Geological Survey Guidebook 29, (1994), pp 137-160.

5. Miser, H.D.: Geologic Map of Oklahoma, 1:500,000: U.S. Geological Survey, (1954).

6. Heath, E. S.: "Evaluation of the William B. Self and T. R. Burrows Leases, Glenn Pool Field," ARCO Reservoir Engineering Report (April 4, 1984).

7. Martinez, G., 1993, *Reservoir Heterogeneity in a Portion of the Bartlesville Sandstone (Desmoinesian), Mayes County Northeastern Oklahoma*, M.S. Thesis, The University of Tulsa, Tulsa, Oklahoma, pp 147.

8. Mishra, J., 1996, *Sequence Stratigraphy of the Bartlesville Sandstone in parts of Okmulgee, Creek, and Okfuskee Counties*, M.S. Thesis, The University of Tulsa, Tulsa, Oklahoma, pp 68.

9. Ye, L., 1997, *Reservoir Characterization and Sequence Stratigraphy of the Pennsylvanian Bartlesville Sandstone, Oklahoma,* Ph.D. Dissertation, The University of Tulsa, Tulsa, Oklahoma, pp 256.

10. Kerr, D. R., Ye, L., Bahar, A., Kelkar, B.M., and Montgomery, S.L.: "Glenn Pool Field, Oklahoma: A Case of Improved Production from a Mature Reservoir," *American Association of Petroleum Geologists Bulletin,* V. 83 (1999) pp 1-18.

11. Allen, J.R.L.: "Studies in Fluviatile Sedimentation: Six Cyclothems from the Lower Old Red Sandstone, Anglo-Welsh Basin," *Sedimentology*, V. 3 (1964) pp 163-198.

12. Miall, A.D.: *The Geology of Fluvial Deposits*, New York, Springer-Verlag (1996) PP582.

13. Thomas, R.G., Smith, D.G., Wood, J.M., Visser, J., Calverley-Tange, E.A., and Koster, E.H.: "Inclined Heterolithic Stratification -- Terminology, Description, Interpretation and Significance," *Sedimentary Geology,* V. 53 (1987) pp 123-179.

14. Grace, M., and Newberry, B.M.: "Geologic Applications of Borehole Electrical Images and Dipmeter," Schlumberger Education Services, Houston, Texas (1990) pp 724.

15. Ye, L., and Kerr, D.: "Use of Microresistivity Image Logs in the Detailed Reservoir Architecture Reconstruction of Glenn Sandstone, Glenn Pool Field, Northeastern Oklahoma," Transactions of the AAPG Mid-Continent Section Meeting (1995) pp 203-213.

16. Hemish, L.A.: "Coal Geology of Rogers County and Western Mayes County, Oklahoma," *Oklahoma Geological Survey Bulletin,* No. 144 (1989) pp 118.

17. Suneson, N.H. and Hemish, L.A., eds.: "Geology and Resources of the Eastern Ouachita Mountains Frontal Belt and Southeastern Arkoma Basin, Oklahoma," Oklahoma Geological Survey Guidebook 29 (1994) pp 294.

18. Kerr, D. R., and Jirik, L. A.: "Fluvial Architecture and Reservoir Compartmentalization of the Oligocene Middle Frio Formation, South Texas," Gulf Coast Association of Geological Societies Transactions, v. 40 (1990) pp 373-380.

19. Van Wagoner, J.C., Mitchum, R.M., Campion, K.M., and Rahmanian, V.D.: "Siliciclastic Sequence Stratigraphy in Well Logs, Cores, and Outcrops," AAPG Methods in Exploration Series No. 7 (1990) pp 55.

20. Van Wagoner, J.C., Posamentier, R.M., Mitchum, Jr., R.M., Vail, P.R., Sarg, J.R., Loutit, T.S., and Hardenbol, J.: "An Overview of the Fundamentals of Sequence Stratigraphy and Key Definitions," in Wilgus, C.K., Hastings. B.S., St. C. Kendall, C.G., Posamentier, H.W., Ross, C.A., and Van Wagoner, J.C., eds., Sea-Level Changes -- An Integrated Approach: SEPM Special Publication No. 42 (1988) pp 39-46.

21. Posamentier, H.W., Jervey, M.T., and Vail, P.R.: "Eustatic Controls on Clastic Deposition I -- Conceptual Framework," in Wilgus, C.K., Hastings. B.S., St. C. Kendall, C.G., Posamentier, H.W., Ross, C.A., and Van Wagoner, J.C., eds., Sea-Level Changes -- An Integrated Approach: SEPM Special Publication No. 42 (1988) pp 109-124.

22. Posamentier, H.W., and Vail, P.R.: "Eustatic Controls on Clastic Deposition II -- Conceptual Framework," in Wilgus, C.K., Hastings. B.S., St. C. Kendall, C.G., Posamentier, H.W., Ross, C.A., and Van Wagoner, J.C., eds., Sea-Level Changes -- An Integrated Approach: SEPM Special Publication No. 42 (1988) pp 110-154.

23. Shanley, K.W., and McCabe, P.J.: "Perspectives on the Sequence Stratigraphy of Continental Strata," *AAPG Bulletin*, V. 78 (1994) pp 544-568.

24. Stork, C. and Clayton, R. W.: "Analysis of Issues in Transmission Tomography using Ray Trace Tomography," 58th Annual International Meeting of Society of Exploration Geophysicists, Expanded Abstracts (1988) pp 1224-1227.

25. Lines, L. R.: "Applications of Tomography to Borehole and Reflection Seismology," *The Leading Edge*, 10, no.7 (1991) pp 11-17.

26. Lines, L. R., Tan, H., and Treitel, S.: "Velocity and Density Imaging Between Boreholes," CSEG Recorder, 16, no.6 (1991) pp 9-14.

27. Lines, L. R., Jackson, R., and Covey, J. D.: "Seismic Velocity Models for Heat Zones in Athabasca Tar Sands," *Geophysics,* 55 (1990) pp 1108-1111.

28. Harris, J. M., Tan, H., Lines, L., Pearson, C., Treitel, S., Mavko, G. Moos, D., and Hoeksma, R. N.: "Cross-Well Tomographic Imaging of Geological Structures in Gulf Coast Sediments," 60th Annual International Meeting of Society of Exploration Geophysicist, Expanded Abstracts (1990) pp 37-40.

29. Lines, L. R., and LeFehr, E. D.: "Tomographic Modeling of a Cross-Borehole Data Set," *Geophysics,* 54 (1989) pp 1249-1247.

30. Lines, L. R., Kelly, K. R., and Queen, J.: "Channel Waves in Cross-Borehole Data," 61st Annual International Meeting of Society of Exploration Geophysicist, Expanded Abstracts (1991) pp 850-854.

31. Lines, L. R., and Tan, H.: "Cross-Borehole Analysis of Velocity and Density," 60th Annual International Meeting of Society of Exploration Geophysicist, Expanded Abstracts (1990) pp 34-36.

32. Owen, T. E., Balogh, W. T., and Peters, W. R.: "Arc Discharge Pulse Source for Borehole Seismic Applications," 58th Annual International Meeting of Society of Exploration Geophysicist, Expanded Abstracts (1988) pp 151-154.

33. Kennedy, W., Wiggins, W., and Aronstam, P.: "Swept-Frequency Borehole source for Inverse VSP and Cross-Borehole Surveying," 58th Annual International Meeting of Society of Exploration Geophysicist, Expanded Abstracts (1988) pp 158-160.

34. Balogh, T. W., Owen, T. E., and Harris J. M.: "New Piezoelectric Transducer for Hole-to-Hole Seismic Applications," 58th Annual International Meeting of Society of Exploration Geophysicist, Expanded Abstracts (1988) pp 155-157.

35. Harris, J. M.: "Cross-Well Seismic Measurements in Sedimentary Rocks," 58th Annual International Meeting of Society of Exploration Geophysicist, Expanded Abstracts, (1988) PP 147-150.

36. Scales, J. A: "Tomographic Inversion via the Conjugate Gradient Method," Geophysics, 52 (1987) pp 179-185.

37. McGaughey, W. J., and Young, R. P.: "Comparison of ART, SIRT, Least-Squares, and SVD Two-Dimensional Tomographic Inversions of Field Data," 60th Annual International Meeting of Society of Exploration Geophysicist, Expanded Abstracts (1990) pp 74-77.

38. Justice, J. H., Vassiliou, A. A., Mathisen, M. E., Bulau, J. R., Singh, S., and Cunningham, P. S.: "Cross-Hole Seismic Tomography-Reservoir Interpretation Case Histories," 60th Annual International Meeting of Society of Exploration Geophysicist, Expanded Abstracts (1990) pp 41-42.

39. Inderwiesen, P. L., and Lo, T.: "Cross-Hole Seismic Tomographic Imaging of Reservoir in Homogeneities in Midway Sunset field, California," 60th Annual International Meeting of Society of Exploration Geophysicist, Expanded Abstracts (1990) pp 22-25.

40. Paulsson, B. N. P., Fairborn, J. W., Cogley, A. L., Howlett, D. L., Melton, D. R., and Livingston, N.: "McKittrick Cross-Well Seismology Project: Part I. Data Acquisition and Tomographic Imaging," 60th Annual International Meeting of Society of Exploration Geophysicist, Expanded Abstracts (1990) pp 26-29.

41. Krohn, C. E.: "Cross-Well Continuity Logging using Seismic Guided Waves," 60th Annual International Meeting of Society of Exploration Geophysicist, Expanded Abstracts (1990) pp 43-46.

42. Lo, T., Inderwiesen, P. L., Howlett, D. L., Melton, D. R., Livingston, N. D., Paulsson, B. N. P., and Fairborn, J. W.: "McKittrick Cross-Well Seismology Project: Part II. Tomographic Processing and Interpretation," 60th Annual International Meeting of Society of Exploration Geophysicist, Expanded Abstracts (1990) pp 158-160.

43. Epili, Duryodhan and McMechan, George A.: "Parallel Implementation of 3-D Prestack Kirchhoff Migration with Application to Field Data," 65th Annual International Meeting of Society of Exploration Geophysicist, Expanded Abstracts (1995) pp 168-171.

44. Bozkurt, G.: *Crosswell Tomography in Anisotropic Media: Glenn Pool Field, Oklahoma*, Ph.D. Dissertation, The University of Tulsa, Tulsa, Oklahoma (1998).

45. Bahar, A.: *Co-Simulation Of Lithofacies And Petrophysical Properties,* Ph.D. Dissertation, The University of Tulsa, Tulsa, Oklahoma (1994).

46. Verly, G.: "Sequential Gaussian Co-Simulation: a Simulation Method Integrating Several Types of Information", Proceedings of 4th International Geostatistical Congress, pp 11.

47. Xu, Wenlong, and Journel A. G.: "GTSIM: Gaussian Truncated Simulations of Lithofacies," Report-6, Stanford Center for Reservoir Forecasting (May 1993).

48. Damsleth, Elvind, et al.: "A Two Stage Stochastic Model Applied to a North Sea Reservoir," paper SPE 20605, presented at the 65th SPE Annual Meeting (1990).

49. Ahuja, B. K.: *Integration of Geological and Petrophysical Information Using Geostatistical Methods – Self-Unit Study,* M.S. Thesis, The University of Tulsa (1993).

50. Welch R.A.: "Berryhill Glenn Sand Unit Reservoir Study," Internal Report of ARCO Oil & Gas Company (1989).

51. Paranji, S.: *Integrated Reservoir Description and Flow Simulation Case Study: Glenn Pool Field*, MS Thesis, The University of Tulsa (1997).

52. Deutsch, C.V and Journel, A.G: *Geostatistical Software and Library and User's Guide*, Oxford University Press (1992).